

INTERNATIONAL ENERGY AGENCY
energy conservation in buildings and
community systems programme

9th AIVC Conference

Effective Ventilation

Proceedings

Volume 2



***Air Infiltration and
Ventilation Centre***

University of Warwick Science Park
Barclays Venture Centre
Sir William Lyons Road
Coventry CV4 7EZ
Great Britain

This report is part of the work of the IEA Energy Conservation in Buildings & Community Systems Programme.

Annex V Air Infiltration and Ventilation Centre

Document AIC-PROC-9-88-2
ISBN 0 946075 40 9

Price: £30.00 Sterling
Distribution: Unrestricted

Participants in this task:

Additional copies of this report may be
obtained from:

Belgium, Canada, Denmark, Federal Republic of
Germany, Finland, Italy, Netherlands, New Zealand,
Norway, Sweden, Switzerland, United Kingdom and
United States of America.

Air Infiltration and Ventilation Centre
University of Warwick Science Park
Barclays Venture Centre
Sir William Lyons Road
Coventry CV4 7EZ
Great Britain

9th AIVC Conference

Effective Ventilation

(held at Novotel Hotel,
Gent, Belgium
12 – 15 September 1988)

Proceedings

Volume 2

© Copyright Oscar Faber Partnership 1989.

All property rights, including copyright are vested in the Operating Agent (Oscar Faber Consulting Engineers) on behalf of the International Energy Agency.

In particular, no part of this publication may be reproduced, stored in a retrieval system or transmitted in any form or by any means, electronic, mechanical, photocopying, recording or otherwise, without the prior written permission of the Operating Agent.

CONTENTS		(i)
Volume 2		
Preface		(iii)
Posters:		
P1	The large area quantitative visualization method of air streams. G. Gottschalk, P.A. Tanner and P. Suter	1
P2	Displacement ventilation by different types of diffusers. P.V. Nielsen, L. Hoff and L.G. Pedersen	13
P3	A comparison of upward and downward air distribution systems. D.J. Croome	31
P4	Air heating systems in airtight multifamily residential buildings. P.O. Jagbeck, G. Werner and K. Engvall	43
P5	Further studies of passive ventilation systems - assessment of design and performance criteria. R.E. Edwards and C. Irwin	61
P6	Zone to zone tracer gas measurements: laboratory calibration and values of air flows up and down stairs in houses. S.B. Riffat, J. Walker and J. Littler	85
P7	Development of an efficient control algorithm for a multizone constant concentration tracer gas air infiltration measurement system. R. Compagnon, A. Kohler, C. Roecker and C-A Roulet	103
P8	A study of the ventilation characteristics of a suspended floor. J.P. Lilly, J.M. Piggins and R.J. Stanway	123
P9	Numerical simulation of indoor turbulent air flows caused by cross-ventilation and its model experiments. J-I Tsutsumi, T. Katayama, T. Hayashi, Q. Zhang and H. Yoshimizu	141
P10	Multi-zone contaminant dispersal analysis using an element assembly approach. J. Axley	157

P11	A numerical study of buoyancy-driven flows of mass and energy in a stairwell. A.S. Zohrabian, M.R. Mokhtarzadeh-Dehghan and A.J. Reynolds	183
P12	A simplified approach of air infiltration in multizones buildings. D. Caccavelli, J.J. Roux and F. Allard	205
P13	Analysis of the influence of topography on the exposure of buildings. J-A Hertig and J. Ehinger	221
P14	The influence of a controlled natural ventilation on the indoor radon decay products concentration: a case study. R. Crameri, Ch. Schuler, D. Furrer and W. Burkart	237
P15	IEA Annex XIV: Energy and Condensation. E. Senave	245
P16	Examinations about the air humidity in lived dwellings depending on different air ventilation systems using a new characteristic value. F-P Schmickler	253
P17	Field experiences of airborne moisture transfer in residential buildings. J. Oldengarm	263
P18	Ventilation habits in residential buildings. H. Erhon	277
P19	Flow conditions in a mechanically ventilated room with a convective heat source. P. Heiselberg and P.V. Nielsen	287
P20	Ventilation and indoor air quality in a modern office building. R.A. Grot, A. Persily, A.T. Hodgson and J.M. Daisey	303
P21	Application of mathematical modelling to the evaluation of building ventilation systems. J.B. Fang, R.A. Grot and T. Kurabuchi	327

PREFACE

International Energy Agency

In order to strengthen cooperation in the vital area of energy policy, an Agreement on an International Energy Programme was formulated among a number of industrialised countries in November 1974. The International Energy Agency (IEA) was established as an autonomous body within the Organisation for Economic Cooperation and Development (OECD) to administer that agreement. Twenty-one countries are currently members of the IEA, with the Commission of the European Communities participating under a special arrangement.

As one element of the International Energy Programme, the Participants undertake cooperative activities in energy research, development, and demonstration. A number of new and improved energy technologies which have the potential of making significant contributions to our energy needs were identified for collaborative efforts. The IEA Committee on Energy Research and Development (CRD), assisted by a small Secretariat staff, coordinates the energy research, development, and demonstration programme.

Energy Conservation in Buildings and Community Systems

As one element of the Energy Programme, the IEA encourages research and development in a number of areas related to energy. In one of these areas, energy conservation in buildings, the IEA is encouraging various exercises to predict more accurately the energy use of buildings, including comparison of existing computer programmes, building monitoring, comparison of calculation methods, as well as air quality and inhabitant behaviour studies.

The Executive Committee

Overall control of the R&D programme "Energy Conservation in Buildings and Community Systems" is maintained by an Executive Committee, which not only monitors existing projects but identifies new areas where collaborative effort may be beneficial. The Executive Committee ensures all projects fit into a predetermined strategy without unnecessary overlap or duplication but with effective liaison and communication.

Annex V Air Infiltration and Ventilation Centre

The IEA Executive Committee (Building and Community Systems) has highlighted areas where the level of knowledge is unsatisfactory and there was unanimous agreement that infiltration was the area about which least was known. An infiltration group was formed drawing experts from most progressive countries, their long term aim to encourage joint international research and increase the world pool of knowledge on infiltration and ventilation. Much valuable but sporadic and uncoordinated research was already taking place and after some initial groundwork the experts group recommended to their executive the formation of an Air Infiltration and Ventilation Centre. This recommendation was accepted and proposals for its establishment were invited internationally.

The aims of the Centre are the standardisation of techniques, the validation of models, the catalogue and transfer of information, and the encouragement of research. It is intended to be a review body for current world research, to ensure full dissemination of this research and, based on a knowledge of work already done, to give direction and firm basis for future research in the Participating Countries.

The Participants in this task are Belgium, Canada, Denmark, Federal Republic of Germany, Finland, Netherlands, New Zealand, Norway, Sweden, Switzerland, United Kingdom and the United States of America.

EFFECTIVE VENTILATION

9th AIVC Conference, Gent, Belgium
12-15 September, 1988

Poster 1

THE LARGE AREA QUANTITATIVE VISUALIZATION METHOD OF AIR STREAMS

G. GOTTSCHALK, P. A. TANNER, P. SUTER

Swiss Federal Institute of Technology, Energy Systems Laboratory
ETH-Zentrum
CH-8092 Zurich / Switzerland

SUMMARY

The project is aimed to develop the quantitative method of visualization of the air streams in application to the indoor problems of heating , ventilating and air conditioning.

The geometrically well defined light sheet is crossing the examined space and determines the plane of observation. The photographic camera is placed perpendicularly to this plane at a distance of a few meters. The flow is seeded with the soap bubbles of the diameter 3-4 mm. The light is reflected from those bubbles which are crossing the illuminating sheet. The film is exposed in the concerned areas: the trajectories of the tracer are recorded in form of elongated tracks.

The photographic images contain the features of the flow which are revealed and quantified in the digitizing operations. The images existing on the colour slides are splitted into six equal square parts and digitized once for each colour with a camera having a 512x512 pixel sensor. The grey scale levels are so adapted that the black slide area obtain the value zero (or any other but small one) in the digital representation matrix. With either Roberts or Sobel operators edges of the bubble tracks (having any orientation) are detected and enhanced.

The above steps are the basis for extracting the velocity vector field from the experimental images.

1. EXPERIMENTAL TECHNIQUE

1.1 Method and Experimental Set-Up (Fig. 1)

The solid tracer, namely soap bubbles are transported with the air streams. The relatively long exposed film is integrating the time - position dependence resulting in the trajectory images. Interpretating the sub-sections of the tracks as being tangential to the stream lines and resulting from the instantaneous direction of the velocity, the Euler - like description of the experiment is revealed.

Taking into account longer sequences of the tracer positions (i.e. longer partitions which cannot be associated with the one point of observation) the Lagrange - like approach is reflecting the experimental method .Finally it is the spacial / time resolution and the interpolation technique which determines which one of the descriptions is taking over another.

The corrections for the tracer behaviour (inertia ,gravity) are planned to be realized.

Method is orientated to be used not necessarily in laboratory chambers but also in the real spaces. The indispensable condition is the darkening of the room. All the instruments needed for experiment are portable and not disturbing the flow pattern in the room.

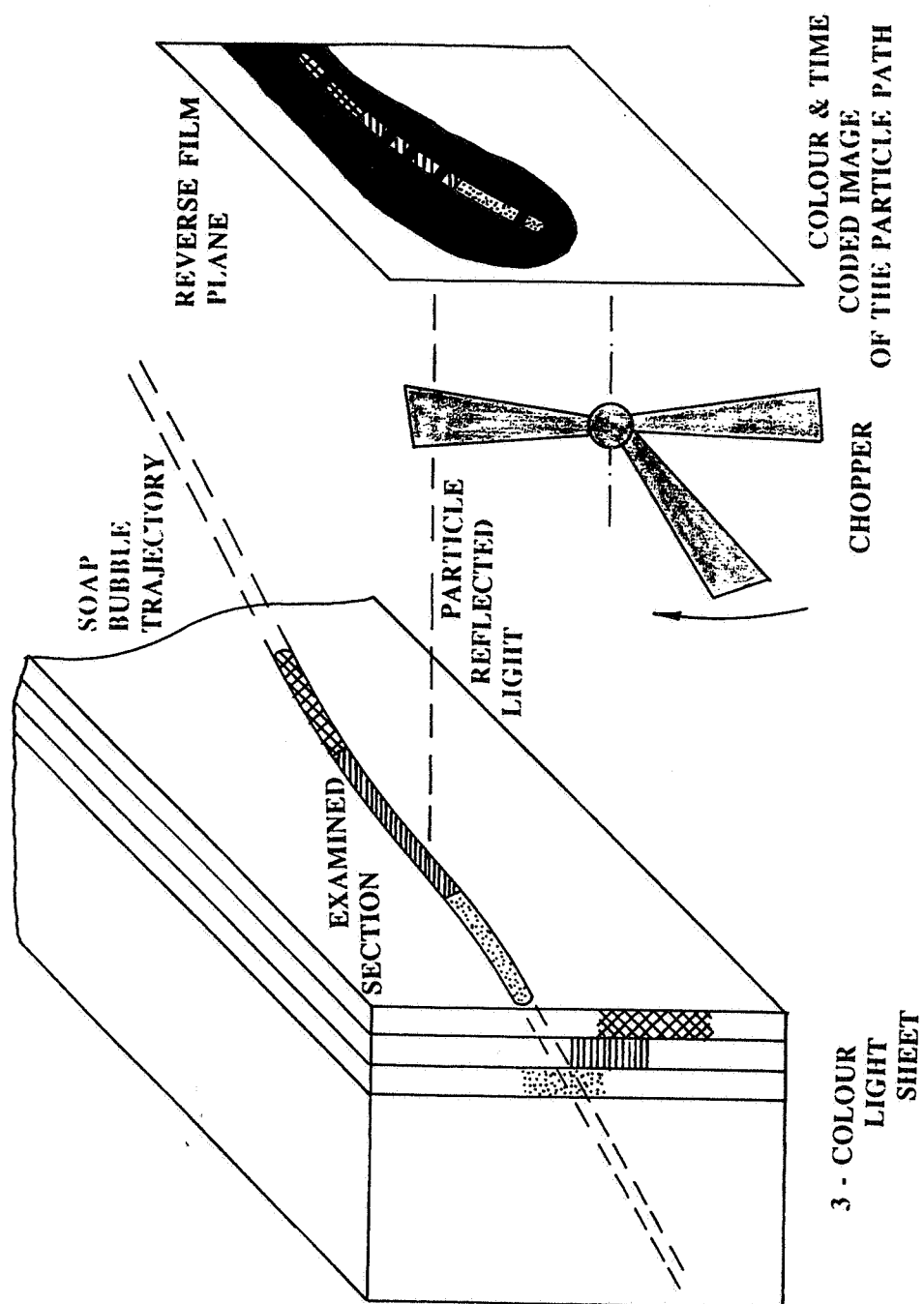


Fig. 1 The scheme of the experiment

1.2 Lighting

The light sheet is consisting of the 3 distinctly separated colours. By that mean the trajectories which are not parallel to the light sheet (ditto observation plane) are resulting in tracks of coloured sequence. Color change is marking the movement of the tracer perpendicular to the observation plane.

Cooling of the light sources is to be realized through the thermally insulated flexible ducting to the outside space.

The light reflected from the room surfaces and other objects should be reduced at the aim to obtain possibly contrast images.

1.3 Tracer and Seeding

The soap bubbles used for seeding the flow are produced by the standard generator (Sage Action Inc., USA). The batch of the bubbles passes through the selector for eliminating those which are too heavy . The homogenous population of bubbles performing the settling velocity in the still air of about 5 cm/s (diameter 3 - 4 mm) is transfered to the experimental space. The average life time is a few minutes .

The helium filling option foreseen by the manufacturer is not utilized. The neighbourhood of the air outlets and other zones of higher speed are the points apt for introducing the tracer. The recorded trajectories of the typical room flow have rectilinear, smooth character indicating the damping effect (like low pass filter). Comparing to the hot wire recording most of the turbulence spectrum is not detectable. The limit frequency of the sinusoidal idealized sollicitation is estimated approximately to $f_{\text{limit}} = 0.5 \text{ Hz}$. This feature is particulary interesting while investigating the averaged flow pattern and its large scale structures .

1.4 The Photographic Technique

Standard reflex camera 24 x 36 mm is used. The images are taken on the colour reversal film 1600 ASA. The shutter is opened for relatively long time (typically 1 s). Only those bubbles which are actually crossing the light sheet are becoming the visible objects on the darkened background during the entire or part time of the shutter action.

1.5 Control of the Image Recording

At the aim to extract the quantitative information from the images the conditions for photographs taking must be strictly controlled .

a. Space

In the observation plane (xy) the real distances are scaled to the image using the physical marks in the experiment. Another mean taken into consideration is the superposition of the experimental images with the reference grid originating from the test shot.

The depth (3rd dimension: along 'z', perpendicular to xy) is controlled by the thickness of the middle light plane.

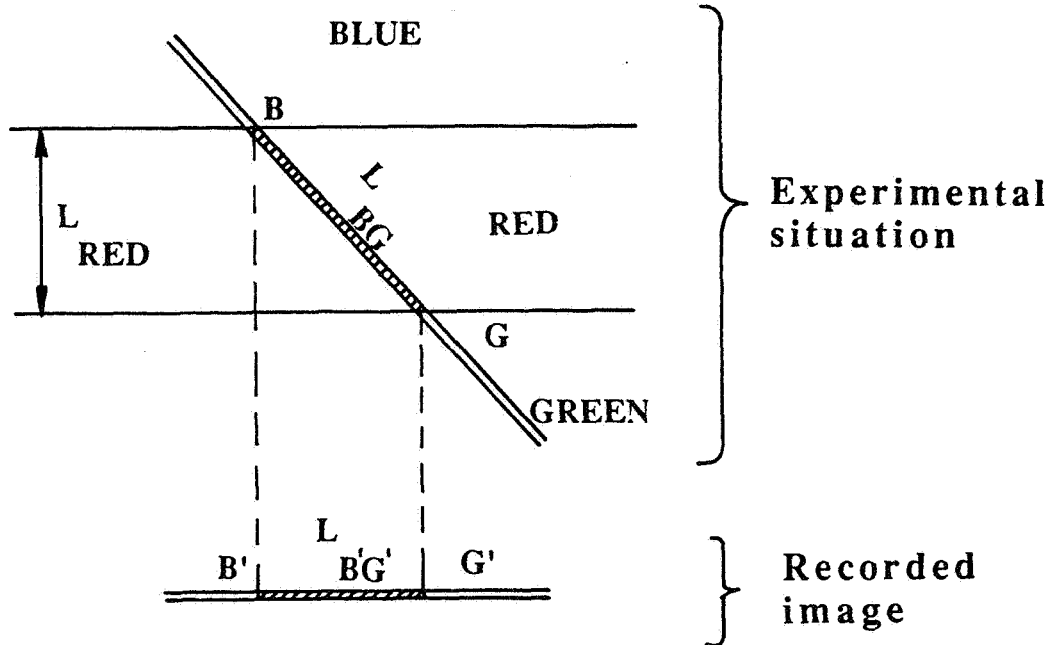


Fig. 2 The reconstruction of the 3rd dimension

The reconstruction of the real depth situation is possible according to Fig. 2:

$$L_{BG} = \sqrt{L_{B'G'}^2 + L_{RED}^2}$$

b. Timing

The 3 - arm non-symmetrical chopper is placed ahead the lenses of the camera. Its speed of rotation is adapted to the range of the tracer speeds observed simultaneously in the photographed plane.

The camera shutter is opened relatively long so that a few complete rotations of the chopper are meanwhile accomplished. That is resulting in "cutting" the tracer trajectories into segments: the long one, shorter and the shortest. Knowing the sense of rotation of the chopper the direction of the tracer displacement is determined.

The "cut-outs" on the trajectory image are the time - marks according to the chopper geometry and the speed of rotation.

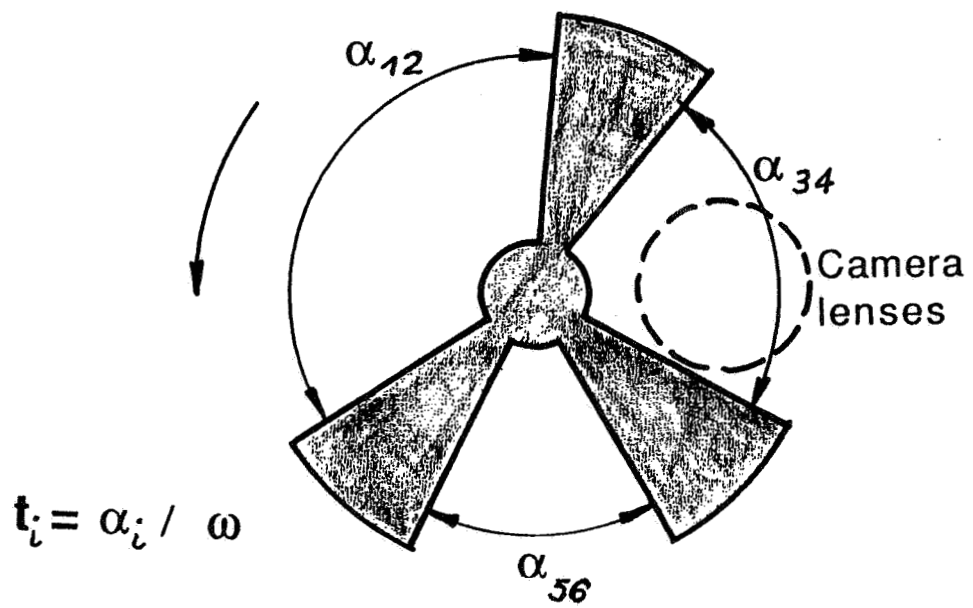


Fig. 3 Chopper

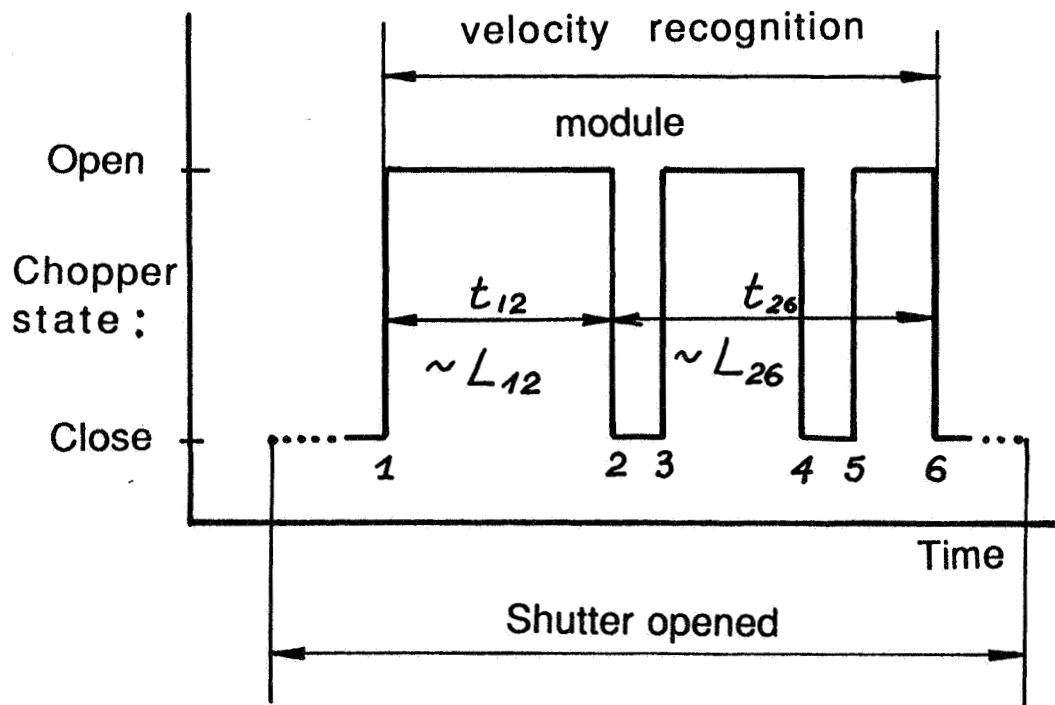


Fig. 4 Timing diagram: chopper/shutter

Taking the sequence of segments: " long - shorter - shortest" as a unit/module of the velocity vector recognition, its value may be calculated for instance:

$$|v|_{xy} = \frac{\frac{L_{12}}{t_{12}} + \frac{L_{26}}{t_{26}}}{2} \quad (\text{see also Fig. 3})$$

Of course the multiple of the recognition module associated to the same trajectory may be used if that facilitates the velocity determination (e.g. because of the length measurement precision).

The camera and the chopper are not synchronized so that the first / last recorded track length is of no signification.

c. Colour

The distinction of the colour on the trajectory image is the mean to determine the 3rd dimension. The purity of the colours is essential to make that successfully. Each of the colours is associated with the separate LUT (Look Up Table) according to the recognition resulting from the light filtering while digitizing.

To accomplish the task the colour control is performed on the each level of the experiment. Namely,

- the light source temperature is known and possibly high
- the filters for producing the colour light sheets are very selective and adapted to the color reverse film sensitivity.
- the digitizing is performed adapting the light source / filters / CCD-camera settings for the best colour distinction after electronic conversion.

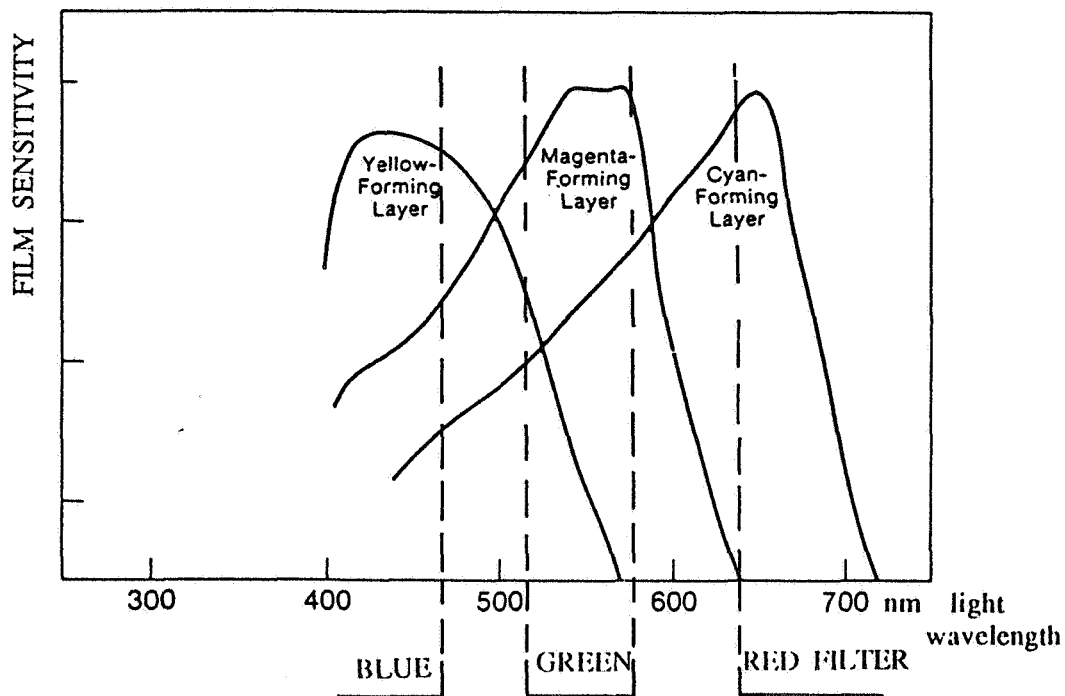


Fig. 5 Reverse film sensitivity vs. light filtering

2.

DIGITIZING AND THE BASIC IMAGE PROCESSING PROCEDURES

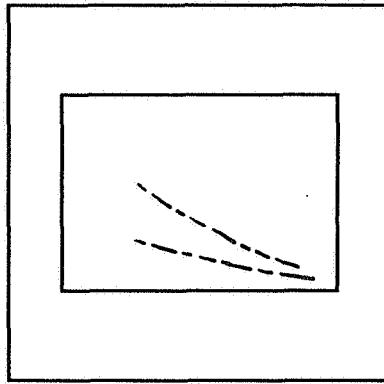


Fig. 6 Image from experiment

The area marked in the slide above is digitized three times (once for each colour) with a CCD-camera (containing a 512x512-pixel sensor). For every colour, information is stored in a specific channel in the computer, that means per slide-area one obtains three different matrices in the computer (three LUT's= Look Up Tables).

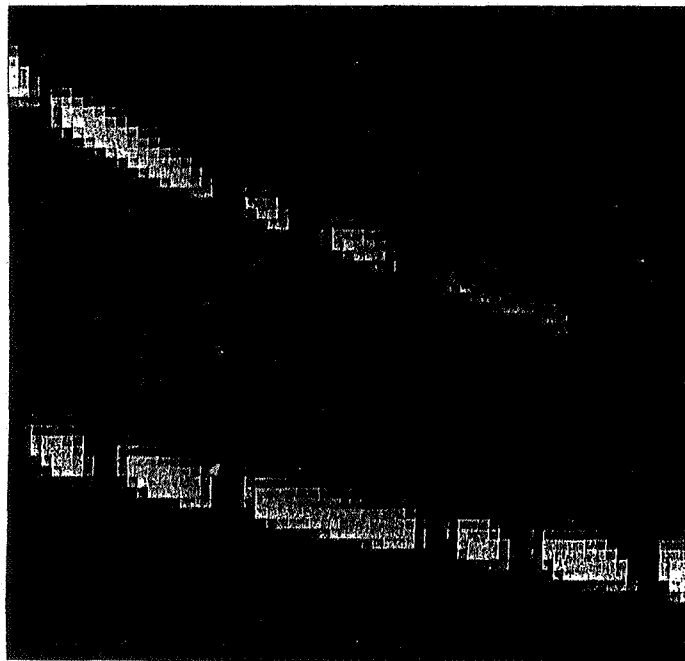


Fig. 7 Digitized image

Shown above is an electronic image, i.e. one 512x512-array for one specific colour. The image consists of pixels with different gray-levels (values between 0 and 128).

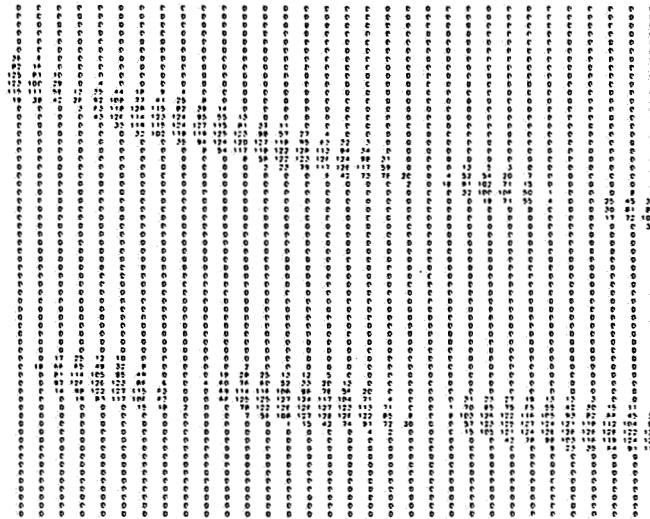


Fig. 8 Numerical representation of the electronic image

Even with this kind of presentation it is possible to visualize the different tracks (there is the advantage that the black background-pixels have the value 0). This matrix represents the basis for the image processing steps which will follow.

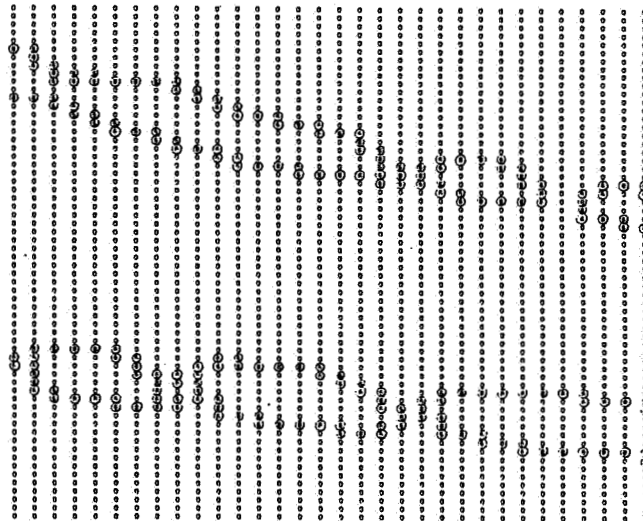


Fig. 9 Effect of edge detection operator

The original matrix looks like this after being modified by an algorithm called "Roberts operator" (for better presentation, pixels which don't have the value 0 are placed in a setting of a circle). Every pixel-value has been calculated with the formulas shown in the next paragraph [4]. The calculation started in the upper left corner and finally stopped at the end of the last row in the corner right below.

2.1 Example of the application of the "Roberts-operator"-algorithm

```

-----> j
| 2 2 2 2 8 8
| 2 2 2 2 8 8
| 2 2 2 2 8 8
| 2 2 2 ② 8 8
| 2 2 2 2 2 2
|
↓
i

```

Let's consider the surrounded pixel with the brightness-value $b(i,j)=2$ in the original matrix that should be modified by the "Roberts-operator". The resulting brightness-value must be calculated as follows:

$$C(i,j) = \sqrt{A^2 + B^2}$$

$$A = b(i,j) - b(i+1,j+1)$$

$$B = b(i+1,j) - b(i,j+1)$$

In this example one gets 0 for A, because $b(i+1,j+1)=2$ is subtracted from $b(i,j)=2$.

The value for B is -6 ($b(i,j+1)=8$ is subtracted from $b(i+1,j)=2$).

The resulting value for C(i,j) is

$$C(i,j) = \sqrt{0^2 + (-6)^2} = 6$$

After being modified by the "Roberts-operator", the area of the original matrix shown above is as follows:

```

-----> j
| 0  0  0  8.5  0  0
| 0  0  0  8.5  0  0
| 0  0  0  8.5  0  0
| 0  0  0  6.0  8.5  8.5
| 0  0  0  0    0    0
|
i

```

The example above illustrates how the image edges became "visible" for further recognition operations:

Length and orientation determination of the tracks in x,y,z-space.

3. CONCLUSIONS

The quantitative visualization of the low-speed air streams in the ventilated/heated spaces using the solid tracer is today technically realistic. The flow pattern of air movement and diffusion may be investigated based on the air velocity vector field. The progress in many associated areas: particle tracking in water, colour CCD-cameras, image treatment, colour photography, are insistently influencing the evolution of the presented method toward a precise and highly automated engineering tool.

4. ACKNOWLEDGEMENT

The authors gratefully acknowledge "Schweizerischer Nationalfonds zur Foerderung der wissenschaftlichen Forschung" for supporting the project (NF: Nr. 2.523-0.87).

5. REFERENCES

- [1] Popovich M. M., Weinberg F. J.:
Laser Optical Methods for the Study of Very Large Phase Objects
Experiments in Fluids 1, 169-178 (1983)
- [2] Kobayashi T., Saga T., Segawa S.:
Some Considerations on Automated Image Processing of Pathline
Photographs
4th International Symposium on Flow Visualization, Paris 1986
- [3] Gonzalez R. C., Wintz P.:
Digital Image Processing
Addison-Wesley Publishing Company, 1987
- [4] Richards J. A.:
Remote Sensing Digital Image Analysis
Springer-Verlag 1986

EFFECTIVE VENTILATION

9th AIVC Conference, Gent, Belgium
12-15 September, 1988

Poster 2

DISPLACEMENT VENTILATION BY DIFFERENT TYPES OF DIFFUSERS

PETER V. NIELSEN, LARS HOFF¹, LARS GERMANN PEDERSEN²

University of Aalborg,
Sohngårdsholmsvej 57, DK-9000 Aalborg, Denmark

¹Birch & Krogboe,
Hovedgaden 54, DK-8220 Brabrand, Denmark

²The Jutland Technological Institute,
Teknologiparken, DK-8000 Århus C, Denmark

SYNOPSIS

The paper describes measuring results of the air movement from three different types of diffusers for displacement ventilation. Two of the diffusers are low-level wall mounted diffusers, one with a low and one with a high initial entrainment. The third diffuser is of the floor mounted type.

The air flow close to the diffusers and in the rest of the room is analysed. Velocity decay in the flow from the low-level diffusers is given as a function of the Archimedes number, and the paper suggests a general equation for this part of the flow. The velocity level and velocity decay in the flow are dependent on the room geometry. The flow is not influenced by the Reynolds number for supply flow above a certain level.

Measurements of the turbulence intensity show a level in the cold flow along the floor which is rather equivalent to the level in an isothermal wall jet.

The floor mounted diffuser generates a circular jet with swirl along a vertical line in the room. The velocity decay in the flow from this jet is high compared to the decay in a conventional, free circular jet.

The ventilation efficiency based on temperatures and vertical temperature profiles are given for the diffusers for different levels of air exchange rates and thermal loads. The ventilation efficiency varies between 1.5 and 2.3 for all diffusers and it is rather unaffected by the type of diffuser.

LIST OF SYMBOLS

Ar	Archimedes number	
a_o	Diffuser supply area	m^2
H	Height of room	m
K	Constant for low-level diffuser	
K_a	Constant for diffuser	
L	Length of room	m
n	Exponent	
Q	Heat emission	W
q_o	Volumen flow	m^3/s
Re	Reynolds number	
T	Temperature	C
T_o	Supply temperature	C
T_{oc}	Mean temperature in the occupied zone	C
T_R	Return temperature	C
u	Mean velocity	m/s
\hat{u}	Instantaneous velocity	m/s
u'	Velocity fluctuation	m/s
u_o	Supply velocity	m/s
u_x	Maximum velocity along floor	m/s
v_o	Supply velocity	m/s
v_y	Maximum vertical velocity	m/s
W	Width of room	m
x	Coordinate	m
y	Coordinate	m
z	Coordinate	m
δ	Thickness of flow at the floor	m
ϵ_T	Ventilation (temperature) efficiency	

1. INTRODUCTION

Ventilation systems with vertical displacement flow have been used in industrial areas with high thermal loads for many years. Quite recently the vertical displacement flow systems have grown popular as comfort ventilation in rooms with thermal loads e.g. offices.

The air is supplied directly into the occupied zone at low velocities from wall mounted or floor mounted diffusers.

The plumes from hot surfaces, from equipment and from persons entrain air into the occupied zone and create a natural convection flow upwards in the room, see figure 1.

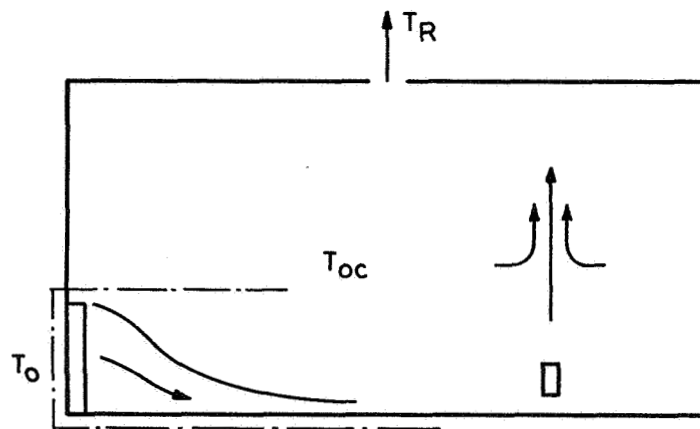


Fig. 1. Room with low-level diffuser, heat source and displacement flow.

The displacement flow systems have two advantages compared with traditional mixing systems.

- An efficient use of energy. It is possible to remove exhaust air from the room where the temperature is several degrees above the temperature in the occupied zone which allows a higher air inlet temperature at the same load.
- An appropriate distribution of contaminant air. The vertical temperature gradient (or stratification) implies that fresh air and contaminant air are separated. The most contaminant air can be found above the occupied zone and the air flow supplied can be reduced.

A general description of the displacement ventilation system has recently been given by Skåret¹, model experiments have been shown by Sandberg and Lindström², and measurements in plumes have been given by Kofoed and Nielsen³.

This paper will deal with the flow from different types of diffusers and it shows the main characteristics of the air movement which takes place in the lower part of the room (within the dotted line in fig. 1). The paper will further deal with the temperature distribution and the ventilation efficiency (temperature efficiency) obtained in the room using different types of diffusers.

2. DIFFUSERS

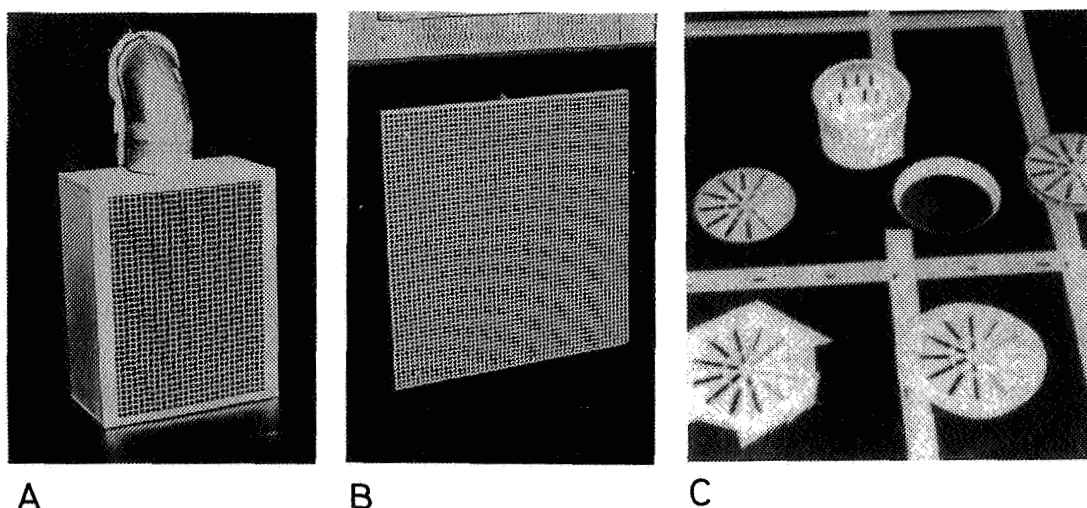


Fig. 2. Two low-level diffusers, type A and B, and a floor mounted diffuser, type C.

Figure 2 shows three different diffusers used in the experiments. The diffusers of types A and B are both low-level diffusers giving a horizontal air flow directly into the occupied zone. They both have a height of about 500 mm, but a different design. The diffuser A has a supply velocity profile which is very constant over the entire supply area, while the diffuser of type B has a supply velocity with a large variation over the supply area, see fig. 3. This variation applies to velocity level as well as to direction, and it means that the local entrainment - or diffusion - is very high close to the opening.

The third diffuser used in the experiments is a floor mounted diffuser called type C. This diffuser gives a vertical circular free jet with swirl and it is used

in practice in groups of four as shown in figure 2.

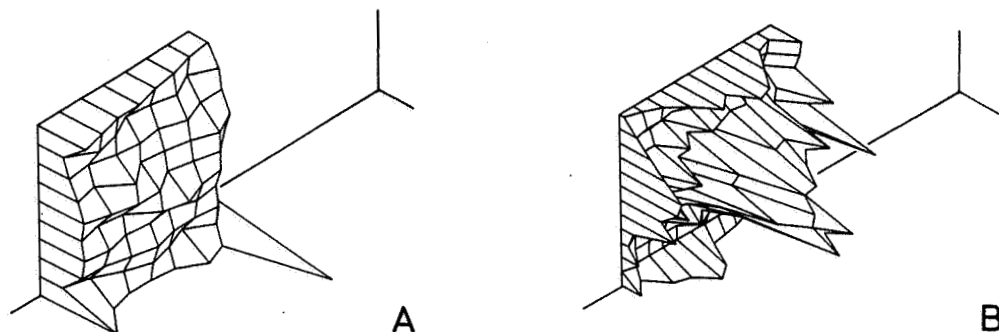


Fig. 3. Supply velocity profile for diffuser A and B.

The experiments take place in a test room of the dimensions $L \times W \times H = 5.4 \times 3.6 \times 2.6$ m. The low-level diffusers are mounted in the middle of the short end wall, while the floor mounted diffusers are located in the middle of the floor. The heat source is installed in the middle plane at a distance of $0.75 \times L$ from the end wall. The return opening is in the middle of the ceiling.

Calculation of temperature efficiency requires measurements of the temperature distribution in the room measurements of the supply temperature T_0 and the return temperature T_R . The temperature distribution in the room is measured at 24 points located at three vertical lines in the room.

3. FLOW FROM LOW-LEVEL DIFFUSERS

The flow pattern close to the openings and the local entrainment of room air influence the air movement in the room. Smoke experiments show that the flow from diffuser A spreads out within a 90° area downstream along the floor. Large temperature differences ($T_{OC} - T_0 \sim 12 - 14$ K) will increase the angle and small temperature differences will decrease the angle giving a flow of a three-dimensional wall jet type for $T_{OC} - T_0 \sim 0$ K.

Smoke experiments with diffuser B show that this diffuser spreads the flow over the whole floor area (180°) at all temperature differences.

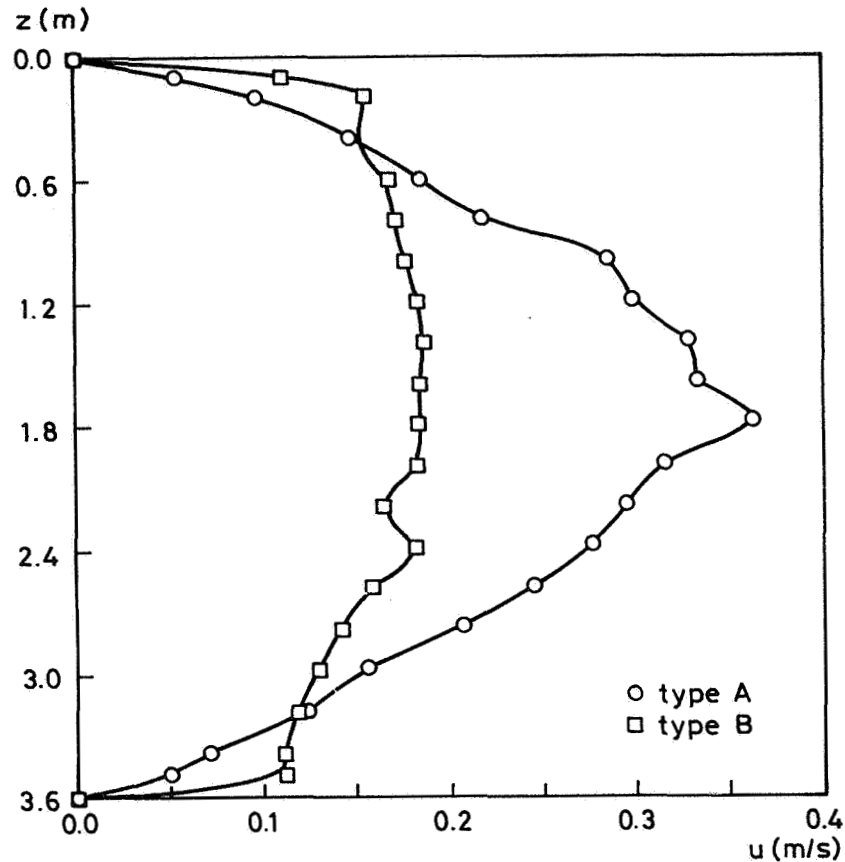


Fig. 4. Velocity distribution close to the floor in a cross-section of the room. $x = 2.4$ m, $y \sim 0.04$ m, $q_0 = 0.056$ m³/s, $T_{oc} - T_o \sim 5$ K.

It is obvious that the two different low-level supply openings - with various initial diffusion - will give a different air movement in the room. Figure 4 shows the maximum velocity close to the floor (4 cm) at a distance of 2.4 m from the diffusers. Figure 4 shows that diffuser A generates a more concentrated flow in the middle plane of the room, while diffuser B spreads the flow over the whole width of the room. This implies that the velocity level will be dependent on room width in the latter case.

Figure 5 shows the velocity decay in the air movement along the floor for both supply openings. The figure indicates that the maximum velocity u_x along the floor is proportional to $1/x^n$ where the exponent n is about 1. The low diffusion in supply opening A results in a high initial acceleration of the air movement due to buoyancy effect on the cold supply air. The velocity level obtained, results in a high velocity in the whole flow

along the floor.

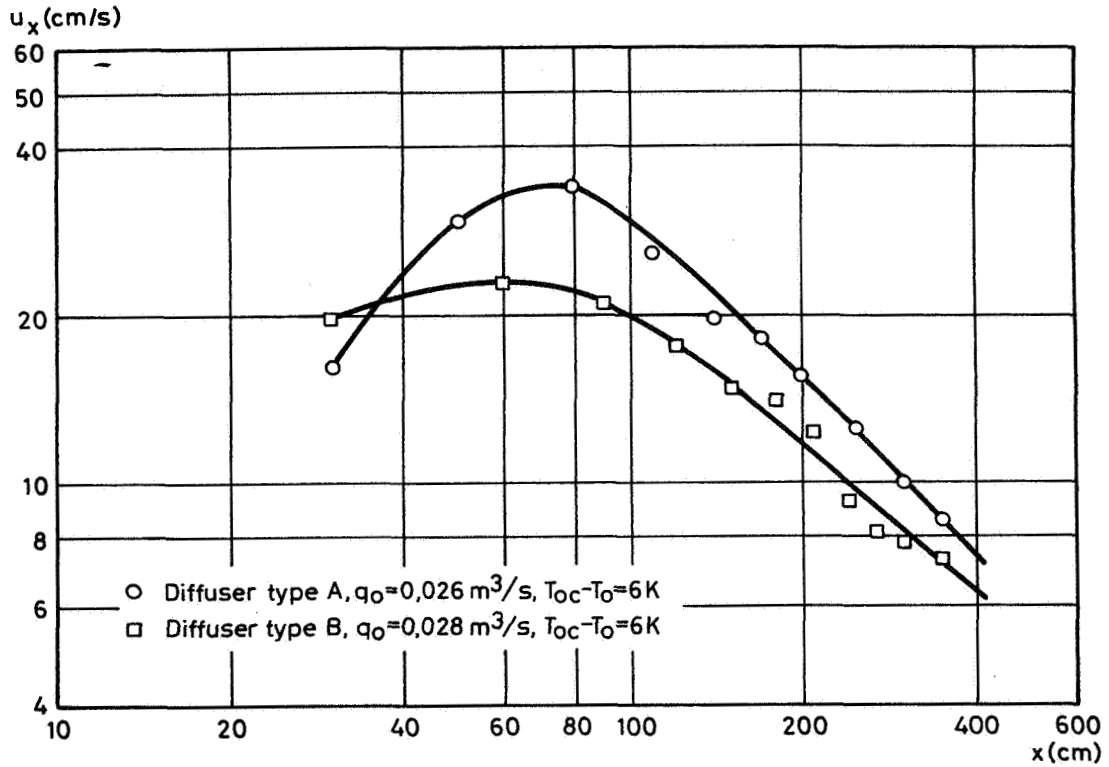


Fig. 5. Maximum velocity in flow versus distance from diffuser.

The flow from diffuser B is also dependent on buoyancy but the acceleration close to the supply opening is smaller due to the high initial entrainment of room air.

It is possible to describe the air movement along the floor by the following equation

$$\frac{u_x}{u_0} = K \left(\frac{\sqrt{a_0}}{x} \right)^n \quad (1)$$

This description is slightly similar to the equation for velocity decay in a wall jet, but the flow is strongly affected by buoyancy expressed by a K-factor which is a function of the Archimedes number Ar .

$$K = \text{func} \left(\frac{\sqrt{a_0} (T_{oc} - T_o)}{u_0^2} \right) \quad (2)$$

The height of the flow along the floor is typical 0.2 - 0.25 m and the maximum velocity is located 0.03 - 0.04

m above the floor surface independently of distance from the diffuser.

The velocity decay in the flow from the diffuser is influenced by the location of the side wall. Figure 6 shows the velocity decay from a low-level diffuser mounted in the middle plane of the room and the velocity decay from the same diffuser mounted close to the side wall. The velocity level in the flow is higher when the diffuser is mounted close to a side wall and the exponent n is smaller.

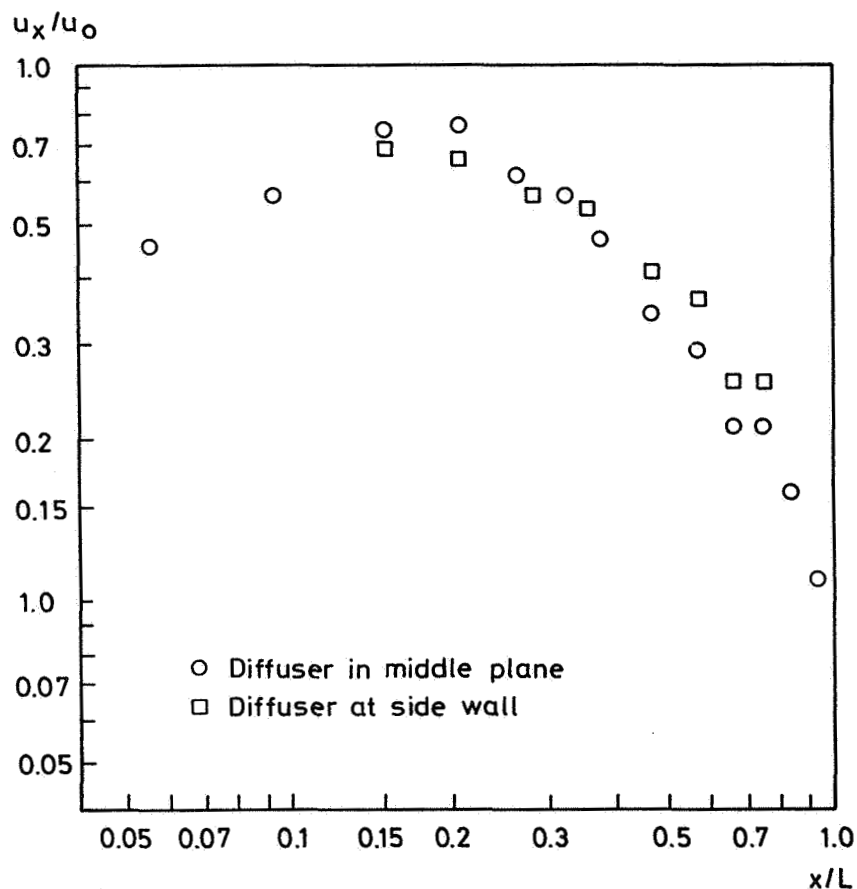


Fig. 6. Velocity decay versus distance for two locations of diffuser type A, $q_0 = 0.026 \text{ m}^3/\text{s}$, $T_{oc} - T_0 = 3.0 \text{ K}$.

It is generally shown by all the experiments that equation (1) is suitable for description of the velocity decay along the floor in a room. But it is also shown that both K and n are functions of diffuser type and diffuser location in the room, as well as room width, implying that it is difficult to separate the influence of diffuser design from the influence of room geometry.

Air movement in ventilated rooms with high supply velocities will be self-similar and will be only slightly dependent on the Reynolds number Re due to the high level of turbulence in the room as shown e.g. by Nielsen⁴.

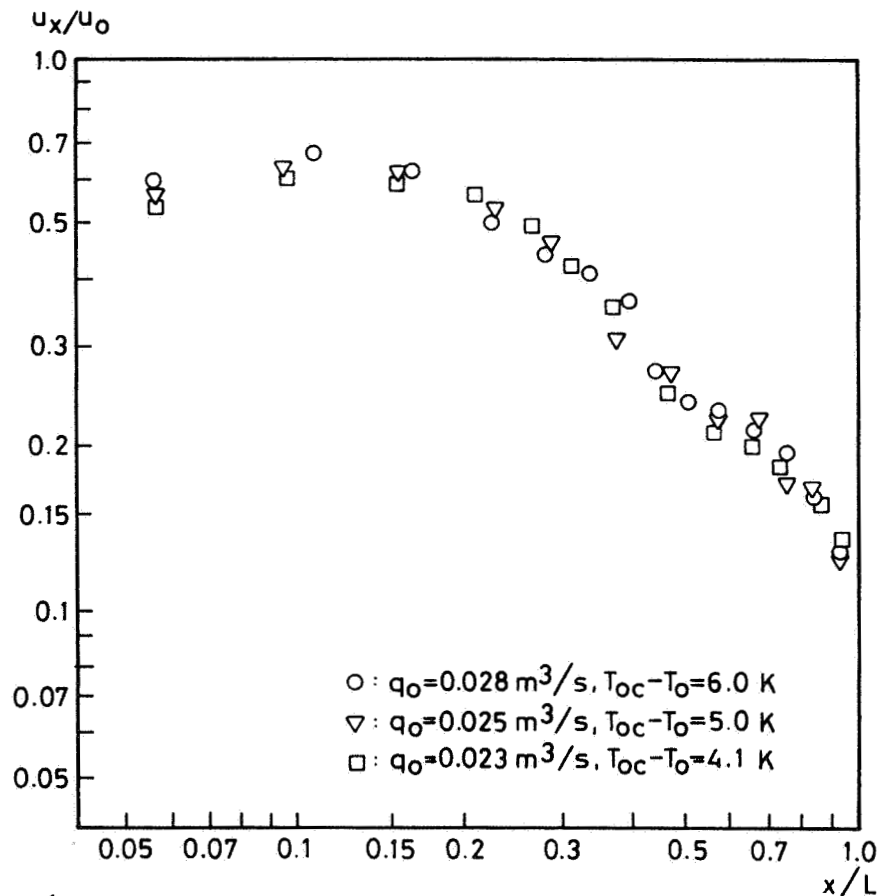


Fig. 7. Velocity decay versus distance measured for identical Archimedes number, for three different Reynolds numbers. Diffuser type B.

Figure 7 shows the results of three experiments with similar Archimedes number and different Reynolds number. The flow is self-similar and it may be concluded that

the air movement has a sufficient turbulence level for $q_0 > 0.023 \text{ m}^3/\text{s}$ and it is thus independent of the Reynolds number. This also means that the coefficient in equation (1) is uninfluenced by the supply velocity u_0 and the Reynolds number Re for a sufficient level of the supply flow q_0 .

Fanger et al.⁵ have shown that the thermal comfort is influenced by mean air velocity and by turbulence. It is therefore important to study the turbulence in the room air movement. An instant velocity \hat{u} can be expressed by

$$\hat{u} = u + u' \quad (3)$$

where u is the mean velocity and u' is an instantaneous deviation from the mean velocity. It is convenient to express a one-directional turbulent intensity by the following expression

$$\frac{\sqrt{u'^2}}{u} \quad (4)$$

which is measured with a hot-wire probe in areas with sufficient mean velocity.

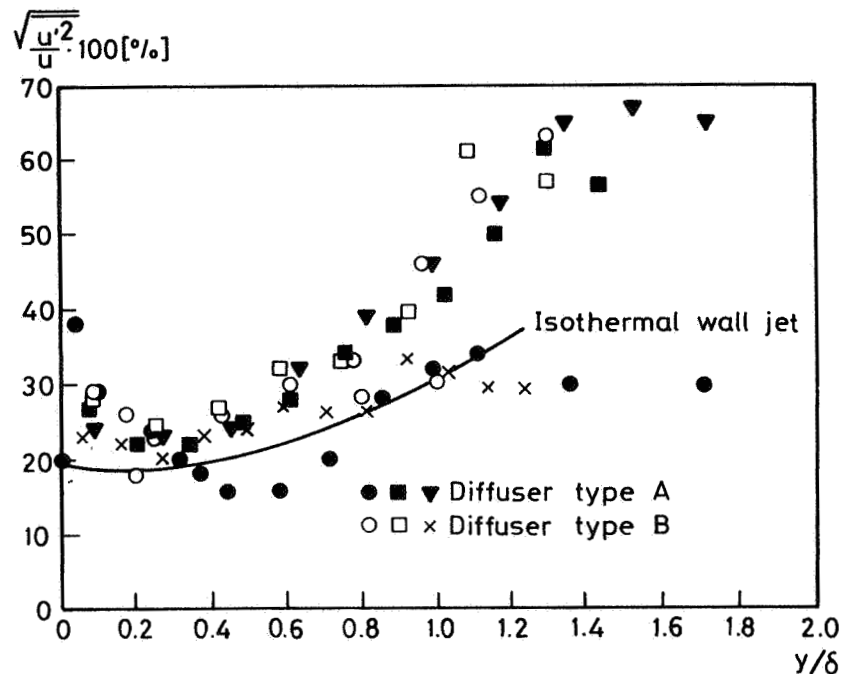


Fig. 8. Turbulence intensity in the flow close to the floor for diffuser A and B.

Figure 8 shows the distribution of turbulence intensity in the flow close to the floor (≤ 0.25 m). All measurements have been taken at a distance of 2.2 m from the diffuser at a flow of $0.056 \text{ m}^3/\text{s}$ for different temperature differences, $0.3 \leq T_{oc} - T_o \leq 6.2$. The thickness δ of the flow is defined as the height to half the maximum velocity $u_x/2$, and the measured turbulence intensity is compared with the level in an isothermal wall jet. It may be concluded that the turbulence intensity in the flow from a low-level diffuser is of the same level as the turbulence intensity in a room with traditional jet ventilation (mixing system).

The measurements in figure 8 only cover a small area of the room. It is not possible to measure the intensity above the flow close to the floor with a simple hot-wire anemometer due to a low mean velocity in that area.

4. FLOOR MOUNTED DIFFUSER

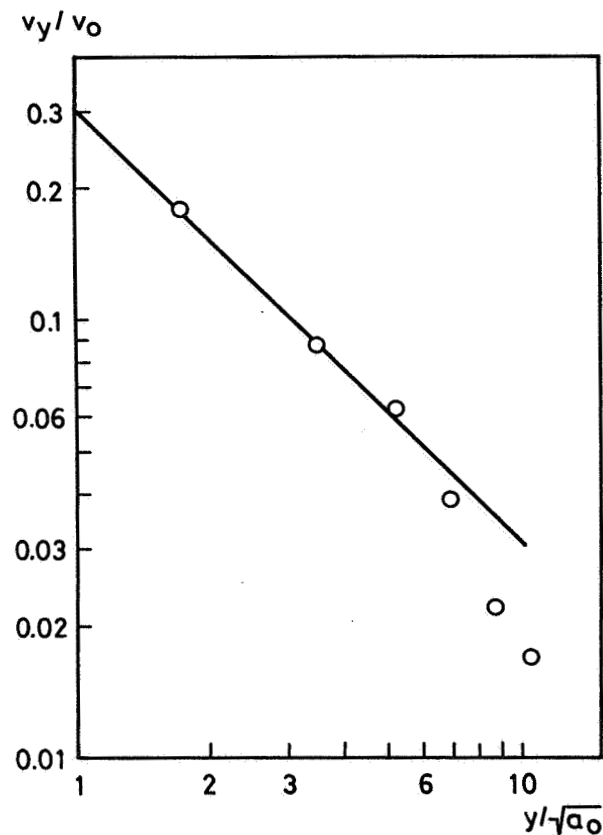


Fig. 9. Velocity decay versus vertical distance for a single floor mounted diffuser (type C).

An alternative method of locating inlet openings for displacement ventilation is floor mounted diffusers. Figure 2 shows a diffuser, called type C, which generates a vertical circular free jet with swirl. It is convenient to compare the velocity decay in this jet with the velocity decay in a conventional circular free jet given by

$$\frac{v_y}{v_o} = \frac{K_a}{\sqrt{2}} \frac{\sqrt{a_o}}{y} \quad (5)$$

The measurements in figure 9 show the velocity decay in a vertical jet with swirl. The measurements correspond to a $K_a/\sqrt{2}$ - value of 0.30 which is about ten times smaller than the same value for a conventional axisymmetric free jet. It is an important conclusion that a jet with swirl has a very fast velocity decay which has also been measured by Balandina and Lovtsov⁶.

The floor mounted diffuser, type C, is often used in a group of four within an area 0.6 m × 0.6 m. In this case the measured velocity level is higher than the velocity level from a single diffuser but both of them have the same level at a height of 0.8 m.

5. VERTICAL TEMPERATURE GRADIENT AND VENTILATION EFFICIENCY

It is important that the diffuser used for displacement ventilation is able to generate good thermal conditions in the occupied zone of the room. It is also important that the ventilation system - including the diffusers - is able to generate a high ventilation efficiency, which will be discussed in this section of the paper.

It is possible to remove exhaust air from the room with a temperature several degrees above the average temperature in the occupied zone, which means an efficient use of energy in the ventilation system. The vertical temperature gradient will show this effect, especially in non-dimensional form, as given in figure 10, when all temperatures are divided by the temperature difference between return and supply.

Figure 10 shows that an increasing flow rate q_o increases the difference between the return temperature T_R and the average temperature in the occupied zone (in a non-dimensional form). This leads to an increasingly efficient use of energy for the diffuser type B at the given heat load.

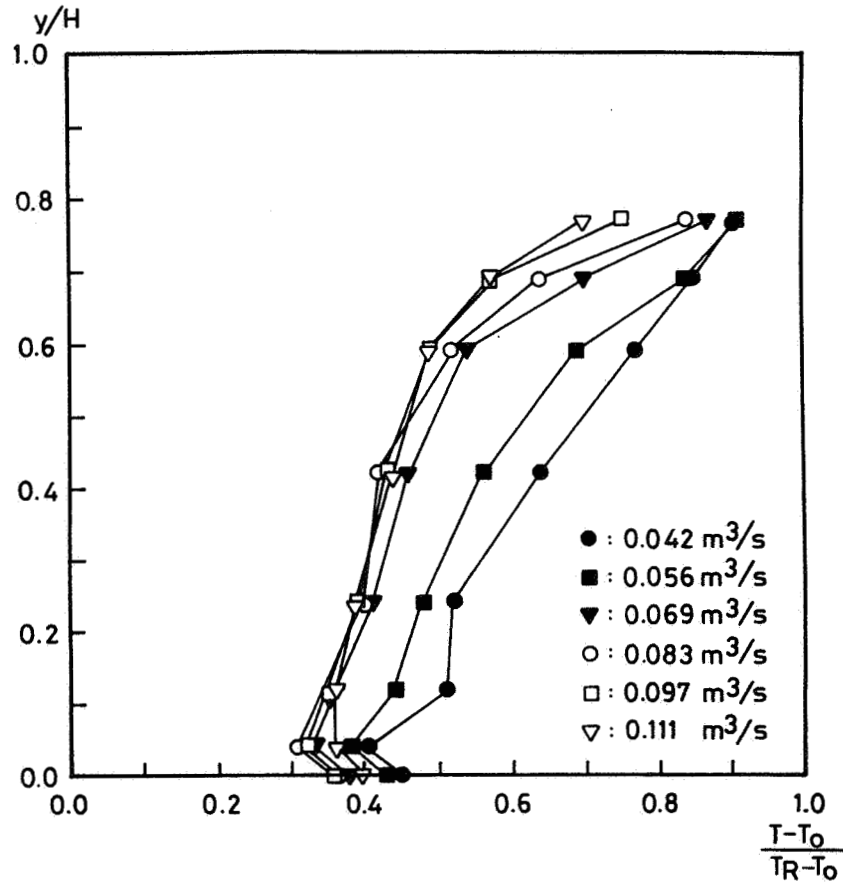


Fig. 10. Vertical temperature distribution for different air flow rates. Diffuser type B. $Q = 500$ W. Measurements by M. Andersen et al.⁷.

The entrainment of air into the hot plume above the heat source, fig. 1, will often generate an area with recirculation of hot and contaminant air below the ceiling of the room. The height to this area will increase with the supply flow q_0 , and smoke experiments show a height of ~ 1.7 m for a volumen of $0.07 \text{ m}^3/\text{s}$ when the heat source has an emission of 500 W. This height is about the height of the occupied zone corresponding to a reasonable design of a system in practice in an office.

The ventilation efficiency based on temperature is given by the equation

$$\varepsilon_T = \frac{T_R - T_O}{T_{OC} - T_O} \quad (6)$$

where T_{OC} in this section is defined as the average temperature of the occupied zone measured at 24 points up to the height of 2.1 m. (The average temperature of the

occupied zone used in section 3 is defined as the temperature at $x, y, z = 3.0, 1.0, 1.8$ m).

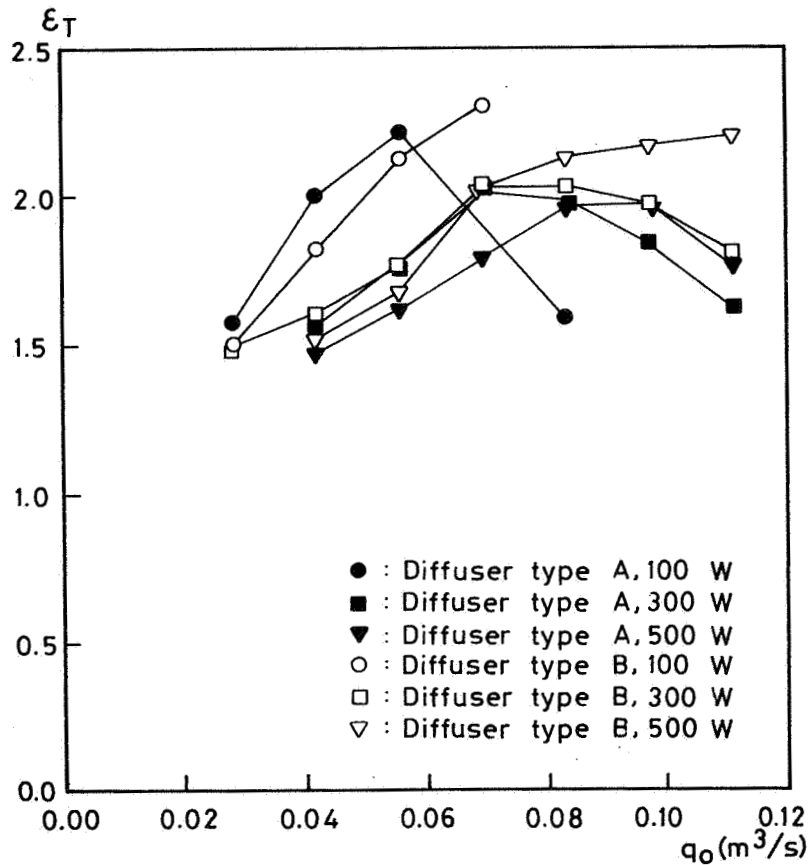


Fig. 11. Ventilation efficiency for diffusers A and B for different flow rates. Measurements by M. Andersen et al.⁷.

Figure 11 shows the ventilation efficiency for diffusers A and B. The efficiency varies between 1.5 and 2.3 depending on the flow rate, which is also the level for the floor mounted diffuser type C.

The ventilation efficiency seems to obtain the same level rather independently of the type of diffuser. Figure 4 shows a typical difference in the flow pattern from diffusers A and B. This difference will influence the local ventilation efficiency giving a slightly higher value in the middle plane of the room when a diffuser of type A is used. However, it will not have any practical influence on the average value of the room. (Correspond-

ingly, the diffuser of type B will give a slightly higher value over the whole width of the room close to the diffuser).

6. REFERENCES

1. SKÅRET, E.,
"Displacement ventilation",
Room Vent 87, International conference on air distribution in ventilated spaces, Stockholm, 1987.
2. SANDBERG, M. and LINDSTÖM, S.,
"A model for ventilation by displacement",
Room Vent 87, International conference on air distribution in ventilated spaces, Stockholm, 1987.
3. KOFOED, P. and NIELSEN, P.V.,
"Thermal plumes in ventilated rooms - an experimental research work",
III Seminar on Application of Fluid Mechanics in Environmental Protection, Silesian Technical University, Gliwice, Poland, 1988.
4. NIELSEN, P.V.,
"Flow in air conditioned rooms",
(English translation of Ph.D.-thesis from the technical University of Denmark, 1974) Danfoss A/S, 1976.
5. FANGER, P.O., MELIKOV, A.K., HANZAWA, H. and RING, J.,
"Air Turbulence and Sensation of Draught",
Energy and Buildings, 12, 1988.
6. BALANDINA, L.J. and LOVTSOV, V.V.,
"Air distribution in the rooms of large volume with rotating jets",
XV International Congress of Refrigeration, Venezia, 1979.
7. ANDERSEN, M., HAUERVIG, A., HJORTSØE, J., MATHIESEN, P.M., NIELSEN, A. and PEDERSEN, M.,
Private communication, University of Aalborg, 1988.

EFFECTIVE VENTILATION

9th AIVC Conference, Gent, Belgium
12-15 September, 1988

Poster 3

A COMPARISON OF UPWARD AND DOWNWARD AIR DISTRIBUTION SYSTEMS

DEREK J. CROOME *

* As from 1st October Professor of Building Engineering at
University of Reading

A COMPARISON OF UPWARD AND DOWNWARD AIR DISTRIBUTION SYSTEMS

Synopsis

Traditionally air has been supplied from the ceiling to the occupants below opposing the buoyancy effects due to heat convected from people, lights and machines. There has also been concern that if air supply outlets are installed at low level near people the chances of draughts and noise are high. The development of swirl air diffusers in Sweden and Germany overcomes these problems and allows a wider consideration of air distribution systems when designing buildings. This also offers flexibility in planning the distribution of electrical systems and piped services. Fresh air is needed at head level if ventilation is to be effective. In high spaces which are densely occupied this is more readily achieved with an upward system.

Introduction

At present there is a conflict between various sources of information concerning the specification of the parameters to ensure a good quality air movement system. Independent surveys of office conditions in the U.S.A. and Europe show that stagnant air conditions are quoted by more than half the subjects as contributing towards lethargy and low productivity (Woods 1985, Croome and Rollason 1988). Laboratory experiments carried out by Fanger and Christensen (1987) claim that the turbulence of the airflow makes people more sensitive to draught than was found in previous studies and then propose a reduction of velocity limits in the present standards in accordance with the percentage dissatisfied (PD) equation.

$$PD = 13800 \left\{ \left(\frac{\bar{v} - 0.04}{a_s - 13.7} + 0.0293 \right)^2 - 0.000857 \right\}$$

For 5% to be dissatisfied this results in a mean velocity (\bar{v}) of 0.08m/s at 20°C (θ_a) rising to 0.1m/s at 26°C. Field surveys and everyday experience tend to contradict these proposals. Clark (1985) using Schlieren techniques has shown that convection velocities around the body especially above the head are 0.2 - 0.4 m/s; these figures are independently supported by measurements taken by van Gunst in the de Doelan concert hall in Rotterdam described by Croome and Roberts (1981). Airstreams with velocities of 0.10 m/s can easily be deflected by the body convection currents thus rendering the airflow system ineffective from the freshness point of view (also see Homma 1987).

The present standards define mean velocities only. This is insufficient and finer details of the air movement pattern need defining especially at head and foot levels. Mayer (1985) has defined the standard deviation for the air movement fluctuations as:

$$S = Tu.V_{50\%} = V_{84\%} - V_{50\%}$$

where Tu = turbulence coefficient (0 - 0.6)

$V_{50\%}$ = velocity exceeded for 50% of the time (mean velocity)

$V_{84\%}$ = velocity exceeded for 16% of the time

Fanger and Christensen (1986) studied the velocity fluctuations around the body and derived the standard deviation in terms of $V_{50\%}$ (at the elbow, at the feet and at the back of the neck), the space air temperature and the heat input into the space. Besides turbulence, the periodicity (T) of the fluctuations is important where fluctuations are defined as

$$\tilde{V} = (S + V_{50\%}) \sin(2\pi t/T + \phi)$$

or

$$\tilde{V} = V_{50\%}(1 + Tu) \sin(2\pi t/T + \phi)$$

Linke (1966) and Regenscheit (1970) have described the basic fundamentals of air motion in air distribution systems. The work of Linke carried out in a lecture theatre with 500 seats at the Technical University in Aachen has revealed the patterns of air movement and temperature distribution resulting from conditioned air being supplied at floor level. Because the main direction of air movement corresponds with that induced by heat released from the occupants, air supplied from floor level produced an even pattern of air flow throughout the auditorium and the vertical temperature gradients were negligible above head level but the temperature from foot to head level varied from 3 to 5°C (Croome and Roberts, 1981), high differentials occurring when the occupancy was high. The advantages of upward systems are mainly in the use of reduced air supply rates by using (i) higher temperature differentials and (ii) occupancy rather than total space volumes for overall heating and cooling requirements. Extraction of the heat from the upward moving air via the lighting troffers, can easily be achieved; alternatively high temperature stratification air can be recirculated to the occupancy zone. Downward systems showed large circular currents with temperature differentials of 4 to 9°C with full occupancy but in this case most of the temperature gradient occurs within 1.5m of the ceiling and the temperature drop from head to foot level was about 1°C. These systems work best in low height spaces and where occupancy densities are low.

Characteristics of Upward and Downward Systems

According to Linke, the Archimedes number is a decisive factor influencing the air movement patterns. For downward air flow distribution systems, the Archimedes number should be $Ar \leq 46$; for upward air flow distribution system, the Archimedes number should be $Ar \leq 360$.

The Archimedes number is defined as

$$Ar = \frac{g \beta \Delta T H}{v^2} \quad (1)$$

Where g = acceleration due to gravity m/s^2
 β = thermal expansion factor ($1/K$)
 ΔT = supply to return air temperature differential ($^{\circ}C$)
 H = height of the auditorium, (m)
 v = air velocity (m/s)

Equation (1) can also be defined in the form of

$$Ar = \frac{g \beta q}{\rho c n^3 H^2} \quad (2)$$

Where q = heat load (W/m^2)
 ρ = air density ($\rho = 1.2 \text{ Kg/m}^3$)
 c = specific heat capacity of the air ($c = 1006 \text{ J/Kg}^{\circ}C$)
 n = air change rate (ach/h)
 g = acceleration due to gravity

Using equation (2) and the Archimedes conditions stated above the minimum air change rate ensuring a stable air movement pattern in the room for a downward system is

$$n > 30.4 \sqrt{q/H^2} \quad (3)$$

and for an upward system is

$$n > 15.3 \sqrt{q/H^2} \quad (4)$$

Comparing equations (3) and (4), it can be concluded that the required air change rate to acquire a stable air movement in a space for a downward system is twice as large as that of an upward system. This is another reason why the upward system is suitable for spaces with large heat gain ($> 140 \text{ W/m}^2$) such as auditoria and where the floor level is heavily occupied by people.

Generally speaking, the supply air temperatures for upward systems are about $18-19^{\circ}C$ and $14-18^{\circ}C$ for downward systems in summer. With higher supply temperatures about 8-10% of the cooling load can be saved resulting in reduced energy costs of about 1.5%.

A comparison of upward and downward systems is shown in Table 1.

- (a) The Archimedes number can be defined in terms of the outlet characteristic

$$Ar = \frac{g \cdot d_o \cdot \Delta \theta_o}{v_o^2} \quad (5)$$

Where $\Delta \theta_o$ = temperature difference at jet entry ($^{\circ}\text{C}$)
 θ_o = room temperature ($^{\circ}\text{K}$)
 d_o = outlet diameter (m)
 v_o = outlet velocity (m/s)
 g = acceleration due to gravity (9.81 m/s^2)

Ar decreases as the air outlet velocity, v_o , increases. With increasing supply to room air temperature differentials, $\Delta \theta_o$, Ar increases (i.e. buoyancy increases) and the more pronounced the curvature of the jet axis becomes.

- (b) The trajectory is calculated by inserting Archimedes number in

$$\frac{y}{d_o} = \frac{x}{d_o} \tan \alpha + Ar \left(\frac{x}{d_o \cos \alpha} \right)^2 \left(0.51 \frac{tx}{d_o \cos \alpha} + 0.35 \right) \quad (6)$$

Where y = the vertical displacement (i.e. deflection from horizontal axis) (m)
 α = inclination angle
 x = horizontal distance from outlet (m)
 t = turbulence factor; for vaned outlet $t = 0.2$

- (c) The axial jet velocity profile is derived using the jet velocity decay equation. (Reigenscheit 1970)

$$\frac{V_x}{V_o} = \frac{x_o}{x} \pm \frac{Ar}{m} \left[1 + \ln \left(2 \frac{x}{x_o} \right) \right]^{\frac{1}{2}} \quad (7)$$

This compares favourably with Koestel's work (Sofrata 1987, Koestel 1954).

The axial velocity varies inversely with the distance from the outlet. The velocity at any point in the jet flow can be divided into two components: Longitudinal velocity v_x and cross-sectional velocity v_y , while v_x is much larger than v_y in most cases so v_y is neglected. It is safe to consider that $v = v_x$, particularly in the main zone of jets, which are mainly used in air-conditioning. Hence, Reigenscheit's equation can be modified using empirical data and expressed as

$$\frac{V_x}{V_o} = \frac{0.48}{tx/d_o + 0.145} \quad (8)$$

The velocity decay equation demonstrates the importance of the Archimedes number as a design factor. Experiments on the behaviour of jets in rooms have shown that the Archimedes number correlates with the air movement patterns in space (Croome and Roberts 1981).

CHARACTERISTICS	DOWNWARD	UPWARD
Vertical temperature gradient:		
i) Foot to head level	Negligible (1-3°C): head temperature are a little warmer	3-8°C lower temperature at foot level
ii) Above head level	4-8°C	Negligible
Supply temperature	14 to 18°C	18°C minimum
Dust	Dust kept at floor level	Dust tends to rise; essential to avoid this in opera houses, concert halls, debating chambers or museums.
Noise	Air velocity at outlet needs to be sufficient to be effective at head level	
Maintenance		More supply grilles to clean
Number of supply outlets	Can use a small number of outlets but less flexibility to control	Necessary to use a large number of small outlets
Energy	Air has to deal with lighting gains before those from people	Air absorbs heat gains from people before those from lighting. Savings in energy can be large in high, well insulated and densely occupied spaces

Table 1: THE CHARACTERISTICS OF DOWNWARD AND UPWARD VENTILATION SYSTEMS

Supply Air Parameters

- a) Work by Linke reported in Croome and Roberts (1981) indicated that a throw giving a velocity of 0.5 m/s at three quarters of the room length, was a suitable criterion to ensure satisfactory room motion without the presence of high velocities in the occupied zone. On this basis the required supply air velocity and the outlet diameter may be determined.

The air outlet velocity (v_o) normally ranges from 5 m/s to 7 m/s for high level outlets in downward air distribution systems; a limitation on the velocity for upward systems is normally observed to avoid excessive sound emission and cold draught in the occupied zone. In the case of sedentary or light work activity, the suitable v_o , for low level outlets is 0.5 to 1.0 m/s. Hence the larger outlet areas are required for a given air flow rate in upward systems. The use of twist outlets gives more scope for achieving penetration of air into the space with less likelihood of draughts or noise (Rowlinson 1987-88).

- b) The allowable supply to room air temperature differential, $\Delta\theta$, for downward distribution may be up to about 11°C but a smaller value, say 5°C, should be selected if air is distributed upwards. This does not mean that a larger amount of supply air volume is needed in upward systems because of the Archimedes criterion referred to previously (see equations 3 and 4) and the use of occupied zone volume instead of total space volume for heating and cooling calculations.
- c) The temperature difference profile is similar to that of the axial velocity, v_x , especially in the main zone of the jets. Hence, the temperature decay law can be expressed in a similar form as for the velocity decay laws:

$$\text{hence } \frac{\Delta\theta_x}{\Delta\theta_o} = \frac{T_x - T_n}{T_o - T_n} = \frac{0.35}{tx/d_o + 0.145} \quad (9)$$

Where T_x = core temperature of the jet flow
 T_n = room air temperature
 T_o = temperature at jet entry.

Microclimate Air Distribution System

A microclimate or task air distribution system is suitable for buildings such as auditoria and lecture theatres, where seats are fixed in permanent locations. The air distributed from the air conditioning system is supplied through the ducts beneath the

seats and is delivered through outlets located at the back of each seat, supply air jets being formed at seated head level. When an air stream travels from an outlet, the kinetic energy is increased in creating turbulence due to the entrainment of secondary room air into the jet stream, (convection currents in the head region due to the mixing effect of the secondary air plus the effects of buoyancy). It is sensible psychologically to provide occupants with some control of air flow direction and/or velocity, usually a simple manual damper control, thus avoiding draughts or increasing freshness as required. The inclination angle of the vane ranges from 0° to 20° from the vertical axis. The inclination angle is usually adjustable and therefore settings could be selected to meet the various preferences of the individuals. The velocity of air at the outlet should not exceed about 1.5 m/s; Sodec (1984) shows that the front of the face can enjoy short intermittent velocity amplitudes of 0.6 m/s.

Task ventilation systems have been designed for desks in offices; similar systems can be envisaged for beds in hospitals. One form of micro-climate air distribution is a system built into the seating structure. The conditioned primary air is generally fed from a pressure chamber accommodated in the chair mounting supports. Indoor air mixes with the primary air and the supply air emerges at the top of the back-rest, at an angle of 0-20° to the vertical axis. In each case, the direction of discharge is selected in such a way that the head of the seated individual is located not in the direct path of the jet, but rather within its induction zone. The momentum of the jet is set so as to ensure stability of the jet direction within the occupied zone and this can be varied in all load situations. Sodec (1984) reported that systems of this type serve to meet the following demands:

- Stability of air distribution within the occupied zone without the substantial circular room air patterns that develop in downward systems.
- Provision of the human respiratory system with a direct supply of conditioned air.
- Provision of adequate convection within the seating area by means of the primary-secondary air intermixing action.

The features of the micro-climate system on which the outlets are mounted to the top of the back-rest are:

- The cold supply air is discharged into the upper half of the occupied area.
- The lower half is conditioned by induction of the secondary air.
- The air discharge velocity at the air outlet is approximately 1.5 m/s; this caters for adequate induction of the indoor air.
- No formation of stagnant patches of cold air.
- Direct discharge of fresh draught-free supply air into the occupied zone without having first to enter from floor outlets.
- Effective air distribution in the occupied area.

Typical design parameters are:

- air volume flow rate: 8.5-10 l/s per outlet
- minimum supply air temperature: 18°C
- induced secondary air: 3.5-5 l/s
- sound power level: 18-26 db (A)
- pressure loss: 30-50 Pa
- air velocity in hollowed seat pedestal: 1.5-2.6 m/s

The return air temperature underneath the ceiling can be as high as 30°C, which will not cause discomfort in theatres because of the extensive room height. Within the occupied area itself the air temperature is 18-24°C owing to the direct arrangement of the seats, an air volume flow rate of 8.5-10 l/s per outlet at $\Delta\theta = 12\text{K}$ will suffice to meet the requirements of the room. The proportion of induced secondary air is approximately 40-60% of the primary air volume flow rate.

Compared with downward air supply systems the microclimate air distribution system has several advantages:

- Direct supply of air to the immediate vicinity of the occupants.
- Greater temperature differences between return and supply air of up to 12°C, hence a lower air volume flow rate is necessary.
- Lower pressure losses.
- Lower refrigeration consumption on account of higher supply air temperature (18°C instead of 14-16°C).
- Use occupancy space volumes in heating calculations.
- Reduced investment costs due to smaller central units and distribution ducts.

Combined Air Distribution System

Conditioned air can be supplied through grilles located beneath the auditorium seatings and outlets at the top of the back-rests (Croome and Lin 1987). The system normally needs double-deck floors, which form a plenum pressure chamber or space for under floor ducts. The supply air is distributed evenly through the plenum to the various outlets which are installed in the raised floor. Normally the depth of the plenum should be at least 200mm. Floor ducts are suitable for conveying the supply air to specific areas of the auditorium. Each individual outlet is made to form a direct link with the supply air branches usually by means of flexible ducting. One of the advantages of the combined air distribution system is that it creates a basic conditioned environment for the extensive areas in the auditorium besides a micro-climate for the individual's comfort. Double deck floors also offer flexibility in routing and accommodating other services such as cabling for communication systems.

Types of Floor Mounted Outlets

The recommended outlets suitable for upward air distribution system assume the following forms:

Slot Plates: The flow emitted from a slot plate is similar to that encountered in a perforated plate system. The small individual jets - except the outer ones - do not induce the room air, but rather the adjacent jets of supply air. The reduction of jet velocity takes place by means of the diffuser effect and not by exchange of energy with the environment.

Free Jet Outlets: These produce round, non-twist type air jets; the diameter of the free outlets ranges from 150 to 250mm. The induction of room air is more intensive than for slot plates.

Floor-mounted Twist Outlets: These produce air jets in a swirl corkscrew pattern. As a result of the higher degree of turbulence, a more intensive induction effect of the indoor air is brought about; the air jet is stable and less sensitive to cross convection so that jet penetration is improved (Croome and Rowlinson 1987). Owing to the larger amount of small inclined jet with swirl effect, intensive exchange of energy with the ambient air is attained. The reduction in jet velocity and adjustment of the supply air temperature to the temperature of the room air proceed at a faster rate than is the case with slot plates and free jet outlets. Due to the geometry of the outlet the noise emission is reduced.

REFERENCES

1. CLARKE A.P., 1985, Man and His Thermal Environment (Edward Arnold)
2. CROOME, D. J., LIN, Z. X., 1987, Improved Method for Airmovement Design, Proc. of Room Vent 87 Conference, June 10-12, Stockholm, Session 2a.
3. CROOME, D. J., ROLLASON, D. H., 1988, Freshness, Ventilation and Temperature in Offices, Proceedings of CIB Conference Healthy Buildings 88, Stockholm, September 5-8th.
4. CROOME, D. J., ROWLINSON, D., 1987, Supply Characteristics of Floor Mounted Diffusers, Proc. of Room Vent 87 Conference, June 10-12, Stockholm, Session 1.
5. CROOME, D. J., ROBERTS, B. M., 1981, Airconditioning and Ventilation of Buildings (Pergamon Press) Second Edition.
6. FANGER, P. O., CHRISTENSEN, N. K., 1986, Ergonomics, 29, (2), 215-236.

7. FANGER, P. O., CHRISTENSEN, N. K., 1987, ASHRAE Journal, 29, (1) 30-31.
8. HOMMA, H., 1987, Free Convection Caused by Metabolic Heat Around Human Body, Proc. of Room Vent 87 Conference, June 10-12, Stockholm, Session 2a.
9. KOESTEL, A., 1954, ASHVE Trans., 60, 385-410.
10. LINKE, W., 1966, Kaltetechnik,, 18, 122.
11. LIN, Z. X., 1986, MSc Thesis 'A New Method for Airmovement Design', Bath University.
12. MAYER, E., 1985, Gesundheits Ing., 106, (2), 65-73.
13. REGENSCHEIT, B., 1970, Gesundheits Ing., 91, (6), 172.
14. SODEC, F., 1984, Air Distribution Systems, Report No. 3554E (Krantz Laboratories, Germany).
15. SOFRATA, H. M., 1987, ASHRAE Journal, 29, (1), 38-42.
16. WOODS, J. E. , 1985, Vent Axia Indoor Pollution Seminar, Imperial College of Science and Technology, London, 13 May (Honeywell Physical Sciences Centre, Bloomington, Minnesota).

EFFECTIVE VENTILATION

9th AIVC Conference, Gent, Belgium
12-15 September, 1988

Poster 4

AIR HEATING SYSTEMS IN AIRTIGHT MULTIFAMILY RESIDENTIAL
BUILDINGS

PER OLOF JÄGBECK¹, GÖRAN WERNER¹, KARIN ENGVALL²

¹The Royal Institute of Technology,
Energy Conservation in Buildings Group, EHUB
S-100 44 Stockholm, SWEDEN

²The City of Stockholm Office of Research and Statistics
Box 8320
S - 104 20 Stockholm, Sweden

1. Synopsis

This paper presents an analysis of indoor climate in buildings with forced air heating systems. The results is based on indoor climate measurements and extensive interviews with the occupants. The analysis shows that design criteria is of great importance for the occupants conceptions of thermal comfort in buildings with air heating systems. Forced air heating systems could be a way to provide mechanical supply air with less problems with the thermal comfort, such as draught, than in ordinary supply- and exhaust air ventilation systems. Especially those designs that use overhead ventilators on the interior walls seems to give a good thermal comfort in the occupant zone. If floor ventilators under the windows are chosen, a very careful design has to be made of both the ventilators and adjacent building details. Special attention has to be put into the coordination between designers and builders.

2. Introduction and purpose

The "Stockholm Project" (1) is a large joint experimental research and demonstration project for evaluation of new energy saving technology in buildings. Primarily established products are used, but in each of the six buildings one or more new methods of energy conservation is tested. The energy demand for heating is considerably lower in these buildings compared to a larger group of buildings of similar types, built during the same time period in Stockholm. All the buildings are airtight and well insulated, some of them better than the Swedish Building Code requirement.

In the Stockholm Project three heating and ventilation system types are represented.

- forced air heating + supply- and exhaust air with heat exchangers (SE).
- hydronic heating + supply- and exhaust air with heat exchangers (SE).
- hydronic heating + exhaust air (E).

In this paper the presentation is limited to a comparison between buildings with forced air heating systems + SE-systems and buildings with hydronic heating + SE-systems.

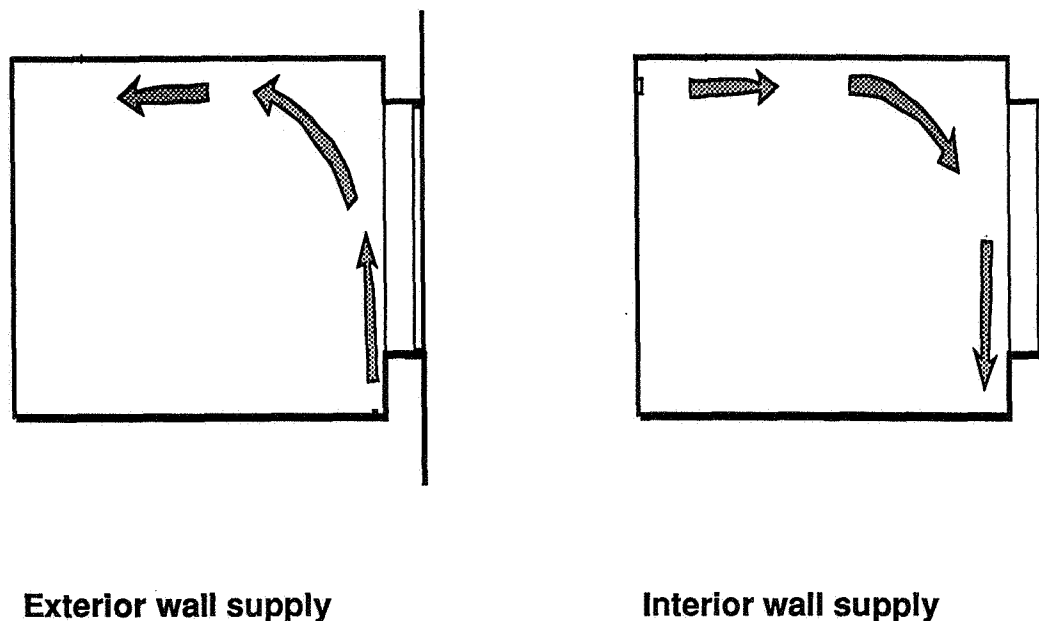


Fig. 1. The two methods of air distribution in the Kejsaren Building, exterior- and interior wall supply

Two different methods of air distribution are being tested and evaluated in the air heated buildings (Fig.1.):

- 1: Exterior wall supply via floor level ventilators under exterior perimeter windows (the Kejsaren Building).
- 2: Interior wall supply from overhead ventilators on interior walls, thereby providing no direct draught protection beneath exterior perimeter windows (the Hstvetet Building).

The aim of this study was to:

- 1: Compare different heating and ventilation systems from the occupants point of view, using sociological interviews.
- 2: Study the thermal comfort in the apartments with air heating systems, using detailed measurements of air movements and temperatures.
- 3: Give advice on further research, development and improvements of the heating and ventilation systems.

The ventilation systems are similar for both buildings with a central mechanical ventilation system combined with air-to-air heat exchanger. Each apartment has an air heating unit in which the incoming ventilation

air supply, at a rate of 0.5 air changes per hour, is mixed with recirculated air from the apartment to provide a total air flow rate equivalent to 1.3 (Kejsaren Building) to 2.5 (Höstvetet Building) air changes per hour respectively.

The two buildings have a very good thermal insulation and air tightness. A very low air circulation rate is thus required to provide the necessary heating load. In the Kejsaren Building the maximum supply air temperature is +45 °C and in Höstvetet Building +35 °C.

Interviews has been done in all buildings in the Stockholm Project. To get a reference the data was supplemented with interviews from an ordinary building built during the same time.

The analysis is based on answers from:

- forced air heating + (SE) in 63 apartments
- hydronic heating + (SE) in 136 apartments
- hydronic heating + (E) in 88 apartments

The parameters studied in this paper are the occupants answer on how they classify their indoor thermal climate, if they have any possibility to achieve thermal comfort, how they classify the air quality.

3. Technical description of the two buildings

3.1 The Kejsaren Building

The ten apartments in the Kejsaren building (2) are being heated by forced warm air supplied by an air heating system. Each apartment has its own separate air heating unit, in which the incoming ventilation, at a rate of 0.5 air changes per hour, is mixed with filtered recirculated air from the apartment to provide a total air flow rate equivalent to 1.3 air changes per hour. The air temperature is controlled by thermostats to balance each apartments transmission losses.

In five of the apartments, air is distributed from the exterior walls at floor level beneath the windows. A simpler system is being tested in the other five apartments, where air is being supplied from ventilators placed the interior walls of the rooms, which means that there is no direct protection against cold downdraught, such as radiators beneath the windows.

3.2 The Höstvetet Building

The 71 apartments in the Höstvetet Building (3) are being heated by a forced warm air heating system similar to the exterior wall supply system in the Kejsaren building. Each apartment has also in this building its own separate air heating unit. The supply air, at a rate of 0.5 air changes per hour, is mixed with filtered recirculated air from the apartments to provide a total air flow rate up to 2.5 air changes per hour depending on the heating load. The heat for the unit is supplied by the domestic hot water circuit, which in this building serves two purposes.

4. Evaluation methods

4.1 Interviews

Personal interviews has been done in all of the Stockholm Project Buildings to gather information from the occupants. One person from each household was chosen. Almost all households has participated in the interviews, which were made one year after the occupants moved into their apartments.

The occupants experience of the indoor climate was studied from many angels. The first questions was related to general aspects on heating and ventilation, air quality, noise etc. Each subject was then studied more deeply with more specific questions, related to the technical systems and time of the year.

The heating was studied by questions of wanted indoor temperature, even or uneven temperature, if the apartment temperature was regarded too hot or too cold and if the occupants regarded the floor temperature hot or cold.

The ventilation in the apartments was studied by questions on the ventilation in general, draught problem, air quality and bad odour problem.

The indoor climate and thermal comfort was then evaluated from the questions of both heating and ventilation. The occupants also had the opportunity to express if they had had any possibilities to achieve thermal comfort. In the indoor climate section questions of general character was also used, such as health problems and the their relation to the apartment.

In the analysis of the indoor climate the occupants experiences was related to different household data, to the building design, and to the heating- and ventilation systems. The result was then compared to measurement data from technical evaluation.

4.2 Thermal comfort measurements in the apartments

The Buildings of the "Stockholm project has each been monitored (4) continuously in more than two years. Data based on five minutes intervals is recorded as hourly mean values in a database. Indoor temperatures are recorded in approximately five of the apartments.

Using that data a comprehensive study was made (5). To further study the air heating systems an intensive study was made during two days in February 1988, as a part of the indoor climate evaluation in the Stockholm Project (6). The weather was cloudy during these two days, and the outdoor temperatures were -1 - -3 °C..

The parameters studied in this paper were:

- Air speed close to the ventilators
- Air speed in the room
- Air direction
- Supply air temperatures
- Indoor air temperature

The measurements were made accordingly to ISO 7726 (7).

5. Results

The results presents the indoor climate experiences of the occupants in relation to the ventilation system used in the building. It also presents the measurements of air velocities in some selected apartments in the two buildings. The data from measurements are then compared to the experiences of the indoor climate in the selected apartments.

5.1 Experiences of indoor climate - Interviews

5.1.1 Ventilation

Slightly more than half of the occupants answers that they consider the ventilation of the apartments as good (Fig. 2.), but there are also many who are dissatisfied, especially with the ES-systems. The highest percentage of satisfied occupants are found in the buildings with E-systems.

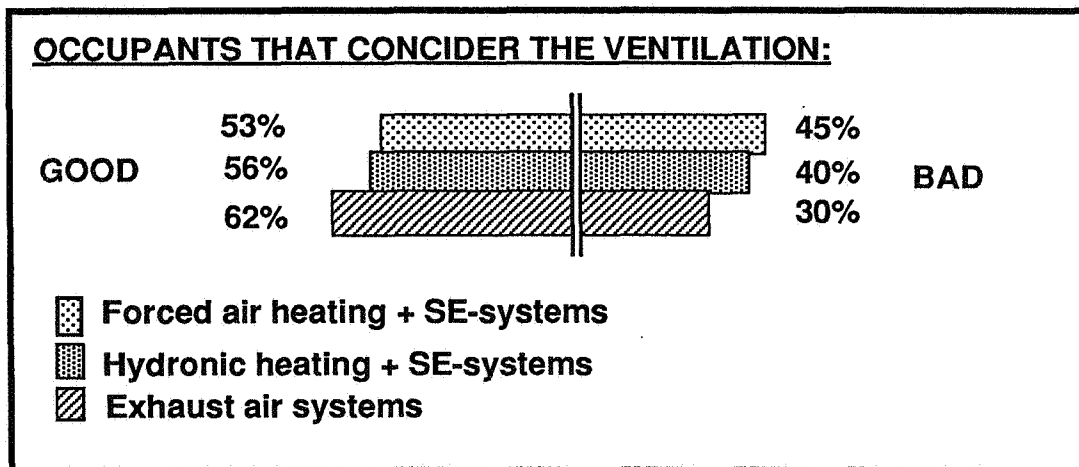


Fig. 2. The occupants general experience of the ventilation system during the winter. Occupants who answers that the ventilation is either good or bad are not represented in the figure.

5.1.2 Noise from the ventilation system

As a result of the improved insulation technology used today in Sweden, the noise from the outside of the buildings has decreased, and one of the consequences is that the occupants pay more attention to indoor noises. Especially in buildings with SE-systems combined with radiators the occupants are disturbed by noises from the ventilation system. In those buildings 47% of the occupants are disturbed (Fig 3.).

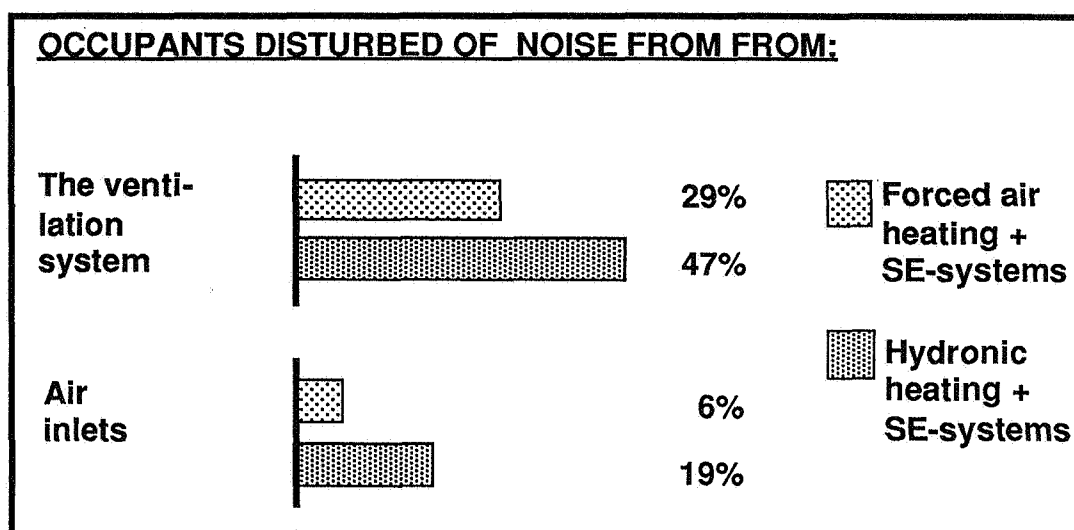


Fig. 3. The occupants experience of noise from the ventilation system.

5.1.3. Air quality

The air quality was described by the occupants with a series of descriptive words (Fig. 4.).

When studying the answers on air quality the occupants in buildings with air heating systems complains more about dusty and stagnant air than those living in buildings with supply- and exhaust ventilation systems. There are also less occupants in these buildings that regard the air free of odours. Even at the question of how the occupants regard the air quality as a whole, air heating systems got the lowest ranking. This indicates that there are other factors that affects the answers, as for example the occupants uncertainty of the air heating systems function and that they find the systems hard to control. Questions as: What kind of air is coming into the apartment?, Is it exhaust- or supply air?, Do I get enough fresh air or do I have to open a window?, are frequent.

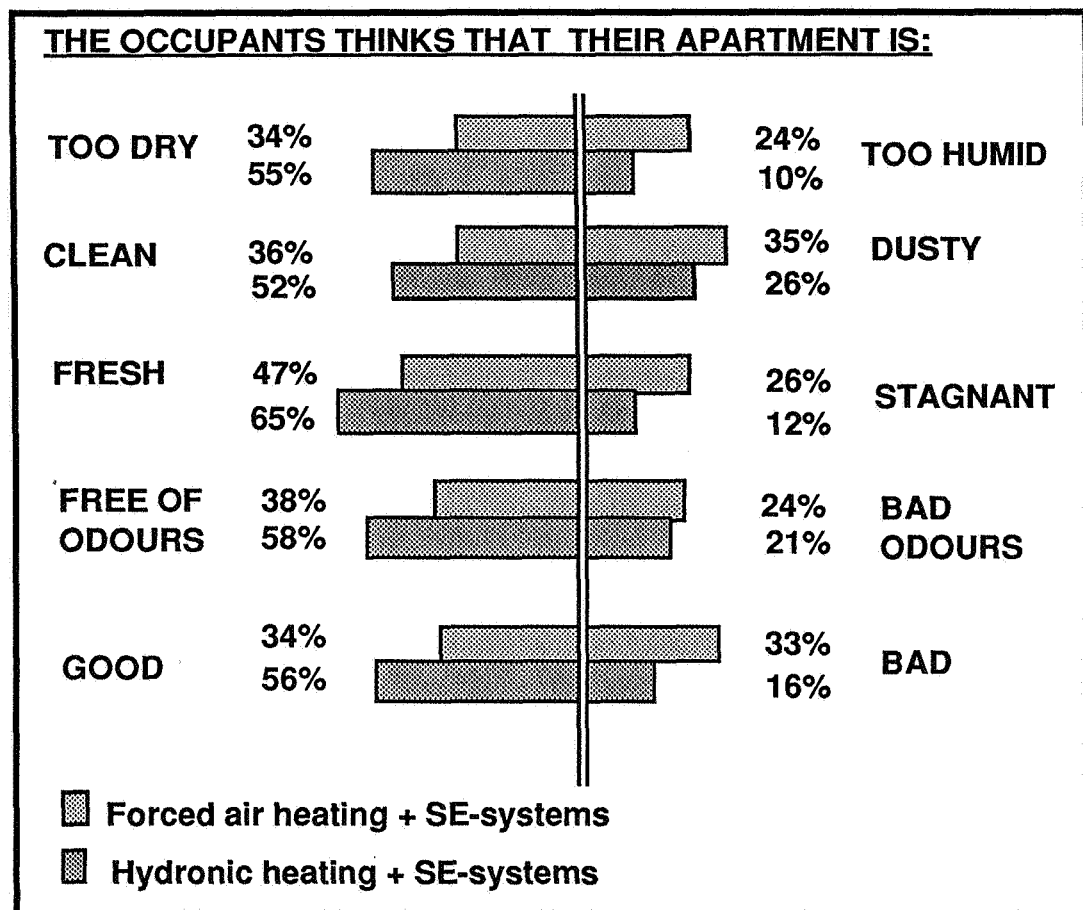


Fig. 4. The occupants experience of the air quality in the apartment during the winter. Occupants who answers that the ventilation is either good or bad are not represented in the figure.

5.1.4. Indoor temperature

In all of the buildings, the occupants consider it to be too cold in their apartments (Fig. 5.). 51% of the occupants in apartments with air heating systems and 63% of the occupants in building with supply- and exhaust air ventilation systems find the temperature is too cold during the winter. In the apartments with air heating systems there is also a group of occupants who considers the indoor temperature too warm. This could be a result of the difficulties to control the temperature in the different rooms in the apartments. On the question on the most negative aspect on forced air heating, the occupant often specifically express dissatisfaction with the indoor air temperature adjustment possibilities.

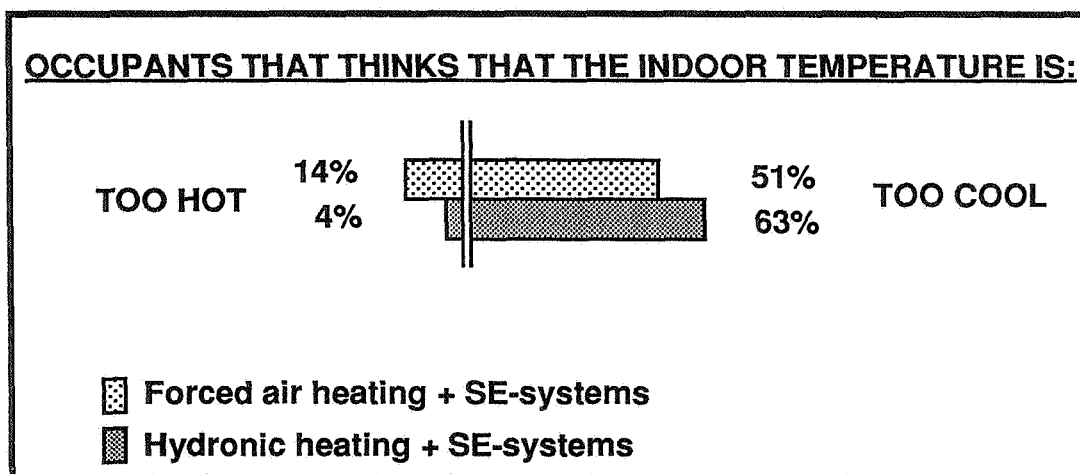


Fig. 5. The occupants experience of the indoor temperature in the apartment during the winter. Occupants who answers that the ventilation is either good or bad are not represented in the figure.

5.1.5 Draught

The experience of draught in the apartment is closely related to the experience of the indoor temperature, which is a possible explanation of the differences in the answers from the two air distribution systems (Fig. 6.). The survey shows that in building with supply- and exhaust air ventilation systems and hydronic heating systems there are a higher number of occupants who feels draught than in buildings with forced air heating systems. Explanations of this could be high air velocities in combination with lower temperatures and / or badly designed ventilators.

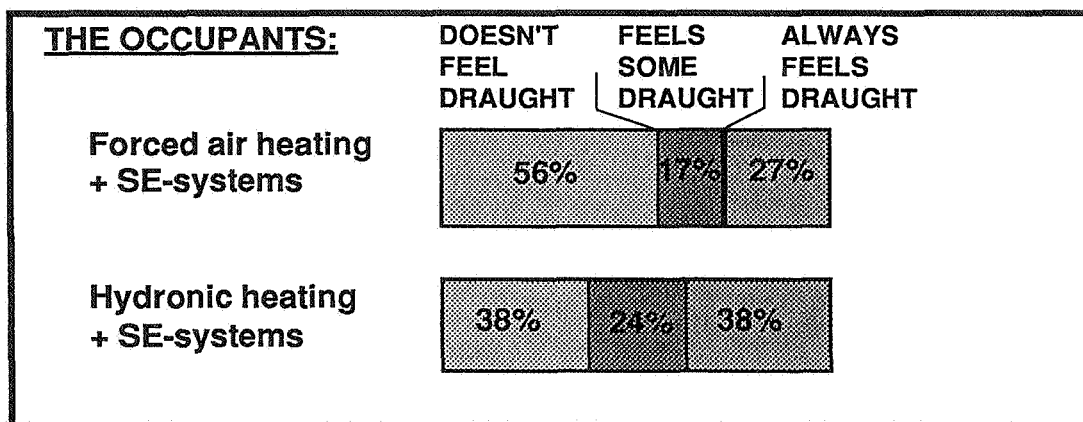


Fig. 6. The occupants experience of the draught in the apartment during the winter.

5.2. Thermal comfort in the Kejsaren Building. interviews - measurements

In five of the apartments in Kejsaren the occupants have expressed that the temperature is too cold during the winter. The most noticeable difference between the two air distribution systems are that there are more complains of draught and cold floors (Fig. 7) in the apartments with air ventilators at floor level beneath the windows.

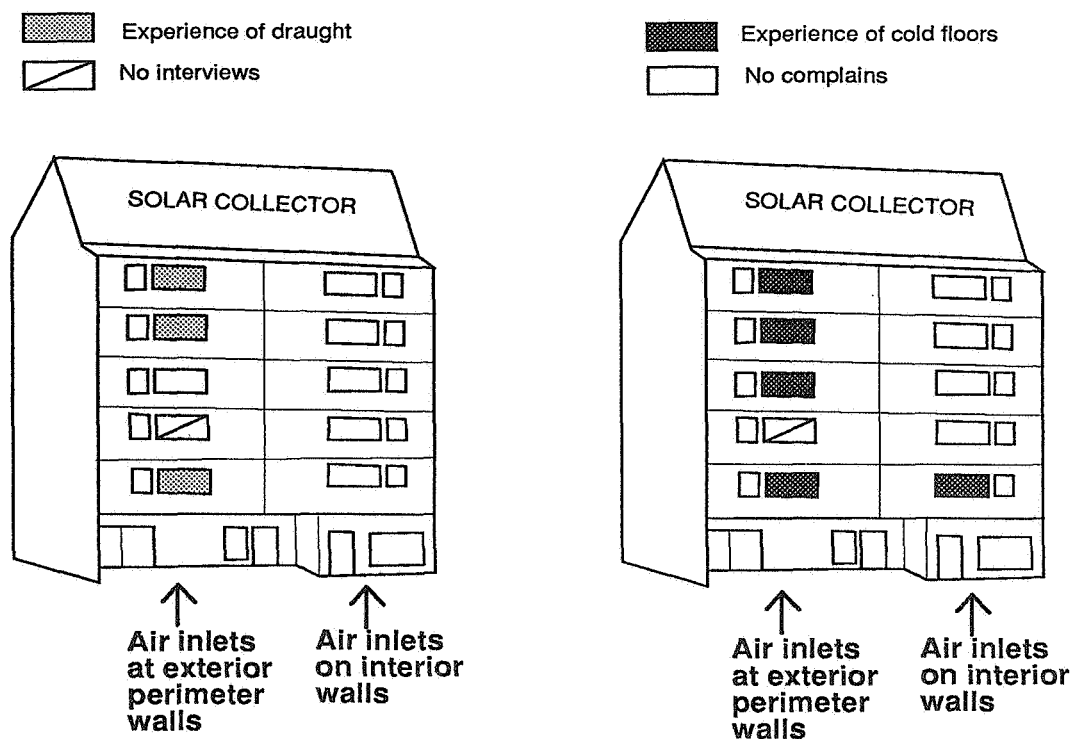


Fig. 7. The occupants experience of draught and cold floors in the Kejsaren apartments during the winter.

5.2.1 Floor level ventilators under the windows. Kejsaren

Air movement pattern in the living room and in a bedroom with ventilators placed in the floor, close to the exterior wall (Apartment A) are shown in Fig. 8 and Fig. 9. A small obstacle forces the air into an unwanted direction. Here a small protruding edge of the window-sill (approximately 8 mm) causes draught problems in the occupant zone close to the windows.

Even though the air temperature is rather high the tenant in this apartment feels that it is too cold during the winter. This is also true for different rooms in the apartment. During the winter there are problems with draught in both bedrooms and living-room, especially from the air ventilators, balcony door and windows up to a level of approximately 2 meters. This corresponds well with the measurements of air movements. No special consideration has been taken to the ventilator in the furnishing of the apartment to avoid the feeling of draught.

In another apartment (B) experiments were made to improve the design (Fig. 10.). A lid with channels that should direct the air flow in the right direction was mounted over the ventilators. However, the pressure drop through those channels then became too high and a air stream was forced out along the floor, wich affects the feeling of cold draught and cool floors.

No cold downdraught could be detected at the windows.

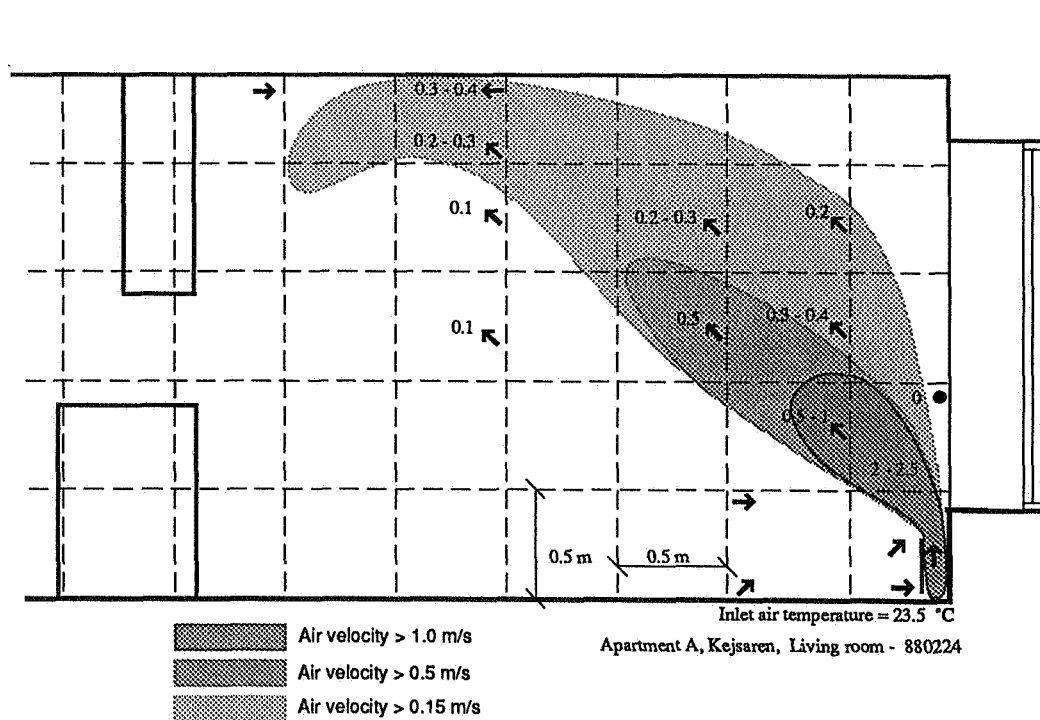


Fig. 8. Section through a sittingroom with exterior wall supply, apartment A, Kejsaren.

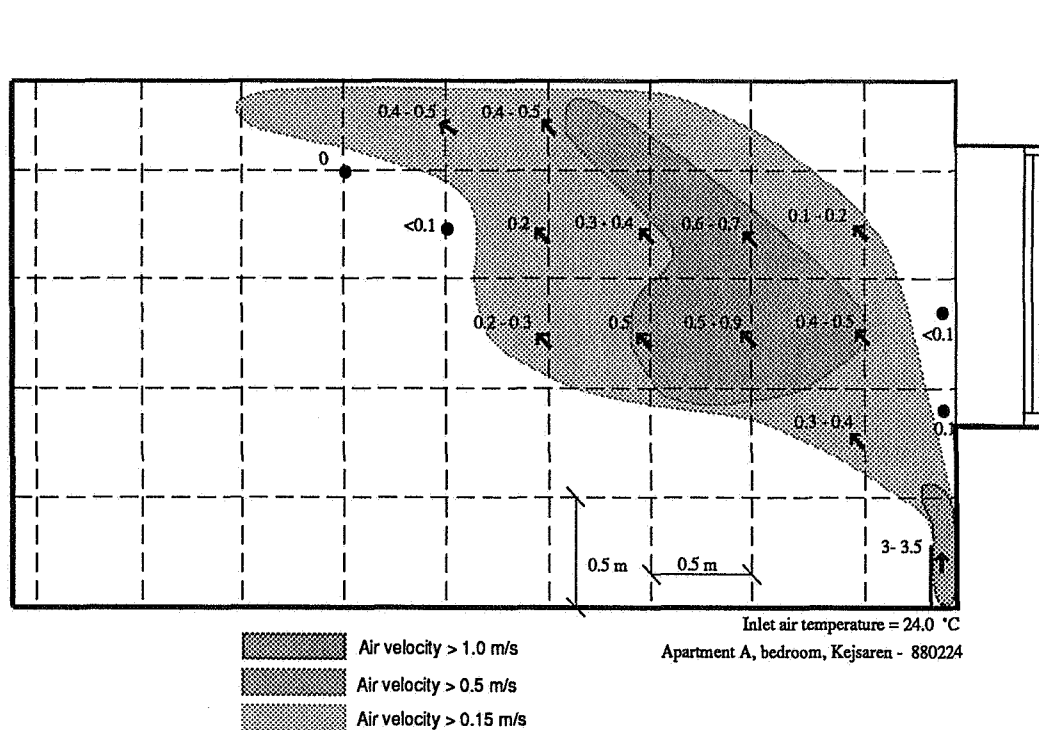


Fig. 9. Section through a bedroom with exterior wall supply, apartment A, Kejsaren.

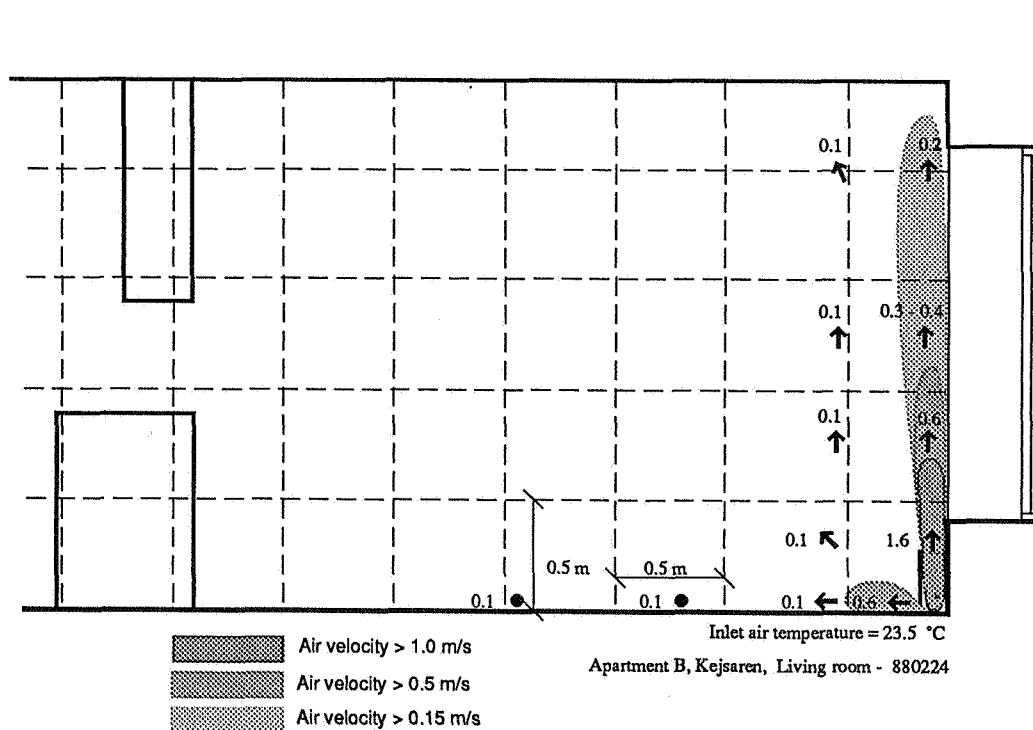


Fig. 10. Section through a sittingroom with exterior wall supply, apartment B, Kejsaren.

5.2.2 Overhead ventilators on interior walls, Kejsaren

The method to distribute the air through overhead ventilators on interior walls close to the ceiling gives an even air flow under the roof and small influence on the occupant zone. The air flows out as a thin layer close to the ceiling and all the air movement is reduced to this zone.

Apartment C, (Fig. 11.): In this apartment situated at the first floor, the occupant express that the indoor air temperature is too cold during the winter and too warm during the summer. They use clothing to try to achieve thermal comfort during the winter, but only succeed to do that in the bedrooms. In this apartment no discomfort related to draught has been perceived. No special consideration was taken to the ventilators when the apartment was furnished.

No cold downdraught could be noticed close to the windows, except for air movement at the edge of the window-sill. That air stream dissolved fast and no significant draught problems could be detected in the occupant zone.

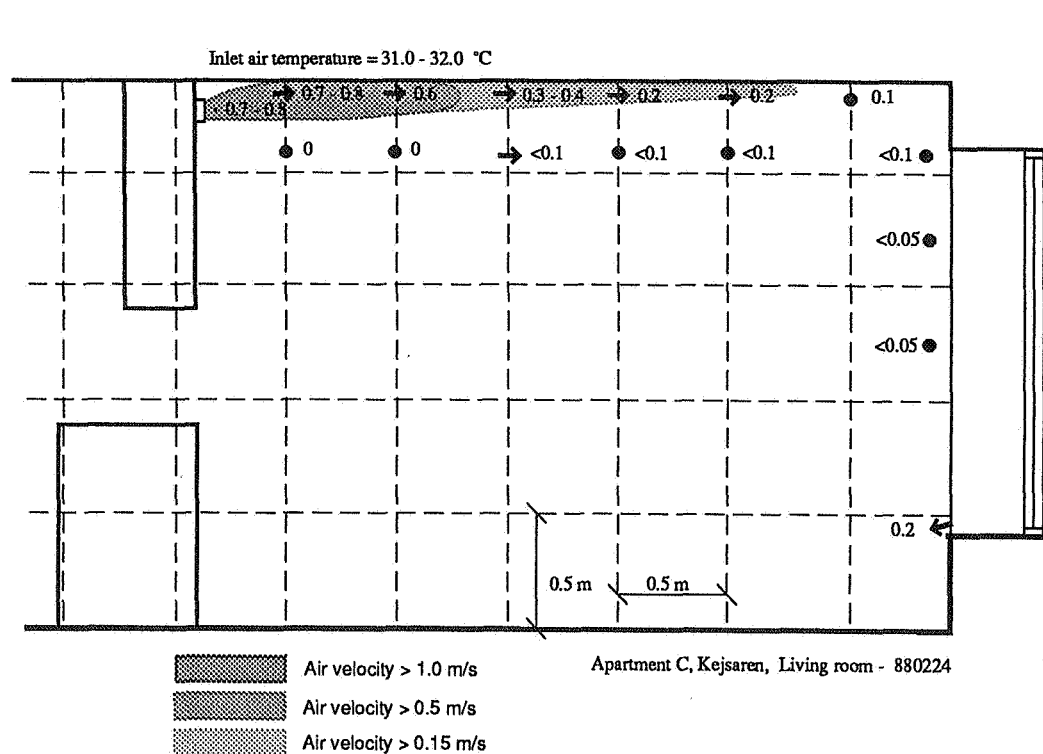


Fig. 11. Section through a sittingroom with interior wall supply, apartment C, Kejsaren.

Apartment D (Fig. 12.): In this apartment the occupants express thermal comfort satisfaction during both winter and summer, in both bedrooms and living-room.

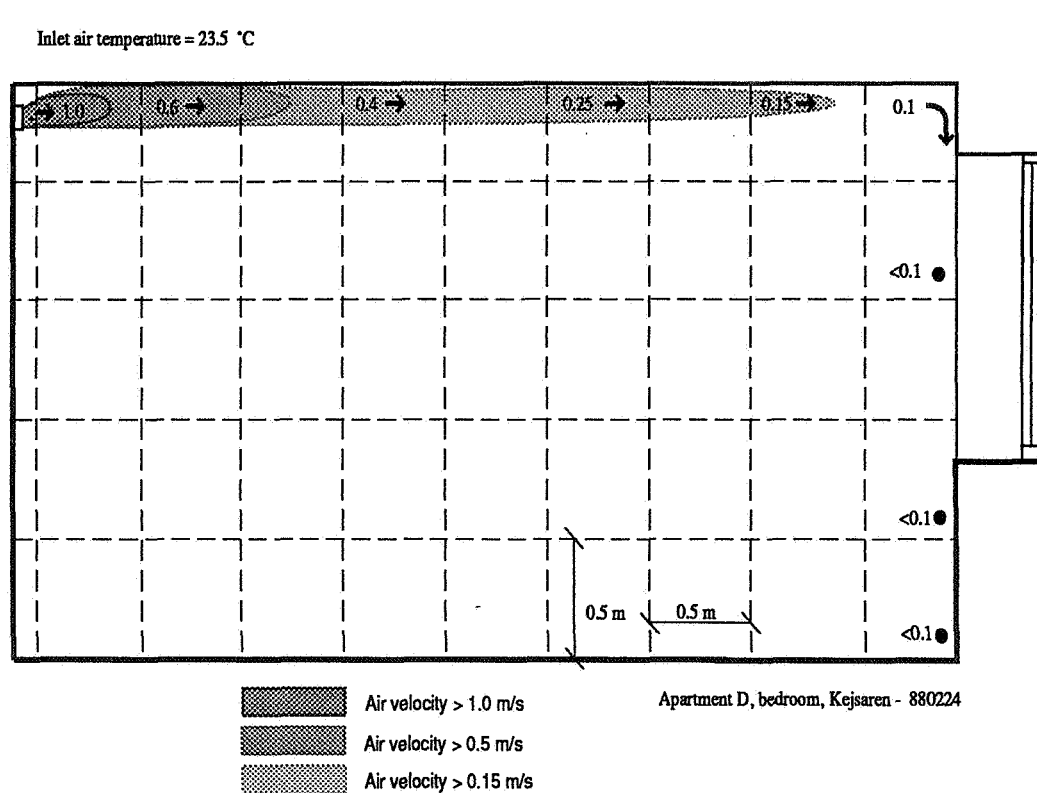


Fig. 12. Section through a sittingroom with interior wall supply, apartment D, Kejsaren.

5.3. Thermal comfort in the Høstvetet Building. interviews - measurements

This building has a window-sill which forces the air into the occupant zone (Fig. 13.). Even here small obstacles forces the air to turn into the room (Fig 14.). Compared with the supply air in the Kejsaren Building (Fig.8.), the influences on the air movements are much smaller.

The occupant in this apartment express satisfaction with the indoor temperature during the winter but complains about too high indoor air temperatures during the summer. The occupant doesn't neither express any complains of draught, even if the figure shows that there are high air velocities in the occupied zone. This could be due to the fact that the occupant has adjusted the furnitures after the placement of the ventilators.

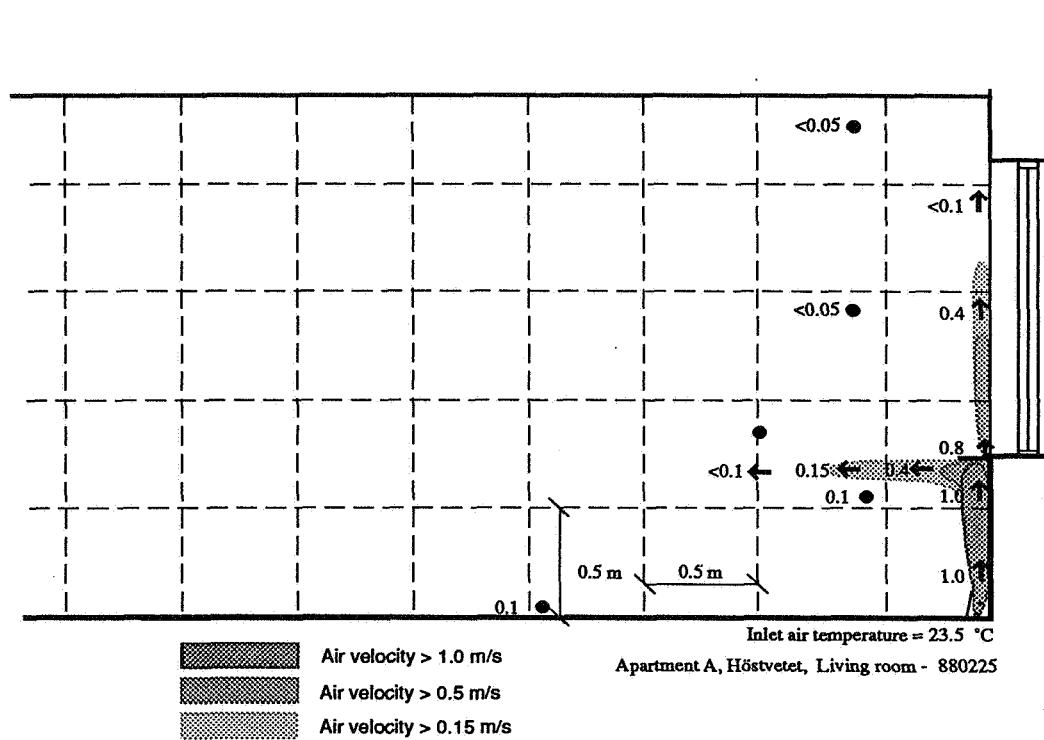


Fig. 13. Section through a sittingroom with exterior wall supply, Höstvetet.

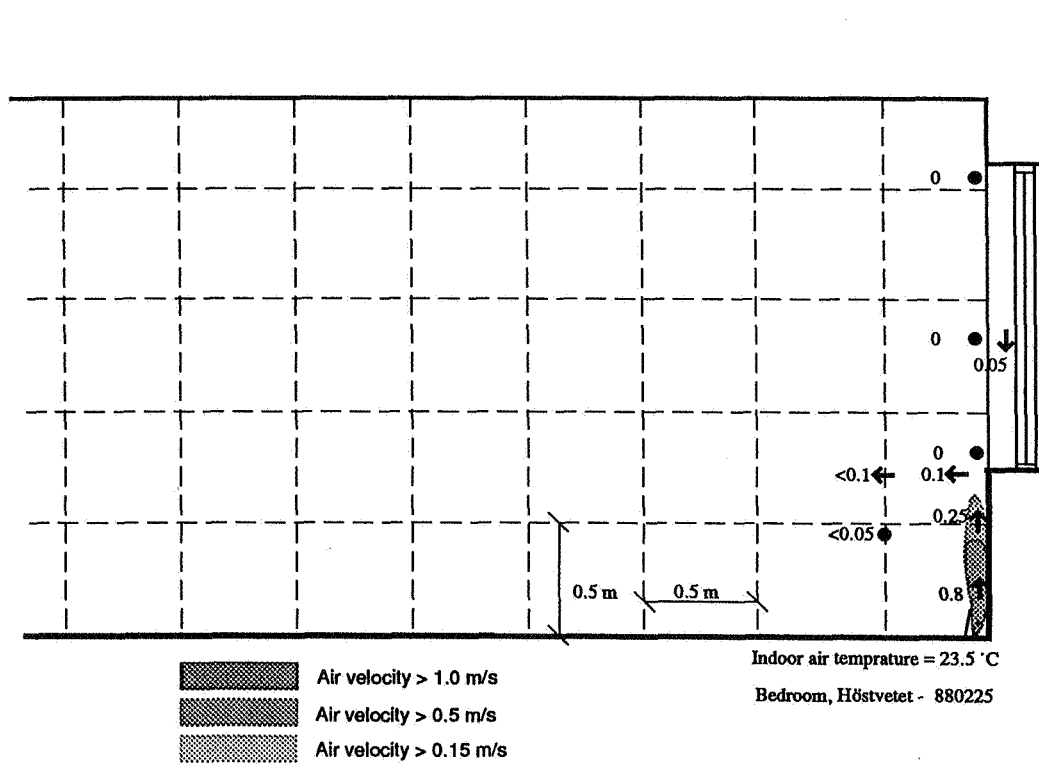


Fig. 14. Section through a bedroom with exterior wall supply, Höstvetet.

6. Discussion

In Sweden, there is a lively discussion about mechanical ventilation system in energy efficient and airtight buildings today. It is well known today that many factors affects the indoor climate. Not only the heating ventilation system but also building materials, thermal cold bridges, tightness and other building design criteria is of great importance. Healthy buildings with installations that provide good air quality without any inconvenience for the occupants, such as for example noise problems, is requested. A broad approach is thus important, not only when evaluating indoor climate, but also when evaluating the building design, the heating and ventilation systems, the indoor air quality and the occupants experience and use of the building. The occupants often express a general feeling of uncertainty when exposed to new mechanical ventilation systems, such as forced air heating. Better possibilities for individual adjustment of the indoor temperature and a better air quality is required.

This study indicates that air heating systems could be a way to provide mechanical supply air with less draught and with less thermal comfort problems than in ordinary supply- and exhaust air ventilation systems. Especially those designs that use overhead ventilators on the interior walls seems to give a good thermal comfort in the occupant zone.

If floor ventilators under the windows are chosen a very careful design has to be made of both ventilators and to the details in their surroundings. Special attention has to be put into the coordination between designers and builders.

7. Recommendations

Forced air heating system has the advantage that there are less complains about draught, but it has a disadvantage in that the occupants doesn't consider the air quality to be as good as with the other systems. Here the technology should be improved by:

Design the ventilation systems for better air quality. Ventilation systems that cause an unhealthy indoor climate in the apartment must be avoided.

Design the ventilators for better performances of both draught and noise.

Design systems for individual adjustment possibilities in the apartments

Give the tenants good information if there are individual adjustment possibilities in the apartments.

Develop methods to measure and display ventilation- and air quality data in each apartment.

8. References

1. ELMROTH, A., JÄGBECK, P.O., JOHANNESSON, C.M., HAMBRAEUS, M. "The Stockholm Project, Energy-Efficient Multi-Unit Buildings, a Full Scale Development Project", Proceedings from Clima 2000, Copenhagen, 1985.
2. SWEDISH COUNCIL FOR BUILDING RESEARCH, "Kejsaren", S6E: 1986, Stockholm
3. SWEDISH COUNCIL FOR BUILDING RESEARCH, "Suncourt, Low Energy Multi-Family Housing", S7E: 1986, Stockholm
4. HAMBRAEUS, M., WERNER, G. "The Stockholm Project - Program for Measuring and Analyzing new Multi-Family Buildings", Proceedings from "Thermal Performance of The Exterior Building III", ASHRAE/DOE/BTEEC Conference, Florida, 1985.
5. JÄGBECK, P.O., ERIKSSON, S.O. AND WERNER, G. "Indoor Climate Control, a Comparative Studies of Six Different Solutions For Heating and Ventilation and the Possibilities of Individual Control." Proceedings from CIB conference "Healthy Buildings", Stockholm, 1988.
6. JÄGBECK, P.O. Indoor Climate in New Multi-Unit Buildings, The Stockholm Project, A Full Scale Demonstration Project, Proceedings from Clima 2000, Copenhagen, 1985.
7. ISO 7726 "Thermal Environments - Instruments and Methods for Measuring Physical Quantities", Geneva, 1985.

EFFECTIVE VENTILATION

9th AIVC Conference, Gent, Belgium
12-15 September, 1988

Poster 5

FURTHER STUDIES OF PASSIVE VENTILATION SYSTEMS - ASSESSMENT
OF DESIGN AND PERFORMANCE CRITERIA.

R.E.EDWARDS 1, C.IRWIN 2.

1. DEPARTMENT OF BUILDING ENGINEERING,
UMIST, P.O. BOX 88, SACKVILLE STREET,
MANCHESTER, M60 1QD, ENGLAND.
2. WILLAN BUILDING SERVICES LIMITED,
2 BROOKLANDS ROAD,
SALE,
CHESHIRE, M33 3SS,
ENGLAND.

ABSTRACT

Increases in building air tightness for purposes of energy saving have, unfortunately, also led to a significant increase in the number of instances of condensation damage, particularly in domestic properties. The cost effective control of condensation is a large problem in the United Kingdom, especially for local authorities with large housing stocks. The use of ducted passive ventilation systems, relying upon stack and wind effects to provide extraction, has several advantages, one of which is that the occupants of dwellings fitted with such systems need little, if any, knowledge of the principles involved, or instructions in its use, to derive maximum benefit.

This paper describes two programs of research carried out on two houses fitted with passive systems: the first house is a highly airtight, timber framed structure, whilst the second is a significantly leakier council owned property of traditional construction. The effect of passive ducts upon the ventilation rate in each dwelling is measured and related to internal/external temperature difference, windspeed and direction. The measured ventilation rates are used to calculate likely rates of moisture extraction during occupation, and the resulting effects upon condensation risk are assessed in the light of the predicted minimum ventilation rates necessary in order to avoid condensation. Theoretical calculations of the expected flow rates through passive systems are presented, and are shown to be in broad agreement with measured values. Finally, design considerations of importance when specifying passive systems are discussed.

INTRODUCTION

Modern energy saving techniques have led to increased risks of condensation upon cold surfaces within the occupied spaces of dwellings. Batty et al (1) estimate that as much as 12kg of water can be released as vapour within a house in a day. It is clear that localized extraction of water vapour in high production rate areas (for example bathroom and kitchen) would be highly advantageous.

A simple, potentially cost effective method of moisture extraction which has been suggested as suitable for use in the United Kingdom is passive stack ventilation, or PSV.

(2) It should be noted that such systems have been in use in most of the rest of Europe for a substantial length of time. These systems use ductwork, terminating at roof level, to provide direct extraction of moist air from areas of high moisture production. The driving forces for extraction are the temperature induced buoyancy force (the "stack effect") and wind induced suction. The likely orders of magnitude of each driving force can be estimated as follows. Firstly, the maximum available pressure difference for buoyancy driven airflow in a duct is given by

$$P_b = (p_o - p_h) \cdot h \cdot g \quad (1)$$

where p_o =air density at outside temperature (kg/m^3)
 p_h =air density at room temperature (kg/m^3)
 h =vertical duct length (m)
 g =acceleration due to gravity (9.81 m/s^2)

Secondly, the velocity pressure difference induced by a moving airstream across the duct discharge, P_v , is given by

$$P_v = 1/2 \cdot p_o \cdot v^2 \quad (2)$$

where v =velocity of airstream. (m/s)

Figures 1 and 2 show the pressure differences in a 5m high duct (typical of a kitchen installation) and a 1.5m high duct respectively, (typical of a bathroom installation.) Whilst figure 3 shows the effect of windspeed on wind induced pressure difference. It can be seen that in the majority of cases, the contribution of stack effect is likely to be smaller than the wind induced component: furthermore, the overall flow of air through a duct of a given length will be influenced by resistance effects.

The airflow rate through a duct can be calculated from the following formula:

$$Q = A [2A \cdot P_t / (E \cdot f \cdot L \cdot p)]^{1/2} \quad (3)$$

where Q =volumetric airflow rate (m^3/hr)
 p =mean air density (kg/m^3)
 P_t =total available pressure difference (Pa)
 $= [P_{b2} + P_{w2}]^{1/2}$
 a =cross-sectional area of duct (m^2)
 E =perimeter of duct (m)
 f =friction coefficient of duct (dimensionless)
 L =length of duct (m)

Values calculated from equation (3) are then corrected using the procedure described in detail in reference (3), in order to take account of any air resistance within the ducts due to bends.

Figure 4 shows the calculated airflow through a 1.5m high, 100mm internal diameter duct for a range of internal/external temperature differences and windspeeds, whilst figure 5 gives the same information for a 5m high duct of the same internal diameter.

The main aims of the work described in this paper are threefold:

- 1) To assess the performance of PSV systems installed in two houses of different construction and air leakage characteristics, for a range of weather conditions;
- 2) To determine whether the contribution to the ventilation rate in the bathrooms and kitchens are sufficient to avoid condensation in each house;
- 3) To estimate the effects of the use of PSV systems upon energy consumption, and to compare them with the effects of other means of moisture removal.

EXPERIMENTAL

a) Details of test houses.

The house used for the first site investigation is situated at Willow Park, Chorley, and is part of the Central Lancashire New Town development. The house is described in greater detail in reference (4), but, briefly, is of a special low energy timber frame construction. The whole house volume is approximately 320m³, of which the bathroom and kitchen comprise approximately 13m³ and 34m³ respectively. Figure 6 gives details of the PSV systems used.

The house used for the second investigation is situated at Withington, South Manchester, and is a three bedroomed, semi-detached council house of traditional construction. The whole house volume is approximately 200m³, of which the bathroom and kitchen comprise approximately 6.7m³ and 16.2m³ respectively. Figure 7 gives details of the PSV systems installed. There are three main differences between the systems used in each house. Firstly, 150mm diameter insulated flexible duct is used in the council house installations instead of the previous rigid rectangular ductwork; secondly, the council house installations are terminated at ridge level by means of Redland gas flue Ridge Ventilators; and finally, Bahco registers are used as ceiling terminals in the council house installations.

b) Measurement details.

The ventilation and air movement measurement performed during these two site investigations were made using the multiple tracer gas technique developed at UMIST (5) Briefly, the technique uses a modified portable gas chromatograph, and is capable of measuring ventilation rates in, and airflows between, three interconnected cells.

The program of measurements performed in the low energy house is given in full in reference 4. The number of different permutations of test conditions used during this study was greater than for the council house study due to extreme airtightness of the house and the presence of window head trickle ventilators.

The following program of measurements was performed in the council house:

- i) no PSV systems in use;
 - ii) bathroom PSV system in use;
 - iii) kitchen PSV system in use;
 - iv) both PSV systems in use;
- In addition, the following subsidiary parameters were measured during each investigation:
- i) internal/external temperature difference;
 - ii) air velocities in ducts;
 - iii) internal/external pressure differences;
 - iv) relative humidity in both kitchen and bathroom;
 - v) windspeed and direction.

RESULTS AND DISCUSSION.

a) Low energy house.

Measured ventilation rates, together with other data, are presented in table 1. (kitchen) and table 2. (bathroom). Several points are worthy of note:

- i) The PSV systems are sensitive to windspeed. Table 1 shows that an increase in windspeed from 2m/s to 5m/s from the west increases the airflow rate in the kitchen duct by between 27% and 40%, depending upon room conditions. From other tests discussed in greater detail in reference it becomes apparent that both systems are highly susceptible to the influence of wind direction.
- ii) Comparison of table 1 with table 2 shows that the bathroom system outperforms the kitchen system for the same windspeed and direction for example, for the case of a 2m/s westerly wind, the bathroom system extracts at a 40% higher rate than the kitchen system.

This is in conflict with the results of Johnson et al (5), who state that the greater stack effect in the longer kitchen duct will always lead to higher extraction rates in kitchen ducts as opposed to bathroom ducts. This argument does not, of course, take into account the influence of resistance effects due to duct length.

Equation 3 predicts duct airflows of approximately $33\text{m}^3/\text{hr}$ and $40\text{m}^3/\text{hr}$ for the bathroom and kitchen ducts respectively, for the test conditions experienced. It would appear that the extreme airtightness of the house has the effect of throttling the PSV systems. It is possible to increase duct airflow rates significantly by opening the kitchen door: however, air movement tests described in more detail in reference (4) show that this practice encourages the flow of moist air into the rest of the house, and is therefore not to be encouraged.

Aside from the other points mentioned above, it should be noted that at windspeeds in excess of 9m/s , the flow of air in both systems actually reversed, thus providing an inflow of air into the house.

b) Council House.

Measured ventilation rates, together with other data are presented in table 3 (kitchen) and table 4 (bathroom). Key features of the results are as follows:

i) As in the case of the low energy house, the systems are sensitive to the influence of wind speed, however, wind direction does not seem to have as significant an effect.

ii) Duct airflows are generally higher than for the low energy house. Table 5 compares duct airflows in both houses for comparable operating conditions.

iii) Airflow rates in the bathroom system are again higher than for the kitchen system under identical conditions. Expressed as a percentage of the overall air change rate, bathroom system airflow rates are comparable to those measured in the low energy house: for the kitchen system, however, the percentage is significantly higher.

iv) The effect of temperature upon duct airflows can be seen more clearly in this case. Temperature is the dominant factor at low wind speeds, but becomes less significant as wind speed increases. It can be seen that the measured airflow rates are in good agreement with the airflow rates predicted in figures 4 and 5.

V) flow reversal was again observed. However, in this case, the threshold windspeed for the onset of flow reversal was only 7m/s. Without carrying out a similar program of tests in a similar house, it is not possible to state categorically whether this reduction in threshold windspeed is due to the choice of terminal, or else is a function of building envelope air tightness. In the opinion of the authors, the former possibility is the more likely.

SYSTEM EFFECTIVENESS - ENERGY IMPLICATIONS OF PSV USE

Using the criteria outlined by Meyringer (6), and adjusting these in order to reflect the likely daily moisture production within the typical bathroom and kitchen, it is possible to estimate the minimum ventilation rates required in order to avoid surface condensation. These values are given in table 6. In the case of the low energy house, inspection of tables 1 and 2 shows that use of the bathroom PSV system gives a ventilation rate of approximately 1.04 ach, whilst the kitchen PSV system gives ventilation rates of between 0.84 and 1.1 ach. Thus it can be seen that even under the low wind speeds experienced during this study, the PSV systems should, in most cases, give a background ventilation rate which is adequate to prevent surface condensation. In the case of the council house, the PSV systems also give ventilation rates above the minimum; however, the rates are well in excess of the minimum required, and hence the systems could be wasting energy by over extraction. It could be argued that these calculations have been made on the basis of the assumption of a constant rate of moisture production and that in practice, higher rates of extraction might be of benefit in order to cope with peaks of moisture production. However, from the energy efficiency viewpoint, it is undesirable that over extraction takes place regularly. One possible solution to this problem would be the provision of a humidity-sensitive throttling system for each PSV duct installed in a house. Such a device would preferably be non-electrically operated, in order to reduce the maintenance and running cost. Another solution might be to reduce the size of PSV ducts so as to give condensation control during conditions of average moisture production, whilst providing a humidity controlled booster fan in the PSV duct. Such a system would give a better response to rapid increases in moisture production rates, but would incur higher maintenance and running costs than the "humidity throttled" option.

d) Optimisation of system design.

In order to optimise the performance of a PSV system, several important design and installation points have to be taken into consideration:

i) The number of bends in a system should be minimised. Offsets or 135 degree bends are to be preferred in circumstances where bends are necessary; in any case, 90 degree bends should be avoided at all costs.

ii) Flexible ducts are valuable components to have available as an option when PSV systems are being designed. It is imperative, however, that when they are used, they are fully extended, or else the resistance to airflow resulting will be significantly greater than for a comparable length of rigid ductwork. It should be impressed upon installers that in circumstances where flexible ductwork is used that the ductwork should be cut to length, rather than allowing excess ductwork to hang loosely, or in the worst case, to be coiled up in the roofspace.

iii) It would be appropriate to remind any PSV system designer that the use of insulated ductwork in the roofspace is essential, in order to minimise the risk of condensation within ducts.

iv) On the basis of the results obtained in the two studies, it is recommended that, wherever possible, a PSV system should discharge by means of a ridge tile ventilator. The lower threshold windspeed for flow reversal is a small price to pay for the less wind direction sensitive system performance obtained.

v) The use of a common discharge terminal for two or more PSV systems may have a certain economic or aesthetic appeal. However, from a technical point of view, it is very important that each system in a dwelling discharges independently.

vi) The inferior performances of the PSV systems in the low energy house are due to an inadequate supply of air to feed the systems, underlining the importance which should be attached to the careful planning of airflow routes into and within a dwelling, in order to ensure that the PSV systems operate to their full capabilities.

vii) If the dwelling being fitted with PSV systems is in an exposed area, it may be the case that volume control dampers have to be used in order to prevent over-extraction.

CONCLUSIONS.

Programs of test work on two contrasting types of house have shown that in both cases, PSV systems provide an efficient means of condensation control within zones of high water vapour production. However, the two studies serve to emphasise two contrasting factors which should be taken into account when designing PSV systems.

The extreme airtightness of the low energy house prevents the PSV systems from extracting to their predicted capability, whilst in the council house, it's high background air leakage means that over extraction is likely to occur, particularly at high wind speeds. On the one hand, it is essential to provide adequate air inlets so as to feed ducts, on the other, it is important to minimise over extraction for reasons of energy efficiency. Over extraction is best controlled by one of two means; firstly, by providing humidity-sensitive throttling of ducts; or secondly, by providing a mechanical boost to extraction. Two installations using the former principle are currently undergoing field trials.

REFERENCES.

1. BATTY, W J, O'CALLAGHAN, P W AND PROBERT, S D.
Applied Energy, Volume 17, 1984, pp 1-14.
2. JOHNSON, K A, GAZE, A I and BROWN, D M.
Proceedings of the 6th AIC Conference, Paper 4, Netherlands, 1985.
3. CIBSE Duct sizing guide (Book C, section C4), 1970.
4. EDWARDS, R E and IRWIN C.
Proceedings of the 7th AIVC Conference, Paper 16, England, 1986.
5. IRWIN, C, and EDWARDS, R E.
Building Services Engineering Research and Technology, Volume 8, 1987, pp 91-96.
6. MEYRINGER.
Air Infiltration Review, Volume 7, No 1, November 1988.

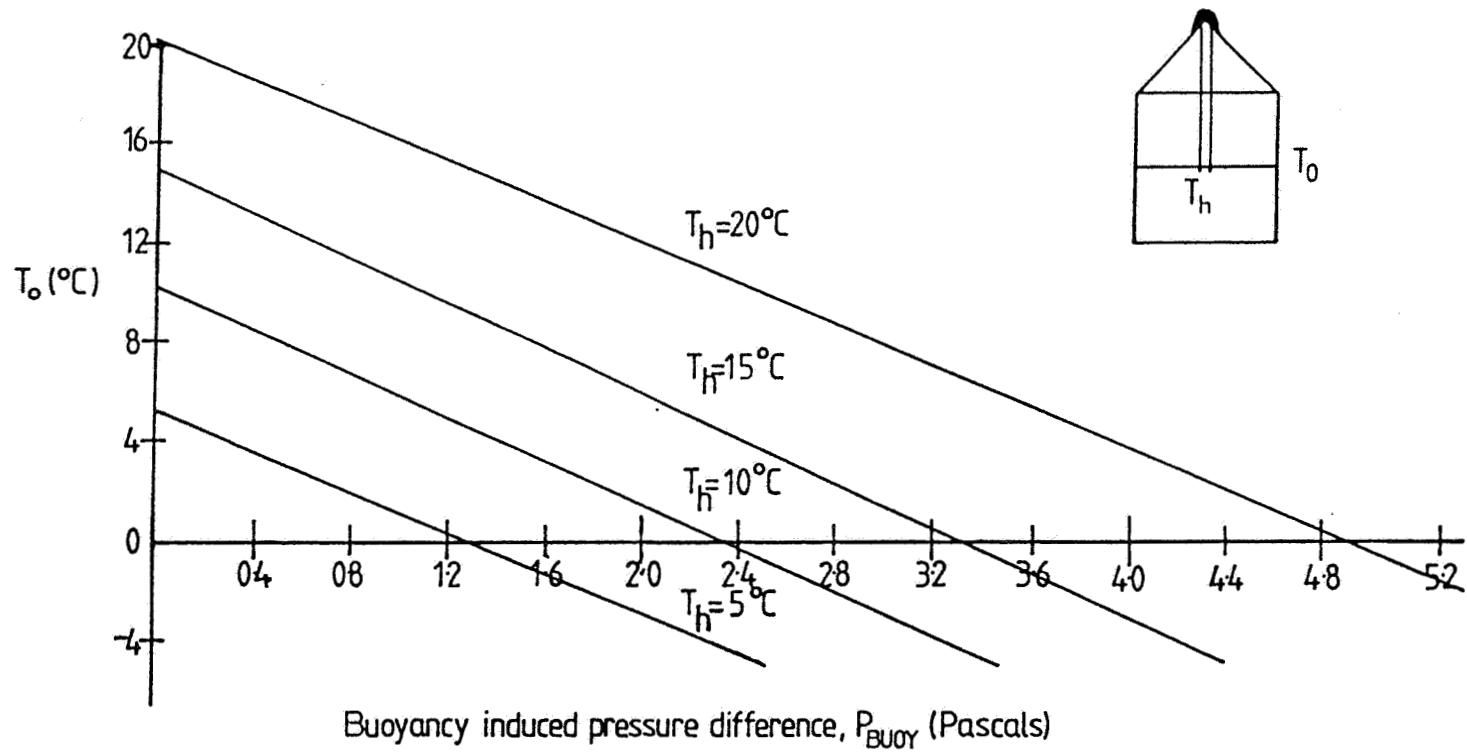


Figure 1: Buoyancy induced pressure difference 5 mtr duct.

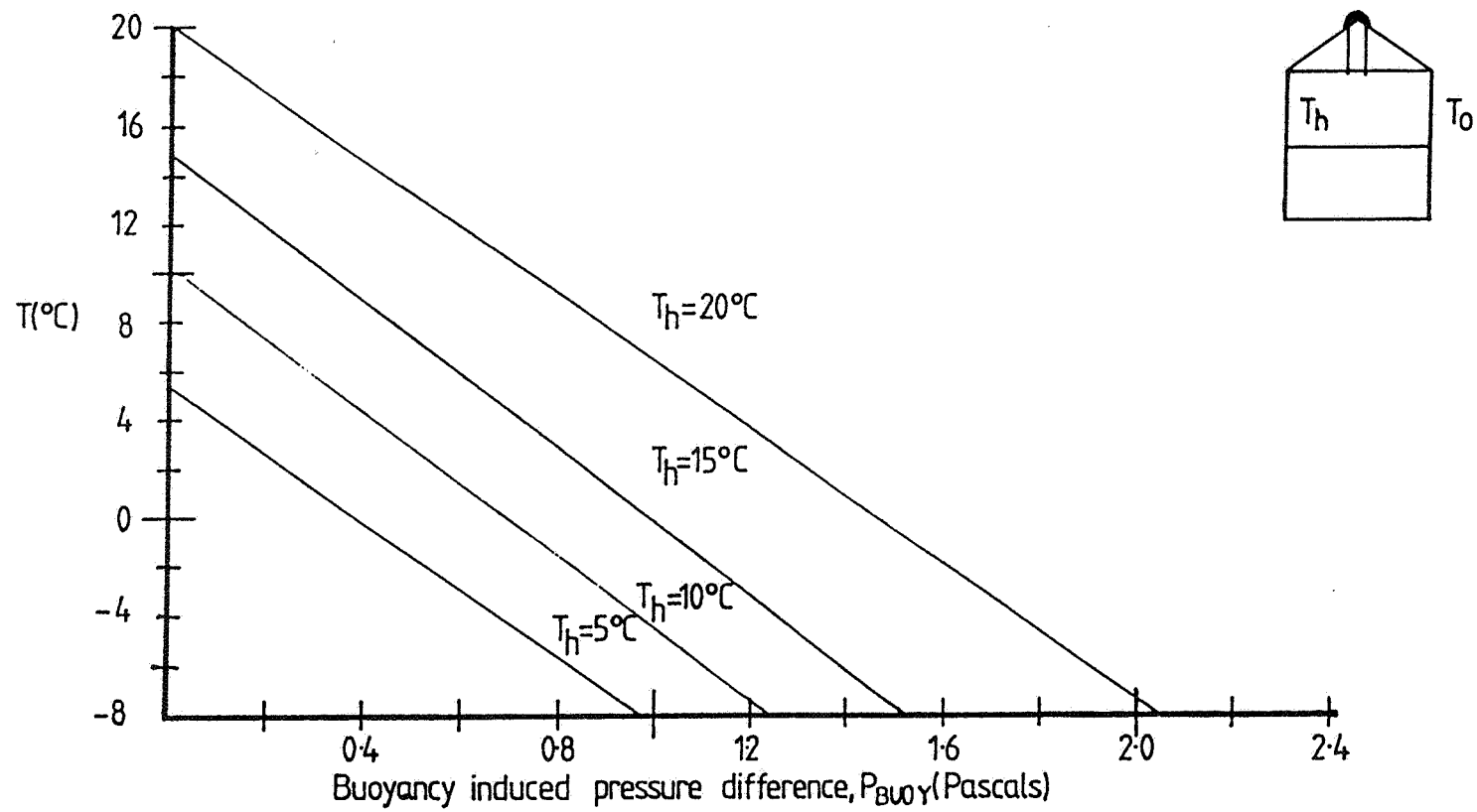


Figure 2: Buoyancy induced pressure difference 1.5 mtr duct.

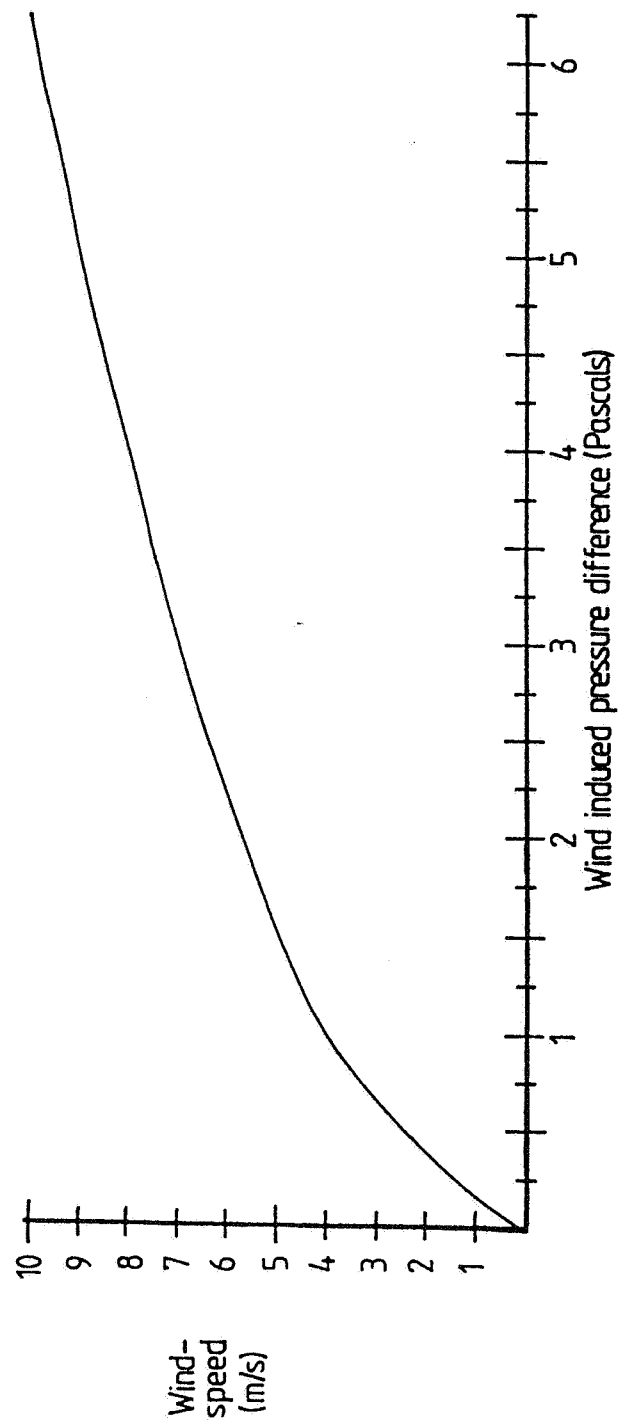


Figure 3: Wind induced pressure difference.

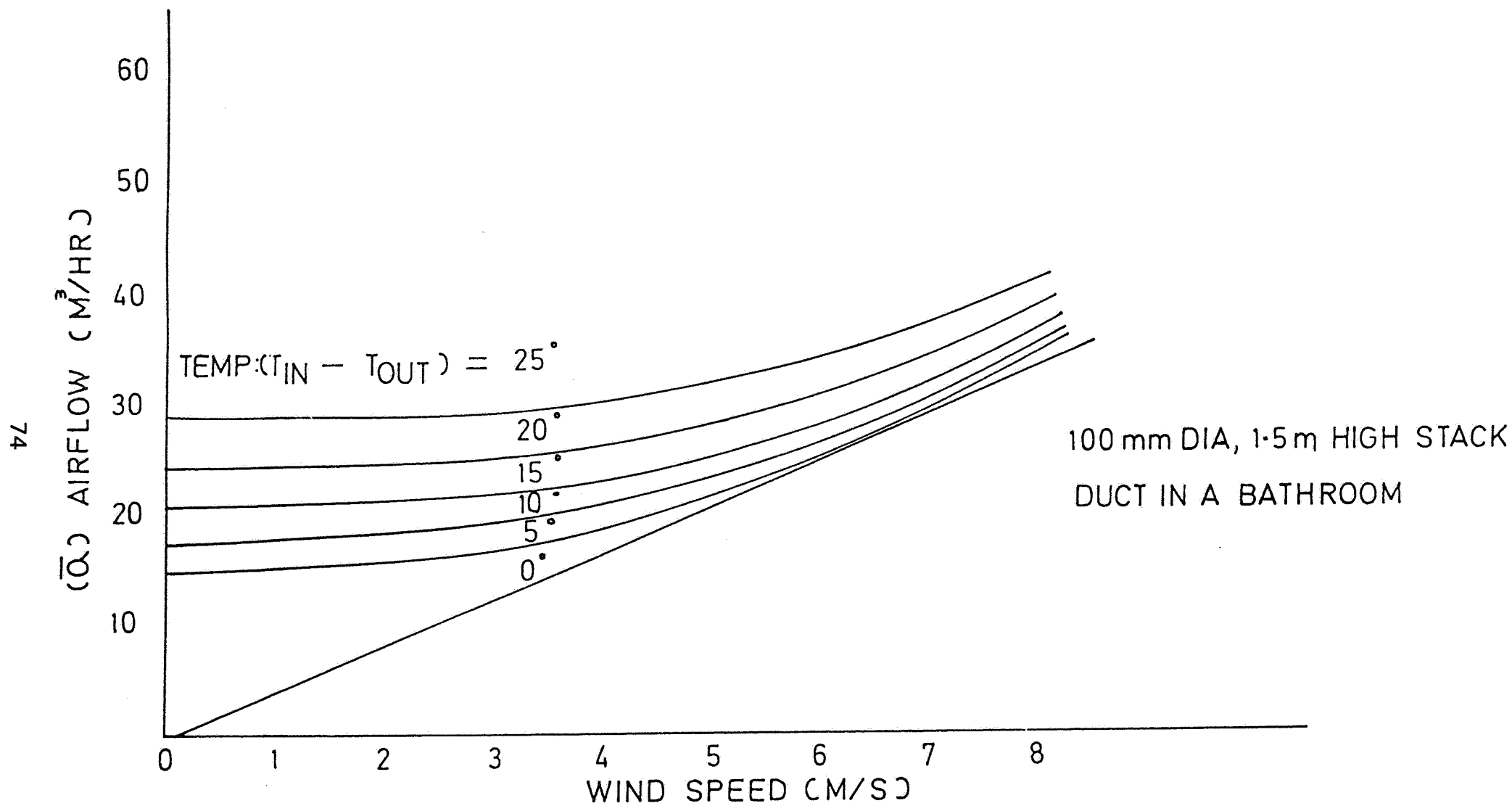


Figure 4: Calculated airflow 1.5 mtr high, 100 mm
dia duct.

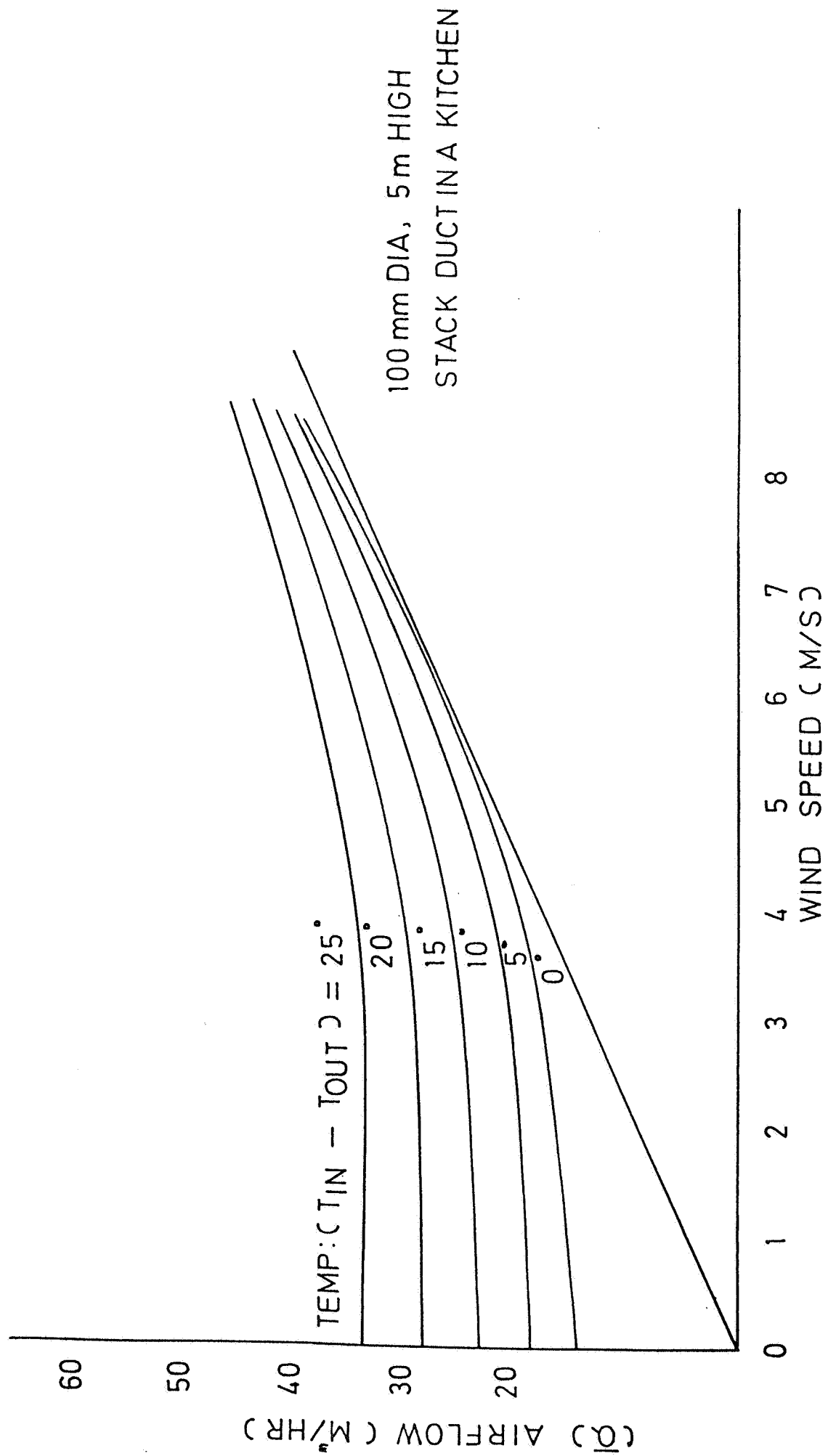


Figure 5: Calculated airflow 5 mtr high, 100 mm dia duct.

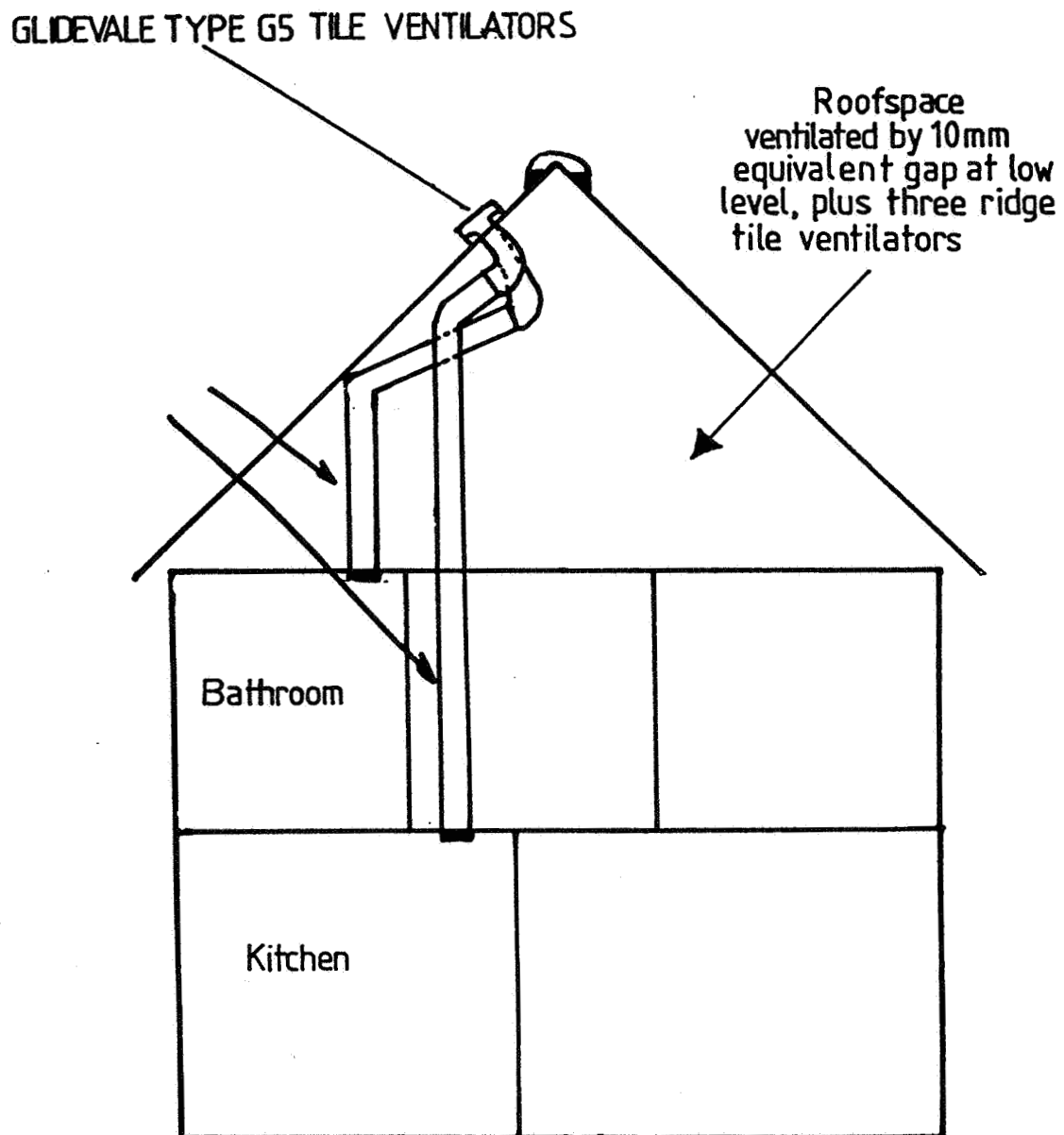


Figure 6: PSV Layout: Low energy house.

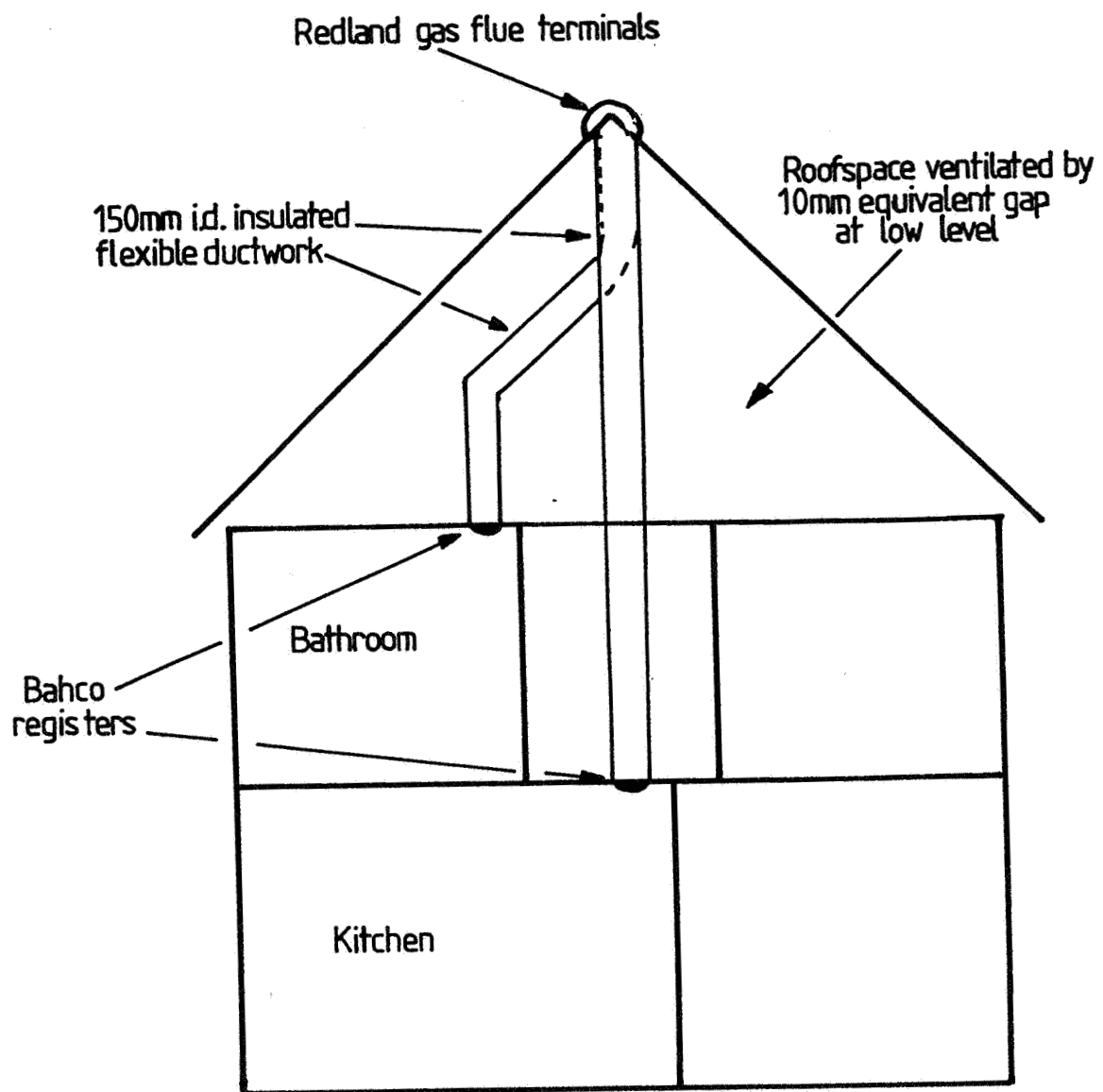


Figure 7: PSV Layout: Council House.

9th AIVC PAPER.

Tables

1. Low energy house - kitchen results.
2. Low energy house - bathroom results.
3. Council house - kitchen results.
4. Council house - bathroom results.
5. Comparison of system performances.
6. Minimum ventilation rates.

Conditions	ACH	NK m ³ /hr	Duct Flow m/s	m ³ /hr	% of NK due to duct		Speed (m/s)	Direct.	T°C
All sealed	.23	7.82	-	-	-	-	2	W	11
Trickle vents open	.59	20.06	-	-	-	-	2	W	12
Duct and trickle vent open	.84	28.56	0.11	5.9	20.7	-	2	W	12
Duct and windows 2"	3.00	102.00	0.15	8.1	7.9	-	2	W	12
Duct open only	.37	12.58	0.10	5.4	42.9	-	2	W	12
Windows open 2" only	2.57	87.38	-	-	-	-	2	W	12
All sealed	.31	10.54	-	-	-	-	5	W	13
Trickle vents open	.63	21.42	-	-	-	-	5	W	13
Duct and trickle vent open	1.17	39.78	0.15	8.1	20.3	-	5	W	12
Duct and windows 2"	3.67	124.78	0.25	13.5	10.8	-	5	W	12
Duct open only	.53	18.02	0.14	7.6	42.2	-	5	W	12
Windows open 2" only	2.74	93.16	-	-	-	-	6	W	13

TABLE 1: Results for kitchen ventilation tests

Conditions	ACH	NB m ³ /hr	Duct flow m/s	Duct flow m ³ /hr	% of NB due to duct	Wind	
						Speed (m/s)	Direct. T°C
All sealed	.35	4.55	-	-	-	2	14
Trickle vent open	.58	7.54	-	-	-	2	14
Duct and trickle vent open	1.04	13.52	.16	8.6	63.6	2	14
Duct and windows 2"	3.19	41.47	.24	12.9	31.1	2	14
Duct open only	1.03	13.39	.15	8.1	60.5	2	14
Windows open 2"	2.72	35.36	-	-	-	2	14

TABLE 2: Results for bathroom ventilation tests

Nk ach	m ³ /hr	Duct Airflow		T°C	Direction	Wind Speed (m/s)	Comments
		m ³ /hr	% of Nk				
1.661	26.9	-	-	26.2	SE	3.0	Duct Sealed
1.956	31.7	-	-	14.5	S	5.0	" "
.939	15.2	-	-	10.0	W	3.5	" "
1.100	17.8	-	-	14.1	NE	6.5	" "
1.195	19.4	13.1	67.5	7.5	SW	3.0	Duct Open
2.226	36.1	20.4	56.5	15.4	SW	4.0	" "
2.808	45.5	20.4	44.8	18.9	S	5.0	" "
3.055	49.5	18.9	38.2	16.9	S	5.5	" "
1.568	25.4	11.7	46.1	9.0	NE	6.5	" "
1.297	21.0	14.6	60.6	13.7	NE	6.0	" "
2.139	34.7	18.9	54.4	9.3	S	6.0	" "
2.029	32.9	17.5	53.2	9.3	S	5.5	" "
1.197	19.4	14.6	75.2	9.2	SE	2.0	" "

Table 3: Council house kitchen

ach	NB m ³ /hr	Duct Airflow		T°C	Wind		Comments
		m ³ /hr	% of Nk		Direction	Speed (m/s)	
1.236	8.3	-	-	21.4	SE	3.0	Duct Sealed
1.743	11.7	-	-	15.8	S	4.0	" "
1.319	9.3	-	-	18.2	SE	4.5	" "
2.006	13.5	-	-	14.5	S	5.0	" "
4.251	28.6	20.4	71.3	29.3	S	5.0	Duct Open
4.580	30.8	21.9	71.1	24.5	S	5.5	" "
5.111	34.4	23.3	67.7	22.2	S	6.0	" "
4.633	31.2	20.4	65.4	24.6	SW	4.0	" "
5.038	33.9	20.4	60.2	22.0	SW	5.0	" "
3.106	20.9	13.1	73.2	8.7	SW	6.0	" "
3.316	22.3	14.6	65.5	12.7	NE	6.0	" "
3.416	22.9	17.4	75.9	16.1	NE	6.0	" "
3.864	25.9	20.4	78.8	17.1	NE	6.0	" "
2.799	18.8	13.1	69.7	9.6	W	3.5	" "
3.106	20.9	13.1	62.7	10.0	W	6.0	" "

Table 4: Council house bathroom

House	Kitchen Duct Airflow (m ³ /hr)	Bathroom Duct Airflow (m ³ /hr)
Low Energy	5.9 - 8.1	16.5
Council	8.1 - 12.9	18.9

Table 5: Comparison of System Performances

House	Kitchen		Minimum Ventilation Rate		Bathroom	
	ach		m ³ /hr	ach	m ² /hr	
Low Energy	0.96 - 1.25		32.5 - 42.5	0.85 - 1.1	11	- 14.0
Council	0.96 - 1.25		15.5 - 20.25	0.85 - 1.1	5.6	- 7.1

Table 6: Minimum Ventilation Rates

EFFECTIVE VENTILATION

9th AIVC Conference, Gent, Belgium
12-15 September, 1988

Poster 6

ZONE TO ZONE TRACER GAS MEASUREMENTS:
LABORATORY CALIBRATION AND VALUES OF AIR FLOWS UP AND DOWN
STAIRS IN HOUSES.

S B RIFFAT, J WALKER AND J LITTLER

Research in Building Group
The Polytechnic of Central London
35 Marylebone Road
London
NW1 5LS
UK

ABSTRACT

This work is concerned with measuring air flows between the floors of houses. A simple measuring technique is described in which two portable SF₆ systems were employed. The design and construction of the portable system are presented. A comparison of air flow patterns in a superinsulated house and a standard house is made. Results showed that the air flow between the upper and lower floors of the superinsulated house was about 20 m³/h compared with 100 m³/h in the traditionally built house. The method has also been validated in the laboratory by measuring air flows between two small chambers using both the tracer systems and an independent flow device.

INTRODUCTION

The study of infiltration and interzonal air movement in houses is important for both energy conservation and indoor air quality control. The heat losses caused by air infiltration in traditionally built houses can account for up to 40% of the heating energy requirements¹. As a result a large number of superinsulated houses are being built in Scandinavia, North America and more recently in the UK². These houses are constructed in such a way that air leakage through cracks and openings in their envelopes no longer serve as a major source of ventilation and so mechanical ventilation systems may be employed. Inadequate air change rates give rise to an increase in concentration of indoor air contaminants (e.g. formaldehyde, nitrogen dioxide and moisture) which may influence the health and comfort of the building's occupants. Research is therefore required to evaluate the extent of air ventilation, interzone air movement and dispersion of interior contaminants so that the optimum compromise between energy efficiency and sufficient air change to maintain a healthy environment is achieved.

Air flows between internal spaces in buildings are usually measured using tracer gas techniques³. Several tracer gases have been used in the past but sulphur hexafluoride has been chosen for our work as it has desirable tracer gas characteristics in terms of detectability, safety, and cost and has been used successfully in previous air infiltration studies^{4,5}.

In the past, measurement of air movement in buildings has been accomplished using a single tracer gas technique, but recently multiple tracer gas techniques have found increased application^{6,7,8}. Although measurements can be made more quickly and accurately using a multiple tracer gas method, the cost of the tracer gases and equipment is high.

The purpose of this work is to demonstrate the use of highly portable units fitted with electron capture detectors for measurement of air flow between floors of houses. A single tracer gas method was employed in this work and the accuracy of this technique was assessed using a two-zone calibration rig. We discuss the effect on air flow patterns of 1) using a ventilation system in the superinsulated houses and 2) using a kitchen extract fan in the traditionally built house. The design, and construction of the SF₆ system are described in this paper along with an analysis of the experimental results obtained and an appraisal of the measurement technique.

2. TWO-ZONE MASS-BALANCE EQUATIONS

Figure 1 is a schematic diagram of a house in which the downstairs and upstairs are designated zone 1 and zone 2, respectively. Air can infiltrate from outside the house into each zone (Q_{01} and Q_{02}). In addition, air can exchange between the two zones in both directions (Q_{12} and Q_{21}).

In a test example, the tracer gas may be released first in zone 1 while all its doors and windows are closed. Following tracer gas mixing the communication doors between the two zones are opened. Some tracer will be carried into zone 2 where it will mix with air and some will return to zone 1. If one applies the tracer material balances in each zone, assuming that a steady state exists and that the concentration of tracer gas in the outside air is negligible, then :

the rate of change of tracer concentration in zone 1 at time t is given by:

$$V_1 dC_1 / dt = - C_1 (Q_{10} + Q_{12}) + C_2 Q_{21} \quad [1]$$

where: V_1 is the interior volume of zone 1.

C_1 and C_2 are the concentrations of the tracer at time t in zone 1 and 2 respectively.

Similarly, the rate of change of tracer concentration in zone 2 at time t is given by:

$$V_2 dC_2 / dt = C_1 Q_{12} - C_2 (Q_{21} + Q_{20}) \quad [2]$$

where: V_2 is the interior volume of zone 2.

The other two flow rates can be then determined using the continuity equations as follows

$$Q_{01} = Q_{12} + Q_{10} - Q_{21} \quad [3]$$

$$Q_{02} = Q_{20} + Q_{21} - Q_{12} \quad [4]$$

Mass-balance equations may be solved using the theoretical technique described in ref.9. An alternative method to estimate air flows between internal spaces was used by Sinden¹⁰. The method assumes a multi zone system may be represented by a series of cells of known and constant volumes which are all connected to a cell of infinitely large volume, i.e. the outside space. The mass-balance for zones can be expressed by a series of equations which can then be solved using matrices. A similar method was used in our work, modified by introduction of the discrete time model as explained in detail in ref.11. The estimated air flow rates for specific moments in time are usually incorrect and in some cases are negative values. However, it is important to realise that we are not concerned with air flow rates at specific times, but rather with mean flow rates over finite time intervals usually greater than one hour.

In order to improve the accuracy of the single tracer gas technique for measuring interzonal air flows, a refined experimental method was developed for use in our work. This involved releasing tracer gas first in zone 1 and monitoring the concentrations in the two zones. The experiment was then repeated, this time releasing the tracer gas in zone 2 instead of zone 1. This method provides an alternative to the use of the two-tracer gas technique providing the weather conditions are stable during the measurements.

3 MEASUREMENT SYSTEM

The microcomputer-measuring system is shown in Fig. 2. The system was made up from the following major components:

- (a) Sampling - Injection Unit
- (b) Column
- (c) Chromatographic Oven
- (d) Electron Capture Detector
- (e) Microcomputer and Interface.

Argon, used as the carrier gas, normally flows at a constant rate through the column via the sampling valve. The carrier gas then passes through the detection cell before being vented to the atmosphere. The sampling unit consists of a two-position, 6-port valve, connected to a 0.5 cm³ sampling loop. The valve can be easily rotated to position 1 or 2 using a small motor.

The column was made by packing a 1.5 m length x 4.3 mm internal diameter nylon tube with 60-80 mesh aluminium oxide. The tube was coiled three times and placed horizontally inside an electrically heated oven. The oven was maintained at a constant temperature using a temperature controller. The electron capture detector, which uses Ni-63 radioactive cell, was made by Pye Unicam Ltd. A pump was used to draw air from the test space to create a flow through the sample loop. By rotating the sample valve to position 2, air in the sample loop was injected into the argon flow which carried it into the column and finally to the detector for analysis. The amplified reverse response from the detector cell is then displayed as peaks on the computer monitor. The system incorporates a BBC microcomputer with two 5¹/₄ inch dual sided floppy disc drives, a parallel printer and interfaces for both analogue and digital data. The interfacing of the gas chromatograph and the sampling and injection units was accomplished by specially designed interface cards. The system is very flexible and can be used for unattended operation.

4 MEASUREMENT AND RESULTS

The tracer decay method has been used to measure interzonal air flows in two houses in Milton Keynes, UK. The two houses were sheltered by a number of adjacent houses. The temperature at various points on each floor, external temperature and wind speed during the measurement period are shown in Table 1.

Tests carried out in these occupied houses are detailed below.

4.1 Superinsulated House.

The superinsulated house is a three bedroomed, semi-detached unit, with a floor area of 75 m². The house was built to a superinsulated standard three times more stringent than the current UK building regulations. Vapour barriers were also installed for both the ceiling and walls of the house. A mechanical ventilation system with heat recovery is used to supply a controlled amount of ambient air. The system was manufactured by BAHCO of Sweden and uses an aluminium cross flow heat exchanger. The space and water heating are provided by a gas boiler.

The downstairs floor, zone 1, has a volume of 73 m³ and contains a living/dining room and kitchen. The upstairs, zone 2, has a volume of 107 m³ and contains the bathroom, three bedrooms, stairway and hall. Two identical SF₆ systems were used in these experiments. The first system was used to collect samples from zone 1 while the second was used to collect samples from zone 2. At the beginning of each test the communicating doors between the two zones were closed, and gaps between each door and its frame were sealed with tape to prevent leakage of tracer gas during the initial mixing period. A known volume of tracer gas was released downstairs where it was mixed with air using an oscillating desk fan. To ensure that a uniform concentration had been achieved in zone 1, samples were taken at four sampling points. After a mixing period of about 30 minutes, the sealing tape was removed and the communicating doors were opened. Samples were taken every 3 minutes for a total experimental time of about 90 minutes. The SF₆ systems analysed the samples *in-situ* so providing instantaneous readings of gas concentration in each zone.

A total of four experiments were performed in summer 1987 with the heating system switched off. In two of these experiments the ventilation system was switched off while in the other two the ventilation system was operated at low fan speed. Figure 3 shows a schematic of the two-zone air flows with the ventilation system off. As the temperature difference between the two floors was

about 0.3°C the air changes were found to be similar. Our experiments showed that the tracer decay curve (concentration/time variations) in zone 1 was not a simple exponential function but the sum of two exponential functions. In another experiment the whole house was seeded with tracer gas and the background infiltration rate was measured using the decay method. The air change per hour was found to be about 0.1. This result agrees with that measured after the house was built 18 months previously¹². A blower door pressure test was also performed in this house and the test revealed an air change rate of 1.5 at 50Pa (i.e. approximately $1.5/20 = 2.075$ ac/h under normal conditions). This value is within the performance range standards of Scandinavian houses.

Figure 4 shows schematic of the interzonal air flows with the ventilation system operating in low mode. The results show the ventilation system is effective in achieving the desired air change per hour in each floor of the house. The estimated whole house air change rate per hour is 0.8 ach (144 m³/h) which is larger than the value calculated from duct flow measurements (130 m³/h).

4.2. Traditionally Built House

In order to compare the pattern of air flows of a superinsulated house with a traditionally built house experiments were carried out in a three bedroomed, semi-detached house. In some of these tests all central heating radiators were switched off while in the others only the lower floor was heated. The total volume of the house was about 162 m³ and that of the upper floor was about 95 m³.

Figure 5 shows a plot of tracer gas concentration with time for both the upstairs and downstairs when SF₆ gas was released downstairs and Fig. 6 shows the same when the gas was released upstairs. Fig. 7 displays a schematic of interzonal air flows. This figure shows that Q_{12} is slightly higher than Q_{21} due to a small temperature difference (about 0.2°C) between the two floors. However, the situation was quite different when the living/dining room and kitchen were heated to 20.5°C while the bedrooms were kept at 16.5°C. In this case air flowed into the ground floor and tended to flow upstairs under the stack effect as shown in Fig.8. The heat transfer rate for the ground floor to the first floor and external environment was -1.1 kW, and that from the first floor to ground floor and external environment was 0.24 kW.

The house infiltration rate was estimated to be about 0.6 ac/h (98 m³/h) which is within the recommended ASHRAE standard.

TABLE 1

Experimental Conditions

House	Temperature difference between zones 1 & 2(°C)	Outside Temperature (°C)	Wind Speed (m/s)
<i>Superinsulated</i>			
Ventilation off	0.5	14.6	4
Ventilation on	0.7	20.0	3
<i>Traditional</i>			
Heating off	0.2	23.0	4
Heating on	4.0	8.5	6

5. VALIDATION OF THE TWO-ZONE AIR FLOW MEASUREMENTS

To validate the tracer gas technique used in this work some experiments were carried out under controlled conditions. For this purpose a small scale test rig was built, Fig. 9. This consisted simply of two chambers (215 litres each) connected in a closed loop by a small pump and a flow meter.

The experimental procedure was as follows. At the beginning of each experiment SF₆ tracer gas was injected into chamber 1 in which a small fan was used for mixing of tracer and air. Following the initial mixing, the pump was turned on and the two chambers were connected. SF₆/air samples were drawn from the two chambers using nylon tubing. These samples were then passed to the two SF₆ systems for analysis.

Experiments were carried out for two different values of air flow rates. The calculated and measured (using the flowmeter) flow rates for experiment 1 were 124 and 114 l/h respectively, while those for experiment 2 were 232 and 244. This corresponds to a +9% error for experiment 1 and a -5% for experiment 2. Figure 10 shows a plot of tracer gas concentration with time for experiment 1. This is similar to the accuracy obtained by Afonso *et al*¹⁴ using N₂O tracer gas and a two-compartment laboratory model.

6. KITCHEN EXTRACT FANS

Installation of kitchen extract fans is widely recommended as a remedial measure to limit condensation in houses. The purpose of using a fan is to remove moisture laden air from the zone in which water vapour is generated and also to minimise the flow of warm moist air from the lower floor to the upper floor of the house where condensation normally occurs. Most houses nowadays are provided with extract fans and it is generally assumed that the use of a 150 mm fan (extract rate about 290 m³/h) is effective in preventing migration of moisture from the kitchen to the rest of the house. There is lack of theoretical and experimental evidence to support this assumption, and the effectiveness of kitchen extract fans can only be determined by a more rigorous investigation.

To study the effect of a manually controlled kitchen extract fan on the air flows patterns in the house, two different tests were conducted. In the first test the central heating system was switched off, while in the second test only the lower floor was heated. Figure 11 displays a schematic of interzonal air flow for the first test. The use of an extract fan increases Q_{10} from 59 to 231 m³/h but has only slight effect on interzone air flow. With the extract fan in operation Q_{12} and Q_{21} were 96 and 125 m³ respectively compared to 105 and 97 m³/h with extract fan switched off.

Figure 12 shows the interzonal air flow for the second test. The limit of the extract fan is clearly shown in this figure. For a temperature difference of about 5.6°C, Q_{12} was increased from 96 to 180 m³/h while Q_{10} was reduced from 231 to 121 m³/h. The two tests indicate that the use of a 290 m³/h capacity fan does not prevent moisture movement to other rooms. Calculations were carried out to establish the minimum extract rate which would limit condensation in the kitchen and prevent air flow from the lower floor to the upper floor of the house. Condensation may be avoided if the relative humidity in a zone does not exceed the range of 60-70% (ref.13). Using an RH of 60% and a total moisture release rate of 8 kg/day, the fan extraction rate should be about 600 m³/h. This represents more than twice the rate which is recommended by the BS5250. The effectiveness of an extract fan depends on whether kitchen doors to the rest of the house are open or closed and also on the local wind speed and direction. The location of the fan in the kitchen is also important and ideally it should be positioned close to the cooker and at a high level.

7. CONCLUSIONS AND RECOMMENDATIONS

- (1) The use of the compact microcomputer SF₆ system has proved to be a reliable and practical approach for measuring air movement in houses.
- (2) We have found that the use of the portable SF₆ system is an inexpensive and simple way of estimating the two-zone air flows in houses. However, for multi-zone measurement in large buildings, the use of multiple tracer gases is preferable as it reduces the time required to make these measurements. To compare the measurement accuracy of single and multiple tracer gas techniques we intend to examine air flow between two zones (a room 4m x 4m x 2m divided by a partition containing a doorway) under a variety of temperature differences using both portable SF₆ systems and our new PFC tracer systems developed at the Polytechnic of Central London.
- (3) The air flow rate between the lower and upper floors of the traditionally built house was found to increase significantly with increasing temperature difference.
- (4) The use of manually operated kitchen extract fans was found to be ineffective in reducing air flow from the lower floor to the upper floor of the traditionally built house. Further work is required to establish the optimum extract rate of a fan for prevention of condensation in the kitchen and reduction of moisture movement to the rest of the house.
- (5) To study the interzone convection heat transfer, further experiments are needed to estimate the air movement between, for example, the conservatory and living room, where a higher temperature difference usually occurs.

ACKNOWLEDGEMENTS

The authors wish to thank Directorate General XII of the Commission of the European Communities, and C J Martin of the Energy Monitoring Company Ltd.

REFERENCES

1. HARRJE D T and GROT R A "Automated air infiltration measurements and implications for energy conservation", Proceedings of the International Conference on Energy Use Management, Pergamon Press, New York, 1977, p457-464.
2. RUYSEVELT P, LITTLER J, and CLEGG P, "Experience of a year monitoring four superinsulated houses", Conference on Superinsulated", UK ISES. 1987, p76-89.
3. HARRJE et al "Documenting air movement and infiltration in multicell buildings using various tracer gas techniques", ASHRAE trans, 1985, p91.
4. LAGUS P and PERSILY A K, "A review of tracer-gas techniques for measuring air flow in buildings", ASHRAE trans., Part 2, 1985, p91.
5. HARRJE D T, GADSBY K and LINTERIS G, "Sampling of air exchange rates in a variety of buildings", ASHRAE trans., 1982, p88.
6. PRIOR, J J, MARTIN C J and LITTLER J, "An automated multi-tracer method for following interzonal air movement", ASHRAE, 1985, Honolulu, Paper HI-85 (No.2).
7. DIETZ R N and COTE E, "Air infiltration measurements in a home using a convenient perfluorocarbon tracer gas technique", Environment International 8, 1982, p419-433.
8. LITTLER J, RIFFAT S B and EID M, "Development of a multi-tracer gas system for measuring air flows in buildings", Proceedings of CEC Contractors Meeting, Brussels, November 1986.
9. DICK J B, "Measurement of ventilation using tracer gases", Heat. Pip. Air Condit. 22, 1950, p131-137.
10. SINDEN F W, "Multi-chamber theory of air infiltration", Building and Environment 13, 1973, p21-28.
11. LITTLER J, MARTIN C and PRIOR J, "Deducing interzonal air flows from multi-tracer gas measurements", Research in Building Group Report 84/718/9, 1984.
12. RIFFAT S B, EID M and LITTLER J, "Developments in a multi-tracer gas system and measurements using portable SF₆ system", 8th AIV Conference Germany, 1987.
13. BRUNDRETT G V and GAILBRAITH G H, "Dehumidifiers in houses at Greenock, Scotland", Heating Vent. Eng. 1984, 57, p27-30.
14. AFONSO G F A, MALDONADO E A B and SKARET E, "A single tracer-gas method to characterize multi-room air exchange", Energy and Buildings 9, 1986, p200-273..

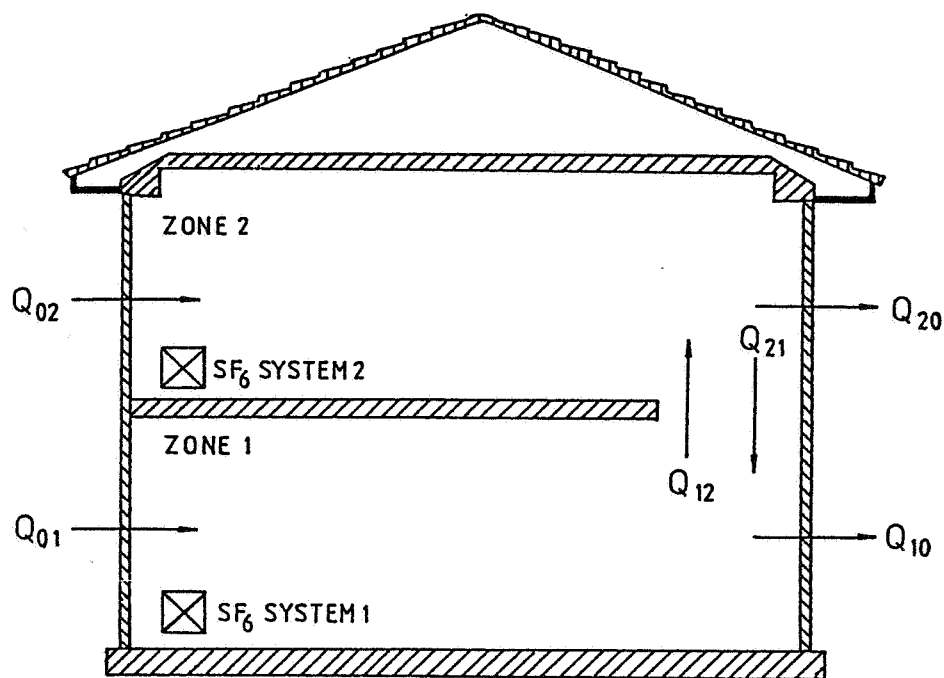


Figure 1.
Schematic of a Two-Zone House.

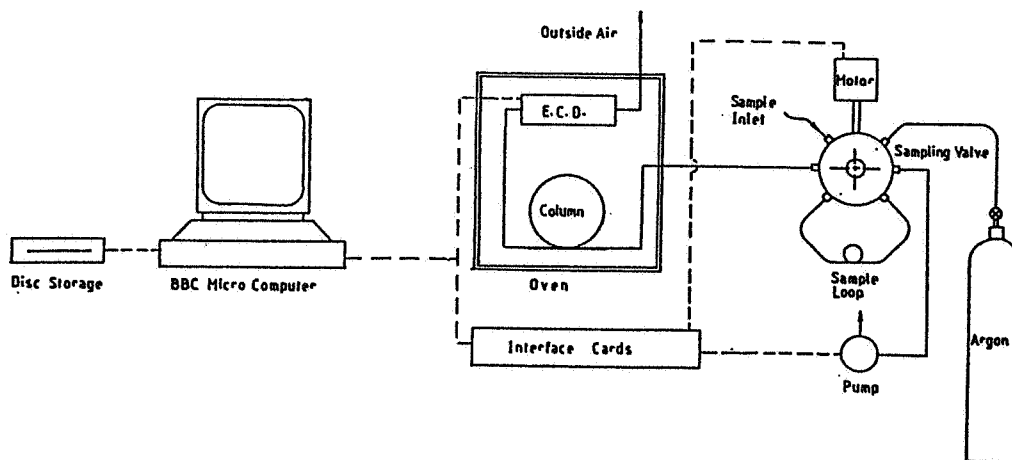


Figure 2.
Microcomputer measuring system for SF₆

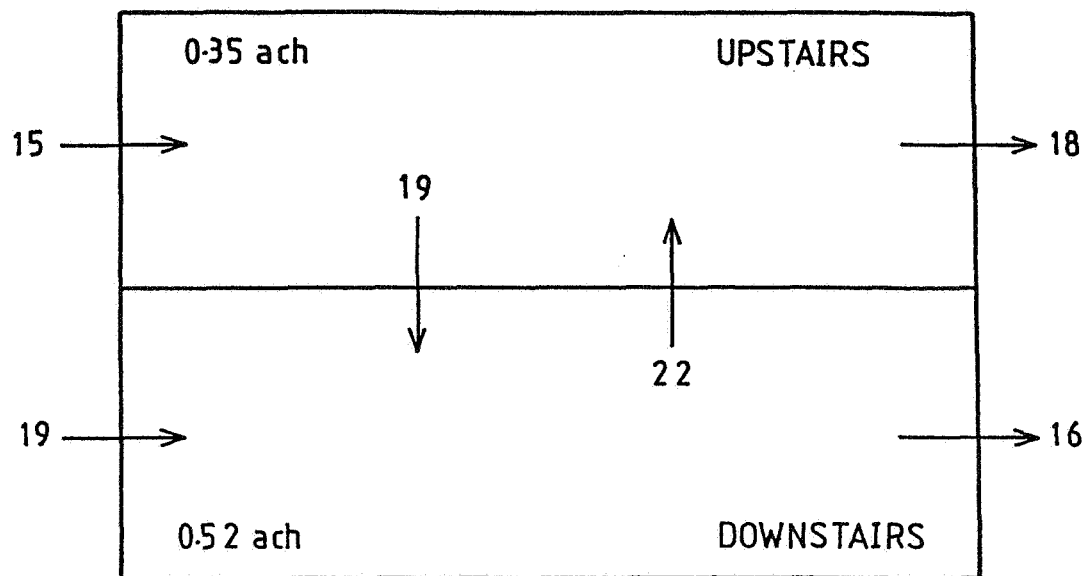


Figure 3.
Schematic of Airflows in Super-insulated House
- Ventilation System Off.

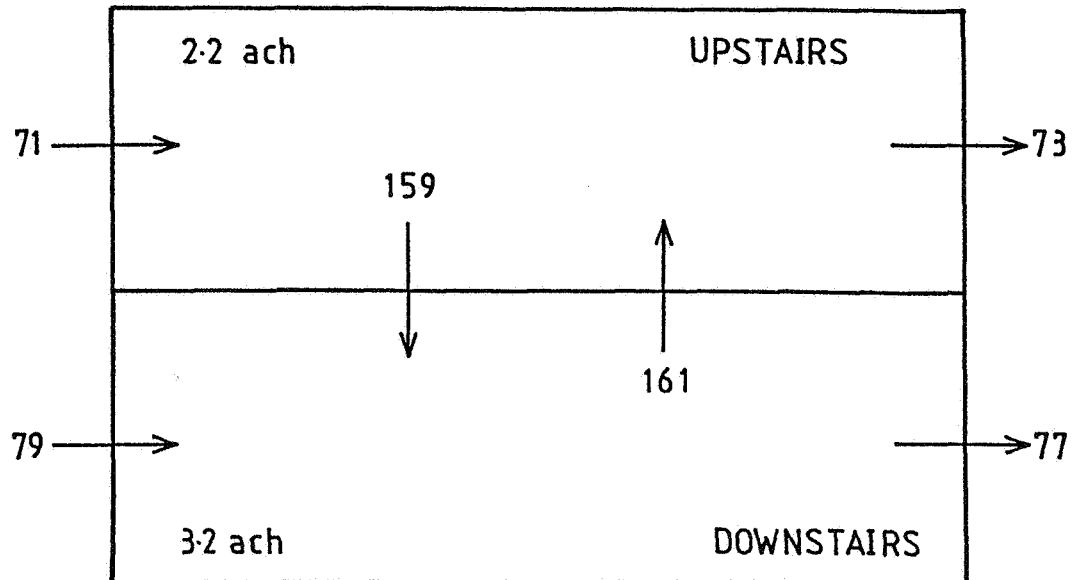


Figure 4.
Schematic of Airflows in Super-insulated House
- Ventilation System On.

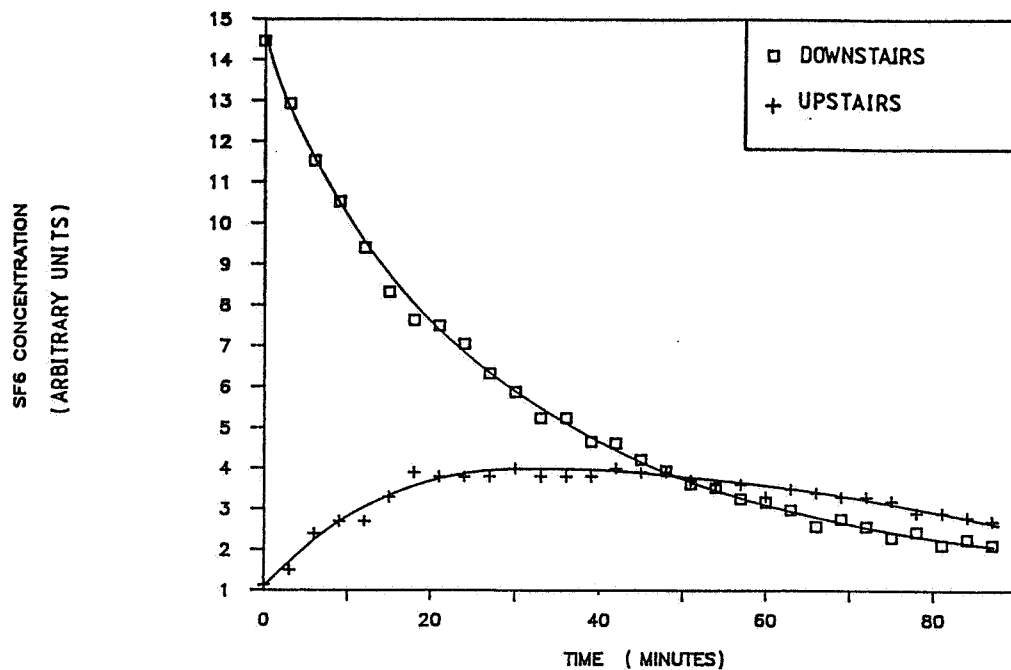


Figure 5.
Evolution of Tracer Gas Concentration in a Traditional House
- SF₆ Released Downstairs.

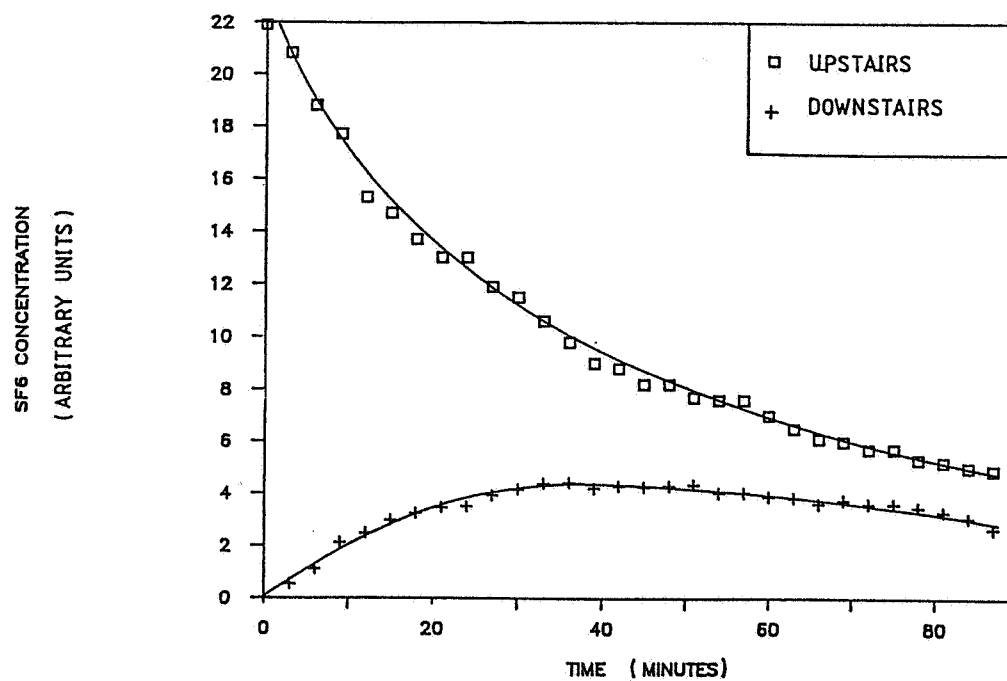


Figure 6.
Evolution of Tracer Gas Concentration in a Traditional House
- SF₆ Released Upstairs.

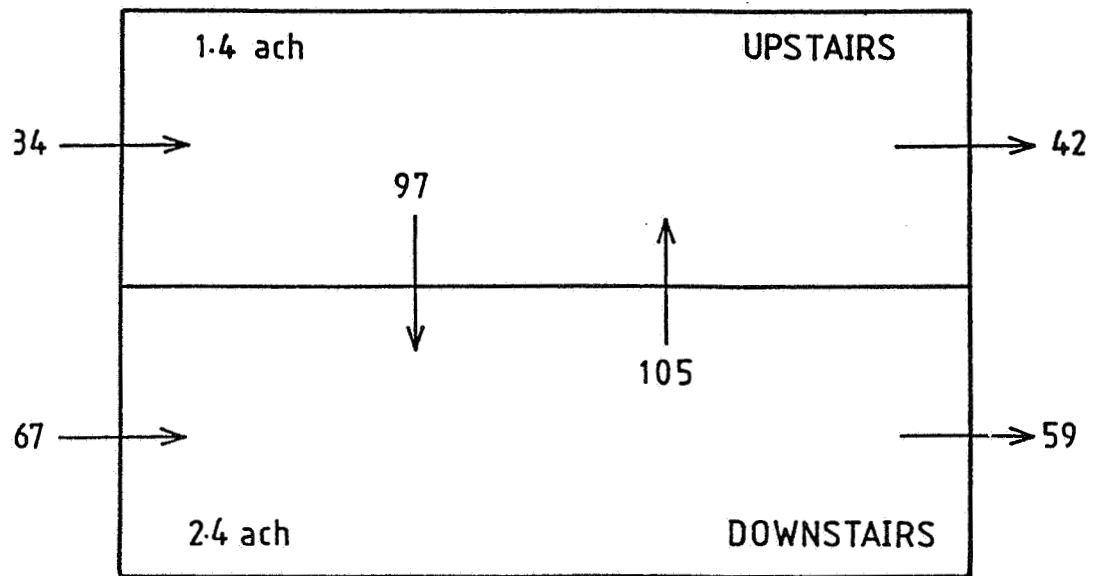


Figure 7.
Schematic of Airflows (m³/h) in Traditional House
- Temperature Difference 0.2 °C.

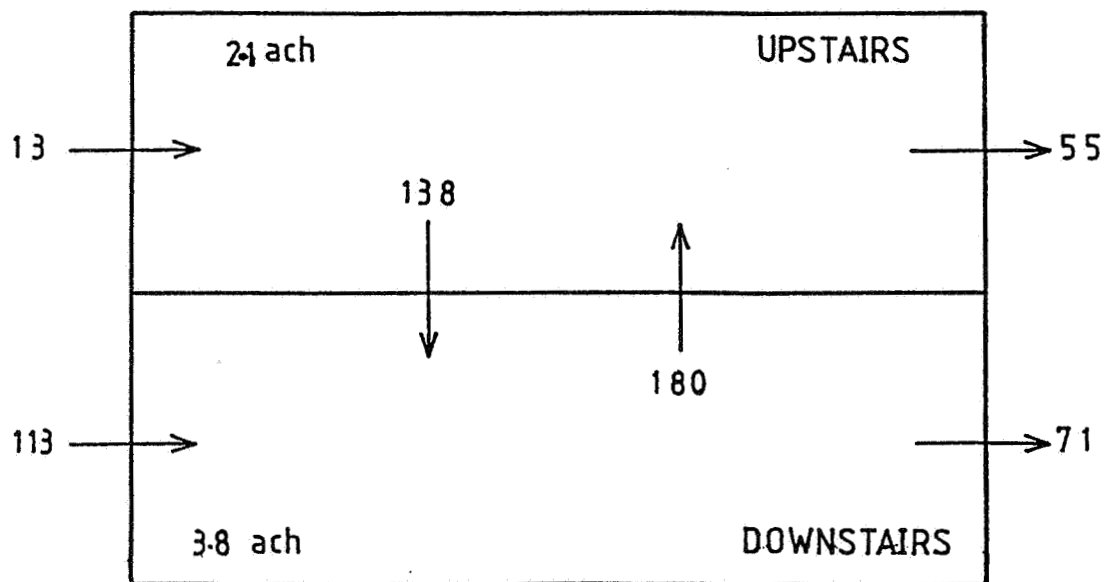


Figure 8.
Schematic of Airflows (m³/h) in Traditional House
- Temperature Difference 4.0 °C.

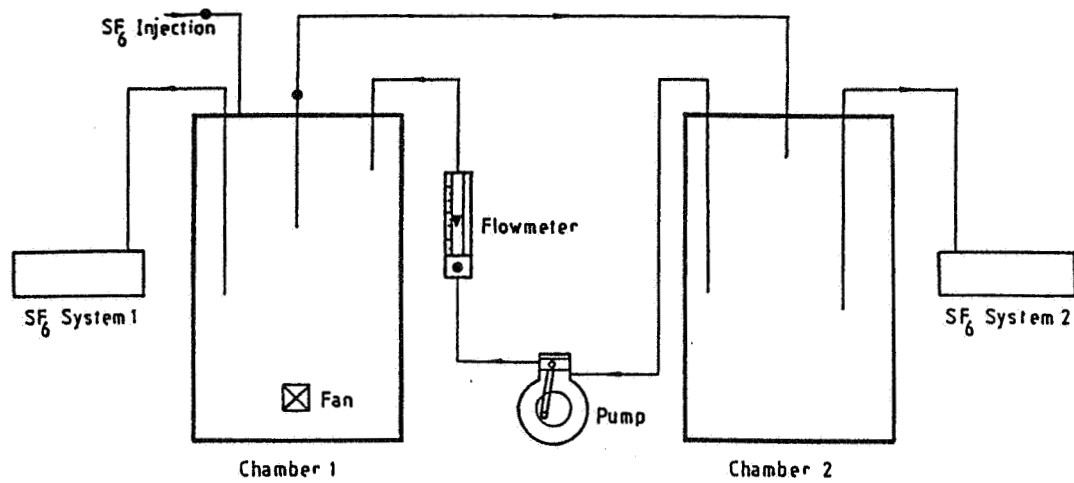


Figure 9.
Test Rig Used for Multizone Method Validation.

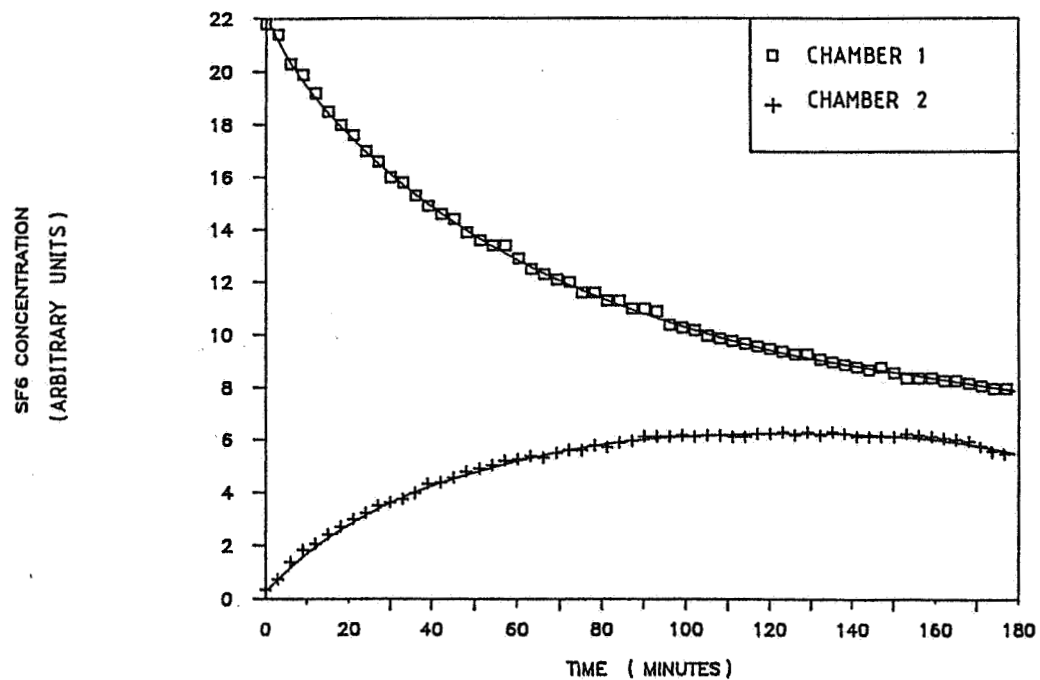


Figure 10.
Tracer Gas Concentration for Validation Experiment 1
- Calculated Flowrate, 124 l/h.

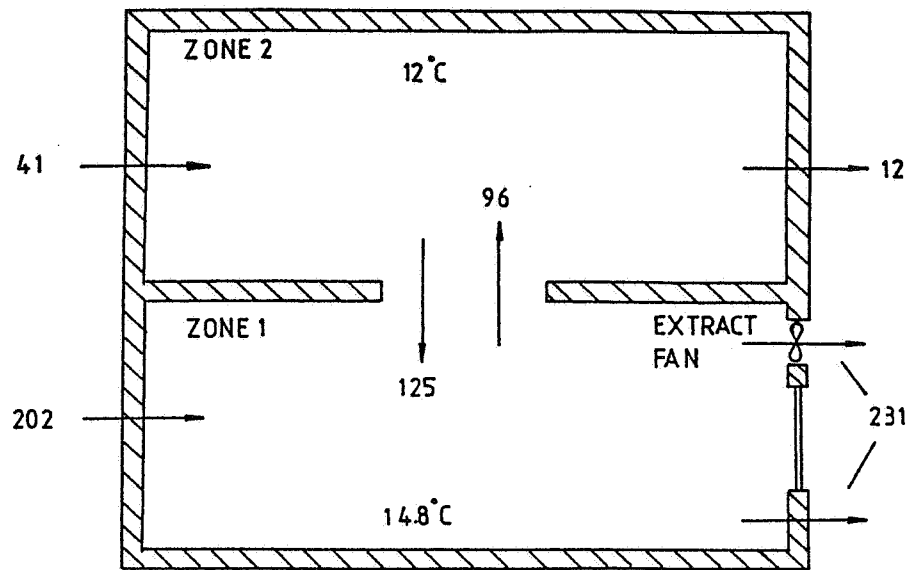


Figure 11.
Airflows with Extract Fan On and 2.8 °C Temp. Difference
- Small Change in Interzonal Airflows Compared to Figure 7.

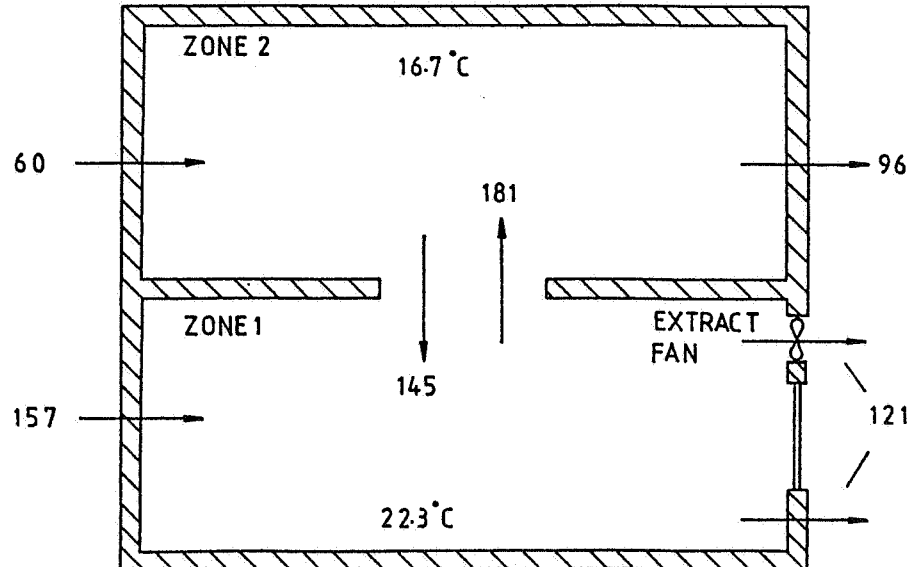


Figure 12.
Airflows at 5.6 °C Temperature Difference
- Reduced Effectiveness of Extract Fan at High Temp Difference

EFFECTIVE VENTILATION

9th AIVC Conference, Gent, Belgium
12-15 September, 1988

Poster 7

**DEVELOPMENT OF AN EFFICIENT CONTROL ALGORITHM
FOR A MULTIZONE CONSTANT CONCENTRATION TRACER GAS
AIR INFILTRATION MEASUREMENT SYSTEM**

**R. COMPAGNON
A. KOHLER
C. ROECKER
C.-A. ROULET**

**Laboratoire d'Energie Solaire et de Physique du Bâtiment
LESO-PB
Ecole Polytechnique Fédérale de Lausanne
CH - 1015 Lausanne
SWITZERLAND**

ABSTRACT

A constant concentration tracer gas (CCTG) measuring system needs a control algorithm to calculate, at each sampling time, the required tracer gas injection rate to keep the gas concentration at a target level. A new control algorithm is presented here in full details. Practical considerations concerning modifications to take into account the physical limitations of the CCTG system and the computing of the optimal control parameters are also presented.

1. INTRODUCTION

The constant concentration tracer gas technique (CCTG) is now commonly used for air flow measurement within buildings. This technique requires a control algorithm to keep the gas concentration at a target level by computing the necessary amount of tracer gas to inject. In an inhabited multizone building, the control algorithm has to respond quickly to large variations of interzonal airflows and/or outside air infiltration.

Few authors^{1,2,3} have described in detail the implemented algorithm of their CCTG systems. As far as we know, they all use common control methods such as P, PI or PID.

We present a different control algorithm, used on our CESAR* system^{4,8}. In order to improve this control method, we developed a computer program simulating a room with variable air change rate which takes the real characteristics of the CCTG system into account. This program allowed us to test some modifications of the theoretical control algorithm and to estimate its optimal parameters.

* CESAR : Compact Equipment for Survey of Air Renewal.

2. THEORETICAL APPROACH

2.1 Single zone model

In a first step, we consider a single zone. The equation governing the tracer gas concentration into the zone is :

$$V \frac{dC}{dt} = -FC + S \quad (1)$$

where V : effective volume of the zone [m³]
 C : tracer gas concentration [-]
 F : air flow leaving the zone [$\frac{m^3}{s}$]
 S : tracer gas injection into the room [$\frac{m^3}{s}$]

This equation assumes that the outside tracer gas concentration is negligible and that the air has a constant density. A perfect mixing of the tracer gas within the zone is also assumed. Even if these assumptions are not always true in real conditions, this model is sufficiently good for control purposes.

Since the CCTG system analyses the concentrations in the zone by sampling at discrete time, the differential equation (1) should be integrated over one sampling time T_s to give a difference equation :

$$C_{k+1} = a_k C_k + b_k U_k \quad (2)$$

where : C_{k+1}, C_k : tracer gas concentration at time $(k+1) T_s$ and $k T_s$ respectively [-]

$$U_k = \frac{S_k}{V} : \text{injection rate } \left[\frac{1}{s}\right]$$

$$a_k = \exp\left(-\frac{F_k}{V} \cdot T_s\right) \quad [-] \quad (3)$$

$$b_k = V \left(\frac{1 - a_k}{F_k}\right) \text{ if } F_k > 0, \quad b_k = T_s \text{ if } F_k = 0 \quad [s] \quad (4)$$

T_s : sampling time [s]

k : sample number [-]

The air flow F_k and the injection rate S_k are assumed to be constant over the integrating time interval $(k T_s; (k+1) T_s)$.

2.2 Control algorithm

The function of the control algorithm is to compute the necessary injection rate U_k to maintain the concentration at a target level denoted W_k (for complete generality the target level may also change during time : therefore it is also denoted by the sample number k). The injection rate is computed using the expression :

$$U_k = -K_s C_k + K_R X_{Rk} + K_w W_k \quad [s^{-1}] \quad (5)$$

with K_s, K_R, K_w : parameters of the control algorithm $[s^{-1}]$

X_{Rk} : an integrating term defined by the difference equation :

$$X_{Rk+1} = X_{Rk} + W_k - C_k \quad [-] \quad (6)$$

This expression is derived by minimizing the quadratic form :

$$J = \sum_{k=0}^{\infty} [(W_k - C_k) Q_e (W_k - C_k) + X_{Rk} Q_R X_{Rk} + U_k R U_k] \quad (7)$$

where Q_e, Q_R and R are weighting factors (see ⁵ for full details).

Different methods are available for the determination of the parameters K_s, K_R and K_w . We choose a method which consists of imposing the poles of the system⁵. This method is far more practical to use for two reasons :

- It is not necessary to make an arbitrary choice of the weighting factors for the quadratic form
- The computing of K_s , K_R and K_w is easier and doesn't require complex computer code as the other methods.

In fact the two poles of the system depend only on the parameters K_s and K_R . The value of the third parameter K_w doesn't have any influence on the pole location but may be used to compensate the effect of one pole.

The relations between the poles and the parameters are :

First case : Real poles Z_1 and Z_2 (Z_1 , is the compensated pole)

$$K_s = \frac{-Z_1 - Z_2 + a_k + 1}{b_k} \quad \left[\frac{1}{s}\right] \quad (8)$$

$$K_R = \frac{(1 - Z_1)(1 - Z_2)}{b_k} \quad \left[\frac{1}{s}\right] \quad (9)$$

$$K_w = \frac{K_R}{1 - Z_1} \quad \left[\frac{1}{s}\right] \quad (10)$$

Second case : Two complex conjugate poles $Z_{1,2} = \text{Re}(Z) \pm i \text{Im}(Z)$
(the real part of the pole is compensated)

$$K_s = \frac{(-2 \text{Re}(Z) + a_k + 1)}{b_k} \quad \left[\frac{1}{s}\right] \quad (11)$$

$$K_R = \frac{((\text{Re}(Z) - 1)^2 + \text{Im}^2(Z))}{b_k} \quad \left[\frac{1}{s}\right] \quad (12)$$

$$K_w = \frac{K_R}{1 - \text{Re}(Z)} \quad \left[\frac{1}{s}\right] \quad (13)$$

where a_k and b_k are defined by (3) and (4).

Through a_k and b_k the parameters are functions of the sampling time T_s and of the air change rate $\frac{F_k}{V}$. There is apparently a problem here as the control algorithm requires parameters which depend on the varying air change rates not known before measurement ! In fact the control algorithm needs only an estimation of the air change rate and the parameters are calculated once for the entire measurement procedure. This point and the optimal location of the poles will be discussed further in chapter 3.

At the beginning of the measurement procedure, the integrating term X_{Rk} has to be initialized to a certain value. Under the assumption that the initial concentration C_0 was kept constant in the past, the initial value X_{R0} is defined by :

First case : Real poles Z_1 and Z_2 (Z_1 is the compensated pole)

$$X_{R0} = \frac{1}{1 - Z_2} \cdot C_0 \quad (14)$$

Second case : Two complex conjugate poles (the real part of the poles is compensated)

$$X_{Ro} = \frac{1}{1 - \text{Re}(Z)} \cdot C_o \quad (15)$$

2.3 Advantages of the algorithm

The proposed control algorithm defined by equation (5) looks like a special case of a traditional PI control algorithm. In fact our algorithm present some advantages over the usual PI control method.

First, a faster response to a step change in the target concentration W_k is obtained by the pole compensation (Fig. 1). This property is very useful for measurement procedures using variable target concentrations in multizone buildings.

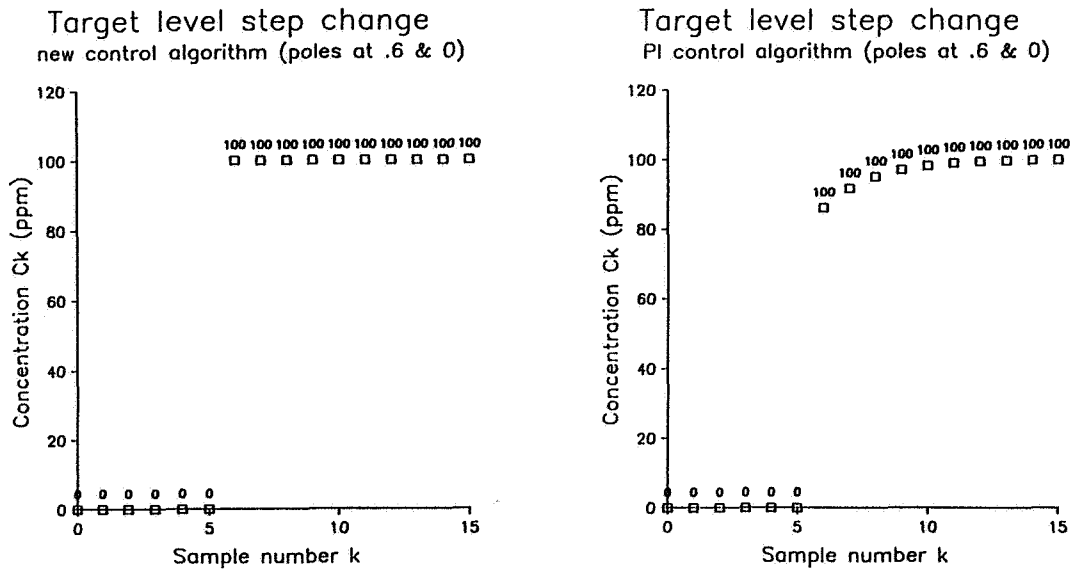


Figure 1 : Response of the control algorithm for a target level step change : the new control algorithm has a faster response than the PI control method. Points are labelled by the actual target level W_k (ppm). (values computed with 1 air change/hour and $T_s = 540$ [s]).

Secondly, the minimization of a quadratic form is well suited to generalize into a multivariable control algorithm. Thus an extension of our algorithm to the case of a multizone measurement system is not difficult. This extension is summarized as follows : equation (1) is rewritten⁶ using matrix notation :

$$V \frac{d}{dt} C = F C + S \quad (16)$$

where	V :	volumes diagonal matrix	$[m^3]$
	C :	concentrations vector	$[-]$
	F :	air flows matrix	$[\frac{m^3}{s}]$
	S :	tracer gas injections vector	$[\frac{m^3}{s}]$

The difference equation (2) becomes :

$$C_{k+1} = A C_k + B U_k \quad (17)$$

where A and B are matrixes derived from the air flows matrix F and the volumes matrix V

$$\text{and } U_k = V^{-1} S_k \quad (18)$$

From equation (17), various methods are available⁵ to compute the parameters matrixes K_s, K_R and K_w necessary for the control algorithm defined (similar to equation (5) by :

$$U_k = -K_s C_k + K_R X_{Rk} + K_w W_k \quad (19)$$

where W_k is the target concentrations vector and X_{Rk} the integrating vector defined by the difference equation :

$$X_{Rk+1} = X_{Rk} + W_k - C_k \quad (20)$$

2.4 Modifications of the algorithm

The tracer gas injection rate the CCTG is able to supply is limited to a certain range : no tracer gas can be removed from the zone and, a maximum injection rate can not be exceeded. Figures 2 and 3 show two cases where these limitations lead to large over- or under-shoots of concentration.

These problems are caused by inappropriate values of the integrating term X_{Rk} . Although the CCTG system cannot supply the necessary injection rate or remove gas to readjust the concentration to target level, the value of X_{Rk} is still incremented as if the system had no limitations. This results in too high or too low values of X_{Rk} , and it takes several steps with over or under concentration to correct the value of this term.

To avoid these problems, it is necessary to correct the value of X_{Rk} when the system is unable to supply the injection rate the control algorithm has asked for. Among the many possibilities to adjust these values, we present here two procedures we have chosen :

First case : $U_k < 0$

Negative values typically occur after a concentration overshoot due to an abrupt decrease of the air infiltration rate into the zone (Fig. 2). As seen above (equation 5), the injection rate is proportional to $W_k - C_k$ and X_{Rk} . During the whole overshoot while $C_k > W_k$, the integrating term decreases. Then, when the concentration goes below the target level, because of the low value of X_{Rk} , the injection rate remains negative and it takes several steps with $C_k < W_k$ to raise the value of X_{Rk} to its new stationary value allowing positive injection rate to be computed.

To avoid this undershooting, the integrating term could be adjusted just before the decreasing concentration crosses the target level. Thus, our procedure works as follows :

Overshoot (1st case) (target level: 100 ppm)
without modification

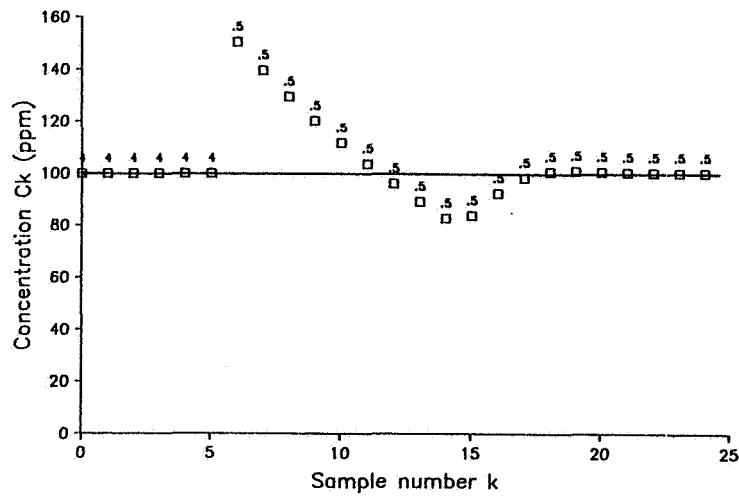


Figure 2 : Concentration overshoot due to an abrupt decrease of the air change rate. Points are labelled by the actual air change rate [h^{-1}] (values computed with $V = 80 \text{ [m}^3\text{]}$ and $T_s = 540 \text{ [s]}$).

Overshoot (2nd case) (target level: 100 ppm)
without modification

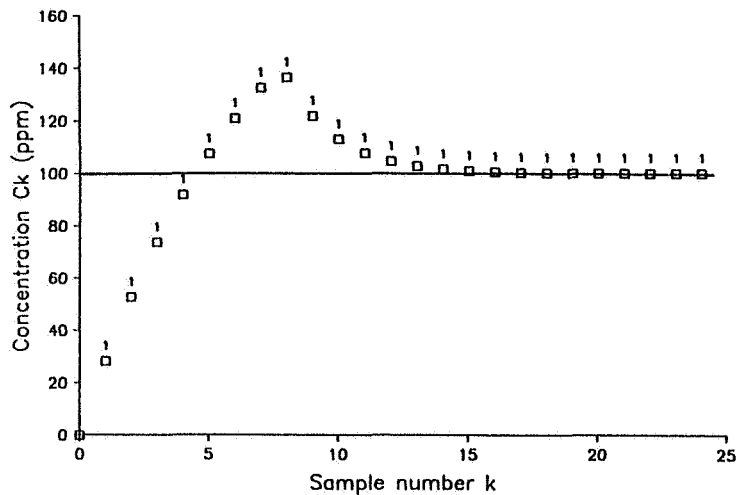


Figure 3 : Concentration overshoot due to the limiting effect of the maximum injection rate U_{\max} the CCTG system is able to supply. All points are labelled by the actual air change rate [h^{-1}] (values computed with $V = 200 \text{ [m}^3\text{]}$, $T_s = 540 \text{ [s]}$ and $U_{\max} = 5.67 \cdot 10^{-8} \text{ [s}^{-1}\text{]}$). These values lead to the maximum concentration increase at the first step : $C_1 = b \cdot U_{\max} = 28,4 \text{ (ppm)}$).

Overshoot (1st case) (target level: 100 ppm)
with modification

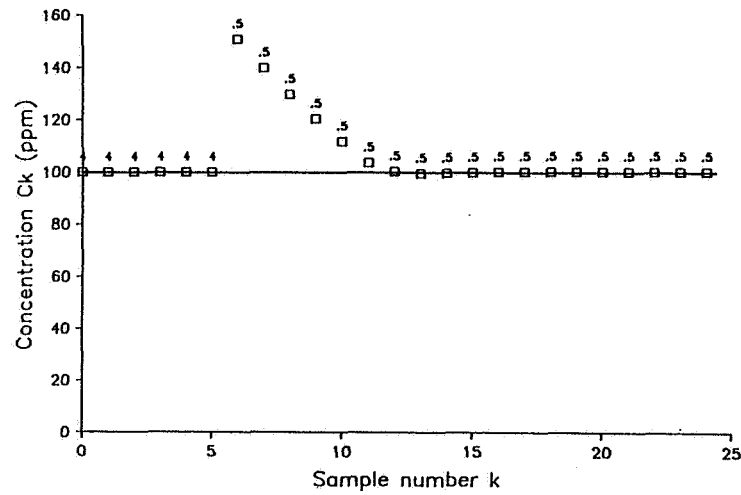


Figure 4 : Effect of the first modification of the control algorithm (compare with fig. 2). All points are labelled by the actual air change rate [h^{-1}]. (values computed with $V = 80 \text{ [m}^3\text{]}$ and $T_s = 540 \text{ [s]}$).

Overshoot (2nd case) (target level: 100 ppm)
with modification

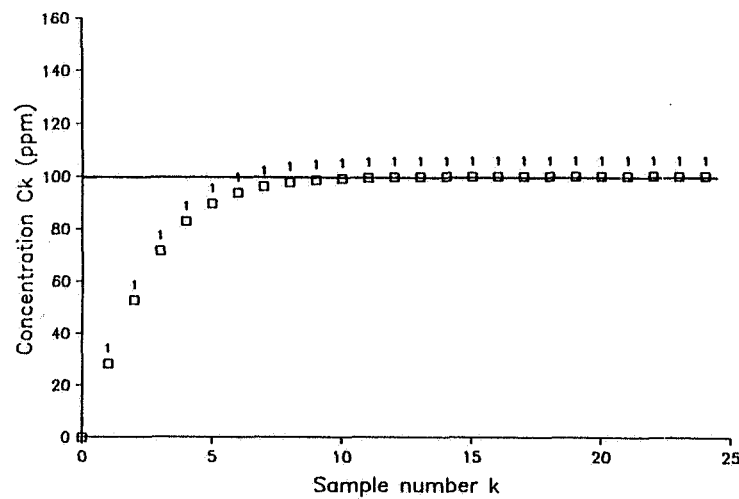


Figure 5 : Effect of the second modification of the control algorithm (compare with fig. 3). All points are labelled by the actual air change rate [h^{-1}] (values computed with $V = 200 \text{ [m}^3\text{]}$, $T_s = 540 \text{ [s]}$ and $U_{\max} = 5.67 \cdot 10^{-8} \text{ [s}^{-1}\text{]}$).

Whenever the control algorithm computes a negative injection rate, the actual infiltration rate is estimated and the concentration for the next step can be extrapolated. If, without any gas injection, the extrapolated concentration is still above target level, nothing is done. But in the other cases, the integrating term is forced to a value leading, through the use of control equation (5), to the necessary injection rate to reach the target level. The following relations are used for this procedure :

(assuming $U_k < 0$)

estimated actual air change rate :

$$n_{\text{est}} = \frac{1}{T_s} \cdot \text{Ln} \left(\frac{C_{k-1} + T_s \cdot \max(0; U_{k-1})}{C_k} \right) \quad \left[\frac{1}{s} \right] \quad (21)$$

(if $U_{k-1} > 0$ n_{est} underestimates the true air change rate)

predicted concentration :

$$C_{p\ k+1} = C_k \exp(-n_{\text{est}} \cdot T_s) \quad [-] \quad (22)$$

necessary injection rate (if $C_{p\ k+1} < W_{k+1}$) :

$$U_k^* = \frac{1}{T_s} C_k \left(\frac{W_{k+1}}{C_{p\ k+1}} - 1 \right) \quad \left[\frac{1}{s} \right] \quad (23)$$

new value for the integrating term :

$$X_{Rk}^* = \frac{U_k^* + K_s C_k - K_w W_k}{K_R} \quad [-] \quad (24)$$

Since the actual air change rate is computed over one sampling time only, its value is sensitive to any measurement error. Therefore equation (23) gives in fact an underestimate of the necessary injection rate to avoid large effects from small measurement errors (it is always easier to add some gas at the next step than to remove some !).

A comparison between fig. 2 and fig. 4 shows the effect of this procedure.

Second case $U_k > U_{\text{max}}$

This case may occur at the beginning of a measurement on a large zone or when the air infiltration rate is very high. For extreme cases, the target concentration will never be reached.

Figure 3 illustrates the problem : the increase of the concentration is limited by U_{max} while the integrating term increases. When the concentration reaches the target level, the high integrating term value forces the control algorithm to inject too much gas. This leads to a concentration overshoot until the integrating term finds its stationary value again.

To avoid this phenomenon, each time the control algorithm asks for an injection rate higher than U_{\max} , the integrating term is forced to a proper value. This value is calculated so that, when used in the control equation (5), the maximum possible injection rate U_{\max} results.

The new value of the integrating term is then :

(assuming $U_k > U_{\max}$)

$$X_{Rk}^* = \frac{U_{\max} + K_s C_k - K_w W_k}{K_R} \quad [-] \quad (25)$$

As shown in figure 5, this procedure gives good results.

3. ALGORITHM TESTING

3.1 Simulation program

In order to test the algorithm, a simulation program was developed⁷. The program simulates a zone with variable air change rate and takes into account the real characteristics of the CCTG system (e.g. time delays due to the pipes, gaz analyzer response time, random errors on the measured concentration, and maximum injection rate U_{\max}).

The tracer gas mixing process within the zone is also simulated using a simple model : The tracer gas is injected in a small fictious volume which is connected to the zone by a constant air flow rate. The small fictious volume and the zone volume are both assumed perfectly mixed. A good mixing into the zone is achieved when the concentration within the fictious volume is close enough to the concentration within the zone. The mixing time constant is defined by :

$$\tau_{mx} = \frac{v}{f} \text{ [s]} \quad (26)$$

where

$v :$	fictious volume	$[m^3]$
$f :$	constant air flow between the fictious volume and the zone	$[\frac{m^3}{s}]$

According to Sandberg and Blomqvist³, this time constant typically lies between 30 [s] and 180 [s]. It can be adjusted by giving proper values to v and f . By assuming f equal to the flow rate produced by the small mixing fan used in the zone ($f \approx 0,015 [\frac{m^3}{s}]$ for the fans we use) the fictious volume lies in the interval between 0,45 and 2,7 $[m^3]$.

3.2 Results

Chapter 2 describes the control algorithm but gives no information on the location of the poles and the estimated air change rate. They are both required to compute the three parameters K_s , K_R and K_w . To investigate these topics, we used our program to systematically try all the possible poles locations for different estimated air change rates. All simulations were performed under the operating conditions listed in table 1.

Sampling time	T_s	= 540	[s]	
Volume of the zone	V	= 80	[m ³]	
Initial concentration	C_o	= 0	(ppm)	
Target concentration	W	= 100	(ppm)	
Fictitious volume	v	= 0.9	[m ³]	
				} $\tau_{mx} = 60$ [s]
Air flow induced by the fan	f	= 0.015	[$\frac{m^3}{s}$]	
Measurement random error	gaussian noise	$\mu = 0$	(ppm)	
		$\sigma = 1$	(ppm)	
Time delays due to the pipes	5.2	[s]		
Analyzer response time	8	[s]		
Maximum injection rate	U_{max}	= $1.42 \cdot 10^{-7}$	[$\frac{1}{s}$]	

Table 1 : Operating conditions used for our simulations.

To remain close to the conditions observed in inhabited buildings, the simulations were performed over 320 samples ($320 \cdot 540$ [s] = 48 hours) with variable air change rates as shown in fig. 6.

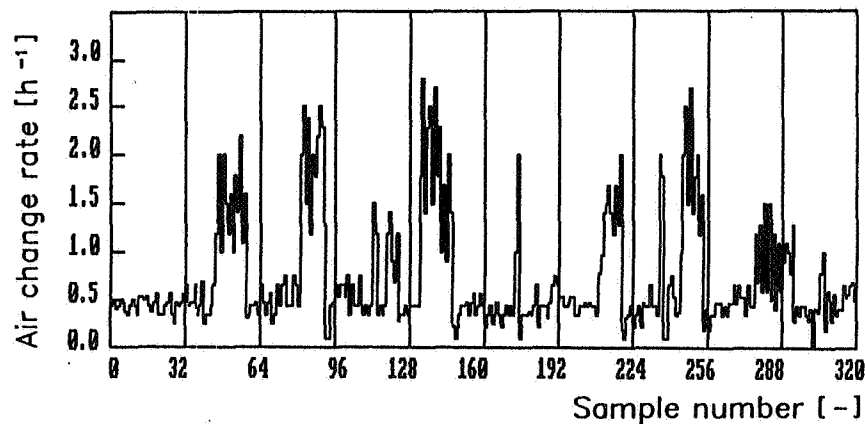


Figure 6 : Variable air change rate used for our simulations.

The simulations results were characterized by three numbers :

- a) the difference between the mean measured concentration and the target level :

$$d = \langle C \rangle - W \quad [-] \quad (27)$$

- b) the concentration standard deviation from the target level :

$$s = \sqrt{\langle (C - W)^2 \rangle} \quad [-] \quad (28)$$

- c) the total negative tracer gas volume the control algorithm wanted to remove from the zone :

$$v_{neg} = V \cdot T_s \cdot \sum_{k=1}^{320} \min(0; U_k) \quad [m^3] \quad (29)$$

$$(\langle \rangle \text{ denotes the "mean" operator} = \frac{1}{N} \sum_{k=1}^N \text{ with } N \text{ the number of samples})$$

It is clear that the optimal control algorithm would lead to ($d = 0, S = 0, v_{neg} = 0$) ! The set of simulations can then be investigated to find out the poles location leading to the smallest vector (d, s, v_{neg}). Figures 7 to 12 present different maps showing the values d, s and v_{neg} for all locations of the poles in real and complex planes.

By studying the maps, in the complex plane (fig. 7 to 9) no complete overlapping appears for the best regions for d, s and v_{neg} . Therefore it is not advisable to locate the poles somewhere in the complex plane.

In the real plane (fig. 10 to 12), the three best regions lie closer to each other. We choose the poles location $Z_1 = 0,6$ (compensated pole) and $Z_2 = 0$ as the "best" values to compute the parameters of our algorithm.

It also appeared that the estimated air change rate required to compute the parameters has only a small influence on the simulation results. It is possible to understand this by looking at figure 13 which shows the dependance of the parameters from the estimated air change rate.

Parameter K_w is the most sensitive parameter but it does not have a strong influence because the dynamic properties of the control algorithm are essentially determined by K_s and K_R which are much less sensitive to the estimated air change rate. It is anyhow important to keep in mind that K_w has a strong influence when a target level step change occurs (e.g. at the beginning of the measurement procedure). It is therefore advisable to choose the minimum expected air change rate for the considered zone.

These conclusions still apply in case of bad mixing ($\tau_{mx} = 180$ [s]) and for other sets of air change rates if their values lie between 0 and 4 [h^{-1}]. For larger variations of air change rates, a recalculation of the control parameters should sometimes be undertaken during the measurement. This procedure and the criteria to apply it, will be investigated during the continuation of this work.

Figure 14 shows the concentrations during 12 hours of a real CCTG measurement using our algorithm with poles located at $Z_1 = 0,6$ $Z_2 = 0$, with an estimated air change rate of 0.1 [h^{-1}]. A fast response to changes in air flow rates can be observed.

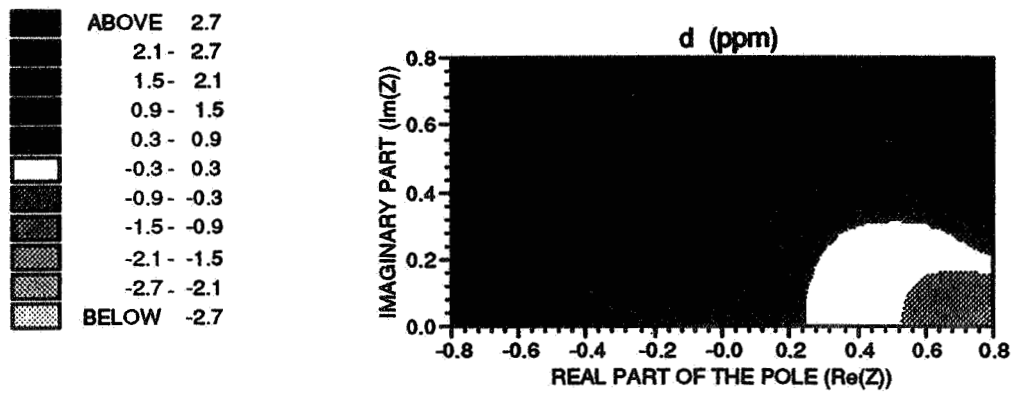


Figure 7 : Difference between the mean measured concentration and the target level in (ppm) for poles located in the complex plane. (Estimated air change rate used for the calculation of the control parameters : $0.5 [h^{-1}]$).

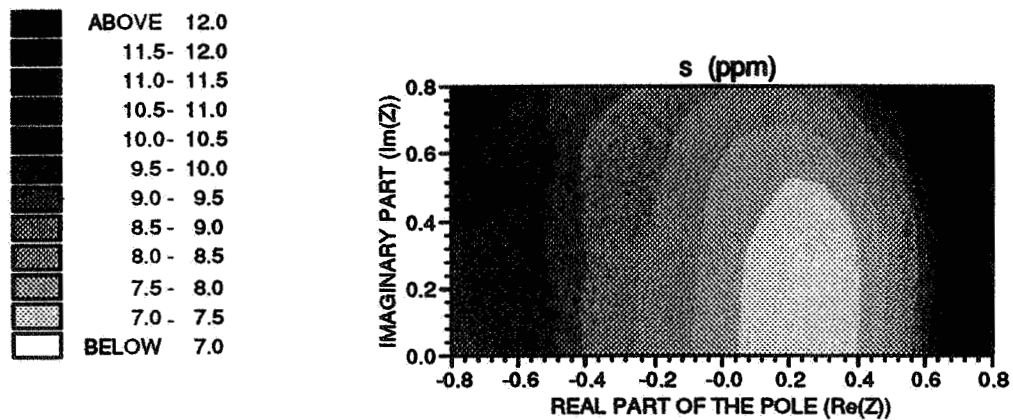


Figure 8 : Concentration standard deviation from the target level in (ppm) for poles located in the complex plane. (Estimated air change rate used for the calculation of the control parameters : $0.5 [h^{-1}]$).

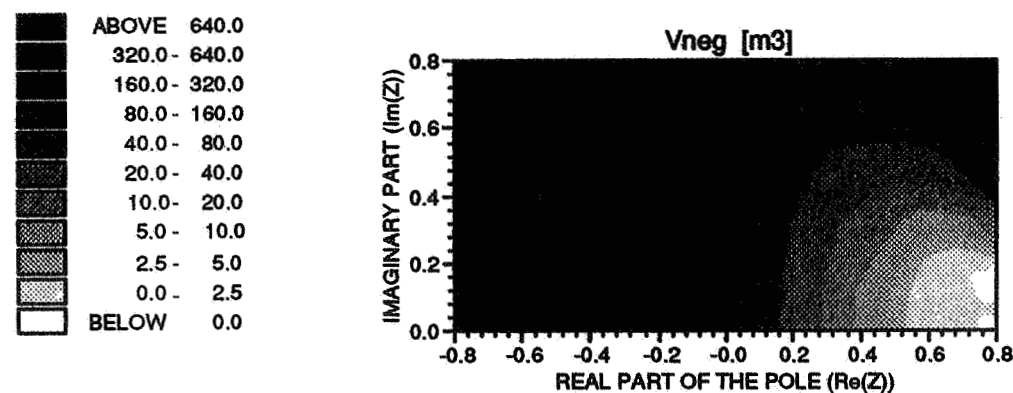


Figure 9 : Total negative tracer gas volume the control algorithm wanted to remove from the zone for poles located in the complex plane. (Estimated air change rate used for the calculation of the control parameters : $0.5 [h^{-1}]$).

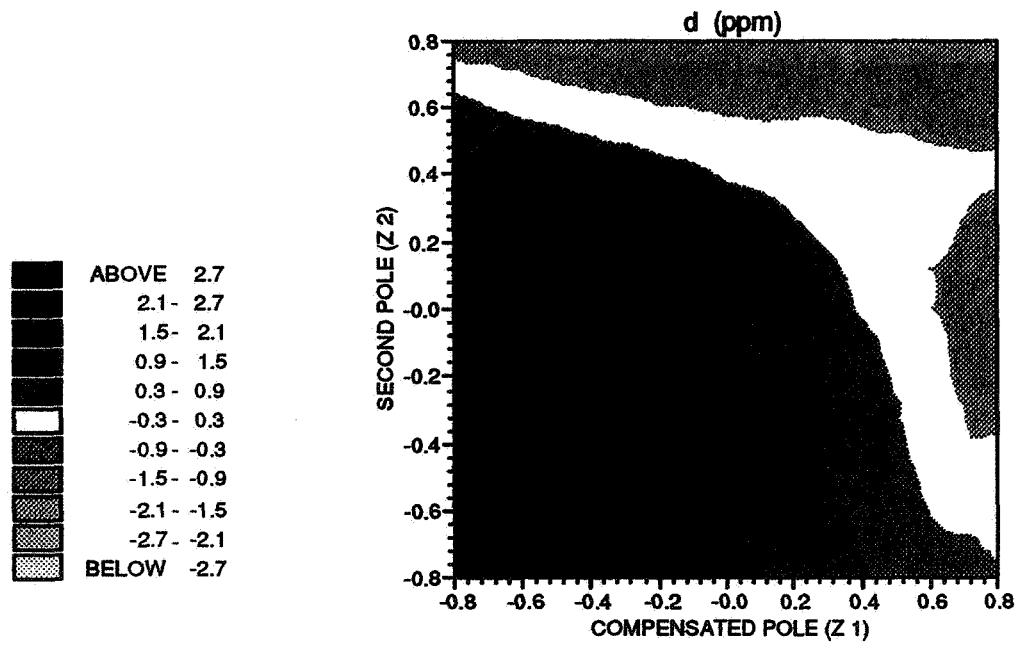


Figure 10 : Difference between the mean measured concentration and the target level in (ppm) for poles located in the real plane. (Estimated air change rate used for the calculation of the control parameters : $0.5 \text{ [h}^{-1}\text{]}$).

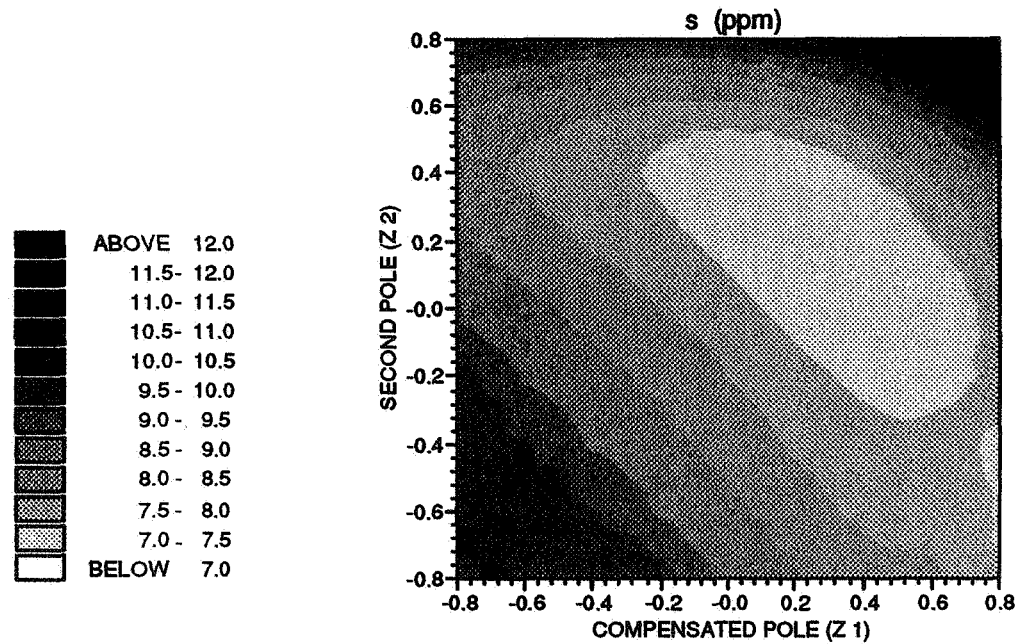


Figure 11 : Concentration standard deviation from the target level in (ppm) for poles located in the real plane. (Estimated air change rate used for the calculation of the control parameters : $0.5 \text{ [h}^{-1}\text{]}$).

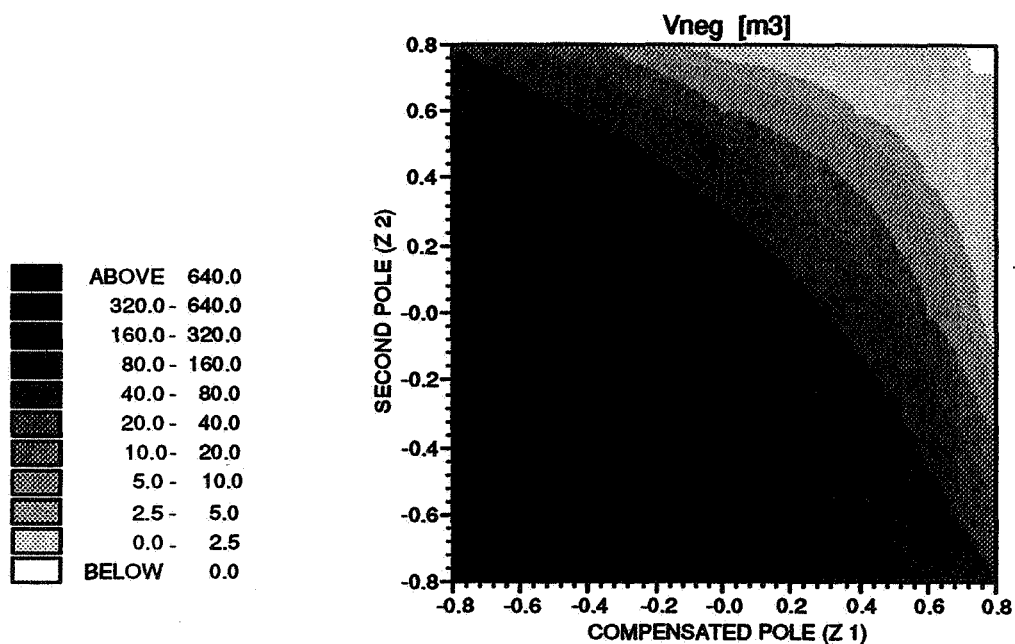


Figure 12 : Total negative tracer gas volume the control algorithm wanted to remove from the zone for poles located in the real plane. (Estimated air change rate used for the calculation of the control parameters : $0.5 \text{ [h}^{-1}\text{]}$).

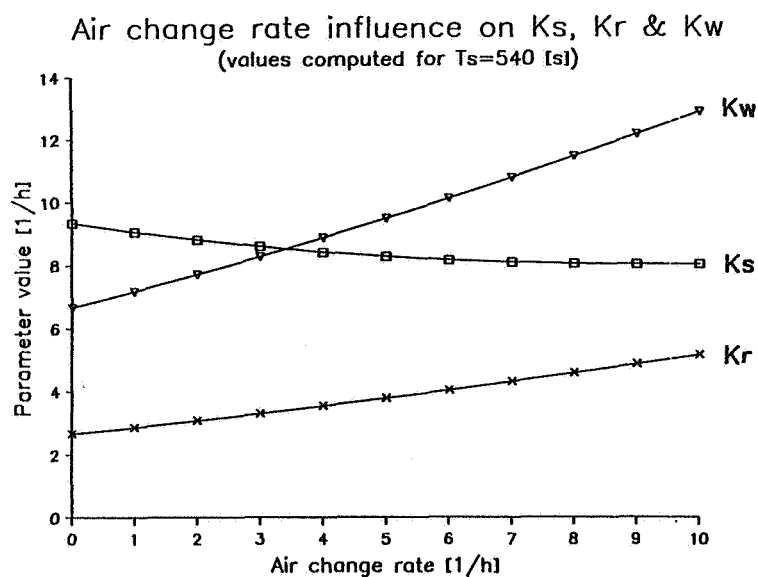


Figure 13 : Values (expressed in $[h^{-1}]$) of the control parameters for various estimated air change rates (poles located at $Z_1 = 0.6$ and $Z_2 = 0$).

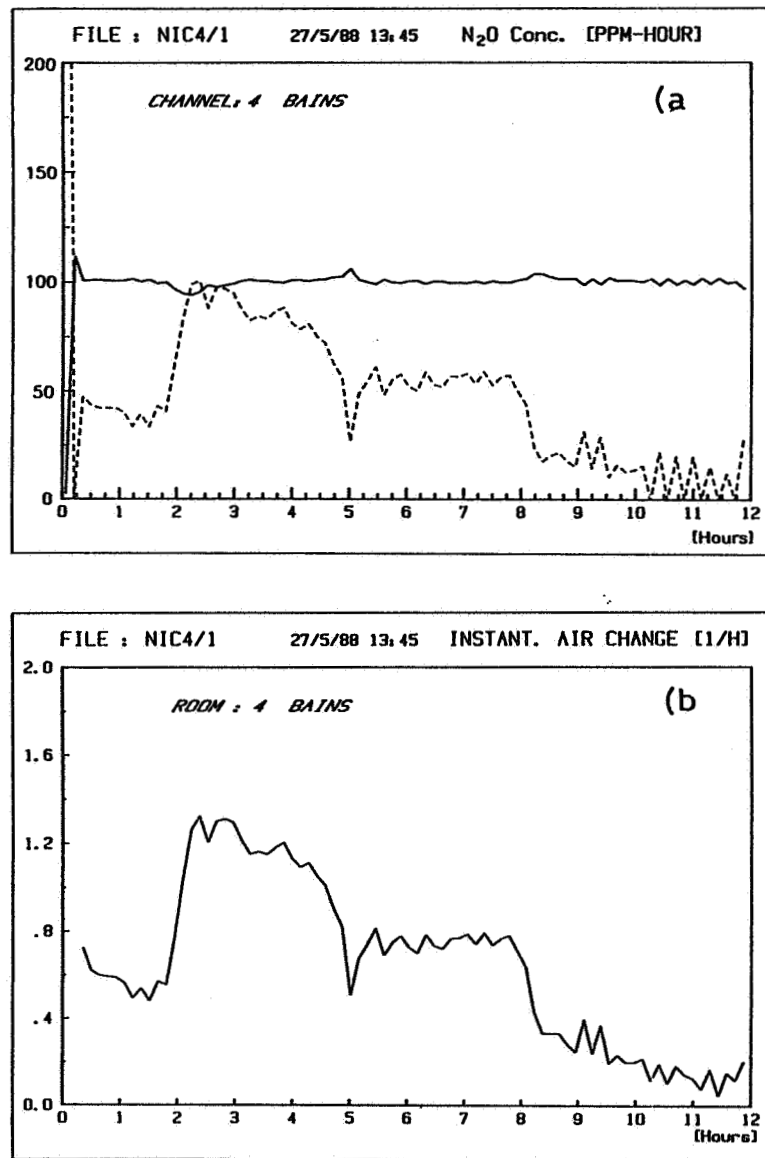


Figure 14 : a) Concentrations measured during 12 hours within a bathroom ($V = 14.1 \text{ [m}^3\text{]}$, target level = 100 ppm, $T_s = 525 \text{ [s]}$). Dotted line shows the tracer injection rate (arbitrary units).
 b) Air change rates deduced from the CCTG measurement. Large air change rate variations due to the mechanical ventilation system can be observed.

We also tried to use the multizone control algorithm briefly presented in chapter 2.3. The first trial did not improve significantly the control ability. There are two reasons for this result :

- the control matrixes K_S K_R and K_w are diagonally dominant : the off-diagonal elements lie one order of magnitude under the diagonal elements which are close to the values of the single zone algorithm.
- The CCTG system is only able to analyze and to dose with tracer gas one zone at a time, which implies that the multizone control algorithm is not completely used. A CCTG system able to analyze and dose many zones simultaneously would take advantage of this multizone algorithm.

Although further work should be useful to refine these findings, it appears that the single zone control algorithm can be used for multizone CCTG system : all zones are simply independently controlled.

4. CONCLUSIONS

A complete control algorithm has been developed and the values required to compute its parameters have been systematically investigated. Some improvements of the theoretical algorithm were developed to avoid inappropriate control behaviour due to the physical limitations of the CCTG system.

The presented algorithm is now implemented on our multizone CCTG system CESAR^{4,8}. The control algorithm considers each zone independently.

Further work is necessary to develop an automatic parameters recalculation procedure when large variations in air change rate are encountered. The possibility for the algorithm to be extended to a multivariable control algorithm also needs further investigations. It is probable that this algorithm would be useful for multizone CCTG system able to analyze and dose many zones simultaneously.

REFERENCES

- 1 Bohac D.L., Harrje D.T.
Improving the accuracy of a constant concentration tracer gas system
In 6th AIC Conference "Ventilation strategies and measurement techniques"
1985 (Airbase # 1796)
- 2 Bohac D.L.
The use of a constant concentration tracer gas system to measure
ventilation in buildings
PV/CEES Report N° 205, Princeton Univ., 1986 (Airbase # 2076)
- 3 Sandberg M., Blomqvist C.
A quantitative estimate of the accuracy of tracer gas methods for
the determination of the ventilation flow rate in buildings
In Building and Environment, Vol. 20 N° 3, 1985 (Airbase # 1947)
- 4 Scartezzini J.-L., Roulet C.-A., Jolliet O.
Continuous air renewal measurements in different inhabited buildings
In 6th AIC Conference "Ventilation strategies and measurement techniques"
1985 (Airbase # 1784)
- 5 Bühler H.
Réglages échantillonnés (Volume 2 : traitement dans l'espace d'état)
Presses Polytechniques Romandes, Lausanne, 1983.
- 6 Sherman M.H., Grimsrud D.T., Condon P.E., Smith B.V.
Air infiltration measurement technique
In 1st AIC Conference "Instrumentation and measuring techniques"
1980 (Airbase # 611)
- 7 Kohler A.
Simulation d'un dispositif de mesure des taux de renouvellement d'air
en vue de tester des algorithmes de régulation
Travail de diplôme d'ingénieur physicien, EPFL, 1987
- 8 Roulet C.-A., Scartezzini J.-L.
Measurement of air change rate in an inhabited building with a constant
tracer gas concentration technique
In ASHRAE trans. 93 part 1, 1987.

EFFECTIVE VENTILATION

9th AIVC Conference, Gent, Belgium
12-15 September, 1988

Poster 8

A STUDY OF THE VENTILATION CHARACTERISTICS OF A
SUSPENDED FLOOR.

J.P. LILLY, J.M. PIGGINS, R.J. STANWAY

British Gas Plc
Watson House Research Station
Peterborough Road
London SW6 3HN

A STUDY OF THE VENTILATION CHARACTERISTICS OF A SUSPENDED FLOOR

By J.P. Lilly, J.M. Piggins, R.J. Stanway.

To be presented at:
The 9th Annual Conference of the
Air Infiltration and Ventilation Centre,
Gent, Belgium.
September, 1988.

ABSTRACT

The ventilation and leakage characteristics of suspended floors are not well documented. As part of a larger study of air flows in housing, the air flow through a suspended floor has been investigated under a number of conditions and methods of ventilation.

The leakage of the suspended floor and the space beneath it has been measured and is compared with the house leakage.

The infiltration to the underfloor space and also the infiltration to the house from the underfloor space through the suspended floor is investigated with natural ventilation and also with different modes of mechanical ventilation.

The leakage of the underfloor space was varied to assess its influence on the ventilation characteristics of the suspended floor and hence on the air quality in the house.

The results could also be of use in the investigation of infiltration of radon into dwellings with suspended floors.

1. INTRODUCTION

The importance of the influence of ventilation on energy conservation, safety, indoor air quality, thermal comfort and heating system design, is well known.

For example, reduced ventilation can have an adverse effect on indoor air quality [1], protective pressure techniques can exclude airborne pollutants [2], and there is also interest in the ingress of pollutants into a dwelling [3].

However, very little is known about leakage and ventilation of one important house component, the underfloor space and its influence on the whole house ventilation.

The Watson House Research Station of British Gas plc has developed methods to measure the leakage [4] and ventilation characteristics [5] of houses. The British Gas ventilation measurement system, Autovent, was adapted to measure house, underfloor and through-floor ventilation rates simultaneously.

The work was undertaken for two reasons. Firstly, more knowledge about underfloor ventilation was needed to assist in the verification of mathematical models of whole-house ventilation. Secondly, data was required giving the relative proportions of house infiltration from beneath a suspended floor due to stack and wind effects and the influence of different forms of mechanical ventilation. However, the data could also be of interest to those investigating the ingress of pollutants into houses.

2. THE TEST FACILITY

The work described in this report was carried out in the test house a view of which is shown in Figure 1. This detached house, which measures 9x6x5 metres contains nine rooms, four of which are bedrooms as shown in the plan of the house in Figure 2.

The construction is of brick and is part solid, part cavity wall. The ground floor is suspended and the house is well carpeted throughout. The house is equipped with a wet central heating system and a warm air system.

The Watson House Autovent [5] was installed in the dining room and was used to measure house ventilation rates and determine flows across the suspended ground floor.

2.1 The underfloor space

The underfloor space, shown schematically in Figure 3, covers a total area of 54m². Its height is 0.94 metres to the joists and 1.1 metres to the suspended floor.

The floor of the space is concrete and the surrounding walls are unplastered concrete block. There is an irregularly shaped partition wall dividing the space into two unequal volumes. This wall, which is also built of concrete block, has holes in it at regular intervals, which allows air movement between the two sections.

The underfloor space is ventilated by seven circular ducts, each of which is 0.15 metres in diameter. There are four ducts in the west wall and three in the east wall. Apart from these ducts, there are no obvious ventilation pathways in the surrounding walls which are in good condition with sound cement work. Similarly, visual inspection of the suspended floor from underneath shows it to be also in sound condition with no obvious leakage paths.

Access to the space is via a trapdoor situated in the hall floor.

3. EXPERIMENTAL METHOD

3.1 Leakage Measurements

Two Watson House leakage testers, see Figure 4, were positioned in the hall and were connected to the underfloor space by a leak-tight seal in the trapdoor.

The leakage of the underfloor space was varied by progressive sealing of the seven vents. In this way, a series of eight sets of leakage measurements was made; the first with none of the vents sealed. Each successive set of measurements involved the sealing of an extra vent, until all seven vents were sealed.

Figure 5 shows how, for each stage of sealing, the leakage $Q(\text{m}^3/\text{s})$ varies with the static pressure difference $\Delta P(\text{Pa})$ between the underfloor area and the house.

The relationship between Q and ΔP is given by:-

$$\Delta P = AQ^2 + BQ + C$$

The curves in the graph have been fitted to the data, using a statistical quadratic curve fit [6].

The coefficients of the curve fits and Q_{50} the leakage at a pressure difference of 50Pa are shown in Table 1, which also shows the same information for the house leakage. Inspection of these values of Q_{50} shows that each vent contributes a similar amount of leakage and that UF_1 , the leakage across the suspended floor, is roughly equal to the additional leakage contributed by the seven vents ($UF_8 - UF_1$).

From Table 1 it is interesting to note that the Q_{50} for the total underfloor leakage with all the vents unsealed and the house have similar values of 1.03 and 1.13 m^3/s respectively.

3.2 Ventilation Measurements

The Autovent, shown in Figure 6, was used in its dual tracer gas mode. N_2O was used as the primary gas, with which ventilation rates were measured using the constant concentration technique. The secondary gas, SF_6 , was continuously injected in the underfloor space and was used to determine the fraction of ventilation air entering the house through the ground floor.

As mentioned, the underfloor space shown schematically in Figure 3, is divided into two unequal volumes by the partition wall. One section (UHAL) lies beneath the kitchen/hall area, the other section (UDIN) is beneath the lounge/dining room area. An injection line was installed in each section in an asymmetric manner in the NE and SW corners. Each injection line was connected to a desk fan which ensured adequate mixing in the sections.

An additional injection line was installed in the UDIN section, through which the second tracer gas was injected at a constant rate. The resultant gas concentrations were monitored in both UDIN and UHAL, and the two values were found to be very similar, thus showing that there was good mixing in the underfloor space.

The initial tests investigated how the air flow through the suspended floor was affected by natural and mechanical ventilation, house pressurisation and depressurisation, wind speed, stack effect and different degrees of underfloor leakage. There are inevitable gaps in the measurements caused by the unpredictability of weather conditions.

House pressurisation was provided by an air supply unit situated in the ceiling of the landing. The unit provided up to 200 m^3/h of air. Depressurisation was provided by an extract unit (0.25 metres diameter, 300 m^3/h) situated in a window in the kitchen. The results of the tests are shown in Table 2.

In order to isolate the effect of a particular parameter, the data has been selected for consistency of wind speed/direction and stack effect.

From analysis of the data the ratio R , has been obtained. R is the ratio of the flow of air entering the house through the suspended floor to the total airflow leaving the house and its derivation, in detail, is shown in Figure 7.

4. RESULTS

4.1 Ventilation Results

An example of how stack and wind speed affect ventilation rate in the house and the underfloor space is shown in Table 3. The effect of doubling the stack while keeping wind speed/direction approximately constant, is to increase the house ventilation rate by a factor of 1.5 and to double the underfloor ventilation rate.

The effect of doubling the wind speed while keeping the wind direction and stack approximately constant, is to increase the house ventilation rate by a factor of 1.6 and the underfloor ventilation rate by a factor of 1.4.

4.2 Natural Ventilation and Pressurisation

For natural ventilation, Table 2 shows that under the prevailing weather conditions with seven underfloor vents unsealed, the total ventilation rate of the house is 0.19 air changes per hour, 60% of this entering via the underfloor space. When the underfloor vents are sealed, the reduction in air change rate is relatively small, from 0.19 to 0.15, but the percentage of air entering the house from the underfloor space reduces significantly to only 18%. However, it was not possible to obtain a matched pair of results and the wind speed and temperature for the sealed vent test were lower than desired.

When the house is pressurised under similar weather conditions, the increased house ventilation rate is roughly the same at 1.08 and 0.99 air changes per hour, with the underfloor vents unsealed and sealed respectively. The proportion of the ventilation air entering the house from the underfloor space is reduced from 60% to 37% with the underfloor vents unsealed and from 18% to 2.7% with the underfloor vents sealed, virtually eliminating any infiltration through the suspended floor.

Under these conditions, and for natural and pressurised house ventilation respectively, the ventilation rates of the underfloor space were $95\text{m}^3/\text{h}$ and $112\text{m}^3/\text{h}$ with the vents unsealed, reducing to $41\text{m}^3/\text{h}$ and $22\text{m}^3/\text{h}$ with the underfloor vents sealed.

4.3 Natural Ventilation and Depressurisation.

Using a kitchen extract fan to depressurise the house resulted in an increase in house ventilation rate from 0.56 to 3.5 air changes per hour. The flow rate through the suspended floor decreased from 75% to 52% of the house ventilation. When the underfloor vents were sealed, the house ventilation rate increased to 3.8 air changes per hour. Some of the variation was due to a larger contribution by stack driven ventilation, although the wind speed was lower, but the proportion entering through the suspended floor reduced to 15%. The underfloor ventilation rates after house depressurisation and underfloor vent sealing changed from $263\text{m}^3/\text{h}$ to $136\text{m}^3/\text{h}$ during the test.

In this set of measurements, an intermediate sealing stage was measured with results in between the extremes presented in Table 2. With four vents unsealed, the depressurised house ventilation rate was 3.3 air changes per hour, 44% of which entered from the underfloor space.

4.4 Natural and Mechanical Ventilation.

The final results in Table 2 show the influence of a balanced mechanical ventilation system. With no mechanical ventilation, and a house airchange rate of 0.76, 0.5 air changes (65%) infiltrates through the suspended floor. When the balanced mechanical ventilation system is switched on, the total air change rate increases to 1.76, 0.86 air changes (49%) coming through the suspended floor.

5. DISCUSSION

The results support the expected behaviour of the ventilation performance of the suspended floor, but they also demonstrate some interesting interrelationships between the ventilation characteristics of the house and its underfloor space.

Air infiltration through the suspended floor provided on average, two-thirds of the house natural ventilation, when the underfloor vents were unsealed. All the forms of mechanical ventilation used decreased the proportion of ventilation entering the house through the suspended floor while increasing the total house ventilation rate. In every case, however, the volume of air entering the house from the underfloor space increased.

House pressurisation and depressurisation increased by a factor of 4 the volume air flow entering the house through the floor, while the house air change rates increased by a factor of 6. Thus, the proportion of air entering the house through the suspended floor decreased.

Balanced mechanical ventilation had less impact, as would be expected. The flow through the floor increased by a factor of 1.7, while the house ventilation increased by a factor of 2.3. Whereas some of the increased air flow from the underfloor space is probably due to an increased stack effect at the time of measurement, not all can be attributed to this. Therefore, the underfloor space must have been acting as an air flow pathway between rooms.

Thus, the use of mechanical ventilation systems resulted in a reduced proportion of the house ventilation air entering via the suspended floor. This was largely due to the increase in infiltration through the exterior fabric of the house and not through a reduction in flow rate through the floor. Air flows into the house via the suspended floor increased unless the underfloor vents were sealed. If the underfloor vents were left unsealed, this would result in reduced concentrations of any products entering the house via the underfloor space. If the vents were sealed, concentrations in the underfloor space would increase, with a possible increase in house pollutant concentrations.

The effect of sealing the underfloor vents resulted in a decreased ventilation rate in the underfloor space and reduced air flows through the suspended floor. When the house was naturally ventilated, the flow through the suspended floor reduced from 60% to 18% of the house total infiltration rate, while the underfloor ventilation rate reduced from $95\text{m}^3/\text{h}$ to $41\text{m}^3/\text{h}$.

With sealed vents, using a pressurised ventilation system, the air flow rate entering through the suspended floor was unchanged, although the house's ventilation rate increased by a factor of 7. The underfloor ventilation changed from $41\text{m}^3/\text{h}$ to $22\text{m}^3/\text{h}$, which would result in an increased rate of pollutant infiltration.

Depressurisation of the house with the underfloor vents sealed resulted in air flow rates through the floor similar to the natural ventilation condition, although the house's total air change rate increased by a factor of 7. When the house was depressurised and the vents were sealed, a small increase in the house ventilation rate occurred due to an increased stack effect. Under these conditions, the sealing of the underfloor vents caused the proportion of air from the underfloor space to decrease by a factor of 3.

6. CONCLUSIONS

The house used for the tests had approximately the same leakage values ($Q_{50} = 0.5\text{m}^3/\text{s}$) for the outer fabric, the suspended floor and the underfloor vents. This resulted in typical house infiltration rates of 0.5 air changes per hour and underfloor infiltration rates of 5 air changes per hour. Approximately 65% of the house ventilation entered via the suspended floor. Sealing the vents in the underfloor space reduced this contribution by a factor of 3 for natural and depressurised mechanical ventilation, and by a factor of 14 when the house was provided with pressurised mechanical ventilation.

The ventilation method had more influence on the contribution of infiltration through the floor when the underfloor vents remained unsealed.

For the weather conditions measured, the most effective way of reducing the concentration of any pollutants entering this house via the underfloor space would appear to be depressurised ventilation with the underfloor vents sealed, i.e. a 'tight' underfloor space. In this situation there was a low proportion of underfloor air entering the house, but a relatively high underfloor ventilation rate. This was mainly due to the high house ventilation rates induced by depressurisation.

Pressurised ventilation with the underfloor vents sealed provided a similar performance, but with a much lower underfloor ventilation rate than in the depressurised case.

7. ACKNOWLEDGEMENTS

The Authors are grateful to British Gas plc for permission to publish this paper.

8. REFERENCES

1. Impact of Reduced Infiltration and Ventilation on Indoor Air Quality.
C.D. Hollowell, J.V. Beak, G.W. Traynor.
ASHRAE Journal, July 1979.
2. Reduction of the Transfer of Airborne Contaminants by Protective-pressure.
H. Feustel.
Hermann-Rietschel-Institut für Heizungs und Klimatechnik, Berlin.
Internal Publication.
3. Radioactivity (Radon and Daughter Products) as a Potential Factor in Building Ventilation.
T. Kusuda, C.M. Hunt, P.E. McNall.
ASHRAE Journal, July 1979.
4. Ventilation in Traditional and Modern Housing.
D.W. Etheridge, D.J. Nevrala, R.J. Stanway.
The Institution of Gas Engineers, 53rd Autumn Meeting, November 1987.
5. Theoretical and Experimental Techniques for Ventilation Research in Buildings.
D.W. Etheridge, R. Gale.
International Gas Research Conference, London, June 1983.
6. Air leakage characteristics of houses - a new approach.
D.W. Etheridge.
Building Services Engineering Research & Technology, Vol.5 No.1 1984.

TEST NAME	LEAKAGE STATUS	COEFFICIENTS FOR $AQ^2+BQ+C=\Delta P$			Q50 (M ³ /S)
		A	B	C	
UF1	V1 TO V7 SEALED	66.4	59.3	-0.6	0.53
UF2	V2 TO V7 SEALED	54.8	36.7	-0.3	0.68
UF3	V3 TO V7 SEALED	51.4	33.7	-0.7	0.72
UF4	V4 TO V7 SEALED	51.9	26.1	-0.4	0.77
UF5	V5 TO V7 SEALED	39.6	28.9	-0.3	0.82
UF6	V6 TO V7 SEALED	23.3	36.8	-1.3	0.89
UF7	V7 SEALED	26.7	27.9	-0.7	0.95
UF8	ALL UNSEALED	22.3	26.2	-0.9	1.03
HL1	HOUSE LEAKAGE	29.4	11.4	-1.1	1.13

TABLE 1.
LEAKAGE CHARACTERISTICS OF THE UNDERFLOOR SPACE AND THE HOUSE.

	VENTILATION CONDITIONS	WIND SPEED M/S	WIND DIR. DEG	STACK °K 0.5	UNDER FLOOR VENT. M ³ /H	SUSPENDED FLOOR VENT. AC/H	TOTAL HOUSE VENT. AC/H	R
SEVEN	NATURAL PRESSURISED	2.88	191	2.19	95	0.11	0.19	0.600
		2.83	191	2.25	112	0.43	1.08	0.370
VENTS	NATURAL DEPRESSURISED	1.86	175	3.44	264	0.42	0.56	0.750
		1.61	182	2.72	263	1.82	3.50	0.520
UNSEALED	NATURAL BALANCED MECHANICAL	2.46	322	1.60	200	0.50	0.76	0.650
		2.57	317	2.60	306	0.86	1.76	0.490
SEVEN	NATURAL PRESSURISED	1.90	172	0.77	41	0.027	0.15	0.180
		2.50	170	2.00	22	0.027	0.99	0.027
VENTS	DEPRESSURISED							
SEALED		1.00	167	4.00	136	0.57	3.80	0.150

TABLE 2
TEST RESULTS

WEATHER PARAMETER VARIED	WIND SPEED M/S	WIND DIR. DEG	STACK °K 0.5	HOUSE VENT. AC/H	UNDER FLOOR VENT. AC/H
STACK	1.76	296	3.3	0.27	4.00
	1.46	279	1.8	0.18	2.10
WIND SPEED	3.69	324	3.3	0.45	5.68
	1.76	296	3.3	0.27	4.00

TABLE 3.
EFFECT OF STACK AND WIND SPEED ON VENTILATION RATE.

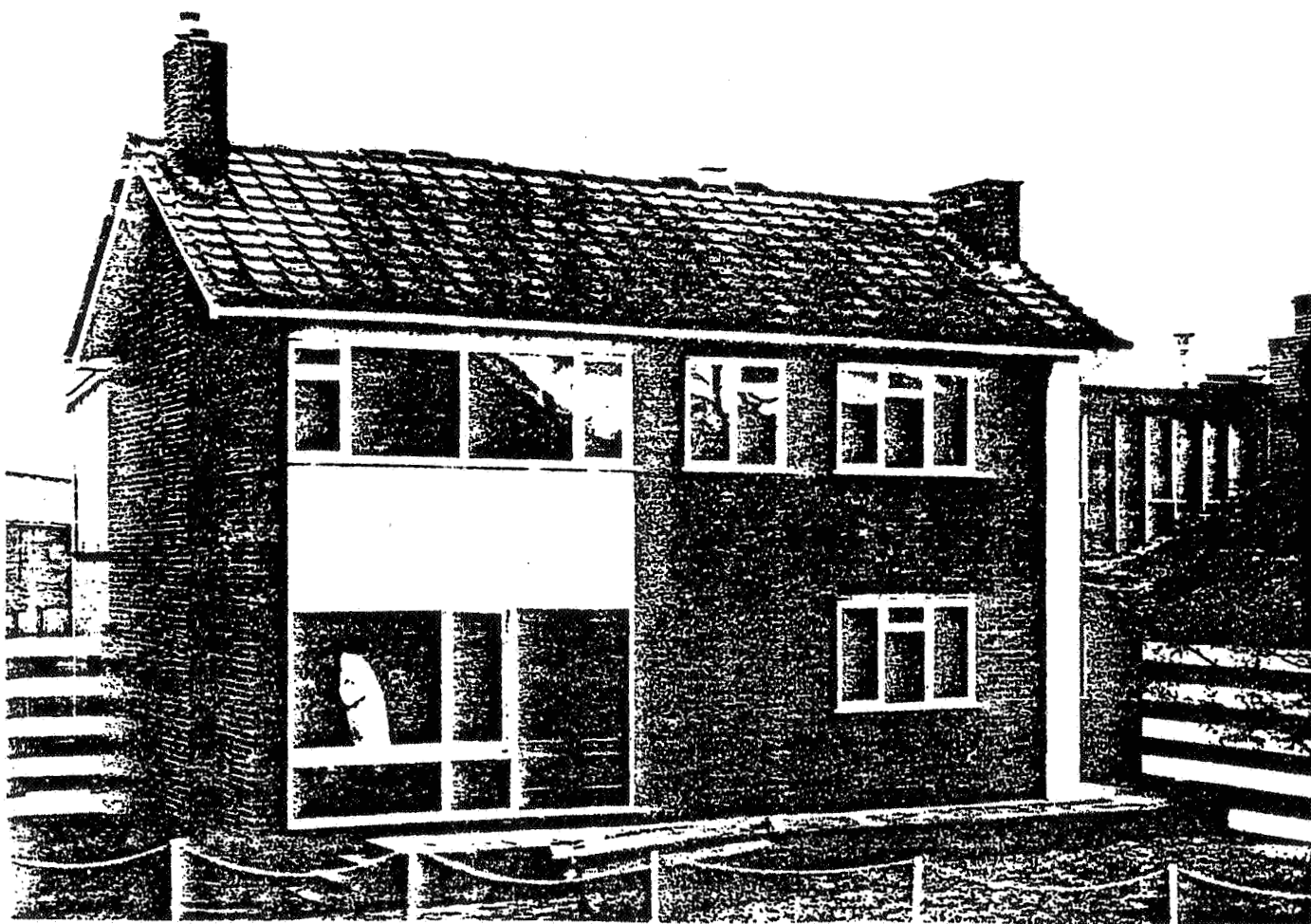
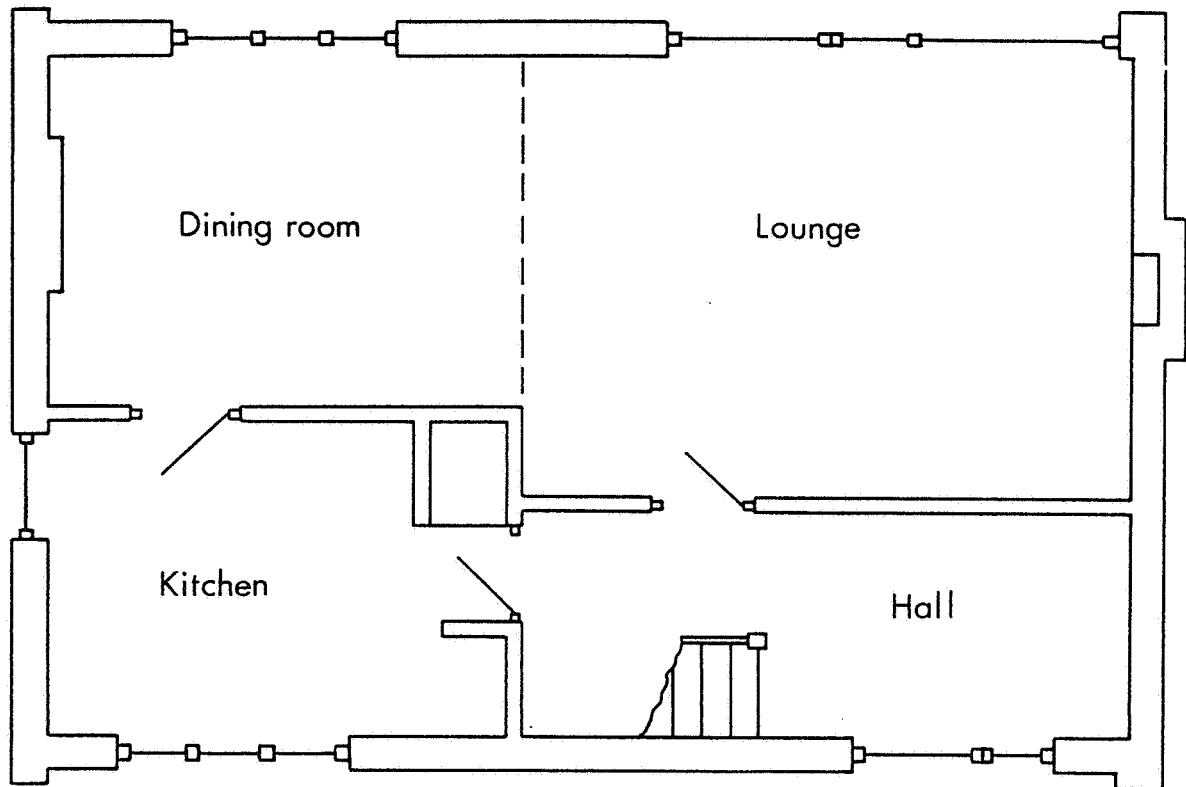


Fig. 1. VIEW OF THE TEST HOUSE SHOWING WEST FACE

Ground Floor



First Floor

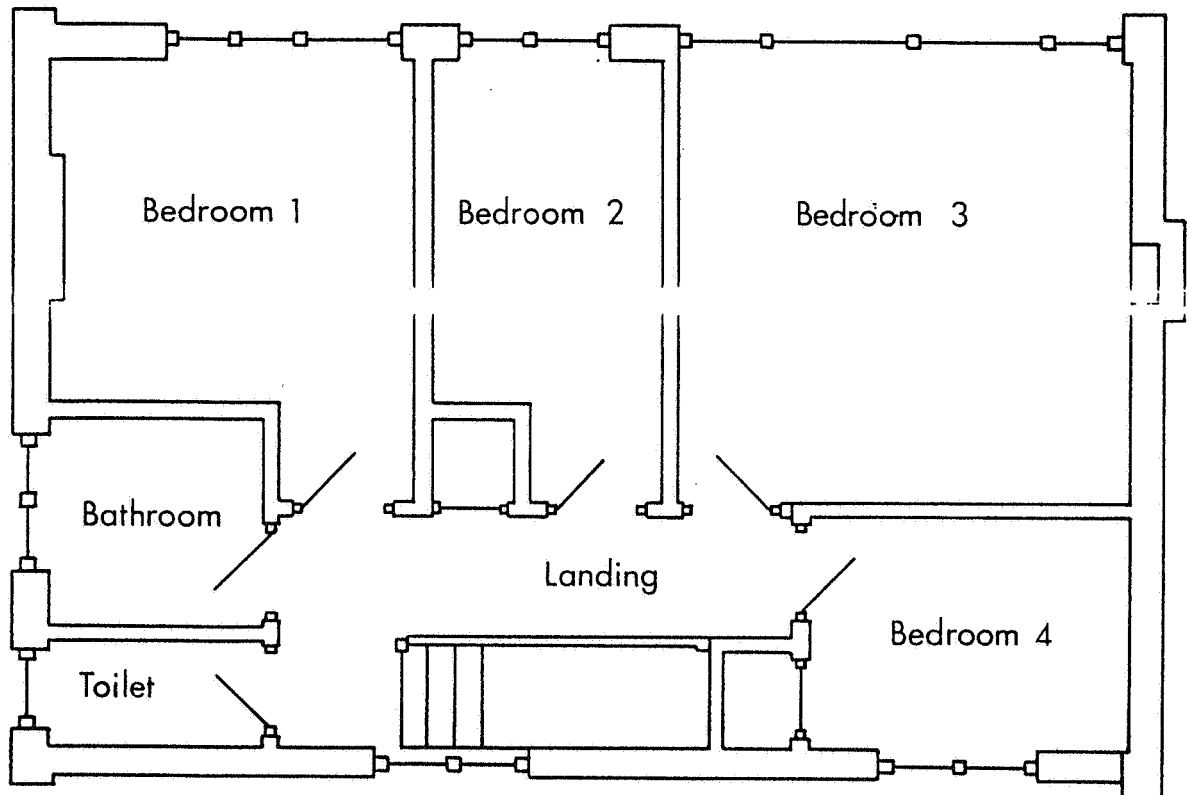
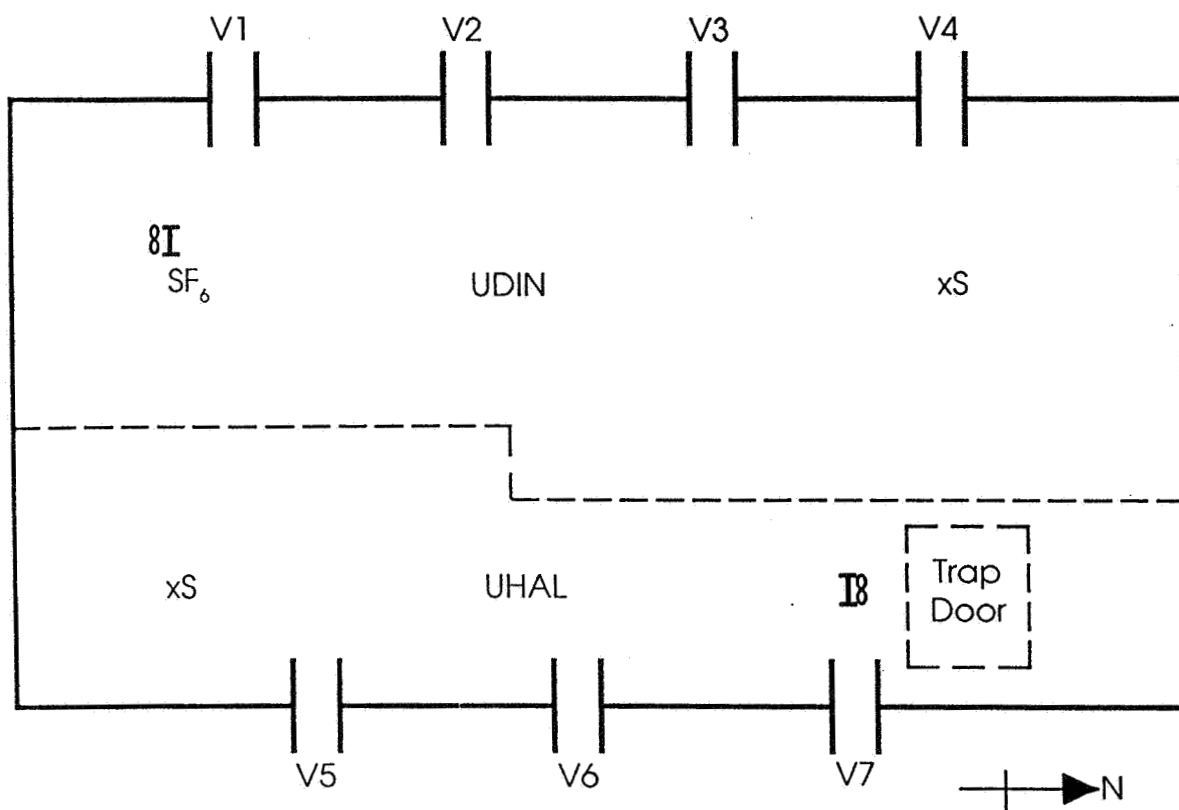


FIG 2 PLAN OF THE TEST HOUSE

y



V - 0.15m vent

I - Injection point

f - Mixing fan

xS - Sample point

UDIN - Space under dining room and lounge

UHAL - Space under hall and kitchen

Fig.3. THE UNDERFLOOR SPACE

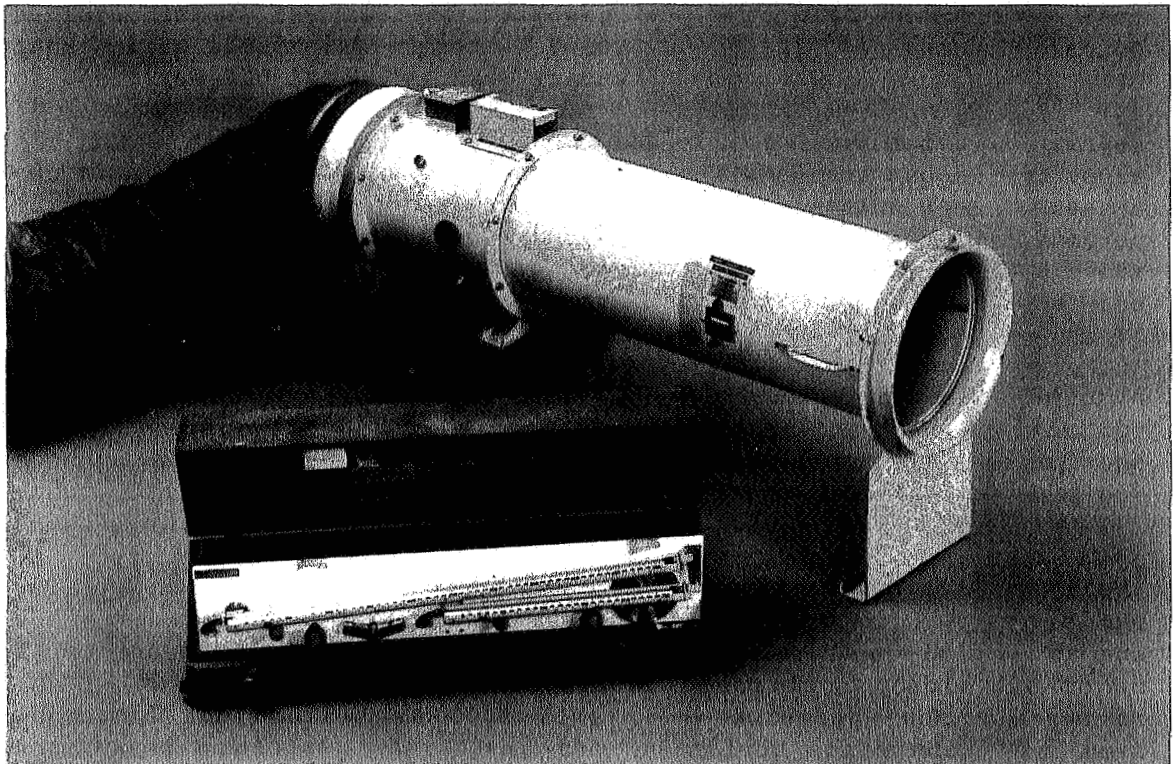


Fig. 4. THE LEAKAGE TEST EQUIPMENT

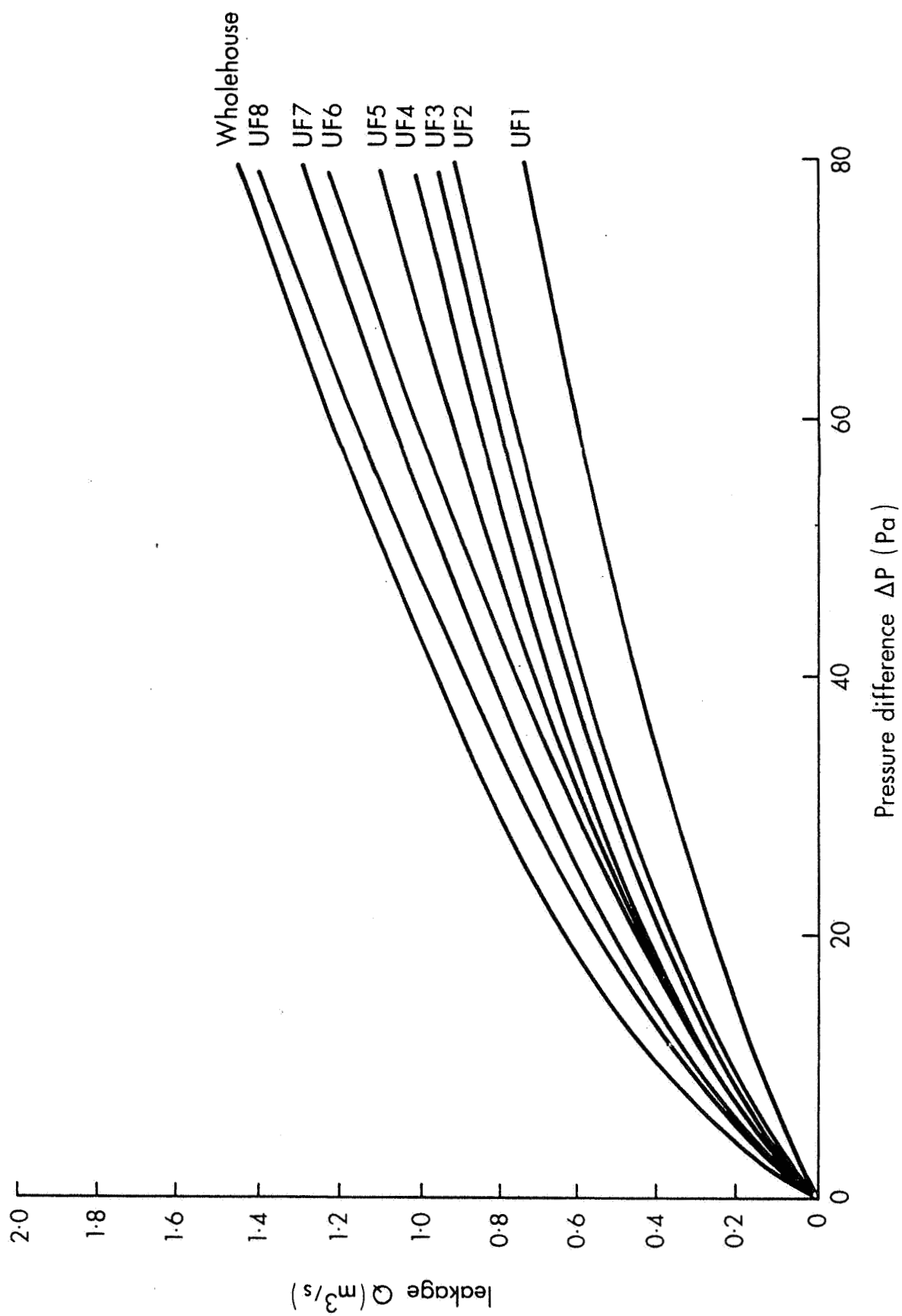
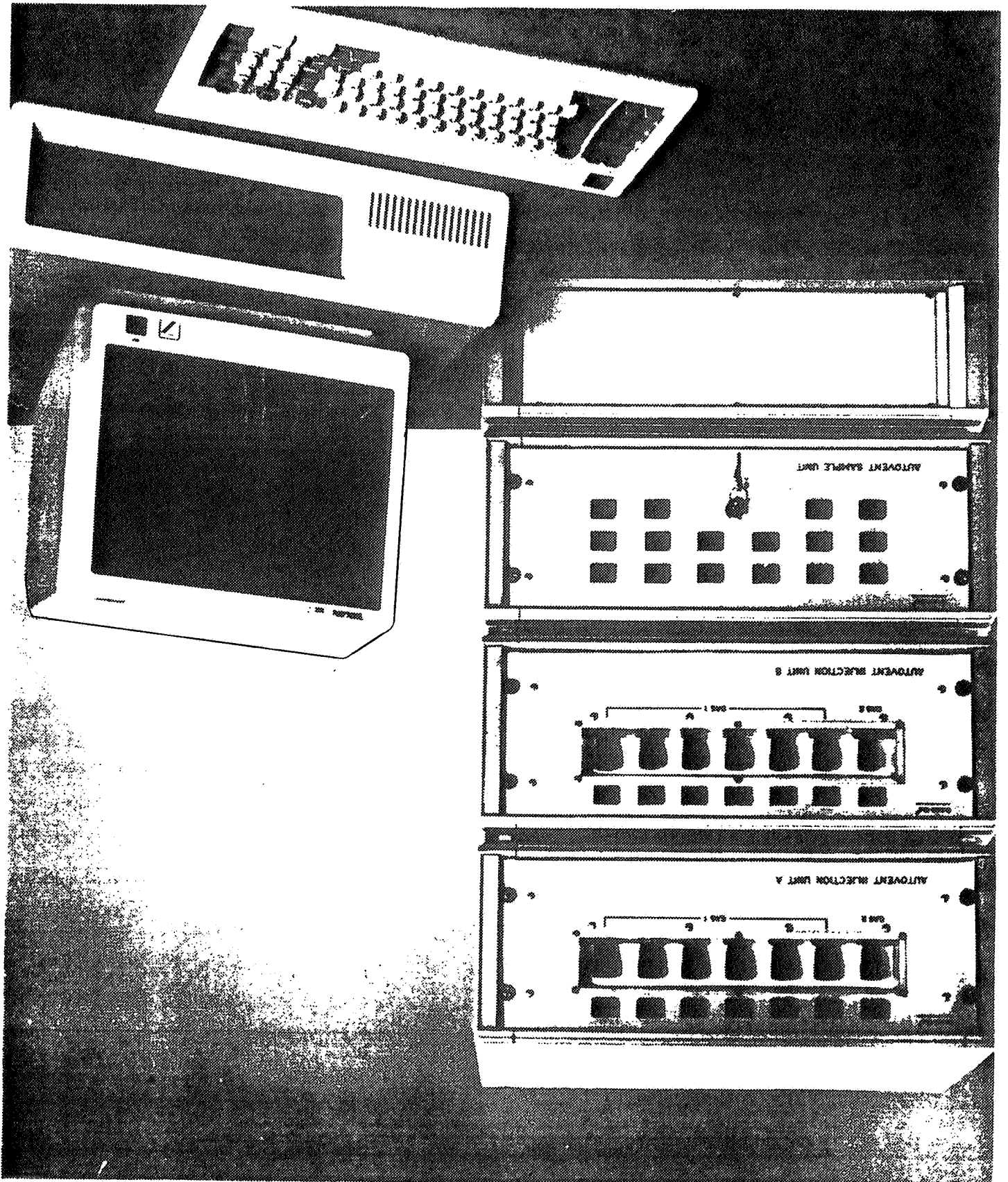
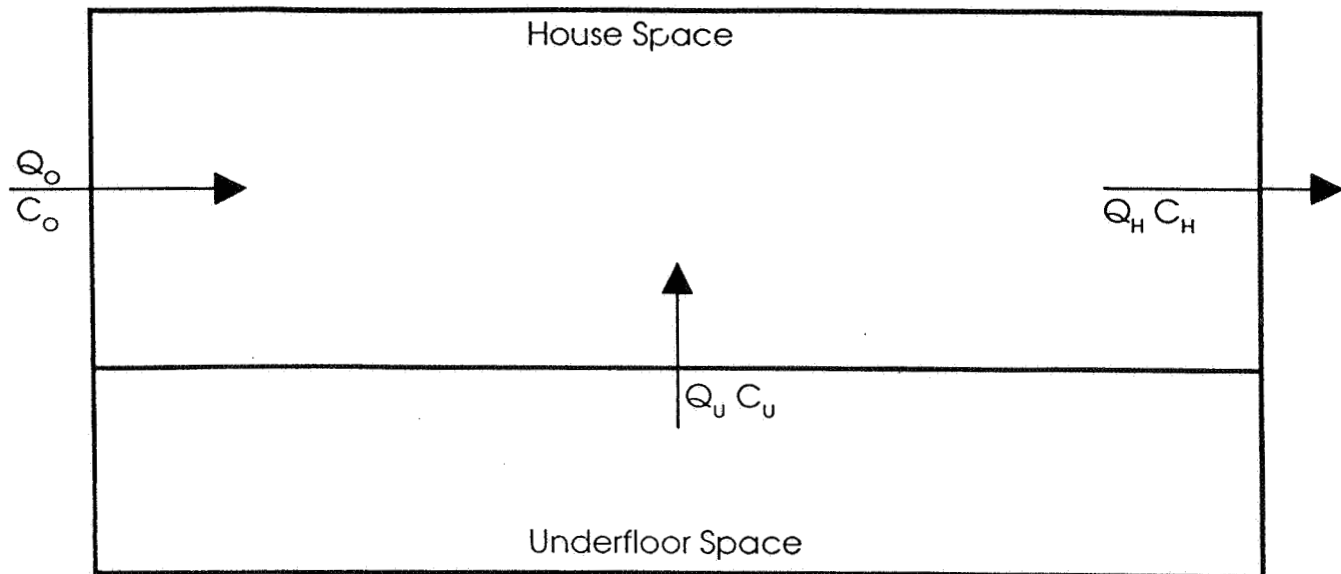


FIG 5 LEAKAGE MEASUREMENTS FOR THE UNDERFLOOR SPACE AND THE HOUSE

Fig. 6. THE BRITISH GAS AUTOVENT





- C denotes SF_6 concentration
- Q denotes air flow rate
- U denotes underfloor
- H denotes house
- O denotes outside

The air flow rate within the house is made up of two components, air infiltrating from the underfloor space and from outside

$$Q_H = Q_o + Q_u$$

Also at equilibrium

$$Q_H C_H = Q_o C_o + Q_u C_u$$

But outside air does not contain SF_6 ie $C_o = \emptyset$

$$\text{and } Q_H C_H = Q_u C_u$$

$$\text{or } R = \frac{Q_u}{Q_H} = \frac{C_H}{C_u}$$

Fig.7. DERIVATION OF R

EFFECTIVE VENTILATION

9th AIVC Conference, Gent, Belgium
12-15 September, 1988

Poster 9

NUMERICAL SIMULATION OF INDOOR TURBULENT AIR FLOWS CAUSED BY
CROSS-VENTILATION AND ITS MODEL EXPERIMENTS

JUN-ICHIRO TSUTSUMI, TADAHISA KATAYAMA, TETSUO HAYASHI,
QINGYUAN ZHANG and HISANORI YOSHIMIZU

Dept. of Thermal Energy System, Kyushu University
6-1 Kasuga-koen Kasuga-shi Fukuoka, 816 JAPAN

SYNOPSIS

Since thermal comfort on human body is influenced by the local air flow speed, it is needed to estimate the distribution of air flow speed in a room for the "effective ventilation". Numerical solution of the equations for the motion of 3-dimensional turbulent air flow and model experiments are conducted for this purpose. The experiment model is a single room model house with 2 windows on the opposite walls. It is actually ventilated by the natural wind. Non-directivity thermistor anemometers are used to measure the 3-dimensional distribution of indoor air flow speed. Several kinds of numerical simulation are carried out on the similar space to the experiment model. Two kinds of mathematical turbulence model are adopted, one is the $k-\epsilon$ 2-equation model, and the other is the Large Eddy Simulation. Two kinds of pseudorandom number are used as the turbulence component of the velocity on the inflowing opening boundary in the LES. The distributions of scalar speed in the sections which are perpendicular to axes of the numerical simulation results are compared with those of the experiment results. They are not entirely corresponding, however, the same tendencies are found.

1. INTRODUCTION

Cross-ventilation is here regarded as natural ventilation through relatively large openings, for instance windows and doors widely opened. It probably makes an adequate air flow rate in a room, and such a air flow often brings about comfortable thermal environment in the warm season¹. It is one of the simplest and the most effective cooling means without air-conditioning. Although thermal comfort on a human body consists of a lot of factors, as air temperature, humidity and radiation, the thermal effect of cross-ventilation depends upon the air flow speed in the vicinity of the human body². However, it is almost impossible to control the air flow speed caused by cross-ventilation in detail. Therefore, it is necessary to predict the distribution of air flow speed in a room in various cases in the step of planning a dwelling house for the "effective ventilation".

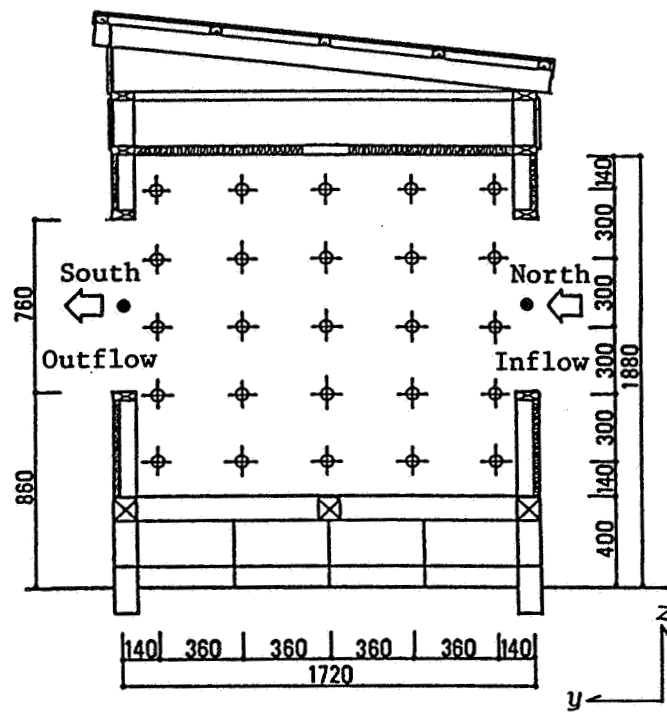
The development of the large capacity and high speed super-computer makes numerical simulation the dominant method for the prediction of the air flow distribution in a room instead of the model experiment. However, there are still some problems left in the numerical simulation. Turbulence is one of the most important problems, and the indoor air flow is almost always regarded as turbulence. The mathematical turbulence model is needed, because the direct simulation of turbulence is impossible or nonsense from the viewpoint of its cost performance. There are two kinds of turbulence model which are recognized practically accurate in various engineering field. One is the $k-\epsilon$ 2-equation model³ ($k-\epsilon$ model), and the other is the Large Eddy Simulation (LES)⁴. Both of them are tested for the simulation of a air flow caused by cross-ventilation in this paper.

The similarity between the result of numerical simulation and the actual flow phenomenon is another important problem of numerical simulation⁵. It is generally examined by compared with the scaled model experiment, if it is impossible or difficult to measure the turbulent values of the real flow. However, it is also difficult to reproduce the large scale turbulence as the natural wind by the wind tunnel or so on. Cross-ventilation is the very air flow which is influenced by the natural wind directly. Therefore, the model house, which is built on the ground and is naturally ventilated, is used for the model experiments to examine the results of the numerical simulation in this paper. There are few documents on the distribution of the air flow in a house which is naturally ventilated^{6,7}. Grasping the air flow distribution caused by cross-ventilation itself is one of the purpose of this paper as its numerical simulation.

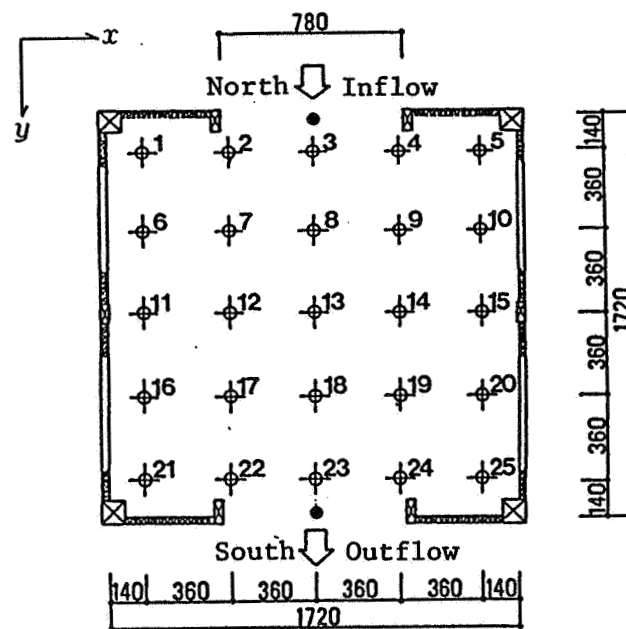
2. MODEL EXPERIMENTS

2.1 Experiment Procedure

The experiment model built on the ground is used for measuring indoor air flow speed caused by cross-ventilation. Its section and plan are shown in Fig. 1 (a), (b), respectively, with the axes of coordinate that is fixed on the model. It has two openings oppositely on its southern and northern wall. They are the same shape of a square, and fixed at the same position in the wall. They are relatively large openings to the whole dimensions of the wall. When the main direction of the wind is north, in other words, the wind direction is perpendicular to the openings, the measurements are carried out. Five non-directivity thermistor anemometers are used to measure the distribution of the indoor air flow speed. These anemometers are fixed on a stand to be situated at measurement heights which are shown in Fig. 1 (a). The stand is moved on the measurement points from No.1 to No.25 by turns which are shown in Fig. 1 (b). Therefore, the measurement points are set on the grid that divide the room space into 5x5x5, and the total number of the measurement points amounts to 125. The air flow speed are measured for 150 seconds at each measurement point. It takes about 80 minutes for a series of the measurement including the moving time. The wind speeds at the centre of the inflowing and the outflowing openings are constantly measured by a 3-dimensional ultrasonic anemometer and a non-directivity thermistor anemometer, respectively. The wind speed and direction above the roof of the model are measured at the height of 4.5m from the ground level by a 3-cup anemometer and an arrow-shaped vane, respectively, as the natural wind data which is not influenced by the model itself. All the data are recorded at the intervals of 2 seconds, and their mean values are found from 60 data.



(a) Section



(b) Plan

Fig. 1. Experiment model with measurement points of indoor air flow velocity (dimensions in mm)

2.2 Experiment Results

The changes on standing of the wind vector above the roof and the wind vector at the inflowing opening on x-y plane and y-z plane measured by 3-dimensional ultrasonic anemometer are shown in Fig. 2 (a), (b) and (c), respectively. The wind directions at the inflowing opening correspond to the wind directions above the roof, the wind speeds at the inflowing opening are about half as much as those above the roof as shown in Fig. 2 (a) and (b). Moreover, it is obvious that the natural wind which flows into the inflowing opening is almost horizontal as shown in Fig. 2 (c). The correlation between the mean inflowing wind speeds and the mean wind speeds above the roof is shown in Fig. 3. The inflowing wind speeds are correlated with the wind speeds above the roof with the high correlation coefficient of 0.91. The correlation between the mean inflowing wind speeds and the mean outflowing wind speeds are shown in Fig. 4. Although those values are scattered somewhat widely, the outflowing flux is nearly equal to the inflowing flux, because the inclination of the regression line is about 45°. The correlations between the mean wind speeds of two openings and their standard deviations are shown in Fig. 5 and Fig. 6. The standard deviations of the inflowing and the outflowing wind speed correspond to their mean values to some extent. Both the inclination value of the regression line of Fig. 5 and that of Fig. 6, which indicate the means of the turbulence intensity at the inflowing opening and at the outflowing opening, are the same value of 36%.

3. NUMERICAL SIMULATION

3.1 Governing Equations of the k-ε Model

The air flow in a room caused by cross-ventilation is regarded as the incompressible isothermal turbulent flow. It is expressed by the continuity equation and the Navier-Stokes (N-S) equations. The ensemble mean of the turbulence is here the objective value to be simulated. The ensemble mean of the continuity equation is as follows:

$$\frac{\partial U_i}{\partial x_i} = 0 \quad (1)$$

where, U_i is the mean velocity component of x_i direction, i is the tensor, $x_1=x$, $x_2=y$ and $x_3=z$. The ensemble mean of the N-S equations become the Reynolds equations with the Reynolds stress term. The Reynolds stress is modelled by the turbulent kinetic energy, k , and the product of the eddy viscosity, ν_t , and the differentials of the mean velocity.

$$\frac{\partial U_i}{\partial t} + \frac{\partial}{\partial x_j} (U_i U_j) = -\frac{\partial \Pi}{\partial x_i} + \frac{\partial}{\partial x_j} \left(\nu_t E_{ij} + \frac{1}{Re} \frac{\partial U_i}{\partial x_j} \right) \quad (2)$$

$$E_{ij} = \frac{\partial U_i}{\partial x_j} + \frac{\partial U_j}{\partial x_i} \quad (3)$$

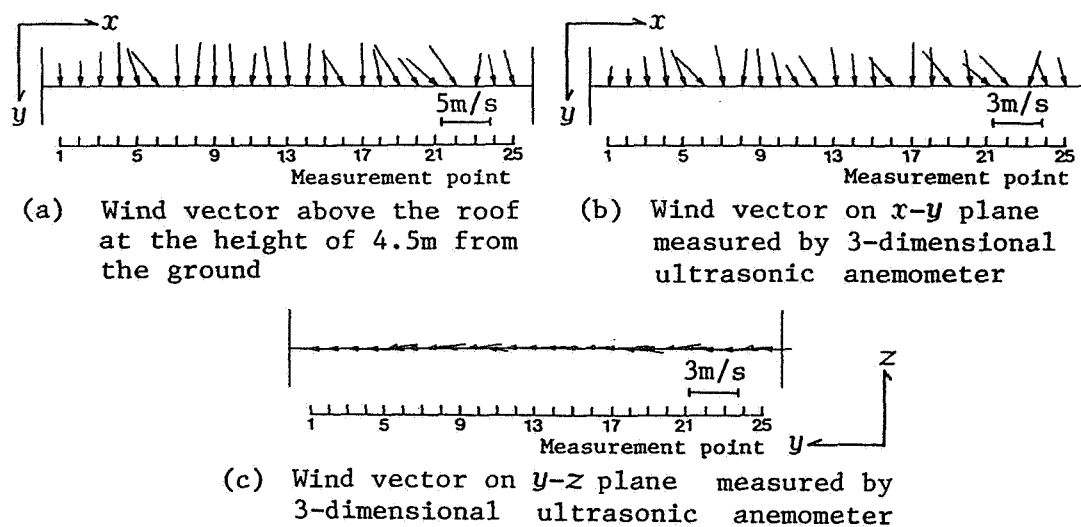


Fig. 2. Changes on standing of the wind vector above the roof and the inflowing wind vector

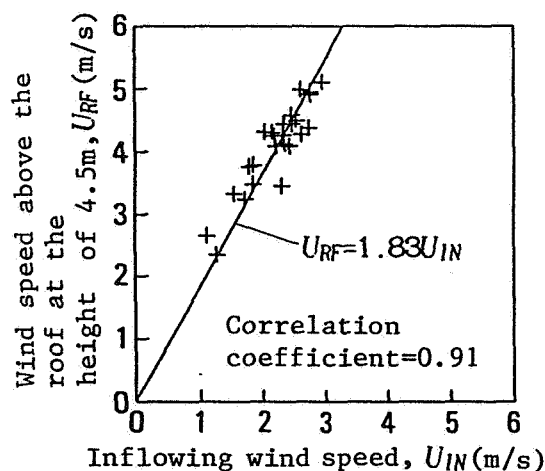


Fig. 3. Correlation between the inflowing wind speeds and the wind speeds above the roof

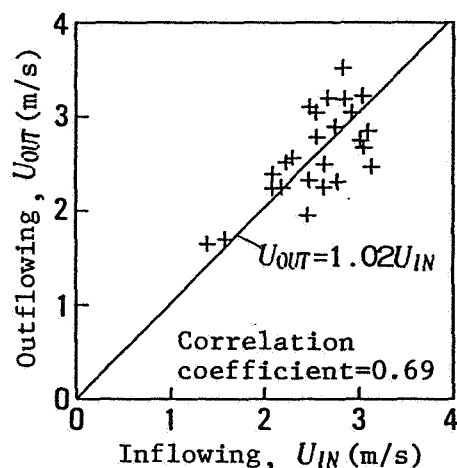


Fig. 4. Correlation between the inflowing wind speeds and outflowing wind speeds

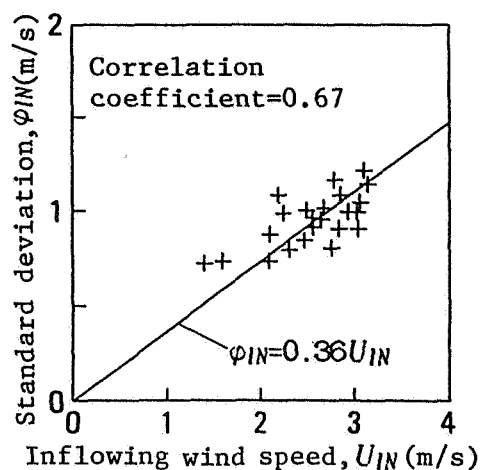


Fig. 5. Correlation between the inflowing wind speeds and their standard deviations

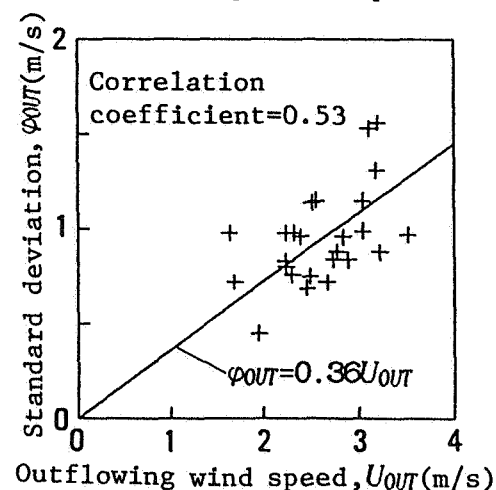


Fig. 6. Correlation between the outflowing wind speeds and their standard deviations

where, t is time, Π is pressure including $(2/3)k$, Re is the Reynolds number. ν_t is found by the algebraical expression of k and the energy dissipation rate, ε , from dimensional analysis.

$$\nu_t = C_D \frac{k^2}{\varepsilon} \quad (4)$$

Then, the equations of k and ε are essential to solve the variables in the mean field. These equations are found from the equations for the fluctuating field.

$$\frac{\partial k}{\partial t} + \frac{\partial}{\partial x_i} (k U_i) = \frac{\partial}{\partial x_i} \left\{ \left(\frac{\nu_t}{\sigma_1} + \frac{1}{Re} \right) \frac{\partial k}{\partial x_i} \right\} + \nu_t E_{ij} \frac{\partial U_i}{\partial x_j} - \varepsilon \quad (5)$$

$$\frac{\partial \varepsilon}{\partial t} + \frac{\partial}{\partial x_i} (\varepsilon U_i) = \frac{\partial}{\partial x_i} \left\{ \left(\frac{\nu_t}{\sigma_2} + \frac{1}{Re} \right) \frac{\partial \varepsilon}{\partial x_i} \right\} + C_1 \frac{\varepsilon}{k} \nu_t E_{ij} \frac{\partial U_i}{\partial x_j} - C_2 \frac{k \varepsilon}{\nu_t} \quad (6)$$

where, C_D , C_1 , C_2 , σ_1 and σ_2 are constants, and these values used here are 0.09, 1.59, 0.18, 1.0 and 1.3, respectively.

3.2 Governing Equations of the LES

The fundamental equations are the continuity equation and the N-S equations which are the same ones as the $k-\varepsilon$ model, however, the averaging procedure is different. All the equations are filtered out and separated into the grid scale (GS) and the sub-grid scale (SGS) variables. The GS variables are solved directly and the SGS variables are modelled by the GS variables. This filtering operation has much the same meaning as the spatial average, but it is not the same process as the ensemble mean. The filtered continuity equation is the same form as eq. (1).

$$\frac{\partial u_i}{\partial x_i} = 0 \quad (7)$$

where, u_i is the GS velocity component of x_i direction. There are three different terms, the cross term, the Leonard term and the SGS Reynolds stress term, from the Reynolds equations. The cross term and the Leonard term are neglected here, and the only SGS Reynolds stress term, which is correspond to the Reynolds stress term in the Reynolds equations but not entirely equal to that, is modelled by the product of the SGS eddy viscosity, ν_{SGS} , and the differentials of the GS velocity components.

$$\frac{\partial u_i}{\partial t} + \frac{\partial}{\partial x_j} (u_i u_j) = -\frac{\partial p}{\partial x_i} + \frac{\partial}{\partial x_j} \left(\nu_{SGS} e_{ij} + \frac{1}{Re} \frac{\partial u_i}{\partial x_j} \right) \quad (8)$$

$$e_{ij} = \frac{\partial u_i}{\partial x_j} + \frac{\partial u_j}{\partial x_i} \quad (9)$$

where, p is pressure including the SGS turbulent energy term. ν_{SGS} is modelled from dimensional analysis by the GS velocities⁸.

$$\nu_{SGS} = (C_s \Delta)^2 \left\{ \frac{(e_{ij})^2}{2} \right\}^{1/2} \quad (10)$$

where, C_s is the Smagorinsky constant, that is here 0.1, Δ is the characteristic width of the filter, which is defined as follows:

$$\Delta = (\Delta x_1 \cdot \Delta x_2 \cdot \Delta x_3)^{1/3} \quad (11)$$

where, Δx_i is the grid width of x_i direction. All the variables used here are non-dimensionalized by the width or height of the openings as the reference length, and the inflowing wind speed as the reference speed. Re based on these reference values in the model experiment becomes 10^5 .

3.3. Numerical Calculation Procedure

The governing equations mentioned above are transformed into the finite difference equations by the explicit forward differences to the time differentials and the centred differences to the spatial differentials on the staggered grid system. The calculation algorithm adopted here is the original MAC method. The grid system is fixed in the objective space which is similar to the experiment model, divided x and y length into 18 equally and z length into 16 equally.

The variables on the inflowing boundary are the given conditions. The tangential velocity components on the inflowing boundary are 0. The normal velocity component in the $k-\epsilon$ model is 1, as the reference speed. As for the LES, three kinds of the normal velocity component are given. One is the constant value, 1, which is the same condition as the $k-\epsilon$ model and it is called "Constant". The others are the normal and the uniform random number, which are called "Normal" and "Uniform", respectively. Their mean values are 1 and their turbulence intensity values are 36% that is the result of the model experiment. The frequency distributions of the given random numbers are shown in Fig. 7. The turbulence intensity in the $k-\epsilon$ model is given by the value of k . That is here 0.2 which is correspond to the turbulence intensity of 36% under the isotropic hypothesis. While ν_{SGS} is calculated directly from the variables on the inflowing opening, ν_t on the inflowing opening is given as follows:

$$\nu_t = k^{1/2} \cdot l \quad (12)$$

where, l is the turbulence length scale, that is 1.0 from the result of the model experiment.

3.4. Boundary Condition

The boundary condition of most variables are given by these values in an external cell. The normal velocity component on the wall is 0. The velocity components tangential to the wall are found from the power law velocity profile as shown in Fig. 8^{9,10}. The normal velocity in an external cell of the wall boundary is found from the flux balance in the external cell and the adjacent internal cell. On the outflowing opening, the tangential components are free slip and the normal component is found from the flux balance in the internal cell neighbouring to the outflowing opening as shown in Fig. 9. The boundary conditions

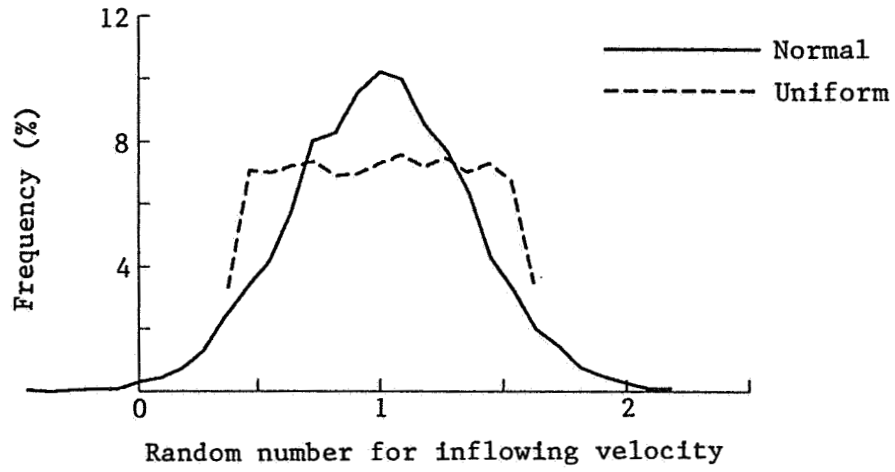


Fig. 7. Frequency distribution of random numbers used for the inflowing boundary in the LES

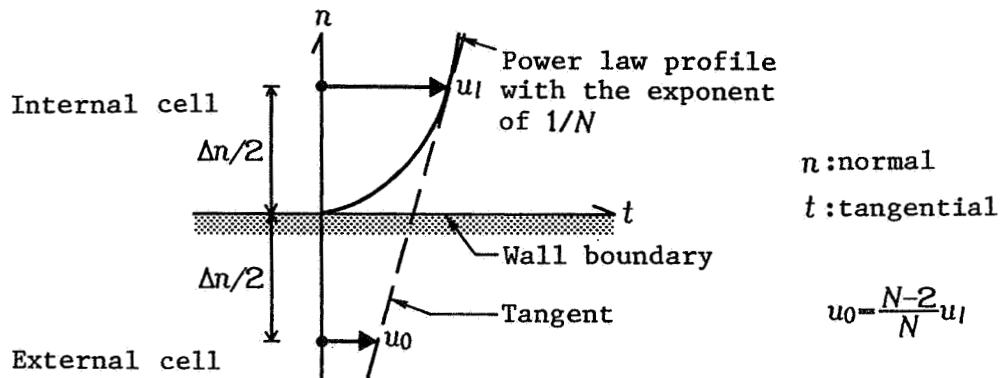


Fig. 8. Boundary condition of the tangential velocity component on the wall

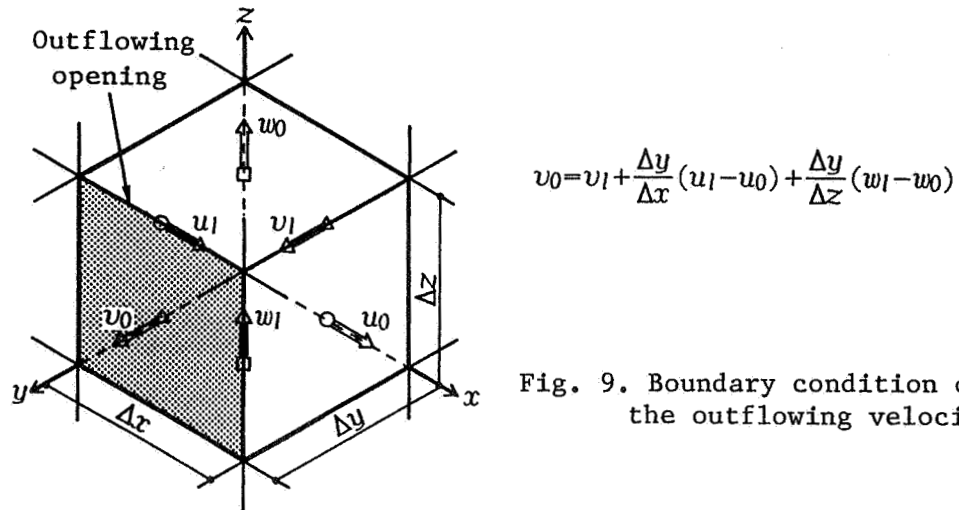


Fig. 9. Boundary condition of the outflowing velocity

of p and Π are found from the basic equations (2) and (8) which are transformed into the difference equations over the velocities on the boundary. The boundary conditions of k , ε and ν_{SGS} on the outflowing opening are free slip. ν_{SGS} and ν_t on the wall are 0. The boundary condition of k on the wall is free slip. The boundary condition of ε is given as follows:

$$\varepsilon = C_D^{\frac{3}{4}} \cdot k^{\frac{3}{2}} / \left\{ \kappa \left(\frac{\Delta n}{2} \right) \right\} \quad (13)$$

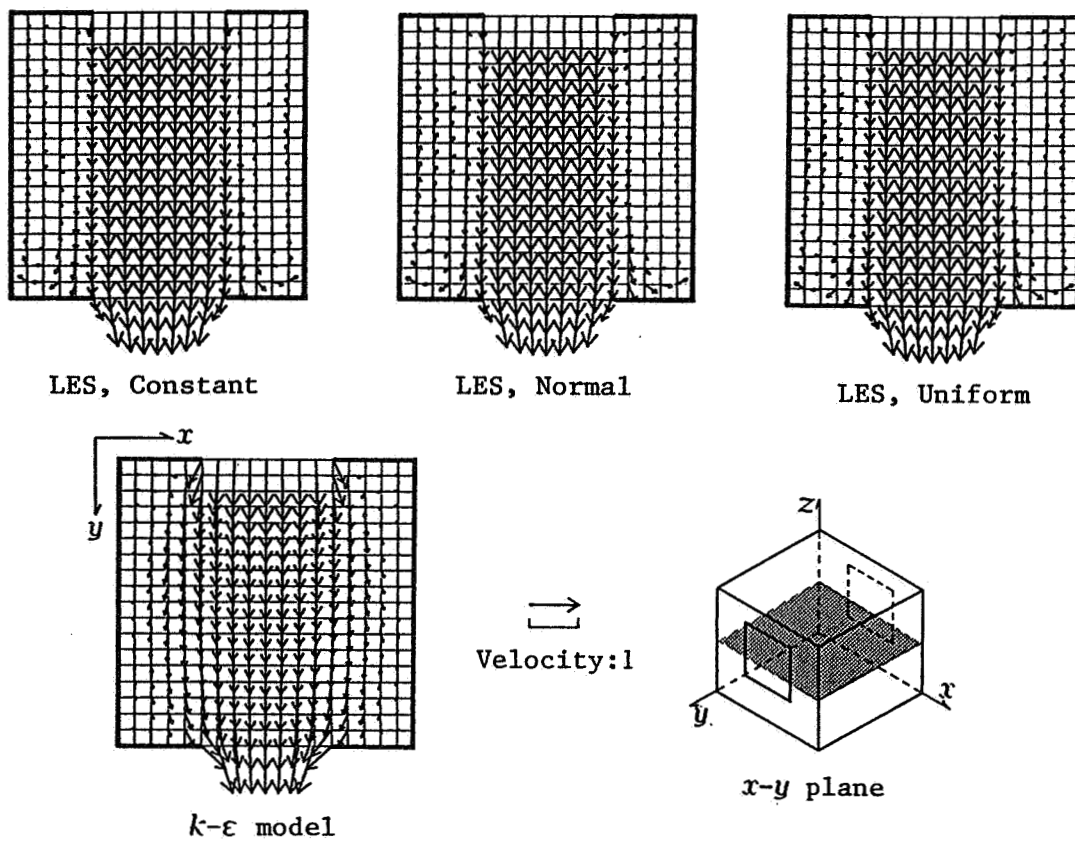
where, κ is the Karman constant, Δn is the grid scale of the normal direction. That is the value of ε in the internal cell adjacent to the wall boundary.

4. COMPARISON BETWEEN MODEL EXPERIMENT AND NUMERICAL SIMULATION

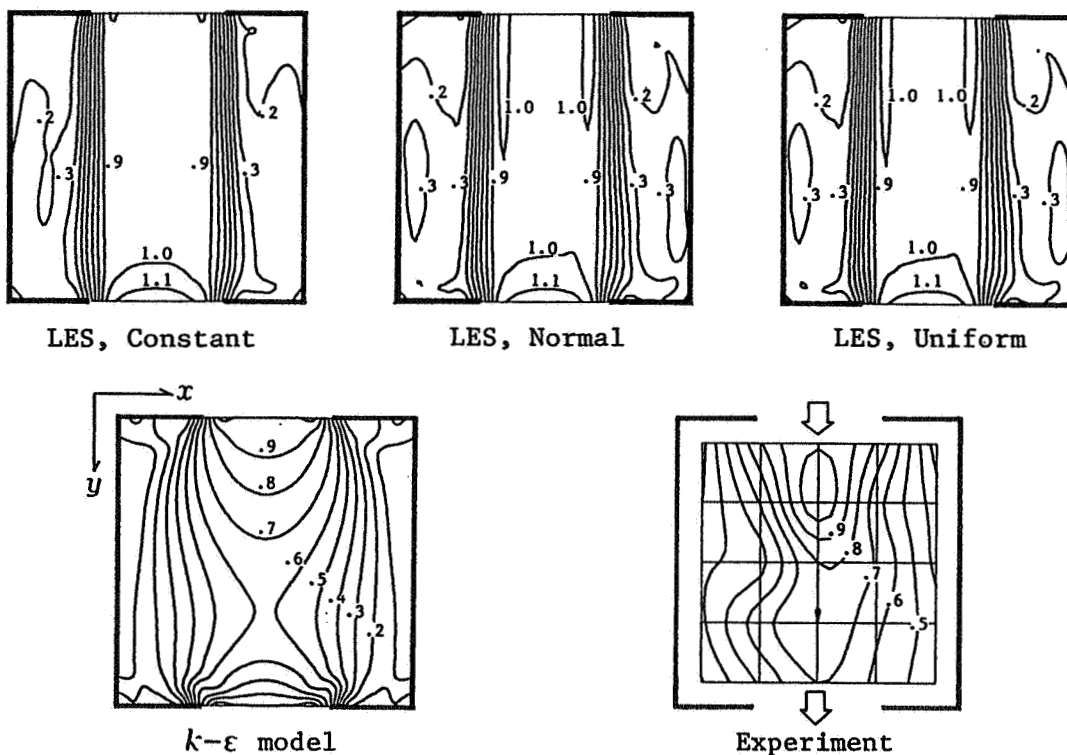
There are four kinds of numerical simulation, one is the k-e model, and the others are the LES. Three kinds of the LES are distinguished by the inflowing boundary condition into the Constant, the Normal and the Uniform. These results are examined, compared with the result of model experiment over the distributions of scalar speed and velocity vector on three sections. These sections are perpendicular to each axis and at the center of the each side length, they are called X-Y plane, Y-Z plane and X-Z plane. The results on the X-Y plane, on the Y-Z plane and on the X-Z plane are shown in Fig. 10, Fig. 11 and Fig. 12 respectively. All the results of the LES are the mean values of 10 time steps.

As for Fig. 10 and Fig. 11, both of them have two openings and there are a lot of common points in the air flow distributions in these section. Therefore, these two sections are examined at the same time. The difference of three kinds of boundary conditions of the LES, particularly the Normal and the Uniform, is not clear. The distributions of the velocity vector by the LES indicate that the air flow passes across the analysis space straightly from the inflowing opening to the outflowing one. The distributions of the scalar speed by the LES in the area from the inflowing opening to the outflowing one are almost uniform. It is regarded as the main flow. The secondary circulations beside the main flow are so weak that contour lines of the scalar speed concentrate to the edges of the two openings. These tendencies do not change by the inflowing boundary. On the other hand, the velocity vectors by the k-e model diffuses right after the inflowing opening gradually, and the scalar speeds by the k-e model decrease up to the centre of the section. They are similar to the results of the model experiments on both sections, although the results of the k-e model keep symmetrical patterns. The distributions of the scalar speed by the model experiments are asymmetric because of the minute fluctuation of the natural wind.

As for Fig. 12, there is little difference, either, between the distributions of the velocity vector by the Normal and that by the Uniform. However, they are a little different from the

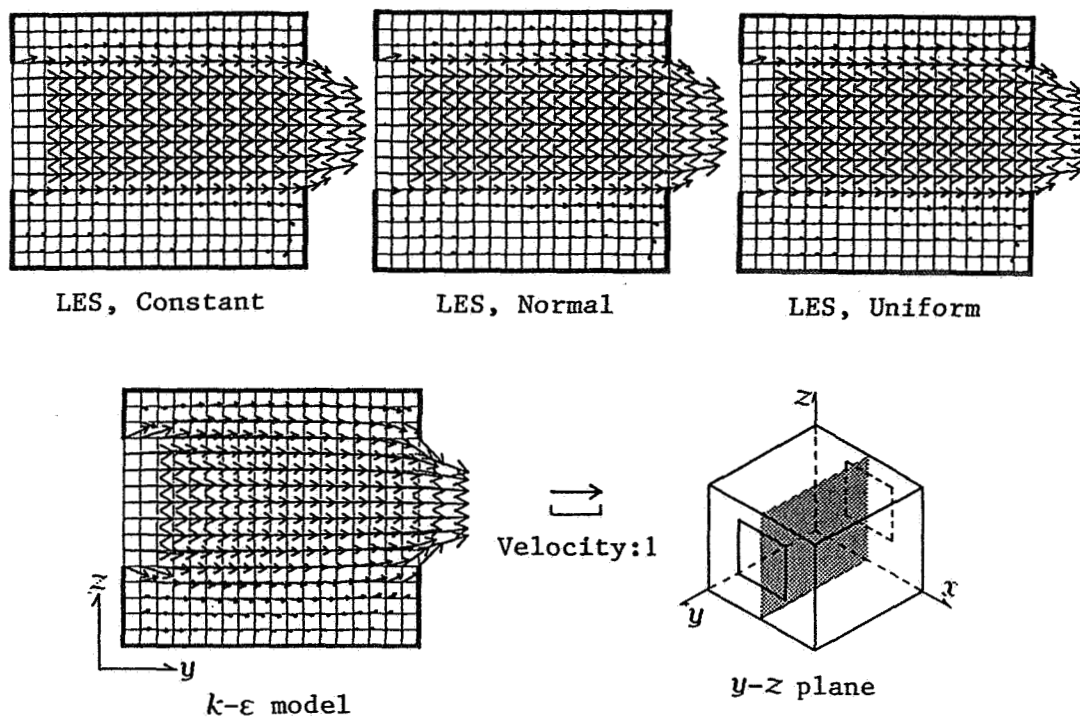


(a) u - v vector on x - y plane

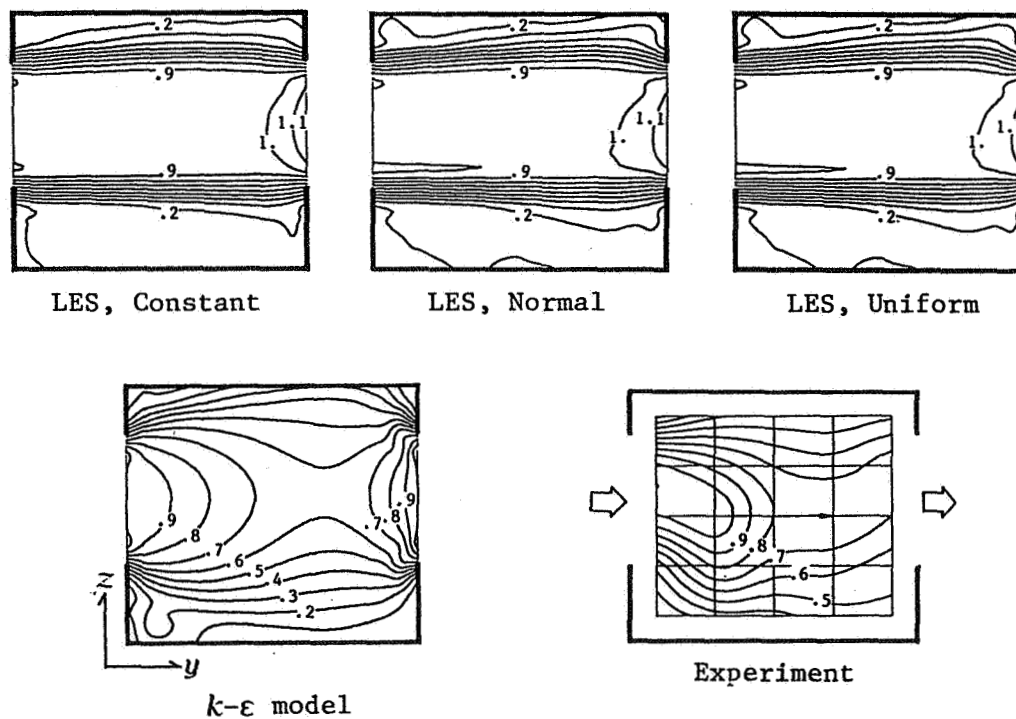


(b) Scalar speed on x - y plane

Fig. 10. Distributions of u - v vector and scalar speed on x - y plane



(a) v - w vector on y - z plane



(b) Scalar speed on y - z plane

Fig. 11. Distributions of v - w vector and scalar speed on y - z plane

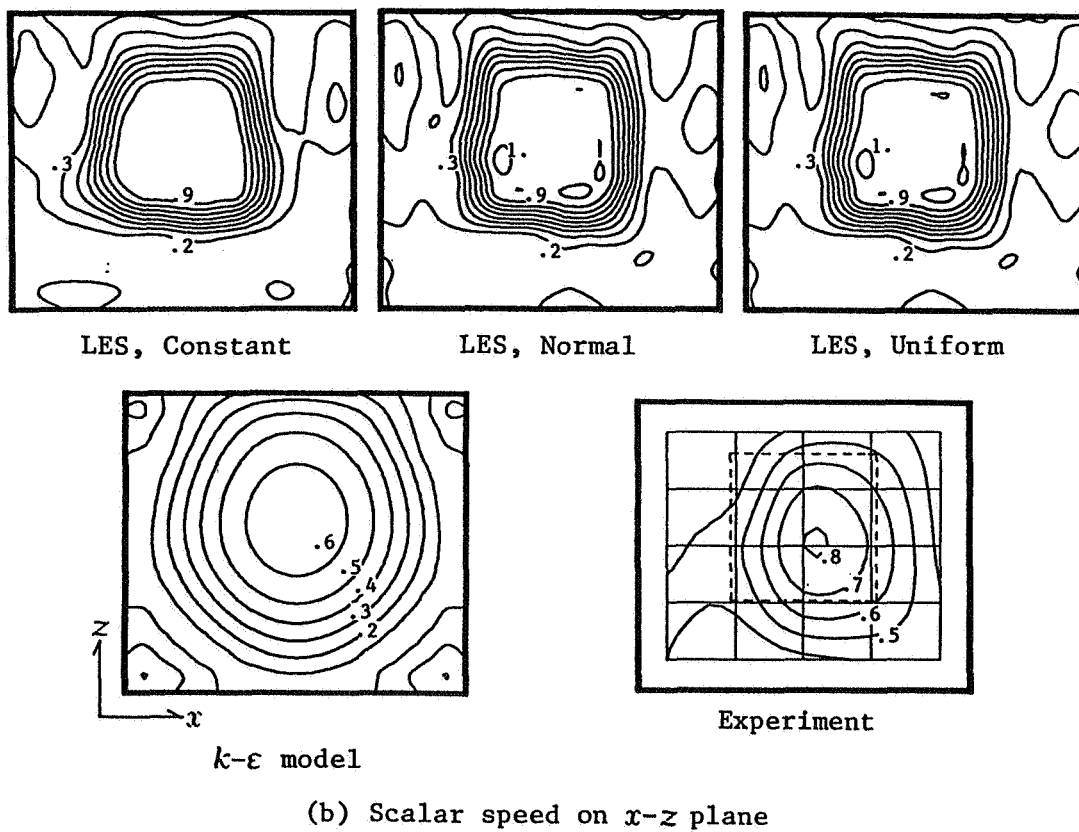
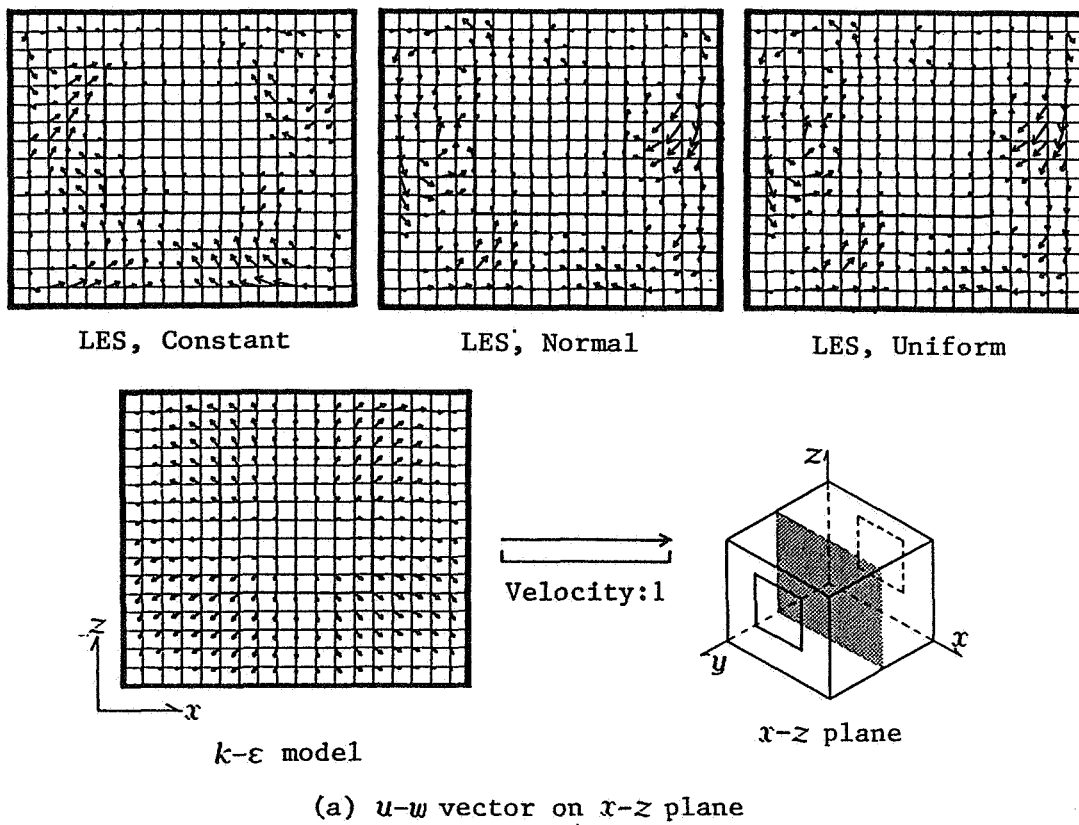


Fig. 12. Distributions of $u-w$ vector and scalar speed on $x-z$ plane

result by the Constant. The distributions of the velocity vector by the LES indicate the secondary circulations around the main flow, while that by the $k-\epsilon$ model indicates the diffusion of the main flow. The distributions of the scalar speed by the LES keep the shape of the opening clearly. On the other hand, the distribution of the scalar speed by the $k-\epsilon$ model show the same tendency as that by the model experiment, although there is a little difference in the values of the contour lines.

5. CONCLUSION

Although there are a lot of documents about the numerical simulation of indoor air flows, those about natural ventilation are limited and those compared with model experiments by the natural wind are more limited. In this paper, four kinds of numerical simulation of turbulent air flow in a room caused by cross-ventilation are carried out, and these results are compared with those of model experiments in the natural wind. There are two major purpose here, one is to grasp the air flow distribution in a model room naturally ventilated, and the other is to simulate such a air flow numerically.

It is difficult to measure the 3-dimensional distribution of air flow speed with a limited number of instruments, because the instruments have to be moved. It takes some long time for a series of the experiments and the measurement data include the long term fluctuation of the natural wind. As for the wind speed, that is eliminated by non-dimensionalization of the mean air flow velocities, as to the wind direction, however, it is impossible. As the stable breeze was blowing in the daytime on the experiment day fortunately, these experiments were able to be carried out under the condition of almost constant wind direction that was perpendicular to the opening. The results of the model experiments seem appropriate distributions of air flow speed.

While this kind of experiment is easy to be influenced by the wind condition, it is necessary to use the large scale turbulence like the natural wind, and it is very difficult to make such a wind artificially in a wind tunnel and so on. Then, numerical simulation is expected as the method to predict the air flow phenomena like this. Two kinds of turbulence model are adopted in the numerical simulation here. However, these models are not refined, they are used in the original and simple form. The boundary conditions on the openings are contrived. On the inflowing boundary, two kinds of random number are used in the LES, the turbulence scale of the model experiments is used in the $k-\epsilon$ model and their turbulence intensity are used in both the model. On the outflowing boundary, the boundary condition that expresses the free outflow is adopted. The outflowing boundary condition well functions, and the flux on both the openings are balanced. However, the inflowing boundary conditions of the LES hardly reform the results. The result of the $k-\epsilon$ model is closer to that of the model experiments than that of the LES, because the random numbers that have no relation spatially and temporally

are used as the inflowing turbulence condition in the LES, while the turbulence length scale from the experiment data is given as the inflowing boundary condition of the $k-\epsilon$ model. This result indicates that the turbulence scale or the kinetic eddy viscosity are needed for the inflowing boundary condition and such a boundary condition should be made and given to the LES.

6. REFERENCE

1. GIVONI, B.
"Man, Climate and Architecture"
2nd Edition, Applied Science Publishers, 1976
2. CLARK, R.P. and EDHOLM, O.G.
"Man and His Thermal Environment"
Edward Arnold, 1985
3. LAUNDER, B.E. and SPALDING, D.B.
"Mathematical Models of Turbulence"
Academic Press, 1972
4. DEARDORFF, J.W.
"A Numerical Study of Three-Dimensional Turbulent Channel Flow at Large Reynolds Number"
J. Fluid Mechanics, Vol.41, Part 2, 1970, pp.453-480
5. ROACHE, P.J.
"Computational Fluid Dynamics"
Hermosa Publishers, 1976
6. NISHIDA, M., KATAYAMA, T., ISHII, A, TSUTSUMI, J., ISHII, Y
"Wind Tunnel Simulation of Cross-Ventilation in Apartment Houses"
Trans. of A.I.J, No.375, 1987, pp.1-9 (in Japanese)
7. MURAKAMI, S., KOBAYASHI, N., KATO, S. and AKABAYASHI, S.
"Experimental Study on Natural Ventilation of Dwelling"
Trans. of A.I.J, No.372, 1987, pp.10-20 (in Japanese)
8. SMAGORINSKY, J.S.
"General Circulation Experiments with the Primitive Equations;
Part 1 Basic Experiments"
Monthly Weather Review, Vol.91, 1963, pp.93-164
9. TSUTSUMI, J., URANO, Y. and NISHIDA, M.
"Numerical Experiments of Thermal Convection in a Room with Natural Ventilation by Large Eddy Simulation and Its Model Tests"
Trans. of A.I.J, No.376, 1987, pp.19-28
10. MURAKAMI, S., MOCHIDA, A. and HIBI, K.
"Three Dimensional Numerical Simulation for Air Flow around Building Part 1"
Trans. of A.I.J, No.360, 1986, pp.1-11

EFFECTIVE VENTILATION

9th AIVC Conference, Gent, Belgium
12-15 September, 1988

Poster 10

MULTI-ZONE CONTAMINANT DISPERSAL ANALYSIS USING:
AN ELEMENT ASSEMBLY APPROACH

J. AXLEY

National Bureau of Standards
Gaithersburg, MD
20899
U.S.A.

ABSTRACT

An *element-assembly* formulation of multi-zone contaminant dispersal analysis theory is described. In this approach a flow system is idealized as an assemblage of *mass transport elements* that model specific instances of contaminant mass transport in the flow system. Equations governing the mass transport phenomena modeled by each element are expressed in terms of contaminant concentration variables, the *nodal concentration variables*, that approximate the contaminant concentration at discrete points, the *system nodes*, in the flow system. The imposition of conservation of mass allows these element equations to be assembled to form spatially discrete but temporally continuous equations that govern the system as a whole. These *system equations* may then be solved to determine the response of the system to contaminant excitation. At its most general level this approach makes no limiting assumptions about the nature of the mass transport phenomena modeled (beyond the assumption of mass conservation) and is, therefore, not limited, in principal, to the well-mixed zone idealization, although, it includes the well-mixed multi-zone theory as a special case.

Element equations for; a) well-mixed zones, b) instantaneous flow transport (with and with out filtering), c) mass transport phenomena governed by first order kinetics, and d) mass transport phenomena governed by the one-dimensional convection diffusion equation are presented. Solution options are outlined, examples of application are presented, and the CONTAM family of programs, that provide one implementation of the theory, is briefly described.

NOMENCLATURE

A	cross-sectional area of flow passage
C	contaminant concentration expressed in terms of mass fraction
αD	dispersal coefficient for species α
g	contaminant mass generation rate associated with an element
G	direct contaminant mass generation rate at a system node
L	length of flow passage
m^e	mass of a volume of flow fluid associated with an element
P	pressure
αR	rate of kinetics process
T	temperature
t	time
\bar{t}	nominal transit time
\bar{u}	bulk (i.e., sectional average) fluid velocity
\mathbf{v}	fluid velocity vector
w	mass transport rate
x,y,z	spacial coordinates
ϕ	upwind parameter
$\alpha \gamma$	dimensionless generation rate of species α
κ	reaction rate coefficient
$\alpha \eta$	filter efficiency relative to species α
ρ	mass density
τ	dimensionless time; system time constants
χ	dimensionless length

Subscripts, Superscripts and other Symbols

species index $\rightarrow \alpha$ $a \leftarrow$ element index
 descriptive index $\rightarrow \text{con } X_j$ \leftarrow node or array element index

a, b, c, \dots . . . specific element indices
 e general element index
 $\alpha, \beta, \gamma, \dots$. . . specific species indices
 α general species index
 i, j, k, l, m, n . . . node (or array element) indices
 k, n time step or iterate indices
 \wedge quantities modified to account for boundary conditions
 \sim quantities modified to account for zero "volumetric" mass terms

Vectors and Matrices

$\{C\}$ system concentration vector
 $\{C^e\}$ element concentration vector
 $\{\Phi\}$ (steady flow/kinetics) system eigenvectors
 $\{E\}$ system excitation vector
 $\{G\}$ system direct (nodal) species generation rate vector
 $\{G\}$ system generation rate vector
 $\{g^e\}$ element-derived species generation rate vector
 $[\kappa]$ kinetics rate coefficient matrix
 $L^e(\{V\})$. . . transformation of vector $\{V\}$
 $[M]$ system mass matrix
 $[M^e]$ diagonal mass matrix associated with kinetics element
 $\{R\}$ kinetics rate vector
 $\{R_o\}$ constant component of kinetics rate vector
 $[W]$ system (mass) transport rate matrix
 $[Z]$ additional (hypothetical) system transformation matrix
 $\{w^e\}$ element mass transport rate vector
 $[x^e]$ element (mass) transport matrix
 $[y^e]$ element mass matrix
 $[z^e]$ additional (hypothetical) element transformation matrix

INTRODUCTION

The central concern of indoor air quality analysis is the prediction of airborne contaminant dispersal in buildings. Airborne contaminants disperse throughout buildings in a complex manner that depends on the nature of airflow into, out of, and within the building system; that depends on the possibility of removal, by filtration, or generation of contaminants; and that depends on the possibility of chemical reaction, radio-chemical decay, settling, precipitation, deposition, or sorption of contaminants. More succinctly, we may say that contaminant dispersal in buildings is, in general, affected by a large variety of often very complex mass transport processes. The purpose of this paper is to present an analytical method to predict contaminant dispersal in buildings that can comprehensively and systematically account for

these complex mass transport processes.

While it is generally recognized that practical methods of contaminant dispersal analysis may be based upon either the microscopic equations of motion¹ [Davidson 87] or the well-mixed zone simplification of the macroscopic mass balance equations for flow systems², the application of these techniques has been largely limited to dispersal driven solely by flow mass transport processes and the possibility of combining macro and microscopic approaches has received little consideration. An element assembly formulation of the contaminant dispersal problem provides a means to not only combine the microscopic and macroscopic techniques but offers a convenient framework for the inclusion of models of the various nonflow mass transport processes that may affect the dispersal of contaminants in a building.

In this paper we shall present an element assembly formulation of the contaminant dispersal problem that generalizes the work done earlier [Axley 87, 88]. An emphasis will be placed on modeling building airflow systems, but the theory and methods developed may be applied to other flow systems as well.

The Contaminant Dispersal Model

We begin by asserting that:

Building airflow systems may be idealized as *assemblages* of discrete *mass transport elements* that model specific instances of contaminant mass transport within the building by relating the time variation of contaminant concentration at discrete points in the building system, the *system nodes*, to the flow and nonflow processes responsible for the dispersal.

This contaminant dispersal model involves, then;

- a) a spatial discretization of the domain of the airflow system (i.e., the selection and identification of the system nodes) and,
- b) the discrete idealization of the mass transport processes responsible for dispersal within the system (i.e., the selection and specification of the mass transport elements).

We shall show that if element equations governing these instances of mass transport are developed within the restrictions of a certain general form then they may be directly assembled to form equations governing the dispersal of contaminants in the system as a whole. Before considering the formal development of this approach, however, it will be useful to consider the element assembly approach from the point of view of a user of this theory.

A User's View of the Element Assembly Approach

Consider the section of a hypothetical two story residence with basement shown below, Figure 1. For this building, let's say, we are concerned with the dispersal of carbon monoxide generated within the furnace of the simple forced-air heating system that serves this residence.

To model contaminant dispersal in a given building system the analyst must first become familiar with the building's airflow system (i.e., HVAC system, infiltration/exfiltration and room-to-room airflow paths) and identify any nonflow mass transport process that may significantly

¹ *Microscopic equations of motion*: differential formulations of the continuity, motion, and energy equations for fluids, (e.g., the Navier-Stokes equation or the Euler equation)

² *Well-mixed zone simplification of the macroscopic equations of motion*: the approach known variously as the "multi-zone", "multi-chamber", "multi-cell", or "compartments" model [Sinden 78, Sandberg 84, Walton 85], that is closely related to similar models used in the chemical engineering field [Wen 75].

affect the dispersal process. With this knowledge in mind, the analyst iteratively selects appropriate contaminant dispersal elements from the *library* of available elements and identifies system nodes to which these elements are "connected" to assemble an *idealization* of the given building airflow system.

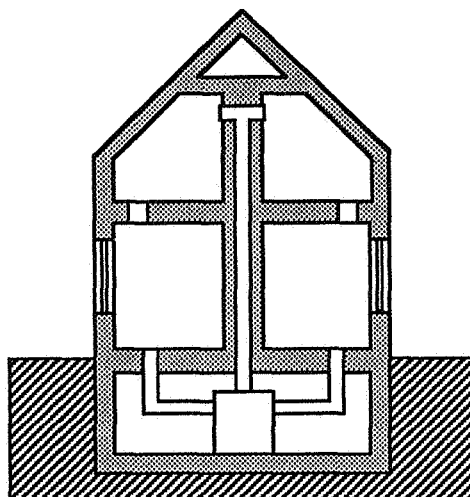


Fig. 1 Hypothetical Two Story Residence

The development of an idealization may often be formulated graphically in a direct and intuitive way. For the hypothetical problem introduced above we may select from the current library of dispersal elements shown in Figure 2.

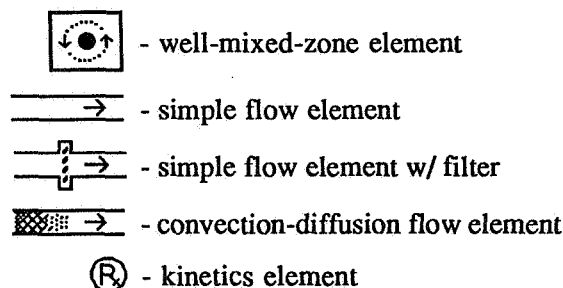


Fig. 2 Current Library of Contaminant Dispersal Elements

Figure 3 shows a possible idealization of this hypothetical building assembled graphically, and hence mathematically, from this library of elements. (The large black dots in this figure correspond to discrete points in the airflow system, the *system nodes*.)

In this example, each of the four rooms, the exterior environment, and the furnace air heating chamber have been modeled with *well-mixed-zone elements*; infiltration, exfiltration, and first-to-second story airflows have been modeled with *simple flow elements*; the HVAC duct flow paths have been modeled with *1D convection-diffusion flow elements* (in an attempt to account for flow delays in this part of the flow system) and the generation of carbon monoxide within the furnace system has been modeled with a *kinetics element*. The kinetics element makes this idealization specific to the analysis of carbon monoxide dispersal in the building system; by removing this kinetics element we would obtain an idealization appropriate for modeling the dispersal of a variety of noninteractive contaminants.

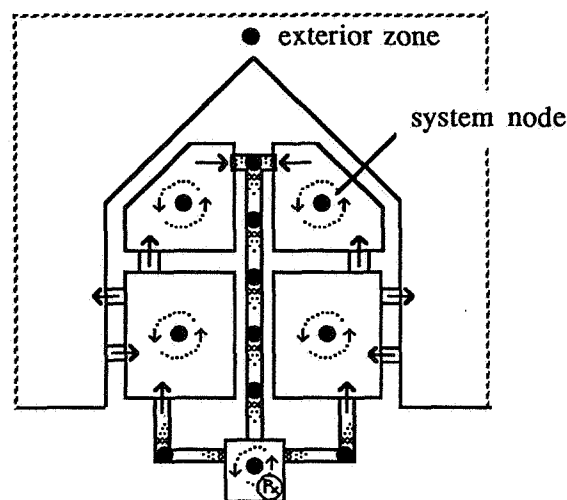


Fig. 3 Idealization of the Building Airflow System

With an idealization in hand the analyst is then in the position to consider any of several solution options, including solutions for steady state concentrations for conditions of steady contaminant generation and steady airflows, evaluation of system time constants for conditions of steady airflows, and evaluation of time histories of contaminant concentrations for various scenarios of steady or unsteady airflows with steady or unsteady contaminant generation rates.

After considering the results of the analysis the analyst may add, delete, or modify elements in an effort, for example, to mitigate an indoor contaminant hazard and then re-analyze the system to evaluate the efficacy of the proposed mitigation measure.

GENERAL FORMULATION

In this section we present a formulation of the contaminant dispersal analysis problem by element assembly that is more general than the formulations presented earlier [Axley 87, 88]. To do so, however, it is useful to repeat parts of the past presentations; the author asks the forbearance of those familiar with these earlier formulations for this repetition.

In indoor air quality analysis we may consider building airflow systems to be three dimensional fields, within which we seek to completely describe the temporal and spatial variation of the *state* of infinitesimal air parcels, providing that the concentration of contaminants within these parcels can be assumed to be uniform³. A parcel, here, is small relative to the scale of the components of the system but large relative to the molecular scale and its state is defined by its temperature, pressure, velocity, and contaminant concentration(s) – the *state variables* of indoor air quality analysis.

The central problem of indoor air quality analysis is, then, the determination of the spacial (x,y,z) and temporal (t) variation of contaminant species concentrations (C) within the domain of the airflow system. This analytical problem will be referred to as *contaminant dispersal analysis*.

For a single *noninteractive*⁴ species, α , contaminant dispersal is driven by the air

³ In some flow systems (e.g., chemical process flow systems) this assumption may not be appropriate; there may be a segregation of components at the micro-scale and, thus, the flow system may not be considered to be a simple continuum.

velocity field (\mathbf{v}) and thus the contaminant dispersal analysis problem, for this case, may be represented, functionally, as:

$${}^{\alpha}C(x,y,z,t) = {}^{\alpha}C(\mathbf{v}(x,y,z,t)) ; \dots \quad (1)$$

where the ellipses, ... , are used to indicate the geometry, initial conditions, and boundary conditions required to complete the definition of the analytical problem. To solve the contaminant dispersal problem, then, the flow field must be either specified or determined.

Two approaches to flow determination may be considered. In the first approach a nonlinear *flow analysis* problem and, in general, a coupled *thermal analysis* problem is formulated and solved, given the environmental excitation (e.g., wind, solar, and thermal excitation) acting on the building system. Alternatively, for existing buildings it may be possible to "measure" building airflows using tracer gas techniques. These techniques are based on the formulation and solution of the *inverse contaminant dispersal analysis* problem. In this presentation we will assume that building airflows are known and will not consider these related problems.

When the kinetics of contaminant reaction, settling, sorption, etc. is important, the contaminant dispersal analysis problem becomes a coupled (and, generally, nonlinear) analysis problem as (the rate of change of) each species' concentration will depend upon both species' concentrations and the airflow velocity field:

$${}^{\alpha}C(x,y,z,t) = {}^{\alpha}C(\mathbf{v}(x,y,z,t), {}^{\alpha}C(x,y,z,t), {}^{\beta}C(x,y,z,t)) ; \dots \quad (2)$$

For such cases we say the contaminant is an *interactive* contaminant and describe the analytical problem as a problem of *interactive contaminant dispersal analysis*.

Basic Approach

The approach to the solution of these field problems taken here is straightforward, but involves several steps. The continuously defined state variables – the contaminant concentrations, ${}^{\alpha}C(x,y,z,t)$, ${}^{\beta}C(x,y,z,t)$, ... – are replaced by a finite set of *discrete system state variables*, $\{\mathbf{C}(t)\}$, that are meant to approximate the value of the continuous variables at discrete points – the *system nodes* – in the airflow system. Equations of a restricted, but very general form, are then defined that may be used to describe the specific mass transport processes that drive the dispersal of contaminants in the flow system. These *element equations* are defined in terms of subsets of the discrete state variables – the *discrete element state variables* $\{\mathbf{C}^e\}$. These element equations may be assembled to form systems of spatially discrete but temporally continuous ordinary differential equations that govern the contaminant dispersal behavior of the system as a whole.

This approach allows consideration of element models based upon both the microscopic equations of motion (e.g., using Finite Element solutions to subdomains of the flow system domain) and macroscopic mass balance equations for flow systems (i.e., the basis of the familiar well-mixed zone models) and has been contrived to be completely analogous to the approaches employed for the solution of the related flow and thermal analysis problems [Axley 86, 87].

Discrete System State Variables

We associate contaminant concentration variables with each of the system nodes and organize these discrete state variables into the *system concentration vector* which for n nodes

⁴ *Noninteractive Contaminant*: a contaminant whose dispersal is not affected by kinetics of reaction, sorption, settling, or other similar or related mass transport phenomena.

is defined as:

- for the dispersal of a single species, α :

$$\{C\} \equiv \{ {}^{\alpha}C_1, {}^{\alpha}C_2, \dots {}^{\alpha}C_n \}^T \quad (3a)$$

- for the dispersal of two species, α and β :

$$\{C\} \equiv \{ {}^{\alpha}C_1, {}^{\beta}C_1, {}^{\alpha}C_2, {}^{\beta}C_2, \dots {}^{\alpha}C_n, {}^{\beta}C_n \}^T \quad (3b)$$

- etc.

Discrete Element State Variables

We model the mass transport processes that determine the nature of contaminant dispersal within the flow system with an *assembly* of mass transport elements. With each element "e" in the assembly we associate one or more nodes – the *element nodes* – and with each node we associate variables that define the state of the element – the *element (state) variables*, (i.e., subsets of the system variables⁵) and note their association with the system variables. Thus, for example, a contaminant dispersal element having three nodes, i, j, and k, would have the element state variables;

- for the dispersal of a single species, α :

$$\{C^e\} \equiv \{ {}^{\alpha}C_i^e, {}^{\alpha}C_j^e, {}^{\alpha}C_k^e \}^T \quad (4a)$$

- for the dispersal of two species, α and β :

$$\{C^e\} \equiv \{ {}^{\alpha}C_i^e, {}^{\beta}C_i^e, {}^{\alpha}C_j^e, {}^{\beta}C_j^e, {}^{\alpha}C_k^e, {}^{\beta}C_k^e \}^T \quad (4b)$$

- etc.

These variables will be identified as the *element concentration vectors*.

General Form of the Element Equations

We attempt to describe the *behavior* of appropriate classes of elements by equations of the general form:

$$\boxed{\{w^e\} = L^e (\{C^e\}) - \{g^e\}} \quad (5)$$

where;

$\{w^e\}$ is a vector of element contaminant mass transport rates into the element from each of the element nodes. For a three-node element with nodes, i, j, and k the elements of this vector are defined as;

- for the dispersal of a single species, α :

$$\{w^e\} \equiv \{ {}^{\alpha}w_i^e, {}^{\alpha}w_j^e, {}^{\alpha}w_k^e \}^T \quad (6a)$$

- for the dispersal of two species, α and β :

$$\{w^e\} \equiv \{ {}^{\alpha}w_i^e, {}^{\beta}w_i^e, {}^{\alpha}w_j^e, {}^{\beta}w_j^e, {}^{\alpha}w_k^e, {}^{\beta}w_k^e \}^T \quad (6b)$$

⁵ As subsets of the system variables, one must distinguish, mathematically, these element variables from the system variables even though, most often, there will be no physical distinction between them.

• etc.

$L^e(\{C^e\})$ is a transformation of $\{C^e\}$ that has the form of a linear transformation and is specific to a given class of elements

$\{g^e\}$ is a vector of element-derived species generation rates.

The vector of species mass transport rates, $\{w^e\}$, for the dispersal of a single species α , may be represented diagrammatically as shown below for a hypothetical three-node flow element that links three well-mixed zone elements, Figure 4, and a single-node kinetics element associated with a single well-mixed zone element, Figure 5. The arrows indicate positive mass transport rates.

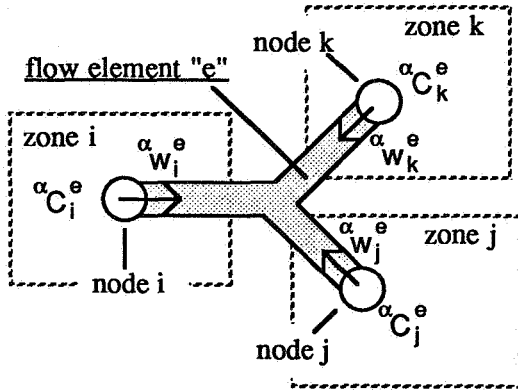


Fig. 4 Hypothetical Three-Node Flow Element

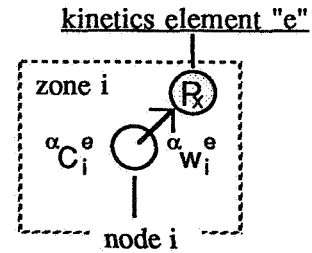


Fig. 5 Single-Node Kinetics Element

For the flow element, mass is transported physically by the airflow moving from each zone into the element; the arrows represent the positive sense of this physical transport. For kinetics elements, mass transport is somewhat more subtle as it involves a conversion of species mass from one form to another. The arrow indicating mass transport in Figure 5 is, thus, directed into the element from the zone node to indicate removal of species α by conversion, rather than physical transport.

It is important to note that it will be necessary to define the element mass transport rate vector so that there will be an element mass transport rate variable corresponding to each of the element concentration variables to account for all possibilities of mass transport.

For contaminant dispersal involving multiple species, then, a single *simple* flow element might be thought to transport each individual species from zone-to-zone while a kinetics element might be thought to transport mass, by conversion from each of the species to any or all of the other species and/or from any of the species to a noncontaminant form that is of no special interest, within the single zone associated with the kinetics element. (Inasmuch as it is difficult to represent these possible multi-species mass transport/conversion phenomena diagrammatically we shall not attempt to do so, here.)

The element transformation operator $L^e()$ is restricted to the form of a linear transformation:

$$L^e(\{C^e\}) \equiv [x^e]\{C^e\} + [y^e]\frac{d\{C^e\}}{dt} + [z^e]\frac{d^2\{C^e\}}{dt^2} + \dots$$

(7)

where;

$[x^e], [y^e], [z^e]$ are square transformation coefficient matrices
 $[x^e]$ is the *element (mass) transport matrix*
 $[y^e]$ is the *element mass matrix*

However, we admit transformation coefficient-matrices that may, in fact, vary with time and/or depend, nonlinearly, on the element concentration vector. As a practically endless variety of element equations may be formulated that have this form, the restriction to this form should not lead to any serious limitation.

System Equations

By restricting the element equations to the form of linear transformations (i.e., equations (5) and (7)) these equations may be directly *assembled* to yield the *system equations* that describe the dispersal of the contaminant species within the whole building's airflow system:

$$\boxed{[W]\{C\} + [M]\frac{d\{C\}}{dt} + [Z]\frac{d^2\{C\}}{dt^2} + \dots = \{G\}} \quad (8a)$$

where;

$$[W] = \underset{e = a, b, \dots}{\mathbf{A}} [x^e] \quad \text{the system (mass) transport matrix} \quad (8b)$$

$$[M] = \underset{e = a, b, \dots}{\mathbf{A}} [y^e] \quad \text{the system mass matrix} \quad (8c)$$

$$[Z] = \underset{e = a, b, \dots}{\mathbf{A}} [z^e] \quad (8d)$$

etc.

$$\{G\} = \{G\} + \underset{e = a, b, \dots}{\mathbf{A}} \{g^e\} \quad \text{the system generation vector} \quad (8e)$$

where \mathbf{A} is the assembly operator, a generalization of the conventional summation operator, Σ . The assembly procedure is based upon the requirement that contaminant species mass must be conserved at each of the systems nodes. It may be represented formally by transformation and summation of element arrays but is practically implemented using relatively simple computational algorithms that accumulate element arrays terms in memory locations of the corresponding system array terms [Axley 87, 88].

SPECIFIC ELEMENT EQUATIONS

The element equations corresponding to the current library of contaminant dispersal elements are presented here and the basis of their development is briefly reviewed. Details relating to the development of these element equations and their use have been presented elsewhere [Axley 87, 88].

Well-Mixed Zone Element

It is often reasonable to model portions of a building airflow system as-if they are perfectly mixed zones. By definition, the concentration of contaminants is uniform within a perfectly mixed zone, thus a single variable for each contaminant species (associated with a single node

located arbitrarily within the zone) is sufficient to describe the spacial variation of contaminant concentration within a well-mixed zone. The rate of change of species mass within a well-mixed zone, or, from an element perspective, the species mass transport into the well-mixed zone "element" from the system node associated with the zone, is defined by the following element equation:

$$\boxed{\{\alpha w_i^e\} = [m^e] \left\{ \frac{d\alpha C_i^e}{dt} \right\}} \quad \text{well-mixed zone element} \quad (9a)$$

or, in terms of the general element transformation arrays defined above:

$$[y^e] = [m^e] \quad \text{for:} \quad \{w^e\} \equiv \{\alpha w_i^e\} \quad (9b)$$

for species α in a well-mixed zone having a volume containing a mass of air of m^e .

Simple Flow Element

Flow through many flow passages in building airflow systems is practically instantaneous (i.e., relative to the dominant time constants of the building's dispersal system) and, therefore, may be modeled as such. The mass transport of a single species, say α , through a simple flow passage with a single inlet and outlet in which flow is assumed to be instantaneous may be described using a two-node *simple flow element*. Given the air mass flow rate $w^e(t)$ from node i to node j we may write the following element equations directly from fundamental considerations:

$$\boxed{\begin{Bmatrix} \alpha w_i^e \\ \alpha w_j^e \end{Bmatrix} = w^e(t) \begin{bmatrix} 1 & 0 \\ -1 & 0 \end{bmatrix} \begin{Bmatrix} \alpha C_i^e \\ \alpha C_j^e \end{Bmatrix} ; w^e(t) \geq 0} \quad \text{simple flow element} \quad (10a)$$

or, in terms of the general element transformation arrays defined above:

$$[x^e] = w^e(t) \begin{bmatrix} 1 & 0 \\ -1 & 0 \end{bmatrix} \quad \text{for:} \quad \{w^e\} \equiv \{\alpha w_i^e, \alpha w_j^e\}^T \quad (10b)$$

It should be noted that the transformation matrix $[x^e]$ is seen to vary with time to account for the time variation of flow through the element. (Figure 6, below, should help to clarify the meaning of the element variables in this case.)

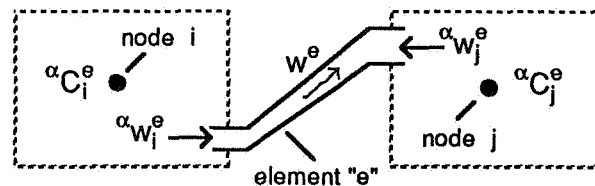


Fig. 6 Simple Contaminant Dispersal Flow Element Variables

The well-mixed, multi-zone theory presented by Sinden [78] and Sandberg [84] is completely equivalent to an element assembly approach limited to the use of well-mixed zone

and simple flow elements. Through the development of additional elements, then, we may extend the conventional multi-zone theory. We also, importantly, provide an alternative formal view of this theory that provides a deeper understanding of the qualitative character of the theory and, therefore, of contaminant dispersal in buildings in general.

Simple Flow Element with Filtration

The simple flow element equations, above, may be modified to account for the action of a filter that removes a fraction, $\alpha\eta$, of the contaminant α as it passes through the element to yield the following element equations;

$$\begin{bmatrix} \alpha w_i^e \\ \alpha w_j^e \end{bmatrix} = w^e(t) \begin{bmatrix} 1 & 0 \\ (\alpha\eta - 1) & 0 \end{bmatrix} \begin{bmatrix} \alpha C_i^e \\ \alpha C_j^e \end{bmatrix} \quad \text{simple flow element w/ filtration (11a)}$$

or, in terms of general element transformation arrays defined above:

$$[x^e] = w^e(t) \begin{bmatrix} 1 & 0 \\ (\alpha\eta - 1) & 0 \end{bmatrix} \quad \text{for:} \quad \{w^e\} \equiv \{ \alpha w_i^e, \alpha w_j^e \}^T \quad (11b)$$

In this case the time variation of the transformation matrix, $[x^e]$, could be due to both the time variation of flow through the element and the time variation of the filter efficiency, $\alpha\eta = \alpha\eta(t)$.

1D Convection-Diffusion Flow Element

In some situations the analyst may be interested in the details of dispersal in some flow passages or may feel the noninstantaneous nature of the flow should not be ignored. If flow in these flow passages may be assumed to be practically one-dimensional (e.g., flow in portions of HVAC ducts) then the details of the convection and diffusion mass transport processes that drive the dispersal may be accounted for using assemblages of two-node *convection-diffusion elements*.

These elements may be developed using a Finite Element solution of the one-dimensional convection diffusion equation:

$$\frac{1}{Pe} \frac{\partial^2 \alpha C}{\partial \chi^2} + \alpha \gamma = \frac{\partial \alpha C}{\partial \tau} + \frac{\partial \alpha C}{\partial \chi} \quad (12a)$$

where;

$$Pe \equiv \frac{w^e L}{\rho A \alpha_D} = \frac{\bar{U} L}{\alpha_D} \quad \text{the dimensionless Peclet Number} \quad (12b)$$

A is the cross-sectional area of the flow passage

α_D is the dispersal coefficient for species α

L is the length of the flow passage

χ is the dimensionless length $\equiv x/L$

τ is the dimensionless time $\equiv t/\bar{t}$

$\alpha \gamma$ is the dimensionless generation rate $\equiv \alpha g L / w^e$

αg is the mass generation rate of species α per unit length of flow passage

\bar{t} is the nominal transit time $\equiv L/\bar{u}$
 \bar{u} is the bulk fluid velocity $= w^e/\rho A$

The Peclet number provides a measure of the importance of convection mass transport relative to diffusion mass transport; at one extreme $Pe = 0$ would correspond to a well-mixed condition and at the other $Pe = \infty$ would correspond to an ideal plug-flow condition.

Following the one-dimensional example discussed by Huebner and Thornton [82] element equations for a two-node flow element may be developed from equation (12) using linear shape functions (i.e., assuming species concentrations vary in a piece-wise linear manner along the flow passage) and applying either the (conventional) Galerkin method or the (upwind) Petrov-Galerkin method in the formulation of these element equations. The resulting element equations are:

$$\boxed{\{w^e\} = [{}_c x^e] + [{}_d x^e]\{C^e\} + [y^e] \frac{d\{C^e\}}{dt} - \{g^e\}} \quad \text{convection-diffusion element} \quad (13a)$$

where;

$$[{}_c x^e] = \frac{w^e}{2} \begin{bmatrix} 1 & 1 \\ -1 & -1 \end{bmatrix} + \frac{\phi w^e}{2} \begin{bmatrix} 1 & -1 \\ -1 & 1 \end{bmatrix} \quad (13b)$$

= the *convection component* of the element mass transport matrix

ϕ = the so-called *upwind parameter*, $0 \leq \phi \leq 1$

$$[{}_d x^e] = \frac{\rho A {}^\alpha D}{L^e} \begin{bmatrix} 1 & -1 \\ -1 & 1 \end{bmatrix} \quad (13c)$$

= the *diffusion component* of the element mass transport matrix

L^e = the length of the element (i.e., a portion of the length of the flow path)

$$[y^e] = \frac{\rho A L^e}{6} \begin{bmatrix} 2 & 1 \\ 1 & 2 \end{bmatrix} + \frac{\phi \rho A L^e}{4} \begin{bmatrix} -1 & -1 \\ 1 & 1 \end{bmatrix} \quad (13d)$$

= the *element volume mass matrix*

or

$$[y^e] \approx \frac{\rho A L^e}{2} \begin{bmatrix} 1 & 0 \\ 0 & 1 \end{bmatrix} \quad (13e)$$

= the *lumped approximation* to the element volume mass matrix

$$[g^e] = \frac{{}^\alpha g L^e}{2} \begin{Bmatrix} 1 \\ 1 \end{Bmatrix} + \frac{\phi {}^\alpha g L^e}{2} \begin{Bmatrix} -1 \\ 1 \end{Bmatrix} \quad (13f)$$

= the *internal generation rate vector*

for species α and fluid mass flow rate, $w^e \geq 0$, through the flow passage from node i to node j.

The use and numerical characteristics of the convection-diffusion element, the inclusion of species generation kinetics, and a comparison to the closely related *tanks-in-series* model commonly used in the chemical engineering field has been presented elsewhere [Axley 88]. Suffice it to say that this element is not for the uninitiated. Numerical solutions to the convection-diffusion equations remains a very active and controversial area of research. The inexperienced analyst is well-advised to become familiar with current literature relating to Finite Element solutions of the convection-diffusion equations before attempting to use this

element.

Two aspects of the convection-diffusion element are especially important. First, the convection-diffusion element is based upon a microscopic description of dispersal and it use provides a first example of combining macroscopic modeling techniques with microscopic techniques in a single analytical method. Secondly, from another perspective a one-dimensional flow regime may be thought to represent an imperfectly mixed zone, therefore, the convection-diffusion flow element may be considered to be an *imperfectly-mixed zone element*. The use of this element in modeling imperfectly mixed zones has yet to be explored, but it is believed it holds much promise.

Kinetics Elements

In some situations the analyst may wish to model mass transport due to chemical reaction, radiochemical decay, adsorption, absorption, settling, deposition, agglomeration, or precipitation of contaminants. The mass transport characteristics of such processes is described by the so-called *kinetics* of the process, a term borrowed from the literature of *reaction kinetics*⁶.

In the present context we consider a kinetic process to involve the contaminant species α , β , ... that interact and/or are transformed in some way to form product species or phases ρ , σ , ..., as:



where we explicitly consider the possible affect of catalysts on the process. The product species or phases may or may not be considered to be contaminants.

In general, the rate of a given kinetic process may depend upon a variety of factors including reactant, product, and catalyst concentrations, temperature, T, pressure, P, and the detailed mechanisms of the kinetic process (i.e., the mechanisms of both chemical and physical processes that, together, govern the kinetics process) therefore, rate expressions take the general functional form of:

$$^{\alpha}R = ^{\alpha}R(^{\alpha}C, ^{\beta}C, \dots ^{\rho}C, ^{\sigma}C, \dots T, P, \dots) \quad (15)$$

where, the rate of kinetics process may be defined in terms of the rate of change of one of the species involved in the process as:

$$^{\alpha}R \equiv \frac{d^{\alpha}C}{dt} \quad ; \text{ rate of kinetics process in terms of species } \alpha \quad (16)$$

Rate expressions for certain general classes of chemical reactions (and presumably the kinetic processes considered here), including single-reactant, consecutive, opposing, and concurrent first order reactions [Moore 81], may take the form of linear combinations of contaminant concentrations:

$$\{R\} = -[\kappa]\{C\} + \{R_o\} \quad (17a)$$

or

⁶ Reaction kinetics involves the study of the rate of change of chemical components in a single or related series of chemical reactions.

$$\begin{pmatrix} \alpha R \\ \beta R \\ \vdots \\ \sigma R \end{pmatrix} = - \begin{bmatrix} \alpha\alpha_K & (-\alpha\beta_K) & \dots & (-\alpha\sigma_K) \\ (-\beta\alpha_K) & \beta\beta_K & \dots & (-\beta\sigma_K) \\ \vdots & \vdots & \ddots & \vdots \\ (-\sigma\alpha_K) & (-\sigma\beta_K) & \dots & \sigma\sigma_K \end{bmatrix} \begin{pmatrix} \alpha C \\ \beta C \\ \vdots \\ \sigma C \end{pmatrix} + \begin{pmatrix} \alpha R_o \\ \beta R_o \\ \vdots \\ \sigma R_o \end{pmatrix} \quad (17b)$$

where we have included the constant component, $\{R_o\}$, for completeness and recognize that, again, the rate coefficient matrix, $[K]$, and the constant component vector, $\{R_o\}$, will, in general, vary with temperature and pressure.

The general rate expression, equation (15), leads directly to the development of a *general kinetics element*. Limiting consideration to kinetic processes occurring within a specific well-mixed zone "e" (were it is assumed that conditions are homogeneous), associated with the system node "i", and containing a set of contaminant species, $\alpha, \beta, \gamma, \dots$, we first identify the relevant element variables as:

$$\{C^e\} = \{ \alpha C_i^e, \beta C_i^e, \gamma C_i^e, \dots \}^T \quad (18)$$

and

$$\{W^e\} = \{ \alpha W_i^e, \beta W_i^e, \gamma W_i^e, \dots \}^T \quad (19)$$

Then from the rate definition, equation (16), and the general form of rate expressions, equation (15), we obtain the general kinetics element equations:

$$\{W^e\} = - [M^e] \{R^e(\{C^e\}, T, P)\} \quad (20a)$$

where;

$$[M^e] \equiv \text{diag} \{ m^e \ m^e \ m^e \ \dots \} \quad (20b)$$

m^e = the mass of the air in the volume of the well-mixed zone "e" associated with the kinetic processes being modeled

$$\{R^e(\{C^e\}, T, P)\} \equiv \begin{pmatrix} \alpha R(\alpha C_i^e, \beta C_i^e, \gamma C_i^e, \dots, T, P) \\ \beta R(\alpha C_i^e, \beta C_i^e, \gamma C_i^e, \dots, T, P) \\ \gamma R(\alpha C_i^e, \beta C_i^e, \gamma C_i^e, \dots, T, P) \\ \dots \end{pmatrix} \quad (20c)$$

or in this case we obtain:

$$[x^e] = 0 ; [y^e] = 0 ; \{g^e\} = [M^e] \{R^e(\{C^e\}, T, P)\} \quad (20d)$$

an element that is defined in terms of only element-derived species generation rates.

The form of equation (20) is deceptively simple. The rate expressions defining these element-derived species generation rates depend on species concentration, in general, so that the general kinetics element introduces a nonlinear species generation contribution (i.e., a species generation rate that depends nonlinearly on the solution vector $\{C\}$), which is distinctly different from the (constant or time dependent) nodal direct generation contribution. The solution of the contaminant dispersal problem involving general kinetics elements will,

therefore, generally require the application of a nonlinear solution strategy in the solution process.

Few interactive indoor contaminants have been studied in sufficient detail to completely define their kinetics, therefore, the consideration of arbitrarily nonlinear kinetics is premature at this time. For the present it is not unreasonable to attempt to approximate many kinetic processes using first order rate expressions of the form of equation (17), which when substituted into equation (20) lead to the *first order kinetics element equations*:

$$\boxed{\{w^e\} = [M^e] [k^e] \{C^e\} - [M^e] \{R_0^e\}} \quad \text{first order kinetics element} \quad (21a)$$

or:

$$\{x^e\} = [M^e] [k^e] ; \{y^e\} = 0 ; \{g^e\} = [M^e] \{R_0^e\} \quad (21b)$$

where, again, one must keep in mind that the rate coefficient matrix and constant rate component will, in general, be temperature and pressure dependent.

SOLUTION OF SYSTEM EQUATIONS

System equations based upon assemblages of the specific element equations presented above will have the following form:

$$[W]\{C\} + [M] \frac{d\{C\}}{dt} = \{G\} \quad (22)$$

To complete the definition of a contaminant dispersal problem it will be necessary to modify this equation to take into account appropriate boundary conditions and, in some instances to account for system nodes having no mass associated with them. With these modifications made the analyst will, typically, consider one of three types of analyses; eigenanalysis, steady state analysis, or general dynamic analysis. These fundamental solution operations are illustrated below in Figure 7. In this section we will briefly review these operations, more complete details may be found elsewhere [Axley 87, 88].

Boundary Conditions

The analyst may wish to specify concentration at some system nodes (e.g., ambient outdoor concentrations or controlled indoor environments) and as a result a subset of the system concentration vector $\{C\}$ will be known. At all other nodes contaminant generation rates may be specified and as a result a complementary subset of the system generation vector will be known. If one makes the algebraic simplifications to equation (22) to account for these specified *boundary conditions*, which, in general, will be time varying specifications, then a reduced system of equations will result involving a subset of the system concentration vector, $[\hat{C}]$, and corresponding submatrices of the system mass and mass transport matrices, $[\hat{M}]$ and $[\hat{W}]$. This reduced system of equations will have a right hand side, the *excitation vector*, $\{\hat{E}\}$, that will include terms relating to both specified generation rates and specified concentrations.

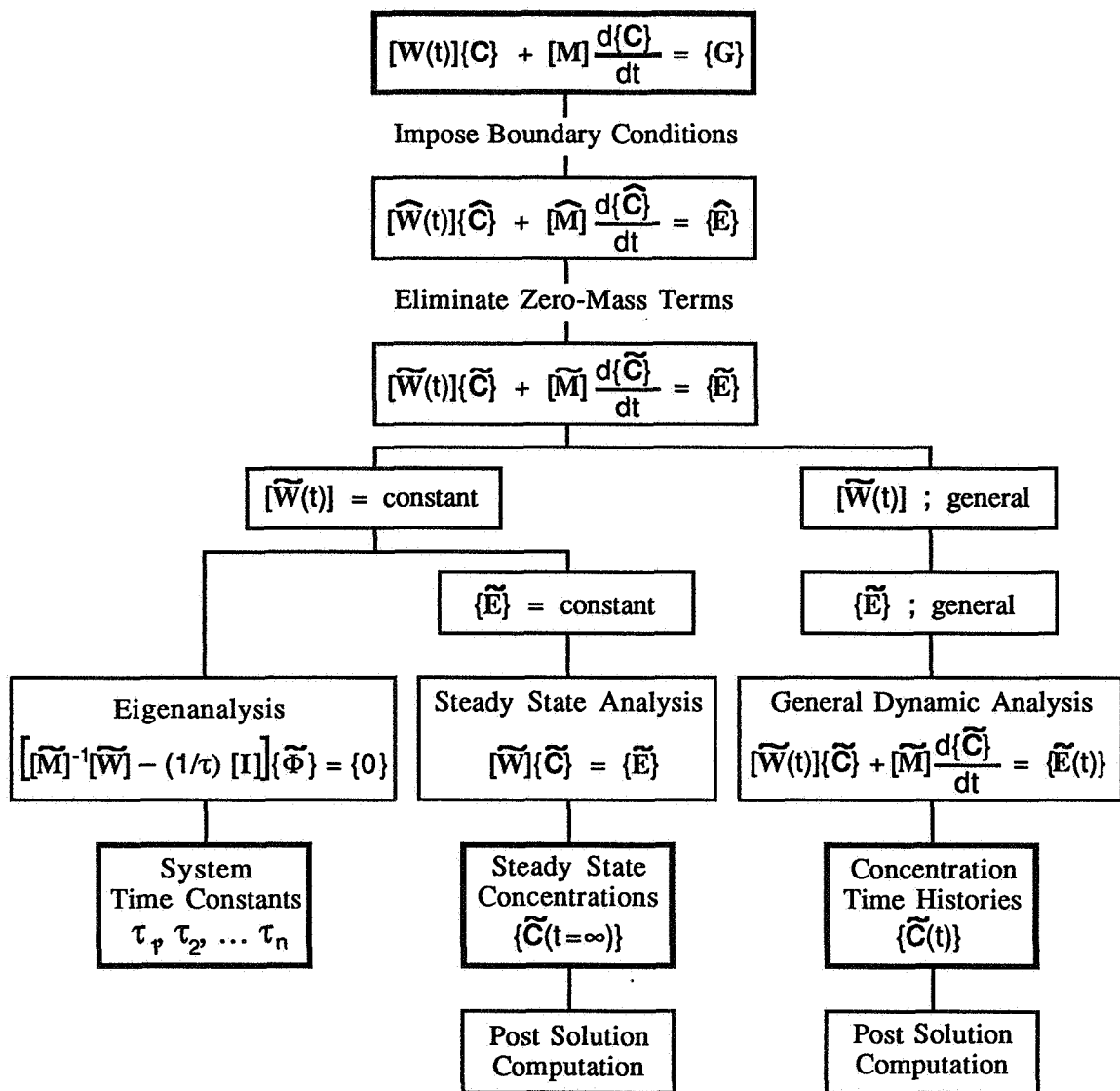


Fig. 7 Solution of System Equations

Zero-Mass Terms

In some instances the analyst may consider the mass contribution to a system node to be negligibly small (e.g., nodes in subassemblies corresponding to HVAC ductwork) and prefer to model these contributions with zero values. Zero mass terms may be accounted for algebraically resulting in a further reduction in the size of the system equations (i.e., the equation in Figure 7 with the tilde, ~, marks). This reduced set of equations will have as its unknowns the subset of the system concentration vector corresponding to those nodes having non-zero mass contributions for which contaminant generation rate time histories are specified.

Solution Options

The system equations obtained after the imposition of one or more concentration-specified boundary conditions and the elimination of zero-mass terms (i.e., the "tilde" equations in Figure 7) may then be used to solve either the eigenanalysis, steady state analysis, or general dynamic analysis problems. It may be shown that these equations will be soluble (i.e., have nonsingular system matrices) when airflow in the system idealization satisfies conservation of

total air mass flow and kinetics rate matrices are restricted to certain forms [Axley 88]. Furthermore, it may be shown that in these cases very efficient, yet numerically stable, solution methods based on LU decomposition without pivoting may be applied to the solution of these problems.

Eigenanalysis: For system idealizations involving steady flow and steady kinetics the analyst may determine the so-called system time constants using standard methods of eigenanalysis.

Steady State Analysis: For problems involving steady flow, steady kinetics, and steady excitation the system eventually will reach a condition of steady concentrations in all zones – the steady state condition. These steady state concentrations, $\{\tilde{C}(t=\infty)\}$, may be directly determined by solving the corresponding algebraic problem. Using these steady state concentrations the analyst may also determine the steady state concentrations at those system nodes associated with zero-mass terms that were "eliminated" from consideration and determine the steady state generation rates required to maintain the concentrations specified at the remaining system nodes.

General Dynamic Analysis: For problems involving steady or unsteady flow, kinetics, and/or system excitation the analyst may solve the complete dynamic problem using a variety of direct numerical integration schemes to compute concentration time histories, $\{\tilde{C}(t)\}$. Using these results the analyst may also determine the concentration time histories at those system nodes associated with zero-mass terms that were "eliminated" from consideration and determine the generation rates required to maintain the concentrations specified at the remaining system nodes.

IMPLEMENTATION & APPLICATION

A program, CONTAM87, has been developed at the National Bureau of Standards to provide an example of one computational implementation of the contaminant dispersal analysis theory presented above. CONTAM87 is the second member of the CONTAM series of programs [Axley 87, 88] that are being developed to provide an integrated set of computational tools for indoor air quality analysis. These tools are presented as a collection of *commands* that complete a variety of basic indoor air quality analysis operations. For example, the command FLOWELEM and its associated data defines flow element characteristics and location in a given element assembly, the command STEADY and its associated data defines and completes a steady state contaminant dispersal analysis problem, TIMECONS and its associated data defines the (steady flow/kinetics) eigenvalue problem and solves it reporting system time constants, etc. Future members of the CONTAM family will provide additional macroscopic flow analysis and inverse contaminant dispersal analysis commands, that may be used to determine airflows in building systems, and, eventually, building thermal analysis commands, based upon earlier work [Axley 86] could be added to provide a complete indoor air quality command processor language.

The programs CONTAM86 and CONTAM87 have been applied to a variety of contaminant dispersal analysis problems and have been employed to simulate new tracer gas methods for determining airflows in building systems. Here we shall present the results of three of these studies to provide some indication of the complexity of problems that may be considered.

NBS Office Building Study

Infiltration studies of a fifteen story office building are presently being conducted by members of the Indoor Air Quality and Ventilation Group at NBS. Some of these studies involve hourly injections of a commonly used tracer gas, SF_6 , into the fresh air supply ports of the building HVAC system. Flows in the supply ducts were measured (with significant uncertainty) by pitot traverse, SF_6 concentration time histories were recorded, and fresh air infiltration was estimated by tracer decay. Using the airflow measurements the upper two floors of this building were idealized as shown in Figure 8.

As indicated by this idealization, fresh air was supplied to each floor through a ceiling plenum space and exhausted via an exhaust duct to the outside. In Figure 9 we compare measured SF_6 concentration time histories (measured centrally within the "space" and at the "exhaust" ports) to computed values of the 15th floor for two supply flow rates: 100% and 75% of the measured flow. In this case, the agreement between measured and computed time histories is within the uncertainty of the measured flows and validation is therefore indicated.

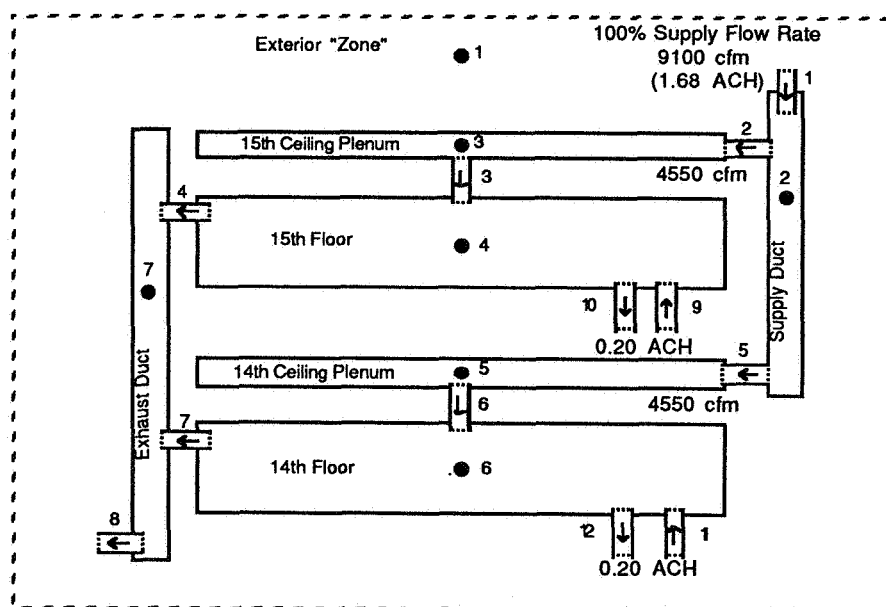


Fig. 8 Idealization of the 14th and 15th Floors of an Office Building

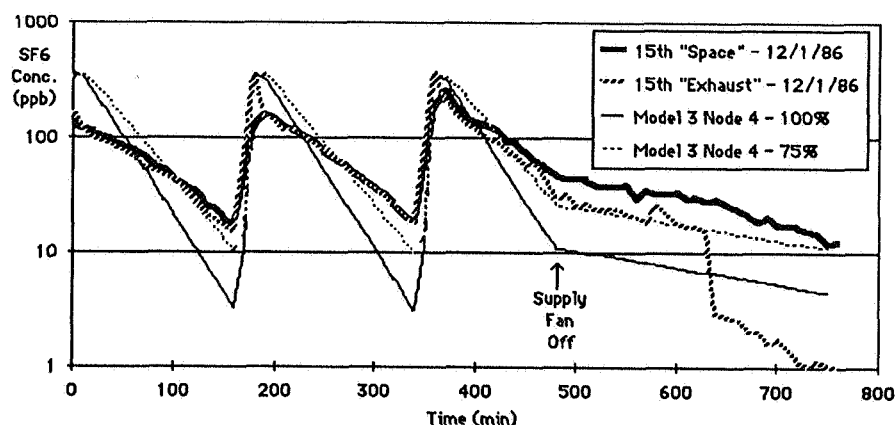


Fig. 9 Comparison of Computed and Measured Response for an Office Building

Carnegie-Mellon Townhouse Study

Borrazzo and his colleagues at Carnegie-Mellon University have conducted detailed field investigations of a two-story townhouse measuring CO, NO, and NO₂ emissions characteristics of the gas appliances within the townhouse and the dispersal of these contaminants throughout the townhouse under a variety of different weather conditions [Borrazzo 87.]. Illustrated in Figure 10 is an idealization of the townhouse and in Figure 11 the dynamic emission characteristics of the principal pollutant source; the gas range. The instantaneous emission rate, $G(t)$, is plotted relative to the steady state value, G_{ss} . The NO₂ emission characteristics were more or less constant and are, therefore, not illustrated. NO₂ is a reactive contaminant and was modeled as so using the measured reactivity of $\kappa=2.4 \text{ hr}^{-1}$.

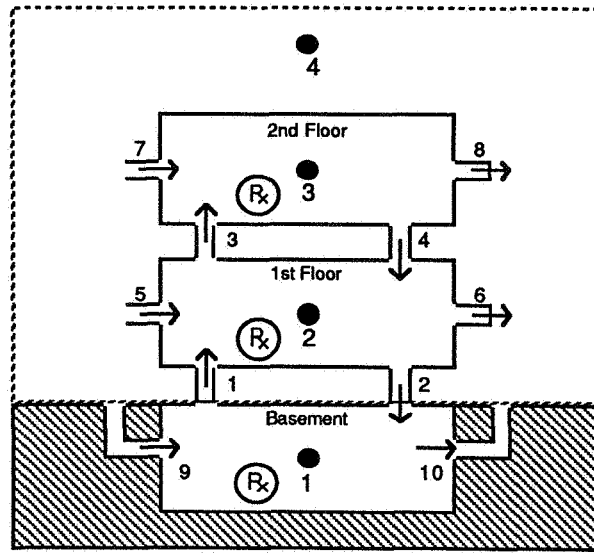


Fig.10 Townhouse Building Idealization

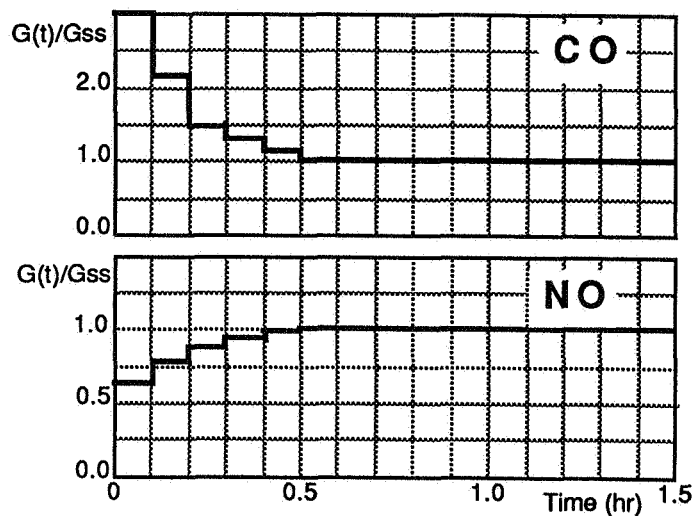


Fig. 11 Range Emission Characteristics

In Figures 11, 12 and 13 we compare computed response with measured data. The details of airflow in this building were unknown in some instances and uncertain in others so several assumptions about flow had to be made to effect the analysis. In particular, it was assumed that the measured whole-building fresh air infiltration rate of 0.21 air changes per hour (ACH) was distributed equally in all three zones, the first-to-second air exchange rate was assumed to be 7.5 ACH, the first-to-basement air exchange rate was assumed to be 0.4 ACH, and all flows were assumed to be constant.

As may be seen, the CO response was under-predicted and the NO response was over-predicted, but both are practically within the reported uncertainty of the emission characteristics (CO: 18% & NO: 6.5%).

Although, the measured NO₂ data is quite suspect, because of scatter and negative values, there appears to be some agreement between this data and the computed response. Inasmuch as this measured data was used to determine the reactivity constant the agreement here may be an artifice. The basis of determination of the reactivity, a single-zone model, and the basis of the computed response are more or less the same as the system behaves, practically, as a single-zone system. Therefore the agreement may reflect no more than this.

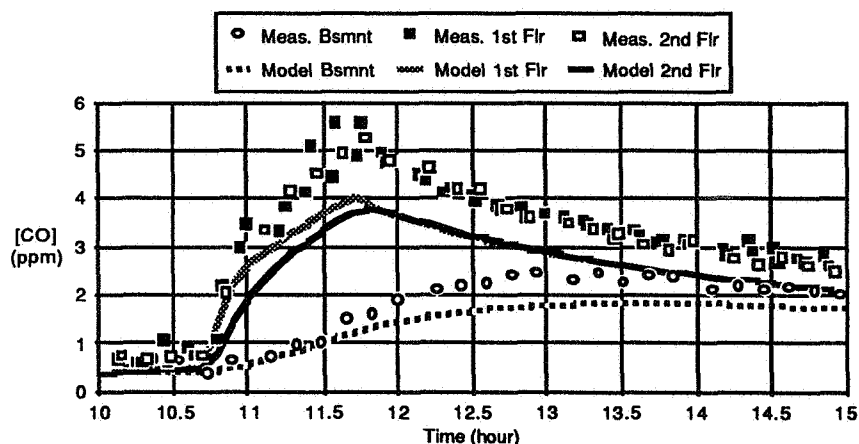


Fig. 11 Comparison of Computed and Measured CO Response

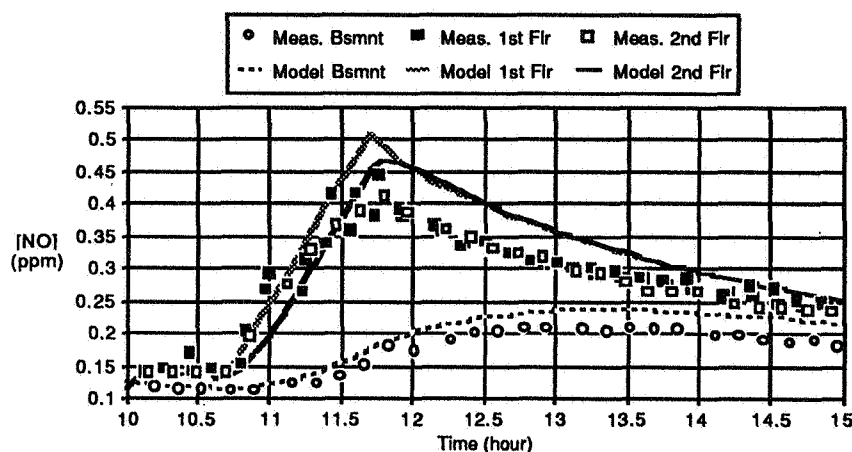


Fig. 12 Comparison of Computed and Measured NO Response

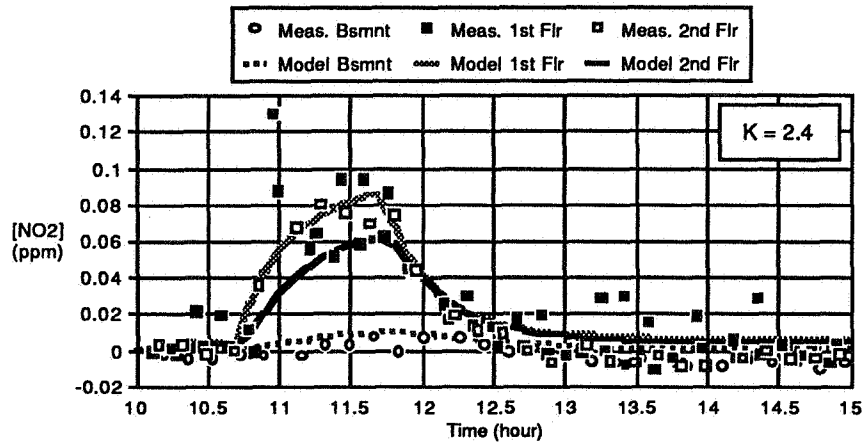


Fig. 13 Comparison of Computed and Measured NO_2 Response
(NO_2 Reactivity = 2.4 hr^{-1})

Convection -Diffusion Study

When employing the convection-diffusion flow element the analyst must take special care to assure an accurate solution has been obtained. In steady state analysis accuracy is affected by element size (i.e., the subdivision of the flow path) and the degree of upwinding chosen. Huebner and Thornton [82] show that instability may be avoided if an upwind parameter is selected satisfying the conditions;

$$\begin{aligned} \phi &\geq 1 - \frac{2}{P_e^e} ; P_e^e > 2 \\ \phi &= 0 ; P_e^e \leq 2 \end{aligned} \quad (23)$$

where;

$$P_e^e \equiv \frac{w^e L^e}{\rho A \alpha_D} = \frac{\bar{u} L^e}{\alpha_D} \quad \text{the element Peclet number} \quad (24)$$

(Note: $P_e^e = (Pe/n)$ for a flow passage idealized by an assembly of n equal-length convection-diffusion elements.) In dynamic analysis, accuracy is also affected by the integration time step selected to complete the dynamic solution and when the lumped mass approximation is employed the analyst may encounter spurious anomalies in the computed solution in some cases [Huebner 82].

Partly because of the challenge of these difficulties and partly because of the importance of the convection-diffusion equation in the area of fluid mechanics, finite element solutions of the convection-diffusion equation have become the focus of considerable research in recent years. Strategies have been put forward to improve the accuracy of the finite element approximation presented above that are, regrettably, beyond the scope of this presentation and the reader is, therefore, advised to review the current and emerging literature. The papers by Hughes and Brooks [82], Tezduyar and Ganjoo [86], and Yu and Heinrich [86] are particularly useful in this regard.

In spite of the numerical pitfalls that await the use of the convection-diffusion flow element

we shall proceed and employ these elements (with the lumped mass approximation) to compute the transport of a contaminant pulse through a length of ductwork. The conditions of this problem are illustrated in Figure 14: fluid flows through a duct of length L and radius R at a mass flow rate w^e ; a contaminant is injected into the inlet stream at a rate $G(t)$ for a short time interval introducing a pulse of contaminant of mass I into the inlet stream; the pulse is convected and dispersed as it moves along the duct. We seek to determine the concentration time history of the contaminant as it emerges from the outlet of the duct.

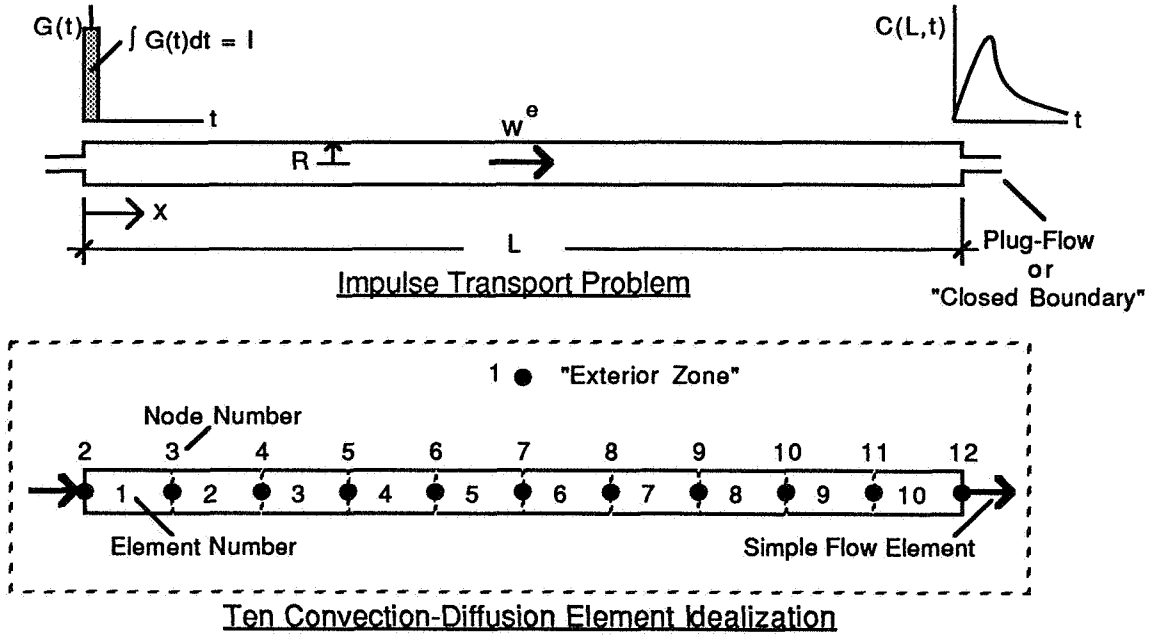


Fig. 14 The Transport of a Pulse in a Duct and the Corresponding Finite Element Idealization

The exact solution to this problem is available for an impulse, for "closed" inlet and outlet conditions, but it is expressed as an infinite sum that is practically difficult to use [Wen 75 pp. 133-137]. For $Pe=0$ the duct becomes a well-mixed system, the initial concentration throughout the duct becomes, simply, $(I/\rho AL)$, and the outlet concentration decays exponentially:

$$\frac{C(L,t)}{(I/\rho AL)} = e^{-t/\bar{t}} \quad ; Pe = 0 \quad (25)$$

For relatively large Peclet numbers the outlet concentration is well approximated by the following expression reported by Nauman and Buffham [83 pp. 101-103]:

$$\frac{C(L,t)}{(I/\rho AL)} = \sqrt{\frac{Pe}{4\pi(t/\bar{t})^3}} e^{\left(\frac{-Pe(1-t/\bar{t})^2}{4t/\bar{t}}\right)} \quad ; Pe > 16 \quad (26)$$

and for very large Peclet numbers the outlet concentration approaches a Gaussian distribution [Wen 75 p. 133]:

$$\frac{C(L,t)}{(l/\rho AL)} = \sqrt{\frac{Pe}{4\pi}} e^{\left(\frac{-Pe(1-t/\bar{t})^2}{4}\right)} \quad ; Pe \gg 16 \quad (27)$$

Approximate solutions to this problem were computed using a 10-element subdivision, as shown in Figure 14, and a twenty-element subdivision. The "closed" boundary condition was modeled using the simple flow element as this element models (instantaneous) plug flow conditions as required. The impulse was approximated by a pulse of finite but small duration. In all studies the upwind parameter, ϕ , was chosen to satisfy the lower bound (i.e., equality) of the stability requirement of equation (23). The results are compared below, Figure 15, to the solutions discussed above, equations (25) to (27).

It is seen that in this case the approximate, finite element solution for the low Peclet number, $Pe=1$, approaches the exact well-mixed solution, as expected. The approximate solution for the higher Peclet numbers has some difficulty in capturing the amplitude of the exit pulse, although, the timing and the form of the pulse appear to be well-approximated. Some part of this error may be attributed to approximating the impulse of the analytic solutions by a pulse of finite duration in the computed solutions.

Some part of the error may be attributed to the coarseness of the finite element subdivision. A comparison of the results of the 10-element and 20-element approximations for $Pe=10$ indicate that a convergent solution was obtained (i.e., further subdivision would not alter the solution), yet when these results are compared to the exact results reported by Wen and Fan [75 Fig. 5-8 p. 136] the amplitude appears to be underestimated by approximately 10%. This same comparison for $Pe=20$ indicates that a convergent solution was almost but not quite achieved. An additional subdivision would presumably reveal convergence, and the error in amplitude estimation was approximately 20%. It is interesting to note that the element Peclet numbers for these two (nearly) convergent solutions – the 10-element solution at $Pe=10$ and the 20-element solution at $Pe=20$ – are both equal to 1.0, a condition that demands no upwinding to maintain numerical stability.

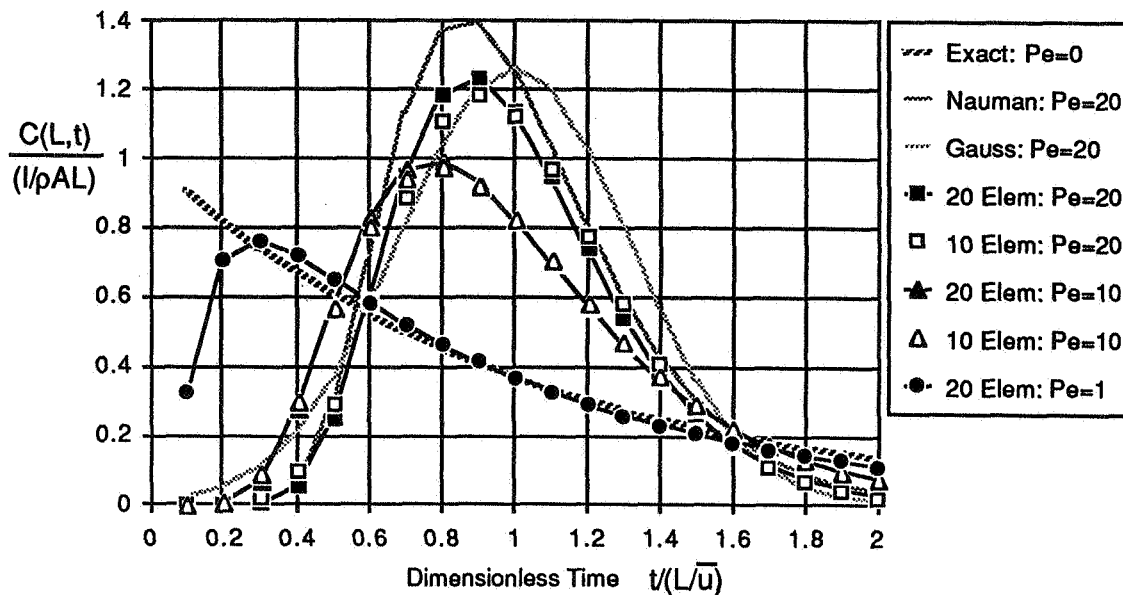


Figure 15 Comparison of Analytic Solutions with Finite Element Solutions for the Pulse Transport Problem

It may be useful to relate these nondimensional studies to more conventional units. The study for $Pe=20$ corresponds to studying the transport of a pulse through a circular duct of 1 m radius having a length of 10 m with a bulk flow velocity of 2 m/s (the practical minimum operational flow rate in HVAC ducts). For these conditions the dispersal coefficient may be expected to be about $1.0 \text{ m}^2/\text{s}$. The results reported in Figure 15 were computed using a pulse duration of 0.005 sec. The dynamic solution was computed using a time step of 0.001 second, in part to capture the short-time pulse accurately and partly to achieve a practically convergent solution.

In practical situations the inaccuracies revealed in these studies are likely to be considered very small and, thus, the convection-diffusion flow element should provide a practically useful analytical tool. Nevertheless, to minimize error the analyst is well advised to seek a convergent solution through both *mesh refinement* (i.e., repeated subdivision of the flow path), starting, perhaps, with a subdivision that results in an element Peclet number of 1.0, and *time step refinement*, starting with a time step sufficiently small to capture the dynamic variation of any excitation with reasonable accuracy, being careful to select an upwind factor so that the stability requirement of equation (23) is always satisfied. When employing convection-diffusion elements in an idealization of a building airflow system it is very likely that extremely small time steps will be required to obtain a convergent solution.

CONCLUSION

From a practical point of view, the element assembly approach is intuitively satisfying and allows consideration of systems of arbitrary complexity. From a theoretical point of view it provides a framework for the consideration of the large variety of mass transport processes that affect the dispersal of contaminants in buildings and offers additional mathematical tools to unravel the formal characteristics of whole-building dispersal models. From a research and development point of view it separates the general problem of indoor air quality analysis into two primary subproblems; element development and development of solution method. Research efforts can, thus, focus on the modeling of specific transport processes, to develop improved or new elements or, alternatively, focus on developing improved methods of solving the resulting equations while accounting for the complex coupling that may exist between the related thermal, dispersal, and flow analysis problems.

The approach has been formulated to be completely analogous and compatible with approaches based upon the Generalized Finite Element Method [Zienkiewicz 83] used to approximate solutions of the microscopic equation of motion for fluids and makes use of the numerical methods and computational strategies that have been developed to support this method and associated methods. It is expected that this compatibility will, eventually, allow the analyst to employ mixed idealizations of building airflow systems wherein a portion of the building airflow system would be modeled in detail using microscopic elements while the rest of the airflow system would be modeled using discrete or lumped parameter elements. In this way the analyst may study the details of dispersal in one area of the system, accounting for whole-system interaction, without the computational overhead of modeling the entire system microscopically. The one-dimensional convection-diffusion element presented in this paper represents the first step in this direction.

REFERENCES

- Axley, J.W., Building Energy Simulation Using Assemblages of Discrete Thermal Elements, *Proceedings of the 11th National Passive Solar Conference*, Boulder, CO, 70-75, June,

1986

- Axley, James, *Indoor Air Quality Modeling: Phase II Report*, NBSIR 87-3661, CBT, National Bureau of Standards, Gaithersburg, MD, Oct., 1987
- Axley, James, *Progress Toward a General Analytical Method for Predicting Indoor Air Pollution in Buildings: Indoor Air Quality Modeling: Phase III Report*, CBT, National Bureau of Standards, Gaithersburg, MD, July, 1988
- Borrazzo, J.E., Osborn, J.F., Fortmann, R.C., & Davidson, C.L., Modeling and Monitoring of CO, NO and NO₂ in a modern Townhouse, *Atmospheric Environment*, **21**, Pergamon Press, 299-311, 1987
- Davidson, L. & Olsson, E., Calculation of Age and Local Purging Flow Rate in Rooms, *Bldg Envir*, **22**, 11-127, 1987
- Huebner, K.H. & Thornton, E.A., *The Finite Element Method for Engineers, 2nd Edition*, John Wiley & Sons, New York, 444-451, 1982
- Hughes, T.J., Analysis of Some Fully-Discrete Algorithms for the One-Dimensional Heat Equation, *International Journal for Numerical Methods in Engineering*, **21**, John Wiley & Sons, 1985
- Moore, J.W. & Pearson, R.G., *Kinetics and Mechanism Third Edition*, John Wiley & Sons, New York, 1981
- Nauman, E.B. & Buffham, B.A., *Mixing in Continuous Flow Systems*, John Wiley & Sons, NY, 1983
- Sandberg, Mats, The Multi-Chamber Theory Reconsidered from the Viewpoint of Air Quality Studies, *Bldg Envir*, **19**, 221-233, 1984
- Sinden, F.W., Multi-Chamber Theory of Air Infiltration, *Bldg Envir*, **13**, 21-28, 1978
- Tezduyar, T.E. & Ganjoo, D.K., "Petrov-Galerkin Formulations with Weighting Functions Dependent Upon Spatial and Temporal Discretizations: Applications to Transient Convection-Diffusion Problems," *Computer Methods in Applied Mechanics and Engineering*, Vol. 59, Elsevier Science Publishers, North Holland, 1986, pp. 49-71
- Walton, G.N., *Estimating Interroom Contaminant Movements*, NBSIR 85-3229, U.S. DOC, NBS, Gaithersburg, MD, August, 1985
- Wen, C.Y., & Fan, L.T., *Models for Flow Systems and Chemical Reactors*, Marcel Dekker, Inc., NY, NY, 1975
- Yu, C.C. & Heinrich, J.C., "Petrov-Galerkin Methods for the Time-Dependent Convective Transport Equation," *International Journal for Numerical Methods in Engineering*, Vol. 23, John Wiley & Sons, 1986, pp. 883-901
- Zienkiewicz, O.C. & Morgan, K., *Finite Elements and Approximation*, John Wiley & Sons, NY, 1983

EFFECTIVE VENTILATION

9th AIVC Conference, Gent, Belgium
12-15 September, 1988

Poster 11

A NUMERICAL STUDY OF BUOYANCY-DRIVEN FLOWS OF MASS AND ENERGY
IN A STAIRWELL.

A.S. ZOHRABIAN, BSc, MSc - PhD Research Student

M.R. MOKHTARZADEH-DEHGHAN, BSc, MSc, DIC, PhD, MASME, AMIMechE -
Lecturer

A.J. REYNOLDS, BSc, PhD, DIC, CEng, FIMechE, MASCE, FRSA -
Professor and Head of Department of Mechanical Engineering.

Department of Mechanical Engineering, Brunel University, Uxbridge,
Middlesex, UB8 3PH, England.

SUMMARY

This paper describes a two-dimensional numerical study, by finite-volume method of buoyancy-driven flow in a half-scale model of a stairwell. The stairwell forms a closed system within which the circulation of air is maintained by the supply of heat in the lower floor. The heat loss takes place from the stairwell walls. The mathematical model consists of the governing equations of mass, energy, momentum and those of the $k - \epsilon$ model of turbulence. The predicted flow pattern and the velocity in the stairway are presented and compared with the authors' experimental data.

NOMENCLATURE

A	area (m^2)
a	coefficient of finite-difference equation
$C_\mu, C_1, C_2, C_3, C_D$	constants in the k- ϵ turbulence model
c_p	specific heat ($\text{J kg}^{-1} \text{K}^{-1}$)
g	gravitational acceleration (m s^{-2})
k	turbulence kinetic energy per unit mass (N m kg^{-1})
Pe	cell Péclet number
\dot{q}_w''	wall heat flux (W m^{-2})
S_ϕ	source term for variable ϕ ($S_\phi = b\phi + c$)
T	absolute temperature (K)
T_w	wall temperature (K)
T_P	temperature at node P next to wall (K)
u^+	non-dimensional velocity in wall region ($u^+ = \frac{u}{u_\tau}$)
u_τ	friction velocity (m s^{-1})
u, v	mean velocity components in x and y directions, respectively (m s^{-1})
y^+	non-dimensional distance from wall ($y^+ = \frac{u_\tau y}{\nu}$)
y_P	distance from node P to the adjacent wall (m)

Greek Symbols

β	coefficient of thermal expansion (K^{-1})
Γ_ϕ	diffusion coefficient for variable ϕ ($\Gamma_\phi = \frac{\mu}{\sigma_\phi}$)
ϵ	rate of turbulence energy dissipation per unit mass ($\text{N m kg}^{-1} \text{s}^{-1}$)
μ	molecular viscosity ($\text{kg m}^{-1} \text{s}^{-1}$)

μ_t	turbulent viscosity	$(\text{kg m}^{-1} \text{s}^{-1})$
μ_{eff}	effective viscosity	$(\mu_{\text{eff}} = \mu + \mu_t)$
ρ	fluid density	(kg m^{-3})
ρ_r	reference density	(kg m^{-3})
ν	kinematic viscosity	$(\text{m}^2 \text{s}^{-1})$
τ_w	wall shear stress	(N m^{-2})
ϕ	general dependent variable	
$\sigma_T, \sigma_{T,t}$	laminar and turbulent Prandtl number, respectively	
$\sigma_\epsilon, \sigma_k$	constants of turbulence model	

Subscripts

n, e, s, w	Control volume faces
t	turbulent

1. INTRODUCTION

A better understanding of buoyancy-driven flows in stairwells is important in relation to energy saving in buildings, design of air-conditioning systems, architectural design, and fire studies. Until recently this type of flow has received relatively little attention, either experimentally or theoretically.

A number of experimental investigations of stairwell flows have been reported by Feustel et al.¹, Marshal^{2,3,4}, Klote and Bodart⁵, Zuercher et al.⁶, Tamura et al.^{7,8}, Chu⁹ and Maguire¹⁰. More recently Reynolds¹¹ and Reynolds et al.¹² developed analytical modelling of the flow processes within stairwells.

In order to improve the understanding of buoyancy-driven flow and the associated energy transfer within the stairwell, the authors have carried out experiments on a half-scale model of a stairwell. These have been reported by Marriott and Reynolds¹³, and Zohrabian et al.¹⁴. Parallel to the experimental investigations, mathematical modelling has also been carried out for prediction of the flow in the stairwell. We have used the $k - \epsilon$ model of Harlow and Nakayama¹⁵, as developed by Launder and Spalding¹⁶.

Studies using the $k - \epsilon$ model have been applied to a variety of engineering problems similar to that of the stairwell. Neilsen et al.¹⁷ and Alamdari et al.¹⁸ studied buoyancy-affected flows in ventilated rooms. Ideriah¹⁹, Markatos et al.²⁰ and Fraikin et al.²¹ predicted buoyancy-induced flows in cavities. In another study Markatos²² predicted the air flow and heat transfer in television studios. Markatos et al.^{23,24}, Cox et al.²⁵ and Kumar et al.²⁶ used a Fire Research Station computer program (known as JASMINE) to analyse the smoke movement in enclosures.

The objective of the present work is to predict the velocity and temperature distributions in the stairwell and to assess the results with the aid of experimental data.

2. THE PHYSICAL MODEL

The half-scale stairwell model geometry is shown in Fig.1. It consisted of a lower and an upper compartment connected by the stairway. The recirculation of air was maintained by continuous supply of heat through a heater positioned in the lower compartment. The area we refer to as the "throat area", shown by the broken line D-D' in Fig. 1, is the area within which most of the measurements were taken. The full details of the experimental rig and the measurement techniques are reported elsewhere¹⁴.

3. THE MATHEMATICAL MODEL

3.1. The governing equations in differential form

In a two-dimensional Cartesian coordinate system, the conservation differential equations for continuity, momentum, energy and those of turbulence energy, k , and its rate of dissipation, ϵ , can be written in the general form

$$\frac{\partial}{\partial x} (\rho u \phi) + \frac{\partial}{\partial y} (\rho v \phi) = \frac{\partial}{\partial x} \left(\Gamma_{\phi} \frac{\partial \phi}{\partial x} \right) + \frac{\partial}{\partial y} \left(\Gamma_{\phi} \frac{\partial \phi}{\partial y} \right) + S_{\phi}$$

where ϕ , Γ_{ϕ} and S_{ϕ} are given in table 1.

The turbulent viscosity, μ_t , in the k - ϵ model is related to k - ϵ (see for example references 15,16,39) :

$$\mu_t = C_{\mu} \rho \frac{k^2}{\epsilon}$$

Based on the concept of eddy diffusivity, $-\rho \overline{v'T'}$ in the k and ϵ equations can be replaced by

$$-\rho \overline{v'T'} = \Gamma_{T,t} \frac{\partial T}{\partial y}$$

3.2. The Governing Equations in Discretised form and the Solution procedure

The first step in deriving the finite-difference equations is to adopt an appropriate grid system. We have adopted the staggered grid system suggested by Patankar and Spalding²⁷, as shown in Fig.2. In such a system the scalar variables (p , T , k , ϵ) are stored at the grid nodes, while u and v velocities are stored at the mid-point between the two adjacent nodes.

The governing equations in discretised form are obtained by integration of the differential equations over the corresponding control volumes, with the aid of a discretisation scheme. The schemes chosen for this study are described in section 3.3. The discretised forms of the governing equations of momentum, thermal energy, turbulence energy and energy dissipation rate can be written as:

ϕ - transport ($\phi = T, k, \epsilon$)

$$(a_p - b) \phi_P = \sum_n a_n \phi_n + c$$

u - momentum

$$(a_p - b)u_p = \sum_n a_n u_n + A_w (p_w - p_p) + c$$

v - momentum

$$(a_p - b)v_p = \sum_n a_n v_n + A_n (p_s - p_p) + c$$

where

$$a_p = \sum_n a_n : \quad a_n = \rho_n v_n A_n f_n$$

and \sum_n denotes summation over neighbours N,S,E,W.

The symbol f_n represents a weighting factor, which is determined according to the chosen scheme. For example, in the hybrid difference scheme for the north boundary of the cell, it can be written as 28,29,30:

$$f_n = \begin{cases} \frac{1}{2} (1 + 2 Pe_n^{-1}) & \text{for } -2 < Pe_n < 2 \\ 1 & Pe_n \geq 2 \\ 0 & Pe_n \leq -2 \end{cases}$$

where Pe is the cell Péclet number.

The main variables in the above equations are u , v , k , ϵ and T . The remaining unknown variable, i.e., pressure, has no equation of its own. To derive the pressure, a special procedure known as SIMPLE (Semi-Implicit Method for Pressure-linked Equations) was used 27,30. The procedure is based on an iterative solution of the governing equations, by which the variables, including pressure, are guessed over the entire field of solution and then corrected as the iteration proceeds. In this procedure the continuity equation is used to derive an additional equation known as the pressure-correction equation. The main variable in this equation is the pressure-correction (p'), which when added to the guessed (current) value of the pressure (p^*) results in an improved value of the pressure ($p = p^* + p'$). This equation is written in the same form as the equations for other scalar variables (T, k, ϵ). The six discretised equations are solved simultaneously using the line-by-line method and the Tri-Diagonal Matrix Algorithm, in the following sequence : u , v , p' , T , k , ϵ .

3.3. The Discretization Schemes

The detailed description of the different discretisation schemes and their mathematical formulation is described by Patankar³⁰. In this study, several schemes have been adopted for comparison. These are central-difference, hybrid and power-law schemes.

In the central-difference scheme a piecewise-linear variation for ϕ is assumed between the grid nodes. According to Patankar³⁰, the central-difference scheme gives accurate results for $|\text{Pe}| < 2$. Outside this limit the scheme is inaccurate^{30,31,32}.

In the upwind scheme the value of ϕ at an interface of the adjacent nodes is assumed to be equal to the value of ϕ at the grid node on the upwind side.

The hybrid scheme was developed by Spalding³³. This scheme is a combination of the central-difference and the upwind schemes. The significance of the hybrid scheme is: (i) For $|\text{Pe}| < 2$ it is identical with the central-difference, (ii) Outside this range it reduces to the upwind scheme.

The power-law scheme³⁴ approximates closely the exponential (exact) variation of the property between the two grid nodes. According to Patankar³⁰, it is premature to ignore the diffusion effects, as soon as the Péclet number exceeds 2, as is the case in upwind scheme. This scheme has the following advantages: (i) it is not expensive to compute, and (ii) at $|\text{Pe}| > 10$ the power-law scheme becomes identical with the hybrid scheme.

4. BOUNDARY CONDITIONS

The usual boundary conditions are the non-slip condition for the velocity, and the definition of the wall temperature or the wall heat flux. However, other modifications to the discretised equations are necessary to account for the contribution of the wall to the adjacent cell, for example, in the form of the shear-stress force. Also, the equations for turbulence energy and energy dissipation have to be modified, as the form given in Table 1 is suitable only for high Reynolds number flows. If a wall thermal boundary condition is in the form of a given temperature, then the wall heat flux has to be calculated. Two of the approaches usually adopted for the special treatment near the walls are the low Reynolds number models, as described for example by Jones and Launder^{36,37} and the wall-function method^{38,16}. The first approach (not adopted in this study) requires a very fine grid within the wall layer, and this makes it unsuitable for complex geometries such as the stairwell. The second approach, that adopted for this study, is based on the assumption that a

standard wall layer has formed at the wall. The boundary-layer equations are then used for the calculation of various parameters such as wall shear stress and heat flux. The details of the wall-function method are described in many sources (see for example references 16,38) and are not repeated here. However, the wall treatment for the thermal boundary conditions is of particular importance in this study and is therefore mentioned here.

For the heater the heat flux is known, see Table 2. It was assumed that an equal amount of heat is transferred to the air from each of the two sides, that facing into the room and that facing the wall, see Fig.1. The heat flux was introduced directly in the equations via the source term. For the stairwell walls, the wall temperatures are specified and the heat flux is calculated from the following relations:

If $y^+ \leq 11.63$

$$\dot{q}_w'' = \frac{\mu C_p (T_w - T_p)}{\sigma_T y_p}$$

If $y^+ > 11.63$

$$\dot{q}_w'' = \frac{\rho C_p C_\mu^{\frac{1}{4}} k^{\frac{1}{2}} (T_w - T_p)}{T^+}$$

where

$$T^+ = \sigma_{T,t} [u^+ + f]$$

and f is a function given by Jayatillaka³⁵ as :

$$f = 9.24 \left\{ \left(\frac{\sigma_T}{\sigma_{T,t}} \right)^{\frac{3}{4}} - 1 \right\} \left\{ 1 + 0.28 \exp \left(-0.007 \frac{\sigma_T}{\sigma_{T,t}} \right) \right\}$$

5. COMPUTATIONAL DETAILS

A grid of non-uniform intervals was employed, the nature of which can be realised from the vector plot, Fig. 3. The grid size was 56 x 37. The choice of minimum grid size was rather restricted due to the geometry of the flow domain, as at least two grid lines were necessary for each step of the stairs, and a reasonable number for the upper and the lower compartments. The maximum grid size was also limited, if the computing time was to be kept

to an acceptable level. The final size of 56 x 37 was chosen after considerable trial.

The computing time per iteration was 4 to 5 seconds on a Pyramid 9820 computer. This merely gives a general idea of the computing time involved because the computing time, in general, depends on many factors. The type of computer and grid size are obviously important. But it also depends on how efficiently the computer program is written and how the initial conditions are defined. Using information from previous runs for the initial conditions reduces the computing time considerably.

The criterion for convergence in studies of this type is to check the gradual reduction of the sum of the residual sources of all the cells (an exact solution would give zero residuals). Also, the computed values of each variable should reach steady values. The sum of the residual sources is normally compared with a suitable reference value. For example, for an open system the sum of mass residuals is compared with the inflow of mass into the flow domain. In this study, in the absence of such an obvious reference value, the variation of the sum of the residual sources was plotted against the number of iterations, and examined. The results showed considerable fluctuations at first, followed by a gradual stabilisation and decrease. The computation stopped when the sum of residual sources for each equation reduced to a relatively small value.

The initial conditions for the variables were as follows :
u was set to 0.1 m/s at the extreme end of the lower compartment (AC in Fig. 1). The u velocities in other locations were computed from the continuity equation. Temperature was set to 20°C. v and p were set to zero. The turbulence energy and energy dissipation rate were obtained from

$$k = 0.03 u^2$$

$$\epsilon = \frac{k^{3/2}}{0.005\ell}$$

where ℓ is the height of the stairwell.

6. RESULTS AND DISCUSSION

The stairwell model we have examined here is a simple configuration compared with the various designs used in buildings. Our experimental work on a half-scale stairwell model¹⁴, showed that the flow was three-dimensional and unsteady. There were a number of separation and recirculation zones. What is more, the relative

importance of viscosity varies dramatically through the field, being very large in corners and near the steps, and relatively small in the body of the flow. An additional difficulty in modeling of the flow is the great variety of heat transfer processes which must be described in adequately realistic fashion. There is heat transfer from every surface and the nature of the flow changes profoundly around the boundaries of the field.

The two-dimensional approach we have adopted here can, therefore, serve to give only a general picture of the actual flow. A three-dimensional approach should provide a better solution. However, any model is based on a set of assumptions which may be violated in one way or another in these wide-ranging conditions. The flow pattern predicted is shown in Fig.3. This shows close agreement with the pattern established by the authors' experimental work¹⁴, as shown in Fig.4. The main features of the flow are the rising column of warm air along the heated walls of the heater, followed by a nearly parallel flow along the ceiling of the lower compartment. As the air flows into the upper compartment, part of it forms a recirculation zone and the other part moves towards the ceiling and, after a circulation in the upper compartment, flows down along the steps to the lower part of the heater.

The predicted velocity profiles at the throat area, using two discretisation schemes, are shown in Fig.5. The experimental values are also included. This figure shows that the velocity values at the throat area are underpredicted in the upper region of the upflow, and in the downflow. However, in comparing the two, one should bear in mind that the experimental results are obtained in three-dimensional flow. The difference may also be attributed, apart from the inadequacy of the mathematical model, to the experimental error inherent in the data. Also it should be noted that the measurements of the wall temperatures showed that they varied along each wall, while average values were adopted in this study. This approach was chosen because a single average value is probably what is available to a designer.

The same argument is valid when comparing the temperatures. The range of temperatures in the throat area obtained by computation was 62 to 76°C. This was high compared with the measured values, which were in the range of 34 to 48°C. In the experimental rig heat losses took place from the sides of the stairwell. This was obviously absent in the two-dimensional model. The over-prediction of the temperature may also be related to the turbulence model, as similar overprediction has been reported by Alamdari et al¹⁸. They suggested that a factor might be introduced into the dissipation term of the turbulence energy equation to reduce the rate of dissipation of turbulence energy near the walls.

An examination of the experimental results for heat losses from the walls showed that about two-thirds of the heat loss took place

through the upper compartment. This is in close agreement with our prediction.

We have presented the results shown in Fig. 5 using two different discretization schemes, namely, the power law and the hybrid schemes. The former should lead to more accurate results in the expense of more computer time. The results shown in Fig. 5 indicate that the difference between the two predicted results is not appreciable.

We have also used the central-difference scheme. However this did not lead to a converged solution. The choice of discretisation scheme is closely related to the range of cell Péclet numbers. They were in the range of -20 to 20 in the lower compartment, and -10 to 10 in the upper compartment. Higher values were obtained near the heater and close to the walls, and much smaller values in the central regions of the recirculation zones. The range of Péclet numbers indicates the reason for failure of the central-difference scheme.

6.1. The Case of an "Open Stairwell"

Work is underway on a so-called "open stairwell". This situation may arise when air enters the stairwell, for example, through cracks. To simulate this case experimentally, two openings (10mm wide) were introduced, one in the lower and one in the upper compartment as shown in Fig. 6. The experiments conducted so far indicate that air is pulled through the opening A, due to the temperature difference between inside and outside of the stairwell, flows a short distance along the floor and then rises along the heater walls. The same amount of air obviously leaves the stairwell from the opening B. The general flow pattern in the stairwell was similar to that shown in Fig. 4. Prediction of the flow is also progressing. A uniform velocity of 0.9 m/s was introduced at the opening A. The results indicate that the jet penetrates farther along the floor than is observed experimentally, apparently due to slow mixing of the jet. This behaviour needs further investigation and the results will be reported elsewhere.

7. CONCLUSIONS

The two-dimensional model, based on the $k-\epsilon$ model of turbulence, appears to be adequate in obtaining some basic information on the flow characteristics in the stairwell. The predicted flow pattern was in good agreement with the pattern established by experiment on a half-scale stairwell model rig. The predicted velocities were reasonable. The proportion of the heat loss from the upper compartment was also in good agreement with the experiment.

THE AIR INFILTRATION AND VENTILATION CENTRE was inaugurated through the International Energy Agency and is funded by the following twelve countries:

Belgium, Canada, Denmark, Federal Republic of Germany, Finland, Italy, Netherlands, New Zealand, Norway, Sweden, Switzerland, United Kingdom and United States of America.

The Air Infiltration and Ventilation Centre provides technical support to those engaged in the study and prediction of air leakage and the consequential losses of energy in buildings. The aim is to promote the understanding of the complex air infiltration processes and to advance the effective application of energy saving measures in both the design of new buildings and the improvement of existing building stock.

Air Infiltration and Ventilation Centre

University of Warwick Science Park
Barclays Venture Centre
Sir William Lyons Road
Coventry CV4 7EZ
Great Britain

Telephone: (0203) 69250
Telex: 312401
Fax: (0203) 410156
ISBN 0 946075 40 9

ACKNOWLEDGEMENTS

The authors would like to acknowledge the helpful information which they received from the Air Infiltration Centre (AIC), and Fire Research Station (FRS). They also wish to thank the Science and Engineering Research Council for financial support given as part of the 'Energy in Buildings' Specially Promoted Programme.

REFERENCES

1. FEUSTEL, H., ZUERCHER, C.H., DIAMOND, R. DICKINSON, B., GRIMSRUD, D. and LIPSCHUTZ, R.
"Temperature and wind-induced air flow patterns in a staircase. Computer modelling and experimental verification".
Energy and Building, 8, 1985, pp. 105-122.
2. MARSHALL, N.R.
"Movement of smoke and fire gases in stairwell".
BRE News, 59, 1983, Spring Issue.
3. MARSHALL, N.R.
"The behaviour of hot gases flowing within staircase".
Fire Safety J., 9, 1985, pp. 245-255.
4. MARSHALL, N.R.
"Air entrainment into smoke and hot gases in open shafts".
Fire Safety J., 10, 1986, pp. 37-46.
5. KLOTE, J.H. and BODART, X.
"Smoke control by pressurised stairwell".
Build. Res. Prac. 12, Part 4, 1984, pp. 216-222.
6. ZUERCHER, C.H. and FEUSTEL, H.
"Air infiltration in high-rise buildings".
4th AIC Conference, Sept. 26-28, Elm., Switzerland, 1983, pp. 9.1-9.17.
7. TAMURA, G.T. and WILSON, A.G.
"Natural venting to control smoke movement in building via vertical shafts".
ASHRAE Trans., 76, 1978, pp. 279-289.

8. TAMURA, G.T. and SHAW, C.Y.
 "Air leakage data for the design of elevator and shaft
 pressurisation system".
 ASHRAE Trans., 82, Part 2, 1976, pp. 179-190.

9. CHU, D.D.H.
 "Assessment and characterisation of airflow in domestic
 stairwell".
 MSc Thesis, Brunel University, 1984.

10. MAGUIRE, D.H.
 "Air movement in domestic stairwell".
 MSc Thesis, Brunel University, 1985.

11. REYNOLDS, A.J.
 "The scaling of flows of energy and mass through stairwells".
 Building and Environment, 21, Part 3/4, 1986, pp. 149-153.

12. REYNOLDS, A.J., MOKHTARZADEH-DEHGHAN, M.R. and ZOHRABIAN, A.S.
 "The modelling of stairwell flows".
 Build. and Envir., 23, No.1, 1988, pp.63-66.

13. MARRIOTT, B.S.T. and REYNOLDS, A.J.
 "Flows of mass and energy through a stairwell - experimental
 studies".
 Report FM 86/1, Dept. of Mech. Eng., Brunel University, 1986.

14. ZOHRABIAN, A.S., MOKHTARZADEH-DEHGHAN, M.R., REYNOLDS, A.J.
 and MARRIOTT, B.S.T.
 "An experimental study of buoyancy-driven flow in a half-
 scale stairwell model".
 To be published in Building and Environment.

15. HARLOW, F.H. and NAKAYAMA, P.I.
 "Transport of turbulence energy decay rate".
 University of California, Los Alamos Science Lab. Report,
 LA3854, 1968.

16. LAUNDER, B.E. and SPALDING, D.B.
 "The numerical computation of turbulent flows".
 Computer Methods in Applied Mechanics and Eng., 3, 1974,
 pp.169-289.

17. NIELSEN, P.V. and RESTIVO, A. and WHITELOW, J.H.
 "Buoyancy affected flows in ventilated rooms".
 Numerical Heat Transfer, 2, 1979, pp. 115-127.

18. ALAMDARI, F., HAMMOND, G.P. and MOHAMMAD, W.S.
 "Computation of air flow and convective heat transfer within space-conditioned rectangular enclosures".
 Proceedings of the 5th Int. Symp. on the use of computers for environmental engineering related to buildings, Bath, July 1986, CIBSE 1986, pp.191-205.
19. IDERIAH, F.J.K.
 "Prediction of turbulent cavity flows driven by buoyancy and shear".
 J. Mech. Eng., 22, No.6, 1980, pp.286-295.
20. MARKATOS, N.C., MALIN, M.R. and COX, G.
 "Mathematical modelling of buoyancy-induced smoke flow in enclosures".
 Int. J. Heat and Mass Transfer, 25, No.1, 1982, pp.699-812.
21. FRAIKIN, M.P., PORTIER, J.J. and FRAIKIN, C.J.
 "Application of a k- ϵ turbulence model to an enclosed buoyancy driven recirculating flow".
 Joint ASME/AICL National Heat Transfer Conference, Florida, 1980, ASME Paper No.80-HT-68.
22. MARKATOS, N.C.
 "Computer analysis of building-ventilation and heating problems".
 2nd Int. PLEA Conference, Crete, 28 June - 1 July 1983, Passive and Low Energy Architecture, Edited by S. Yannas.
23. MARKATOS, N.C. and PERICLEOUS, K.A.
 "Laminar and turbulent natural convection in an enclosed cavity".
 Int. J. Heat Mass Transfer, 27, No.5, 1984, pp.755-772.
24. MARKATOS, N.C. and COX, G.
 "Hydrodynamics and heat transfer in enclosures containing a fire source".
 PCH Physiochemical Hydrodynamics, 5, No.1, 1984, pp.53-66.
25. COX, G. and KUMAR, S.
 "The mathematical modelling of fire in forced ventilated enclosures".
 18th DOE Nuclear Airborne Waste Management and Air Cleaning Conf., Baltimore, 1984, pp.629-639.
26. KUMAR, S., HOFFMAN, N. and COX, G.
 "Mathematical modelling of fires in hospital ward".
 Proc. 14th National Conf. on Fluid Mechanics and Fluid Power, Roorkee, India, 1986, p.III,5.
27. PATANKAR, S.V. and Spalding, D.B.
 "A calculation procedure for heat, mass and momentum transfer in three-dimensional parabolic flows".
 Int. J. Heat Mass Transfer, 15, 1972, pp. 1787-1806.

28. GOSMAN, S.V. and IDERIAH, F.J.K.
"A general computer program for 2D turbulent recirculating flows".
Imperial College London, 1976.
29. IDERIAH, F.J.K.
"Turbulent natural and forced convection in plumes and cavities".
PhD Thesis, University of London, 1977.
30. PATANKAR, S.V.
"Numerical heat transfer and fluid flow".
McGraw Hill, New York, 1980.
31. PATEL, M.K., MARKATOS, N.C. and CROSS, M.A.
"A critical evaluation of seven discretization schemes for convection-diffusion problem".
Int. J. Numerical Meth. Fluids, 5, 1985, pp. 225-244.
32. GOSMAN, A.D., PUN, W.M., RUNCHAL, A.K., SPALDING, D.B., WOLFSTEIN, M.
"Heat and mass transfer in recirculating flows".
Academic Press, London, 1969.
33. SPALDING, D.B.
"A novel finite-difference formulation for differential expressions involving both first and second derivations".
Int. J. Num. Methods Eng., 4, 1972, pp. 551-559.
34. PATANKAR, S.V.
"A calculation procedure for two-dimensional elliptic situations".
Numerical Heat Transfer, 4, 1981, pp. 409-425.
35. JAYATILLAKA, C.V.L.
"The influence of Prandtl number and surface roughness on the resistance of the laminar sub-layer to momentum and heat transfer".
In 'Progress in Heat and Mass Transfer', Vol.1, Pergamon Press, 1969, London.
36. JONES, W.P. and LAUNDER, B.E.
"The prediction of laminarization with two equation model of turbulence".
Int. J. Heat and Mass Transfer, 15, 1972, pp. 301-314.
37. JONES, W.P. and LAUNDER, B.E.
"Prediction of Low-Reynolds number phenomena with a two equation model of turbulence".
Int. J. Heat and Mass Transfer, 16, 1973, pp. 1119-1130.
38. LAUNDER, B.E. and SPALDING, D.B.
"Turbulence models and their application to the prediction of internal flows".
Heat and Fluid Flow, 2, No.1, 1972, pp. 43-54.

39. RODI, W.
"Turbulence models and their application in Hydraulics -
A state of the art review"
International Association for Hydraulic Research Publ., 1980.

Equation	ϕ	Γ_ϕ	S_ϕ
Continuity	1	0	-
u-momentum	u	μ_{eff}	$-\frac{\partial p}{\partial x} + \frac{\partial}{\partial x} (\mu_{eff} \frac{\partial u}{\partial x}) + \frac{\partial}{\partial y} (\mu_{eff} \frac{\partial v}{\partial x})$
v-momentum	v	μ_{eff}	$-\frac{\partial p}{\partial y} + \frac{\partial}{\partial x} (\mu_{eff} \frac{\partial u}{\partial y}) + \frac{\partial}{\partial y} (\mu_{eff} \frac{\partial v}{\partial y}) + g(\rho_r - \rho)$
Turbulent Energy	k	$\frac{\mu_{eff}}{\sigma_k}$	$G_k - C_D \rho \epsilon + \rho g \beta \overline{v'T'}$
Energy Dissipation	ϵ	$\frac{\mu_{eff}}{\sigma_\epsilon}$	$C_1 \frac{\epsilon}{k} G_k - C_2 \rho \frac{\epsilon^2}{k} + C_3 \rho \frac{\epsilon}{k} g \beta \overline{v'T'}$
Energy equation	T	Γ_{eff}	S_T

$$\Gamma_{eff} = \frac{\mu}{\sigma_T} + \frac{\mu_t}{\sigma_{T,t}}$$

$$G_k = \mu_t \left\{ 2 \left[\left(\frac{\partial u}{\partial x} \right)^2 + \left(\frac{\partial v}{\partial y} \right)^2 \right] + \left(\frac{\partial u}{\partial y} + \frac{\partial v}{\partial x} \right)^2 \right\}$$

The empirical constants have been adopted from Launder and Spalding¹⁶ and take the following values :

$C_\mu = 0.09$, $C_D = 1.0$, $C_1 = 1.44$, $C_2 = 1.92$, $C_3 = 1.0$, $\sigma_k = 1.0$, $\sigma_\epsilon = 1.3$

TABLE 1. The differential equations of the mathematical model .

WALL	AB	BC	CD	DE	EF	FG	GH	HI	IJ	JA
Temperature °C	60	40	40	28	30	27	27	27	30	40
Heat Flux from the two walls of the heater = 1600 W/m^2										

TABLE 2. Thermal Boundary Conditions

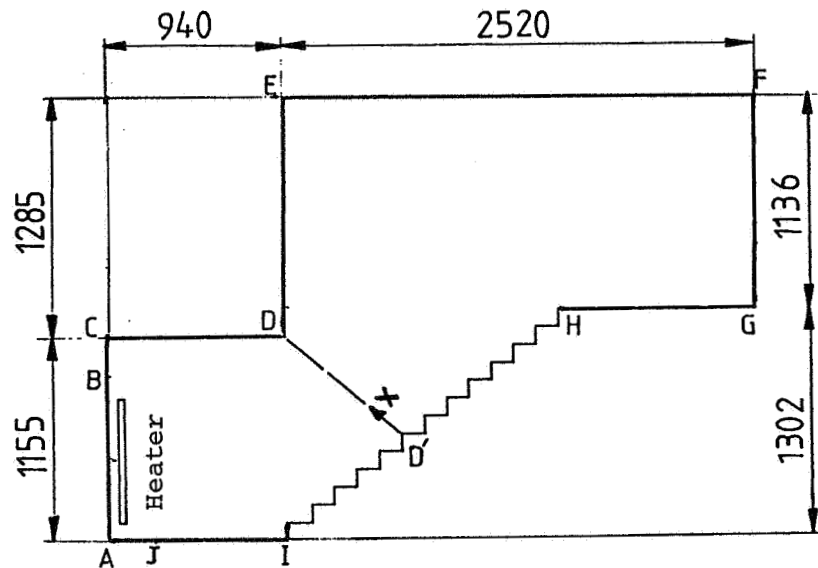


Figure 1. Stairwell model geometry. DD' indicates the throat area. (Dimensions are in mm).

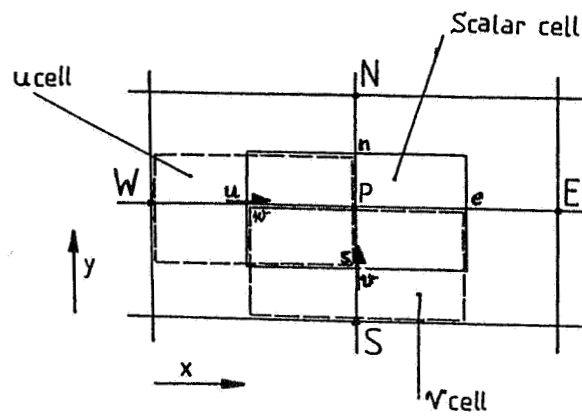


Figure 2. Control volumes of staggered-grid system.

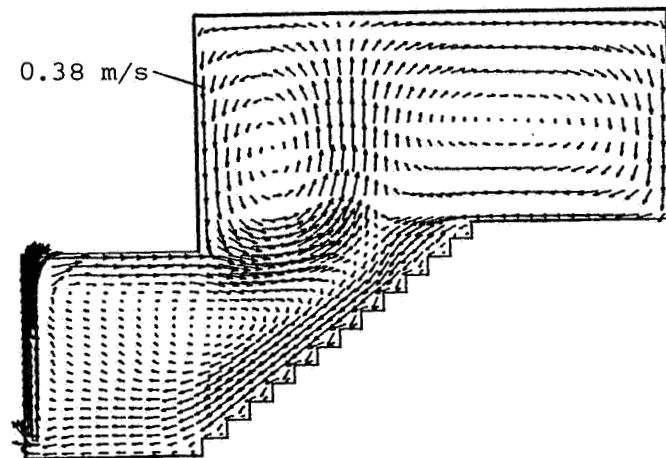


Figure 3. Predicted vector plot of the flow field.

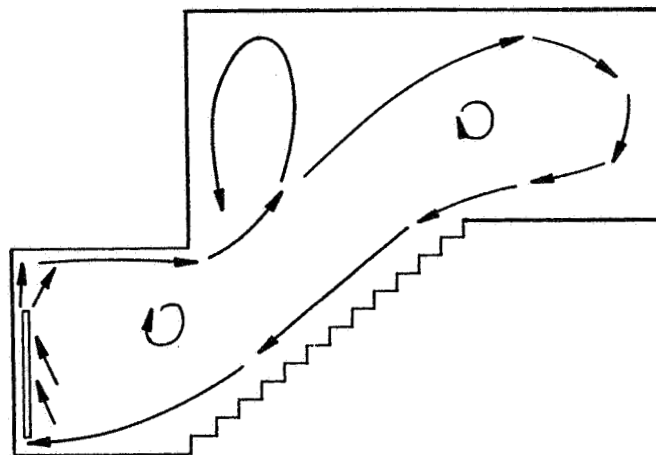


Figure 4. A two-dimensional view of the flow pattern in the stairwell.

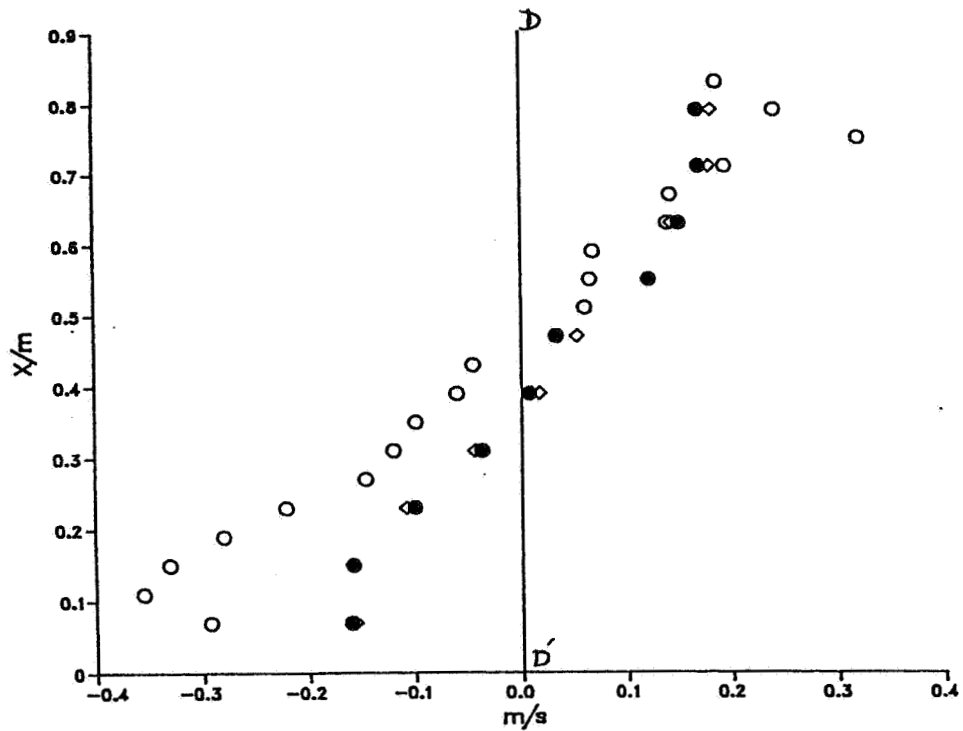


Figure 5. Predicted (2D) and measured (3D) profiles of the component of velocity (Perpendicular to DD') at the throat area.
 O - experiment • - prediction (hybrid scheme)
 ♦ - prediction (power-law scheme).

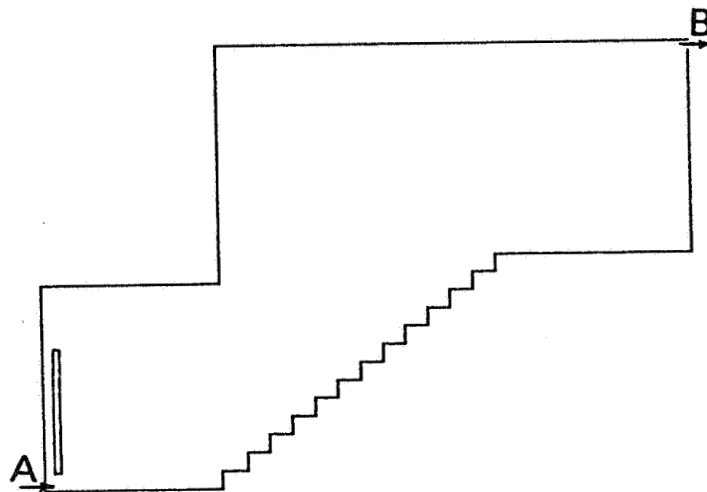


Figure 6. Schematic diagram of the open stairwell.

EFFECTIVE VENTILATION

9th AIVC Conference, Gent, Belgium
12-15 September, 1988

Poster 12

A SIMPLIFIED APPROACH OF AIR INFILTRATION IN MULTIZONES BUILDINGS

CACCAVELLI D., ROUX J.J., ALLARD F.

Laboratoire Equipement de l'Habitat - INSA Bât. 307
20, Avenue Albert Einstein
69621 - VILLEURBANNE (FRANCE)

SYNOPSIS

The specific value of different flows resulting from air exchanges between rooms or with the outside is not always important. An extensive model is not suitable when only estimations or tendencies have to be drawn (very time consuming).

So we developed a simplified infiltration model for predicting airflows in single rooms and between different zones of a building. We integrated this model into a building transient thermal simulation program set up to a micro-computer system.

So as to obtain this model, we used simplified assumptions. We planned those simplifications into two directions:

- separate study of the actions induced by wind and stack effect,
- separate study of mass and heat transfers.

In this way, our approach consists in searching for a satisfying compromise between an appreciable saving of time and consistent results.

The model is devised as follows :

- a transitional step where the ingoing airflows are calculated once for all under the successive agency of wind and stack effect. this step leads to the storage of the different flows into matrices reflecting both effects.
- a connecting step where airflows resulting from wind and stack effect are combined.

LIST OF SYMBOLS

A_j	= Physical open area, m^2
C_j	= Airflow coefficient, m^3/s at 1 Pa
C_p	= Pressure coefficient
g	= Acceleration of gravity, $9.81 m/s^2$
K_j	= Leakage coefficient, $m^3/s.m^2$ at 1 Pa
P_r	= Reference pressure, Pa
$\overline{P_v}$	= Average dynamic pressure, Pa
$\overline{Q_{exh}}$	= Net mass flow rate from an exhaust system, Kg/s
$\overline{Q_{m_j}}$	= Mean mass flow rate through opening j, Kg/s
$\overline{Q_{v_j}}$	= Mean volume flow rate through opening j, m^3/s
\overline{V}	= Average wind speed, m/s
$\overline{V_{met}}$	= Average meteorological wind speed, m/s
z	= Height of calculated point, m
$\overline{\Delta P_j}$	= Mean pressure difference across opening j, Pa
ΔT	= Time step, s
β_j	= Flow exponent
ρ	= Air density, Kg/m^3

1. INTRODUCTION

Nowadays, due to a better insulation of buildings, ventilation takes a great part in energy consumption¹.

However, we should not retain only energetic aspect. Whether ventilation is intentional (mechanical ventilation) or unintentional (infiltration) it has repercussion both on hygienic conditions (contaminant migration) and on risks of damaging the building (water vapor condensation).

It is necessary that we should provide the estimation of these ventilation rates taking into account a lack of clear information on some data (pressure coefficient, air permeability,...).

2. PRINCIPLES OF VENTILATION

Infiltrations through the building envelope are driven by a pressure difference across the shell.

The two motive forces primarily responsible for this pressure difference are :

- _ wind through its velocity and direction produces higher -than-ambient pressures on the windward faces and lower pressures on the others,

- _ stack effect caused by the temperature difference between indoor and outdoor air.

Under this pressure drop, an airflow across the unintentional openings of the shell takes place. This airflow may either be a comer or a goer. It is unintentional because it depends only on weather conditions. The renewal of air, which is due to voluntary ventilation, is added in algebraic value to this crossing flow.

Now, we will study the action of these two motive forces.

2.1. Wind effect

Wind generates over all obstacles a pressure field which fluctuates in time .

The sudden pressure in a given point can be expressed by the relation :

$$P(z,t) = \overline{P}_v(z) + P'_v(z,t) \quad (1)$$

where $\overline{P}_v(z)$ denotes the average pressure during ΔT and $P'_v(z,t)$, the sudden fluctuation .

However, during our calculation of air infiltration, only the notion of average pressure is kept ($\Delta T=3600$ s) .

The average dynamic pressure $\overline{P_v}$ over a building is linked to the mean wind velocity \overline{V} at a reference point by the relation

$$\overline{P_v}(z) = \frac{1}{2} \rho \cdot C_p \cdot \overline{V}(z)^2 \quad (2)$$

The average wind speed on a specific location is linked to the wind speed measured at the nearest meteorological station by a logarithmic relation² :

$$\overline{V}(z) = k \cdot \text{Log}_e \left(\frac{z}{z_0} \right) \cdot \overline{V}_{m \text{ et } t} \quad (3)$$

where $k, z_0(m)$ are constants which depend on surface roughness . They have been assessed for different terrain classes (Table 1) .

	TERRAIN PARAMETERS FOR STANDARD TERRAIN CLASSES				
	Ocean or other body of water	Flat terrain with isolated obstacles	Rural area	Urban, industrial area	Center of large city
z_0	0.005	0.07	0.3	1	2.5
k	0.166	0.202	0.234	0.266	0.292

Table 1 : Terrain parameters

Pressure coefficients vary according to different parameters :

- _ shape and size of the building,
- _ exposure of the building,
- _ kind and direction of the wind .

These pressure coefficients are determined by testing a scale model of the building in a boundary layer wind tunnel.

An experimental study by J. GANDEMER³ led to the setting up of a detailed mapping of pressure coefficients for each facade. This study has been made for each parameters combination before-mentioned (figure 1)

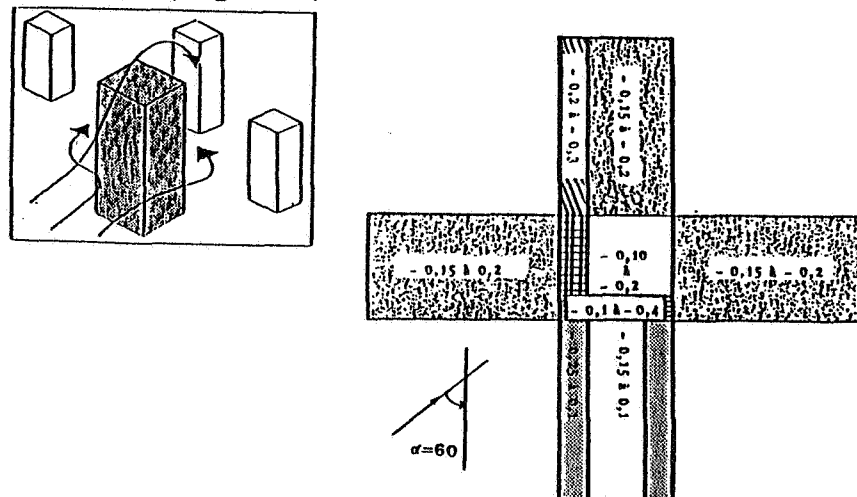


Figure 1 : Mapping of pressure coefficients according to J. GANDEMER for a tall building .

In this way, these results (pressure coefficients) are difficult to exploit. Moreover, an assumption was made which consists of defining, for each facade, a mean pressure coefficient. Thus, we have established⁴ nine configurations of pressure coefficients corresponding to three kinds of building-single-family house, small building and high-rise building), two kinds of wind according to terrain roughness (open country terrain and suburban terrain) and with or without neighbour surroundings. Table 2 shows the discrete values of pressure coefficients according to the angle of incidence of wind for a tall building.

Tall Building	α	0	30	60	90	120	150	180
Country terrain without surroundings	F	0.6	0.6	-0.05	-0.8	-0.6	-0.5	-0.4
	R	-0.9	-0.6	-0.6	-0.9	-0.6	-0.6	-0.9
Country terrain with surroundings	F	0.2	0.1	-0.2	-0.35	-0.3	-0.25	-0.2
	R	-0.35	-0.3	-0.35	-0.3	-0.25	-0.3	-0.35
Suburban with surroundings	F	0.25	0.1	-0.2	-0.4	-0.4	-0.35	-0.3
	R	-0.5	-0.4	-0.4	-0.5	-0.4	-0.4	-0.5

Table 2 : Pressure coefficient versus angle of incidence of wind ($^{\circ}$) ;(F=Facade, R=Roof)

From pressure coefficient values obtained each 30 degrees, that is twelve values by symmetry, the interpolation according to the angle of incidence of wind on the facade is realized by using a FOURIER's series⁵ limited to the 6th rank.

2.2. Stack effect

Temperature difference between inside and outside or between two rooms causes air density variations. These variations produce in their turn pressure differences and hence either infiltration or exfiltration across the shell (figure 2).

Stack effect pressure, calculated at a height z , between zones (i) and (m) is written as follows :

$$P_i(z) - P_m(z) = P_{r_i} - P_{r_m} - (\rho_i - \rho_m) \cdot g \cdot z \quad (4)$$

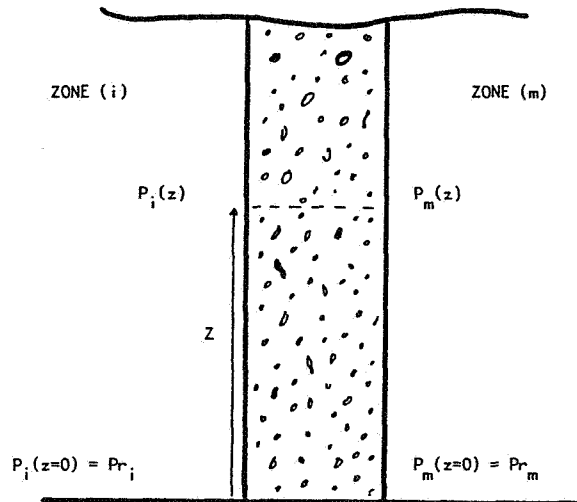


Figure 2 : Definition of different pressures.

2.3. Combined effects of wind and temperature difference

The effects of wind and temperature difference usually act simultaneously to induce unintentional air infiltrations inside a building.

The combined action of these two motive forces is not simple because on the one hand, it depends on the building and on the other, on meteorological conditions of the site.

It is the study of this action which defines the main calculation procedures of airflow.

From equations (2), (3) and (4), the pressure difference calculated at a height z , between zones (i) and (m), under the simultaneous action of wind and stack effect is as :

$$\overline{\Delta P} = P_i - P_m = Pr_i - Pr_m - (\rho_i - \rho_m) \cdot g \cdot z + \frac{1}{2} \rho_i \cdot C_p \cdot \bar{V}^2(z) \quad (5)$$

with :

$$\begin{cases} Pr_i = 0 \text{ if room (i) is outside } (P_{atm} = 0 \text{ Pa}). \\ C_p = 0 \text{ if room (i) is inside.} \end{cases}$$

2.4. Flow equation

This equation characterizes the relationship between mean flow rate through openings and mean pressure difference acting on these openings.

To all kinds of openings, the relationship can be expressed as :

$$\overline{Qv_j} = C_j . (\overline{\Delta P_j})^{\beta_j} \quad (6)$$

The flow exponent value depends on the character of airflow and hence on the kind of openings. For rough and narrow openings, the airflow is laminar whereas, for larger openings it becomes turbulent. This means that for low pressure differences, β_j tends towards 1 whereas, for more important pressure differences β_j tends towards 0.5 .

Many authors* have suggested an intermediary value, $\beta_j = 0.67$ to characterize the typical pressure difference implied in dwelling houses (from 0 to 10 Pa).

Two forms of flow equation are generally used to describe the airflow.

* For intentional openings (air vents, ventilation grilles, ...) we can write :

$$\overline{Qv_j} = C_d . A_j . \sqrt{\frac{2 \overline{\Delta P_j}}{\rho}} \quad (7)$$

The discharge coefficient C_d is a function of the Reynolds number and the ratio of the openings size to the entire surface. But in our calculations, C_d is assumed to be equal to 0.6.

* For unintentional openings (cracks, crevices, background leakage areas, ...) the equation is :

$$\overline{Qv_j} = K_j . A_j . (\overline{\Delta P_j})^{0.67} \quad (8)$$

This equation is normally applied to every leakage component. But the location of the background leakage (leakage between the sill plate and the foundation, frame-wall leakage, electrical outlets, plumbing penetrations, ...) is rather difficult to obtain for an existing building and impossible to predict during the design process. Therefore, we assume that the leakages are uniformly distributed on each facade of the building. With this assumption a single crack permeability coefficient will characterize the leakage of each facade. So, the solution of equation (8) is easier to obtain than before by reducing the amount of complex computer programming and by removing the input of the exact location of the observable cracks.

Two methods may be used to know the crack permeability coefficient of each facade :

_ by measuring air permeability of the shell. To determine this permeability, one of the methods is the fan-pressurization*. the average air leakage through each facade is obtained by dividing air permeability in proportion to the surface of the facade.

_ by adding all individual components belonging to the facade. In design process, we will use the second method.

3. CALCULATION METHOD

The specific value of different flows resulting from air exchanges between rooms or with the outside is not always important. An extensive model is not suitable when only estimations or tendencies have to be drawn (very time consuming).

So we developed a simplified infiltration model for predicting airflows in single rooms and between different zones of a building. We integrated this model into a building transient thermal simulation program set up to a micro-computer system^a.

So as to obtain this model, we used simplified assumptions. We planned those simplifications into two directions:

- _ separate study of the actions induced by wind and stack effect,
- _ separate study of mass and heat transfers.

In this way, our approach consists in searching for a satisfying compromise between an appreciable saving of time and consistent results.

The model is devised as follows :

- _ a transitional step where the ingoing airflows are calculated once for all under the successive agency of wind and stack effect. this step leads to the storage of the different flows into matrices reflecting both effects.
- _ a connecting step where airflows resulting from wind and stack effect are combined.

We will use a standardized description form^a based on GER ALMETH's work to outline this model.

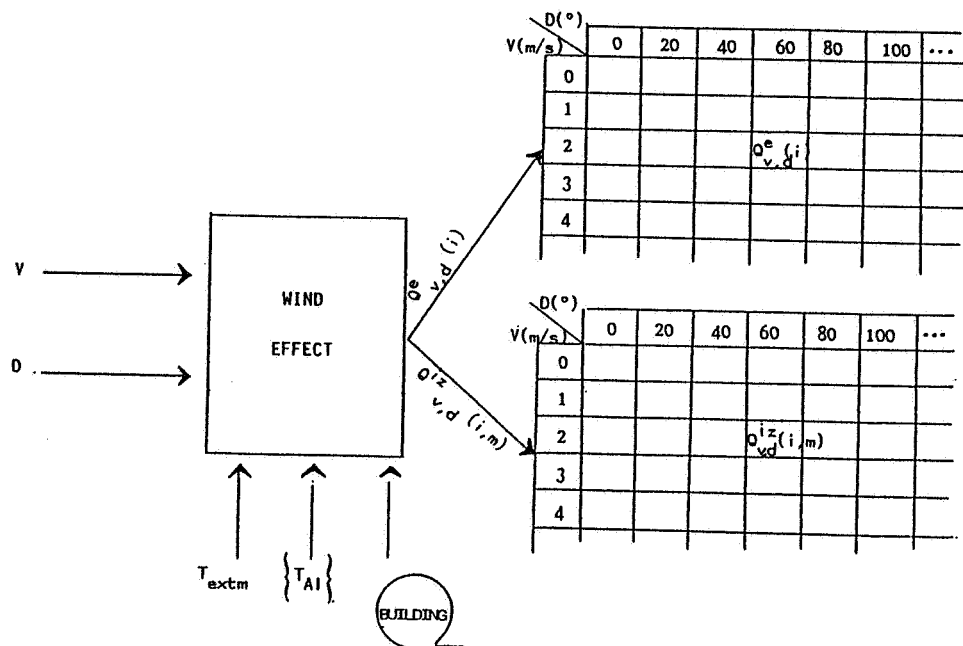
Now, we will study both phases.

3.1. Transitional step

This step depends only on characteristics of the building and weather conditions. The computation time is mainly a function to the number of zones.

3.1.1. Airflows driven by wind effect

The ingoing airflows through each zone are back-calculated for both inputs : wind speed and its direction. Other inputs (inside and outside air temperatures) are assumed to be constant during the studied period.



Nomenclature

Inputs	$\left\{ \begin{array}{l} V \\ D \end{array} \right.$: Wind speed, m/s
		: Direction of wind/south, °
Outputs	$\left\{ \begin{array}{l} Q^e_{v,d}(i) \\ Q^i_{v,d}(i,m) \end{array} \right.$: Net mass flow from the outside towards the inside of zone(i), Kg/s.
		: Net mass flow from zone (m) towards zone (i), Kg/s.
Parameters	$\left\{ \begin{array}{l} T_{extm} \\ \{T_{Ai}\} \end{array} \right.$: Mean outside temperature during the studied period, °C
		: Air temperatures vector.

We limited the set of outside climatic values in order not to obtain oversized matrices :

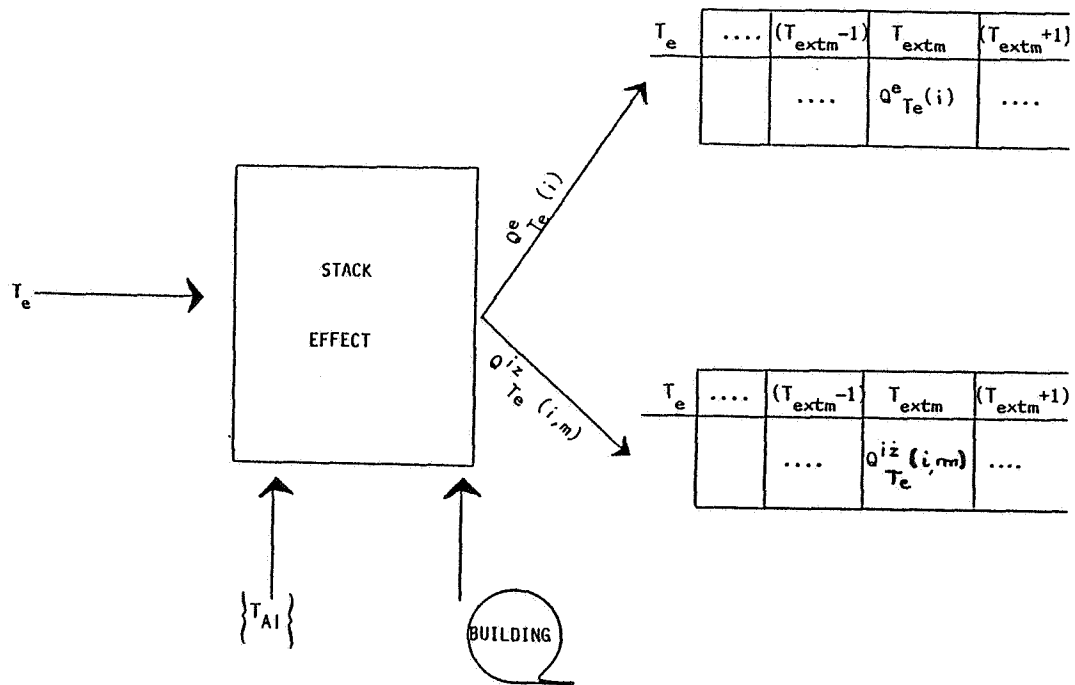
- _ wind speed varies from 0 to 10 m/s with 1 m/s step.
- _ wind direction varies from 0 to 340° with 20° step.

This restriction is in agreement with meteorological values provided by climatic files.

The calculation method of airflows driven only by wind is summed up in table 3.

3.1.2. Airflows driven by stack effect

The ingoing airflows through each zone are back-calculated according to a single input variation : outside air temperature. The other inputs (inside air temperatures) are assumed to be constant during the studied period.



Nomenclature

Input	T_e	: Outside air temperature, °C
Outputs	$Q^e_{Te(i)}$: Net mass flow from the outside towards zone(i), Kg/s
	$Q^{iz}_{Te(i,m)}$: Net mass flow from zone (m) towards zone (i), Kg/s.
Parameters	$\{T_{Ai}\}$: Air temperatures vector

The outside air temperatures variation are obtained from mean outside air temperature during the studied period : T_{extm} . $(T_{extm} - 7) \leq T_e \leq (T_{extm} + 7)$ which means 15 different values for T_e .

The calculation method of airflow driven only by stack effect is summed up in table 3.

3.2. Connecting step

In our simplified method, we have separated wind and stack effects in order to study separately their actions on a building. Now, we have to combine these two effects.

R. CADIERGUES¹⁰ as shown that the combined effects of wind and temperature difference is usually between :
 _ the effect which corresponds only to the predominant force,
 _ the effect which corresponds to the adding of the two motive forces.

ASHRAE¹¹ suggests the following correlation :

$$Q^e_T(i) = Q_{max} \cdot (1 + 0.24 \cdot \left(\frac{Q_{min}}{Q_{max}}\right)^{0.8}) \quad (9)$$

where :

$Q^e_T(i)$ = Net mass flow from the outside towards zone (i)
under the combined action of wind and stack effects,
Kg/s.

with :

$$\begin{cases} Q_{max} = \text{MAX} (Q^{ev,d}(i), Q^{Te}(i)) \\ Q_{min} = \text{MIN} (Q^{ev,d}(i), Q^{Te}(i)) \end{cases}$$

We preferred to use a simplified relation :

$$\begin{cases} Q^e_T(i) = \sqrt{(Q^{ev,d}(i))^2 + (Q^{Te}(i))^2} \\ Q^{is}_T(i,m) = \sqrt{(Q^{is}_{ev,d}(i,m))^2 + (Q^{is}_{Te}(i,m))^2} \end{cases} \quad (10)$$


	WIND EFFECT	STACK EFFECT
WIND VELOCITY	$\bar{V}(z) = k \cdot \text{Log}_{10} \left(\frac{z}{z_0} \right) \cdot \bar{V}_{ref}$	
PRESSURE DIFFERENCE	$\Delta \bar{P} = Pr_i - Pr_{\infty} + \frac{1}{2} \rho_i \cdot C_p \cdot \bar{V}^2(z)$ with : $\begin{cases} Pr_i = 0 \text{ if room (i) is outside} \\ C_p = 0 \text{ if room (i) is inside.} \end{cases}$	$\Delta \bar{P} = Pr_i - Pr_{\infty} - (\rho_i - \rho_{\infty}) g \cdot z$
FLOW EQUATION	$\bar{Q}_{vj} = C_j \cdot (\Delta \bar{P}_j)^{0.5}$	$\bar{Q}_{vj} = C_j \cdot (\Delta \bar{P}_j)^{0.5}$
MASS BALANCE EQUATION FOR EACH ZONE	$\sum_j \bar{Q}_{mj} - Q_{exh} = 0$	$\sum_j \bar{Q}_{mj} = 0$
SOLUTION OF THE FLOW EQUATION	Standard Newton' method generalized to a system of non-linear algebraic equations.	

Table 3 : Simplified method of calculation of air infiltration in buildings.

4. COMPARISON OF OUR MODEL WITH EXPERIMENTATION

We have compared numerical results obtained from our simplified model with an experimental study undertaken in residential suburb of Ottawa, Canada, by the Division of Building Research (D.B.R.).

This energy research project, called MARK XI, was first conducted on the instrumentation¹², then on the measure of airtightness¹³ in four detached two-storey houses.

In particular, we are interested in the standard construction which architectural design is shown in figure 3.



Figure 3 : Architectural design of the standard house.

37 air infiltration measures were made during 1978-1979 heating season¹⁴. Air infiltration rates were measured using the tracer-gas decay method¹⁵, with CO_2 as the tracer-gas. This involves introducing a small amount of CO_2 into the house and measuring the decay of its concentration with time, using an infrared gas analyser. Whereas, air permeability was measured for different pressure drops across the envelope, using the fan-pressurization method. We have estimated air permeability of standard house (normalized by the building volume) at $K_{\text{res}} = .234 \text{ m}^3/\text{h.m}^3$ at 1Pa.

Table 4 sums up a part of experimental tests. It describes climatic conditions under which these measures were made. Either the results are numerical or experimental, they are set out as air infiltration rates.

TEST N°	AIR TEMPERATURE		WIND VELOCITY	WIND DIRECTION	MEASURED VALUES	CALCULATED VALUES
	Inside (°C)	Outside (°C)				
1	22.4	4	4.83	N	.219	.225
2	20.4	-12.7	1.65	N	.264	.258
3	20.7	-2.6	3.93	NW	.274	.234
4	22	-10.6	10.55	NW	.415	.355
5	20.2	.5	2.19	W	.168	.208
6	23.4	-3.4	6.12	W	.301	.256
7	21.8	-4.4	4.43	W	.210	.241
8	21	-4.7	9.61	W	.222	.345
9	22.6	-5.5	5.63	W	.271	.262
10	22.5	-7.4	4.69	W	.267	.256
11	19.8	-9.3	5.68	W	.255	.273
12	22.6	-9.6	5.23	W	.265	.261
13	23.1	-10.6	6.00	W	.303	.280
14	21.3	-12.2	6.30	W	.292	.286
15	21.4	3.9	1.07	W	.155	.199
16	22	.2	7.38	S	.316	.262
17	22.4	3.7	6.48	S	.270	.240
18	20.0	-9.0	5.95	SW	.256	.274
19	22.2	3.8	8.05	E	.214	.293
20	22.4	-1.0	7.64	E	.281	.300
21	22.0	-4.7	8.00	E	.260	.309
22	21.0	-5.6	1.43	E	.236	.228

Table 4 : Experimental conditions and obtained results.

We plotted on a graph (figure 4) , measured infiltration points on x-axis and calculated infiltration points on y-axis. The solid line is the locus of points that represent perfect agreement; the dashed lines define an area of acceptable agreement based on the measurement uncertainties ($\pm 25\%$).

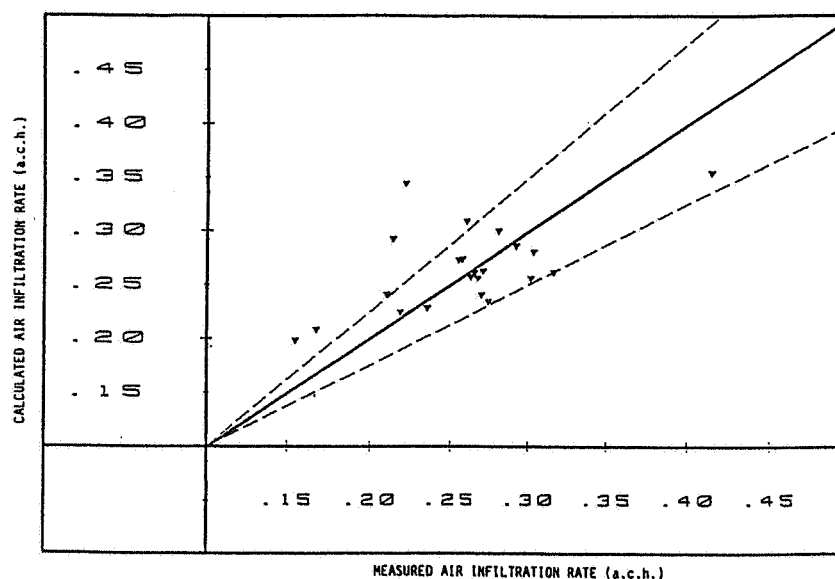


Figure 4 : Comparison between calculated and measured air infiltration rates.

We note a good agreement between experimental and predicted results. The points which are further off the solid line correspond to high level velocity of wind (test n° 4, 8, 16). Two kinds of interpretation, which are not inconsistent, may explain these differences.

_ air infiltration measures by using a tracer-gas decay method depend on climatic conditions. With a strong wind (≥ 7 m/s), these measures may be erroneous.

_ we assumed that only an average pressure coefficient on each facade may characterize the wind impingement on a building. This assumption is not valid when the dynamic pressure becomes predominant in the infiltration process.

This comparison could not be taken as a validation for our model since it is applied to a particular kind of dwelling house. It may be interesting that other cases may be studied especially air exchanges between rooms. Unfortunately, we do not know if any experimentation of this kind was made before.

5. CONCLUSION

We studied a simplified model which treats air mass transfers in a partitioned building.

This model was made to analyze the tendencies in a aided architectural design context. So, we privileged the quickness of computation running instead of a wide investigation scope.

This study must be balanced by noting that, even if physical principles and general laws which induce ventilation phenomena are known, it exists a great incertitude concerning different data (pressure coefficients, air permeability , ...)

ACKNOWLEDGEMENTS

This work was supported by "l'Agence Française pour la Maitrise de l'Energie" under contract N° : 6.04.0025.

REFERENCES

1. ROLDAN, A. ALLARD, F. and ACHARD, G.
"Influence des infiltrations et des transferts aérauliques entre pièces sur la charge thermique d'un bâtiment multizone" ICBEM'87 , Tome 3 , LAUSANNE , Oct. 1987, pp 178-185

2. GANDEMER, J.
"Ecoulements et charges induits par le vent sur les
bâtiments."
Cahiers du CSTB n°2045, livraison 265, Dec. 1985, pp 1-31
3. GANDEMER, J.
"Champ de pression moyenne sur les constructions usuelles."
Cahiers du CSTB n°1492, livraison 187, Mars 1978, pp 1-32
4. FAUCONNIER, R. GUILLEMARD, Ph. and GRELAT, A.
"Algorithmes des simulateurs du comportement thermique des
bâtiments : BILGA et BILGO (suite)."
Annales ITBTP n°458, Oct. 1987, pp 78-116
5. KREYSIG, E.
"Advanced engineering mathematics . "
Wiley (4th edn), New-York, 1979.
6. MOYE, C.
"La perméabilité à l'air des bâtiments d'habitation ."
Cahier du CSTB n° 2019, livraison 262, Sept. 1985 pp 1-20
7. KRONVALL, J.
"Testing of houses for air leakage using a pressure method."
ASHRAE Trans. 84, Part 1, 1978, pp 72-79
8. CACCAVELLI, D. ROUX, J.J. and BRAU, J.
"Modélisation simplifiée du comportement thermique d'un
bâtiment multizone . Prise en compte des phénomènes de
ventilation naturelle ."
Revue Générale de Thermique, n° 311, Nov. 1987 pp 585-596
9. CLEMENT, D. CHOUNET, L.M. DUBOIS, A.M. FAUCONNIER, R.
GUILLEMARD, Ph. LAHELLEC, A. LARET, L. and SORNAY, J.
"Vers une base de connaissances en modélisation thermique du
bâtiment. Elements d'analyse d'une modélothèque."
ICBEM'87, Tome 2, LAUSANNE, Oct. 1987, pp 256-262.
10. CADIERGUES, R.
"Méthode d'étude de la ventilation naturelle . "
PROMOCLIM E, TOME 8E, n° 5, Dec. 1977 pp 307-318
11. ASHRAE Fundamentals 1985
Chapter 22 , pp 22.1, 22.18
12. QUIROUETTE, R.L.
"The Mark XI Energy Research Project : Design and
Construction . "
Building Res. Note n° 131, pp 1-20
13. SHAW, C.Y. and TAMURA G.T.
"Mark XI Energy Research Project : Airtightness and Air
Infiltration Measurements ."
Building Res. Note n° 162, June 1980, pp 1-22

14. LIDDAMENT, M. and ALLEN, C.
"The validation and comparison of mathematical models of air infiltration."
Technical Note AIC 11, Air Infiltration Centre, September 1983, pp 1-113
15. SANDBERG, M.G.
"Predicting a time-varying flow rate using the constant concentration and decay technique."
ASHRAE Trans. 93, Part 1, 1987, pp 1381-1393

EFFECTIVE VENTILATION

9th AIVC Conference, Gent, Belgium
12-15 September, 1988

Poster 13

**ANALYSIS OF THE INFLUENCE OF TOPOGRAPHY
ON CLIMATIC EXPOSURE OF BUILDINGS
(Climatological Data Transfer)**

J.-A. Hertig and J. Ehinger

**LASEN, SWISS FEDERAL INSTITUTE OF TECHNOLOGY
LAUSANNE, SWITZERLAND**

1. INTRODUCTION

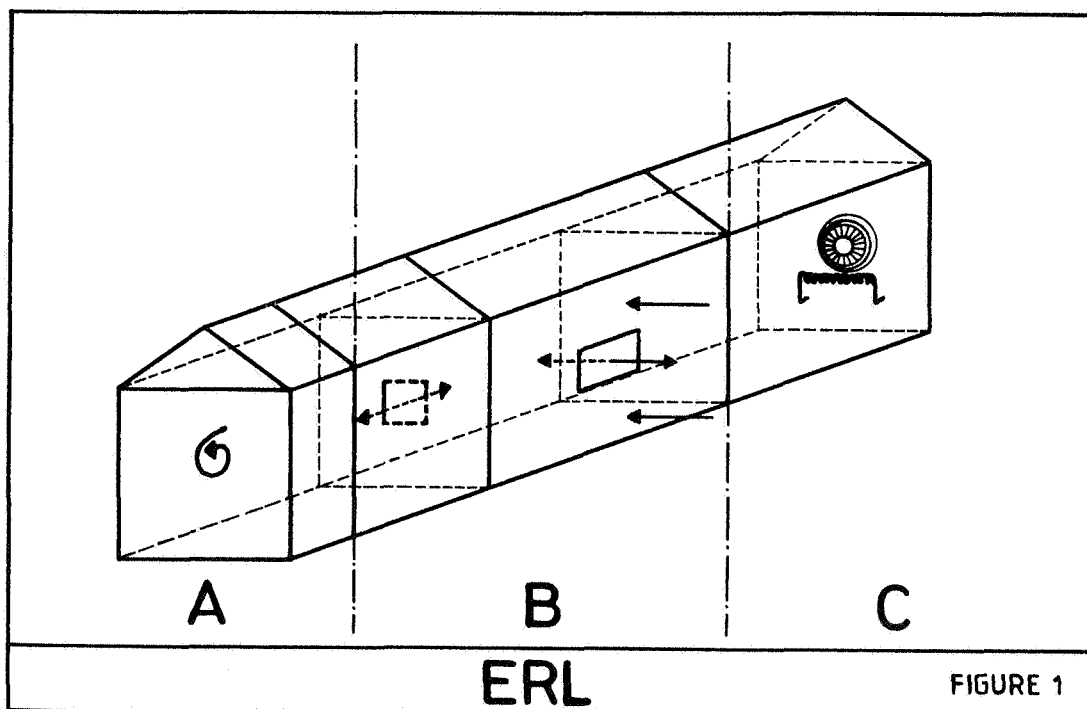
This text contains comments to the poster presented at the 9th AIVC Conference in Gent, Belgium. The project under consideration in the poster (Climatological Data Transfer) is one of the numerous research fields of the Swiss ERL program (Energierrelevante Luftströmungen in Gebäude - Energy Relevant Air Flow in Buildings).

2. OBJECTIVES OF THE ERL PROGRAM

The ERL program is subdivided into three fields of research, namely:

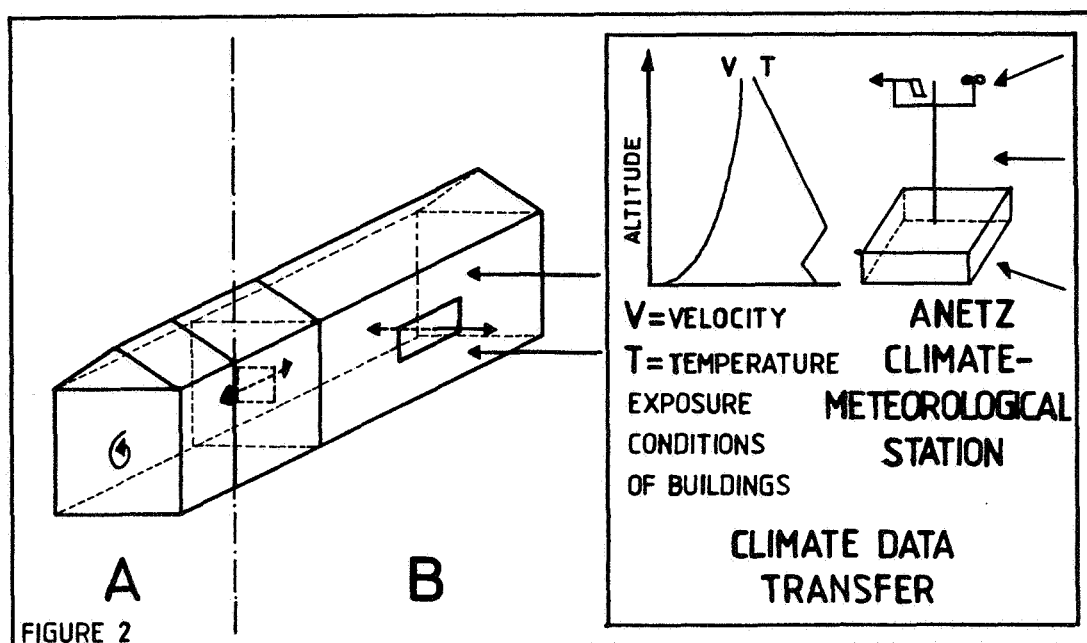
- A: Analysis and modelling of air flow within buildings considered as closed entities
- B: Analysis and modelling of air flow taking place between various buildings, partially open to the exterior environment
- C: Optimisation of ventilation and air-conditioning systems.

The objectives of these three fields of research are interlinked, the final goal of the ERL program being theme C. The climatological data transfer project is included under theme heading B.



3. OBJECTIVES OF THE CLIMATOLOGICAL DATA TRANSFER PROJECT

The main goal of this study is to set up a methodology and a modelling system capable to determining the climatic exposure of buildings situated in a particular location of Switzerland, on the basis of corrected data obtained from the automatic meteorological station network "ANETZ". The envisaged modelling system should be accessible to engineers so that they may know the magnitudes of climatological data which can influence air conditioning and ventilation systems.



LASEN N53I.III

I988.07.22 RR

4. SPECIFICITY OF RESEARCH IN THIS FIELD

Much work has been undertaken in the field of meteorological data analysis, and several authors have studied wind effects on constructions. Such work has generally contributed to the elaboration of various national standards concerning wind loads on buildings. These studies are generally related to strong or extreme wind conditions.

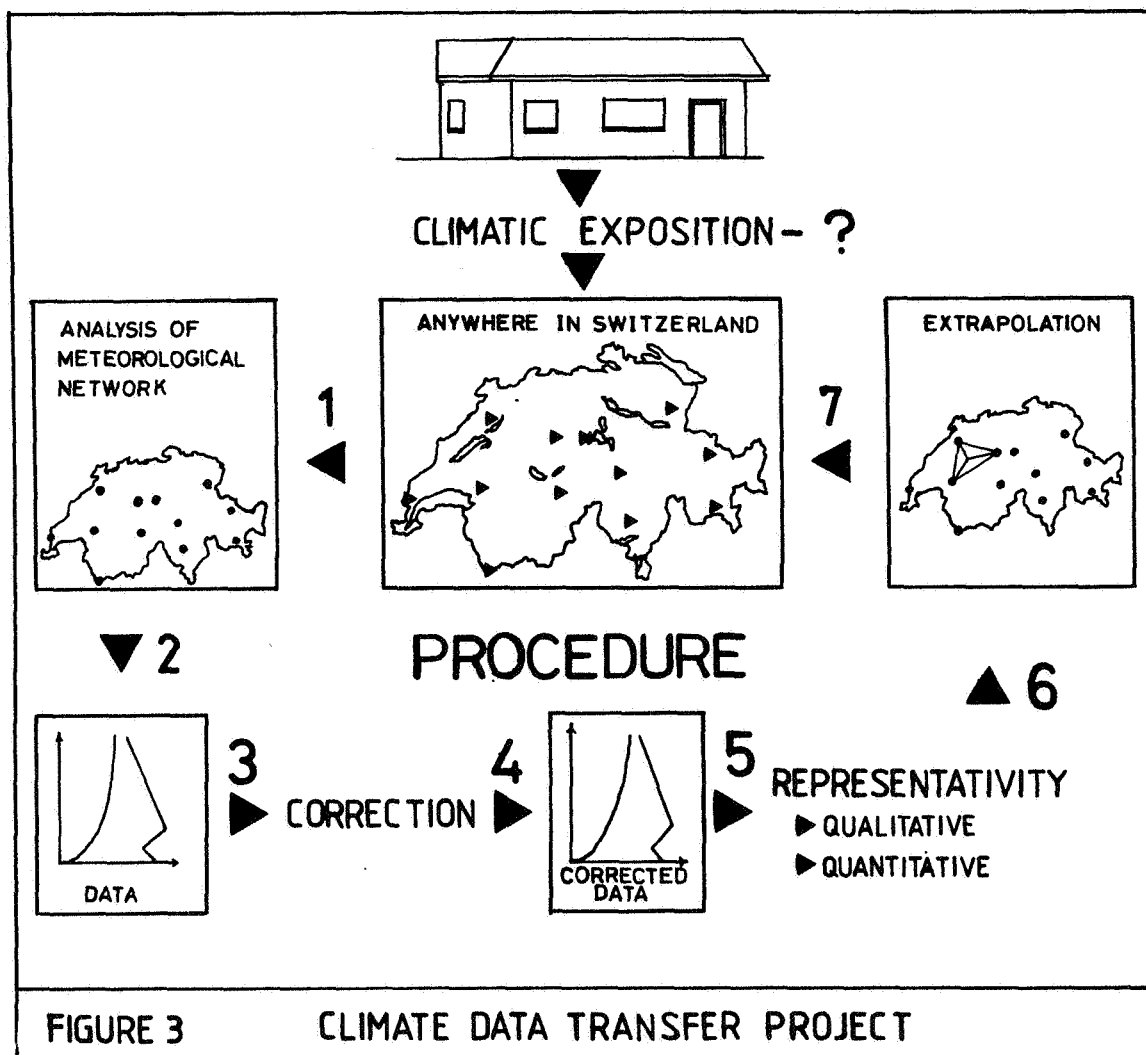
To our knowledge, however, no work has been carried out on light to moderate winds in complex terrain. This is consequently the principal objective of the present study.

5. ORGANISATION OF THE CLIMATOLOGICAL DATA TRANSFER PROJECT

The authors of the present project plan to use data supplied by the automatic meteorological station network ANETZ, which was set up and is administered by the Swiss Meteorological Institute.

However, it has been observed that certain parameters, in particular wind velocity and direction, are perturbed by the proximity of other instruments, the presence of obstacles (trees, buildings), and the complexity of Swiss topography.

Consequently, the first phase of the project consisted in visiting each station in the ANETZ network in order to draw up an inventory of potential problems. The second phase, currently being carried out, aims to establish corrections to the perturbed data mentioned above, while at the same time investigating the representativity of the ANETZ network. The following phases of the project will begin once these preliminary studies have been concluded.



6. ANALYSIS OF THE ANETZ NETWORK

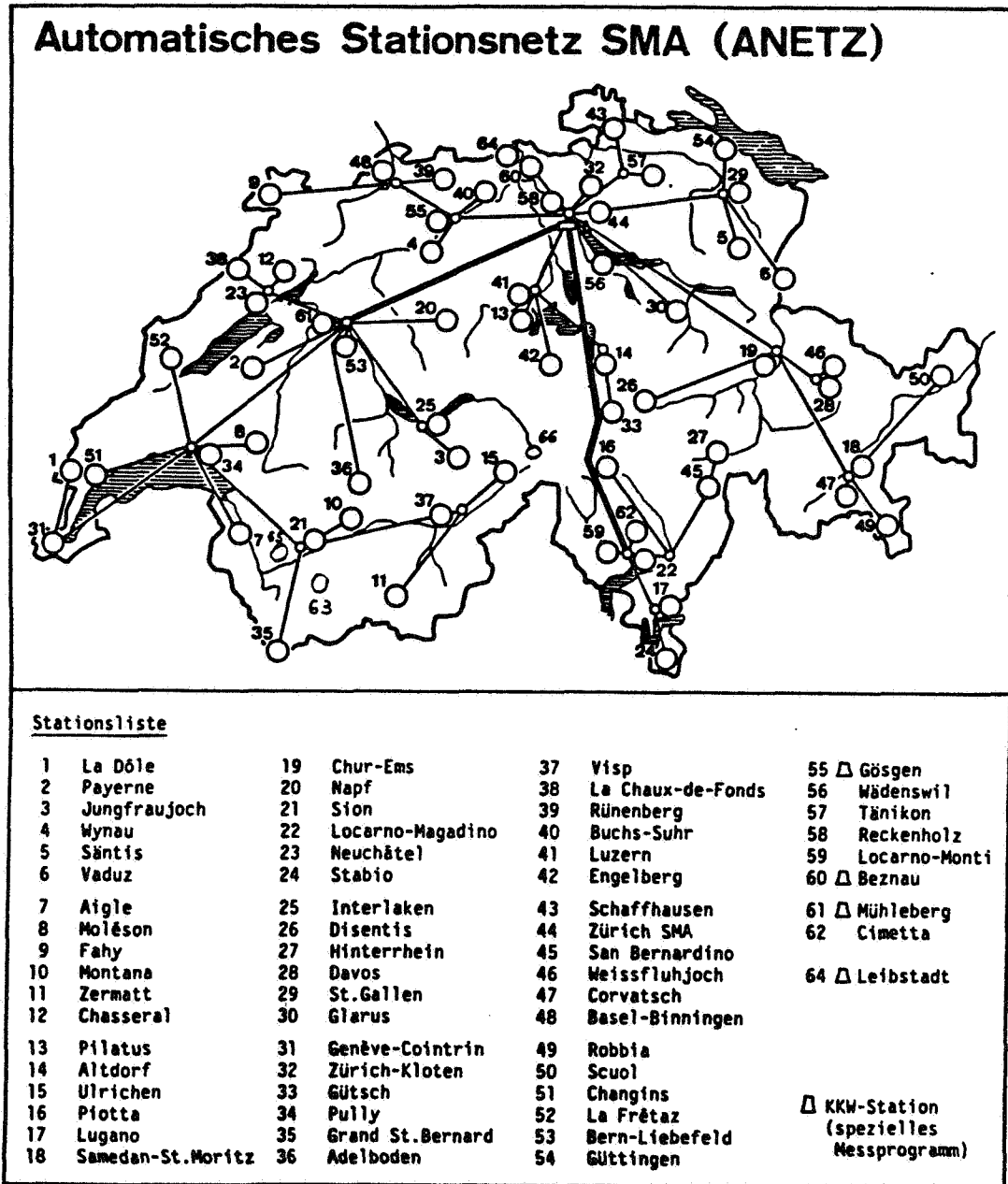


FIGURE 4

LASEN N53I.II3

I988.07.22 RR

The 64 existing meteorological stations have been analyzed. This work comprises three aspects:

a. Observation

On the spot, the following parameters have been noted:

- Estimation of the time evolution of the environment in the vicinity of the station
- Simplified topographic profiles
- Presence of nearby obstacles
- Complexity of local orography
- Principal morphological features
- Surface characteristics and vegetation
- Sources of wind
- Localisation of the instruments
- Interactions between wind-measuring equipment
- Orientation of wind-measuring instruments
- Estimation of the probable behavior of wind-measuring instruments.

b. Photography

At each station, a 360° panoramic view was taken in the vicinity of the instrumented mast, with a 50 mm focal lens. More general views of the station were taken at various locations, and the instruments were photographed in detail. These documents will enable updating of information on each station, and yield precise indications required for wind-tunnel tests (see paragraph 9).

c. Summary of observations

In order to optimize wind-tunnel tests (see sub-heading 9), three types of classification have been established according to the scale of the problem considered. Information gathered during this research forms also the basis of the methodology necessary for the correction of ANETZ meteorological data.

7. INVENTORY OF PROBLEMS

The ANETZ meteorological network is a somewhat complex ensemble and the risk of errors is consequently high. It should be noted, nonetheless, that the network functions remarkably well, and for example breakdowns in data transmission are extremely rare.

The following list gives an idea of the chief potential sources of data error, although at this time it is not possible to estimate the real importance of such errors:

a. Geographical location of the stations

This is chiefly related to the complex orography characteristic of Switzerland, as well as to the presence of natural (trees...) or man-made (buildings...) obstacles.

b. Material chosen

The ANETZ stations are not always equipped with identical instruments, due to the constant upgrading of material and the diversity of climatic conditions. This poses problems as to the uniformity of transmitted data; such data requires correction in order to enable intercomparisons.

c. Technical Reliability of the installations

Numerous breakdowns can occur, such as the breakdown in communications, fortunately very rare, or more subtle problems such as the slow drift of information registered by a particular instrument.

d. Reliability of data

First ANETZ records date back to 1978. It is, however, inadvisable to work with such data prior to the end of the year 1980.

e. Maintenance of the equipment

It is often possible that instruments are not cleaned after rain or the sprinkling of fertilizer used for fields neighboring a particular station.

f. External perturbations

Several external sources of wind can disturb wind measurements at an ANETZ station: Flyover by a helicopter, presence of a nearby road, etc. Damage due to animals is also a particularly disturbing factor for anemometric readings.

g. Interactions between instruments

A lightning rod, mast, or light marker (such as at an airport) located near an anemometer may significantly influence its behavior.

Due to the fact that it is impossible to take into account all these problems simultaneously, the following hypotheses have been put forth:

- The equipment is technically reliable
- They are satisfactorily maintained
- The data is free of technically-induced perturbations.

Only the problems linked to disturbances in anemometer and wind-vane measurements are taken into account. These can be identified on three different scales:

- General orography, with for example the presence of a mountain summit within a few kilometers radius
- Local features, such as the wake produced by obstacles within a radius of a few hundred meters
- Interactions between measurement equipment.

8 . STATION TYPOLOGY

In order to apply a correction to data influenced by the above mentioned factors, individual stations have been grouped together according to three types. Correction factors will be determined by wind-tunnel tests.

8.1 Classification according to anemometer type

- | | |
|-----------------------|-------------|
| a) Schiltknecht type: | 35 stations |
| b) Lambrecht type: | 19 stations |
| c) SIAP type: | 10 stations |

This classification has been further refined by taking into account other features in the neighborhood of anemometers, such as antennas or light markers.

8.2 Classification according to nearby obstacles

It is envisaged to summarize information relative to obstacles in order to establish a "Standard obstacle type" to be tested in a wind-tunnel. The model obstacle should then need only minor modifications in order to reproduce the environments around each station.

8.3 Classification according to topography

The local topography of each station has been classified according to simple geometric forms such as those shown in the following figure.

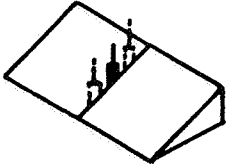
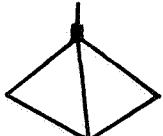



TYPE	DESCRIPTION	SCHEMA	ANETZ NO
A	Station situated on a regular slope		x, ...
B	Station situated on a mountains summit		y, ...
C	Station situated in a valley bottom		z, ...
D	Station situated on a pass		t, ...
E	Topography too complex		u, ...

FIGURE 5

ANETZ STATION TYPES

LASEN N53I.II4

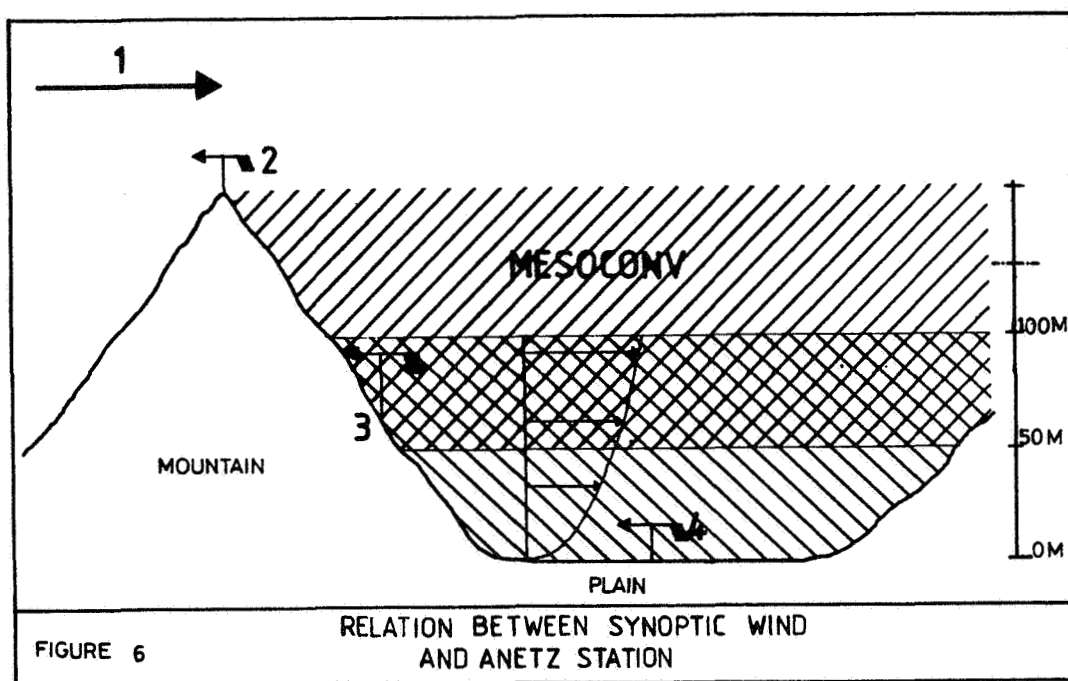
I988.07.22 RR

9. CORRECTIONS AND REPRESENTATIVITY

The methodology established for ANETZ data correction may also be used to identify the representativity of each station, that is to say the area of validity of the measurements.

9.1 Correction strategy

The following figure summarizes schematically typical orography of Switzerland, and ANETZ stations located on flat ground, on a slope, or on a mountain summit.



LASEN N531.II5

.1988.07.22 RR

- (1) Synoptic wind
- (2) High-altitude mountain station
- (3) Station based on a slope
- (4) Station located on flat ground (plain).



MESOCONV

Domain of application of the MESOCONV meteorological models



Domain of application of power and logarithmic wind profile laws.

It is planned to set up a relation between the synoptic wind and that observed at the surface in order to compare data measured by the ANETZ network and extrapolate the measurements to any point in Switzerland.

The method which is envisaged is briefly described below. The relation between the synoptic wind and summit or high-altitude stations will be established by wind-tunnel tests (scale 1:5000) for the twelve stations in this category (Relation 1-2 as shown in Fig. 6).

The link between the upper-level station and slope stations down to about 20 m above a flat surface will be achieved through numerical simulations with a meso-meteorological model (MESOCONV). (Relation 2-3 in Fig. 6)

Power or logarithmic wind-profile laws will enable the link to be made between slope stations and stations located on a plain (relation 3-4).

In this manner, it will be possible to obtain wind relationships between the surface and the synoptic wind.

9.2 Topographic corrections

The aim here is to apply corrections to data perturbed by orography within a 3-5 km radius around the station. The twelve high-altitude stations will be modeled at a 1:5000 scale.

The scale models, mounted on a circular base with a 2 m radius, will be placed on a turntable and experimented upon in a wind-tunnel. The synoptic wind will be reproduced by the wind-tunnel fans. The model will be equipped with a wind-vane and a hot-wire anemometer. For each degree of rotation, wind speed and direction will be measured. This will yield a correction matrix containing 720 values.

As previously mentioned, twelve scale models have been chosen which should enable global corrections on this scale for Switzerland.

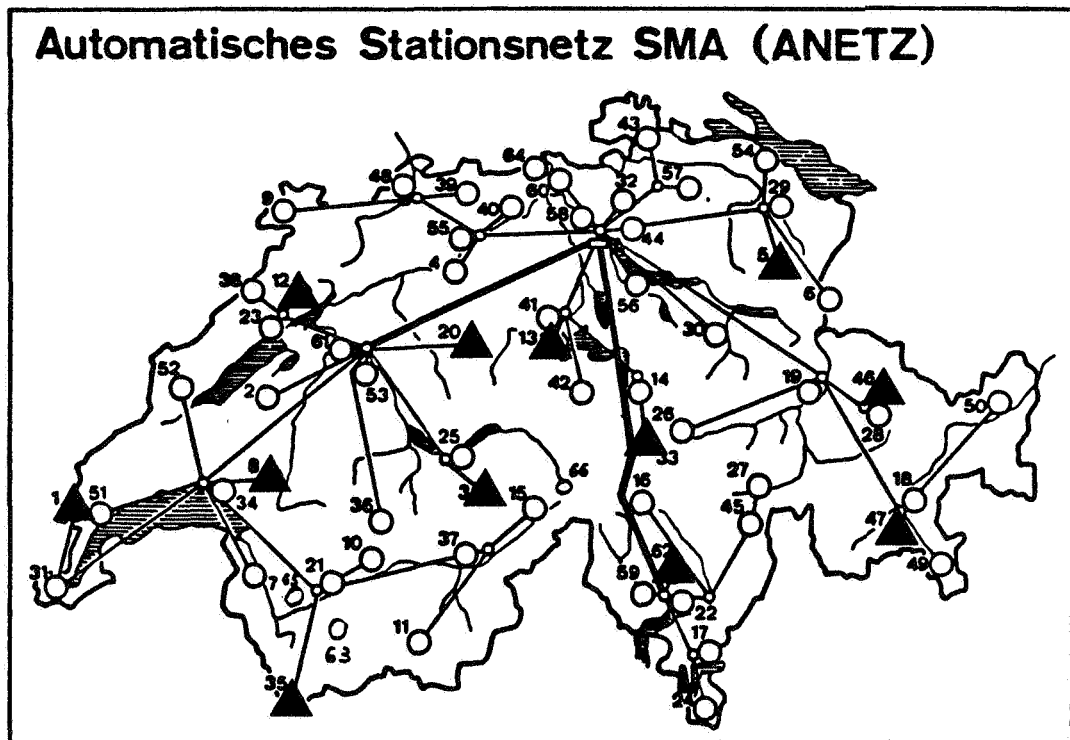


FIGURE 7

9.3 Correction taking into account obstacles

Only those obstacles present within a radius of 300-500 m around the station will be considered. A complete inventory of these features has been drawn up. The configurations of each station will be regrouped into a number of classes, in order to organize the wind-tunnel tests in a rational manner.

A standard model will be constructed, and it will be sufficient to displace certain parts of this scale model in order to reproduce in the wind-tunnel the environment of each station. The wind-tunnel will be used to simulate airflow at 10 m above the ground. The model will rotate degree by degree, yielding a new 720-value matrix (velocity and direction over 360°).

9.4 Correction for wake effects of instruments

The third and last type of correction concerns the anemometers and wind-vanes themselves. These instruments are often surrounded by objects of various forms which generate turbulence, such as antennas, light markers in the vicinity of airports, masts, pylons, or other instruments located nearby for inter-comparison purposes. These latter objects are generally placed between 3 and 5 m from the ANETZ wind instruments. As mentioned previously, a 720-point correction matrix will be established for each wind-tunnel experiment. Because of the similarity of configuration of a number of ANETZ stations, only about 15 wind-tunnel simulations are needed to test the 64 ANETZ stations.

9.5 Global corrections

Non-corrected data supplied by ANETZ stations will be transformed with two correction matrices, thereby yielding the corrected data sets. Only the twelve high-altitude measuring stations will be modified by the two correction matrices.

9.6 Extrapolation from summits to plain and station representativity

The mesoscale meteorological model MESOCONV enables simulations of wind flow in complex terrain to be made. With this numerical model, a ventilation map of Switzerland will be drawn up, taking into account vertical and horizontal wind variations. Studies undertaken with this model should enable the solution of representativity of the ANETZ network (see paragraph 5) quantitatively. The vertical resolution of the model extends from the surface to a height which ranges from 5000 to 10000 m.

9.7 Link between MESOCONV and the surface

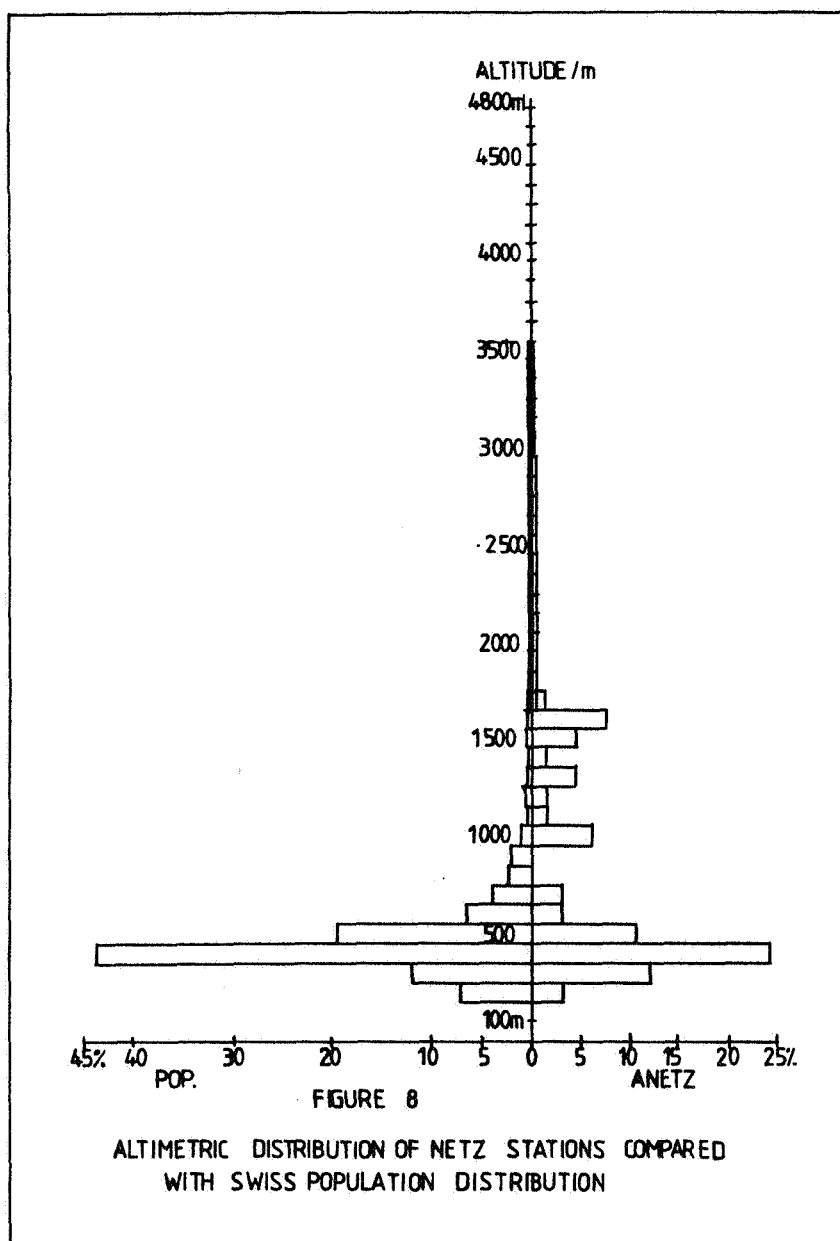
Between the surface and the first MESOCONV model level, wind data at 10 m height can be obtained by applying power law or logarithmic profile relationships, interpolated from data supplied by the numerical model.

10. REPRESENTATIVITY OF THE ANETZ NETWORK

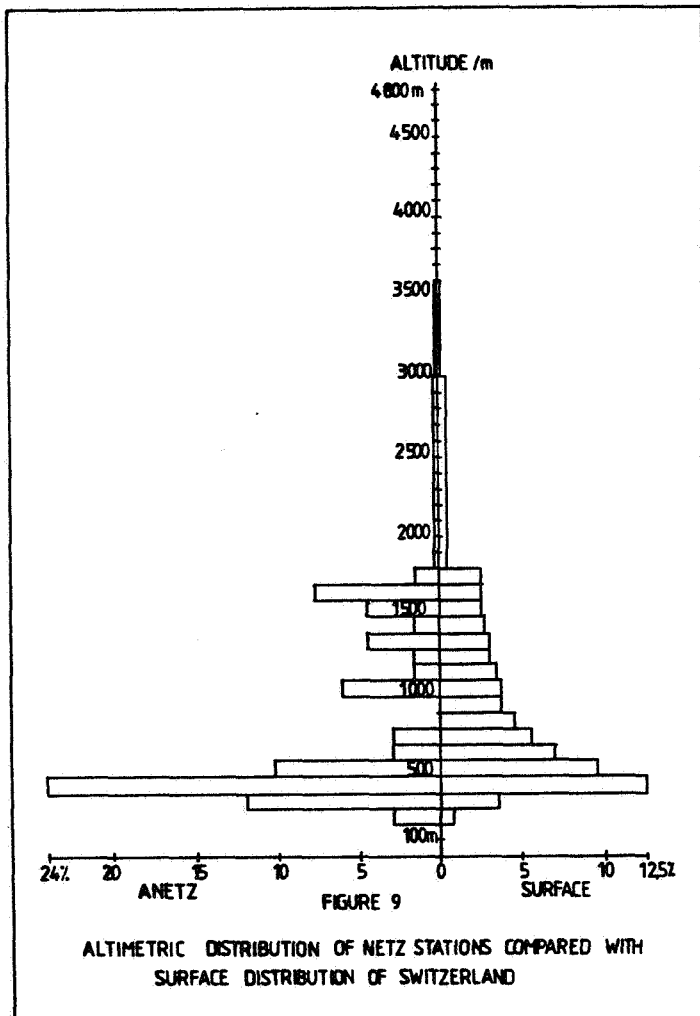
As mentioned above, the area of validity of the ANETZ data will be delimited quantitatively through simulations with the MESOCONV model. Simultaneously, a more qualitative study concerning station representativity will be carried out. This consists in underlining possible gaps in the geographical outlay of the ANETZ meteorological network.

10.1 Altimetric distribution of the ANETZ network

As a first step, the height distribution of the ANETZ network was compared to that of Swiss population as an indicator of density of built-up areas. The following figure summarizes this comparison.



As a second step, the height distribution of the ANETZ stations was compared to the area distribution of various altitudes: for example, 5.6% of the total area of the country lies between 701 and 800 m. The following figure summarizes this relationship.



LASEN N°31.118

1988.07.22 RR

11. CONCLUSION

A further study of the qualitative representativity of the ANETZ network is under way, where one is attempting to relate the horizontal distribution of the meteorological stations to height intervals, exposure of the stations, and Swiss climatology basins.

The methodology presented here will be completed by an inverse concept which will enable us, we hope, to answer the question: "What is the climatic exposure of a construction planned at a particular site?".

EFFECTIVE VENTILATION

9th AIVC Conference, Gent, Belgium
12-15 September, 1988

Poster 14

THE INFLUENCE OF A CONTROLLED NATURAL VENTILATION ON THE
INDOOR RADON DECAY PRODUCTS CONCENTRATION: A CASE STUDY

R. CRAMERI, Ch. SCHULER, D. FURRER AND W. BURKART

Radiation Hygiene Division
Paul Scherrer Institute
CH-5303 Würenlingen, Switzerland

1. ABSTRACT

Air exchange rates in occupied buildings are difficult to assess due to their dependence on a multitude of climatic parameters and inhabitant behaviour. Moreover, the assessment of the influence of the air exchange rate on the radon progeny concentration is hampered by the diurnal and seasonal fluctuations of the indoor radon levels. Experiments involving two adjacent rooms submitted to identical conditions influencing the radon concentration and showing similar temporal variations and levels of radon progeny provide a mean to assess the contribution of a controlled natural ventilation enhancement to the reduction of the indoor radon progeny concentration. First results show, that one additional air exchange per day reduces the mean indoor radon progeny concentration by about 5 %. This indicate that natural ventilation is not sufficient to reduce the indoor concentration of radon decay products to an acceptable level in areas with elevated radon source strength, especially during the winter.

2. INTRODUCTION

Exposure to radon and radon daughters are a well-known cause of lung cancer in miners^{1,2}. The attention payed during the least decade to the indoor radon problem has revealed, that the activity concentration in the living area of many buildings may reach or even exceed the concentrations measured in modern mines^{3,4}. Thus indoor radon progeny are believed to be the greatest "natural" radiation hazard to the general public and therefore one of the most critical indoor air pollutants. The indoor concentration of volatile substances i.e. also of radon and radon decay products is determined by the source strength, the infiltration mechanisms and the air exchange⁵. Moreover, the air exchange rate is influenced by the characteristics of a building⁶, climatic parameters and by the behaviour of the inhabitants opening and closing windows according to a subjective feeling about the indoor air quality. Involving both the feasibility of technical solutions and the private sphere of occupants, field measurements in occupied buildings are quite delicate.

The aim of the present case study was to clarify if the assessment of the influence of the inhabitants on the indoor concentration of radon decay products is feasible. To achieve this goal, all fluctuations of other parameters influencing the indoor radon decay products concentration have to be reduced to a minimum in order to avoid misinterpretations of the experimental results. The case study involves two comparable rooms subjected to approximately the same external parameters influencing the indoor progeny concentration. Controlled changes of the natural ventilation in one of the two rooms keeping the other one as control, allow us to eliminate the major sources of errors and to test the feasibility of such a project.

3. MATERIALS AND METHODS

Continuous measurements of radon decay products were performed with Eberline WLM-1 working level monitors. Field calibration of these sampling units were accomplished with an electroplated alpha source as described earlier⁷. Measurements of air exchange rates were carried out with a tracer gas technique using nitrogen protoxyde (N₂O) as described elsewhere⁸. Both, decay and constant concentration methods were used for the air exchange rate

determinations. To simulate in a realistic way the ventilation behaviour of inhabitants, owners of 100 dwellings were asked by mailed questionnaire about their ventilation attitudes.

4. RESULTS

4.1 The diurnal cycle

Figure 1 shows the diurnal radon decay products fluctuations during one week for the two experimental rooms located on the ground floor of a single family home.

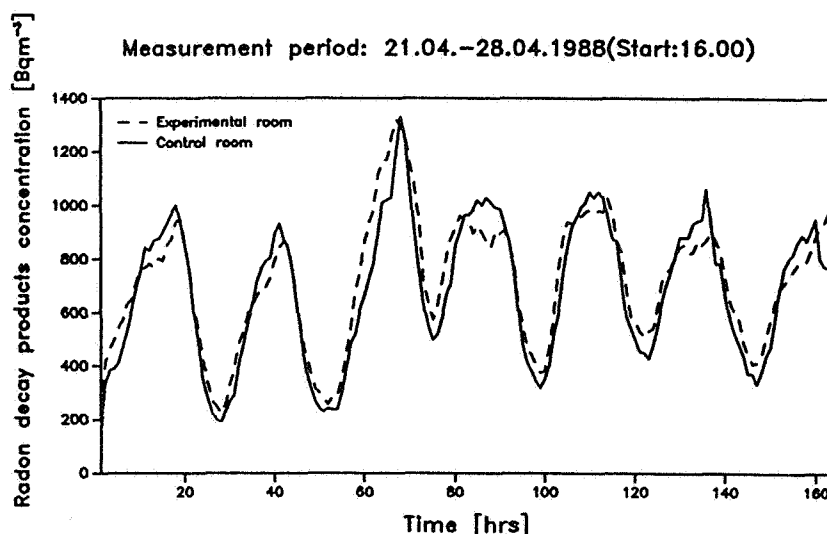


Figure 1. The diurnal fluctuations of the radon decay products concentration in the two examined adjacent rooms

The two adjacent rooms showed almost identical pattern of radon decay products for at least three months in the absence of occupants. The diurnal cycle exhibits, for so far unknown reasons, a maximum in the early morning and a minimum in the late afternoon. Therefore the opening of a window during the decreasing phase of the diurnal cycle would overestimate the influence of the ventilation on the radon decay products concentration. Thus for quantitative assessments the time-dependent variations of the radon decay products concentration obtained for a ventilated room must be considered and compared with the values obtained for the unventilated control room. The analysis of adjacent rooms which are submitted to identical conditions influencing the radon progeny concentration and exhibiting a comparable diurnal cycle (Figure 1) provides a mean to assess the influence of a controlled natural ventilation on the indoor radon daughters concentration.

4.2 Limitations of the radon decay products detection system

Time integrating radon progeny monitors have the disadvantage that they fail to respond quickly to fast changes in activity concentrations. In addition,

because of the half-life of the radioisotopes involved, a time-lag of about 45 minutes between actual and reported radiation level occurs. However, this time-lag does not influence long time experimental records in a significant way.

4.3 Influence of the natural ventilation on the concentration of radon decay products

From the 88 responses to the questionnaire on ventilation attitudes, only 51 were filled in completely. The ventilation attitudes turned out to be highly variable for the different rooms of a building as well as for different buildings. The mean values obtained for different rooms during winter and summer reported in Table 1 give an idea about the extreme variations in different climatic periods. This ventilation behaviour during different climatic periods may partially explain the reported seasonal variations of the mean indoor radon concentrations⁹.

Table 1. Mean window opening time in minutes day⁻¹ (\pm S. D. of the mean) for a sample of 51 homes

Season	kitchen	bathroom	living room	bedroom
Winter	30 (\pm 5)	25 (\pm 4)	25 (\pm 3)	130 (\pm 45)
Summer	300 (\pm 60)	400 (\pm 75)	450 (\pm 67)	700 (\pm 90)

Because the indoor concentration of radon decay products reach maximum values during the winter when room ventilation is reduced in order to save energy, we decided to perform first experiments with short ventilation periods of 10 minutes. Such a period provokes an enhanced ventilation of one air exchange for the experimental room compared to the unventilated control room as determined by tracer gas decay experiments.

A typical record of the influence of this controlled natural ventilation on the concentration of radon decay products in the experimental room during a period of 24 hours is reported in Figure 2.

The response of the working level monitors to changes in the ventilation rate of the experimental room showed to be fast enough to record changes in the concentration of the radon decay products even if ventilation occurs during the decreasing phase of the diurnal cycle. Therefore a quantitative assessment of the influence of the ventilation rate on the radon decay products concentration is practicable. The air exchange rates of the unventilated experimental and control room determined by tracer gas decay experiments were $0.15 \pm 0.01 \text{ h}^{-1}$ and $0.14 \pm 0.02 \text{ h}^{-1}$, respectively. These results are in good agreement with the values of 0.13 h^{-1} and 0.12 h^{-1} obtained during a three weeks' experiment using the constant tracer gas concentration method in the absence of occupants.

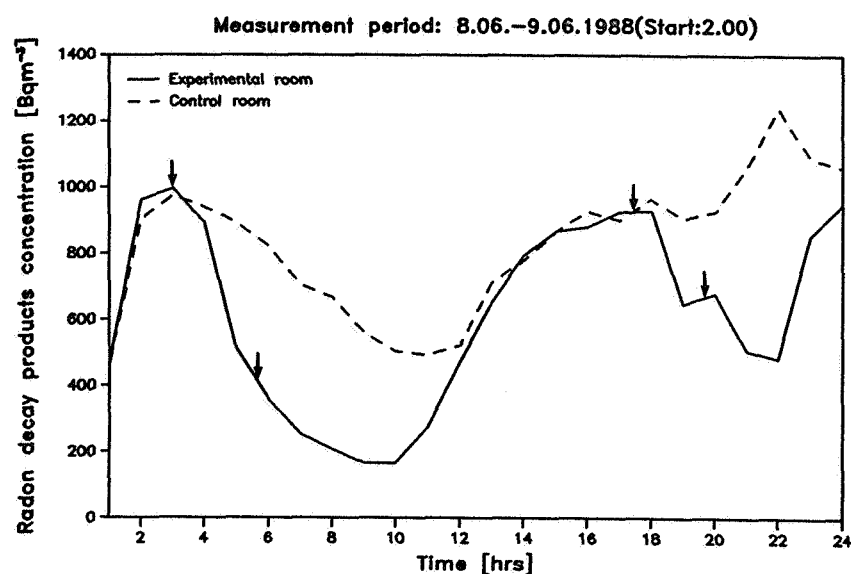


Figure 2 Influence of a controlled natural ventilation on the concentration of radon decay products. Arrows indicate opening of the windows in the experimental room during 10 minutes.

From the preliminary results of the experiments reported in Table 2 we can deduce, that one additional air exchange per day reduces the mean indoor radon decay products concentration by about 5 %. The experimental equipment is sufficient to permit an estimation of the influence of natural ventilation to the indoor concentration of radon decay products. However, for a more accurate quantification long term experiments are required.

Table 2. Influence of a controlled natural ventilation on the indoor concentration of radon decay products

Measurement period	Room	Mean rn-decay products [c] (Bqm ⁻³)	Mean air exchange (h ⁻¹)	Reduction (%)**
08.06-09.06	1	612 (± 58)	0.32*	25
	2	829 (± 43)	0.11	
21.06-22.06	1	687 (± 36)	0.27*	20
	2	860 (± 26)	0.10	
22.06-23.06	1	592 (± 51)	0.29*	20
	2	742 (± 31)	0.12	
23.06-24.06	1	788 (± 47)	0.31*	20
	2	987 (± 21)	0.12	

* Room ventilated during four periods of 10 minutes (ca. 4 additional air exchanges day⁻¹)

** In room 1 as compared to the control room 2

5. CONCLUSIONS

The results of our experiments with a matched pair of rooms displaying similar diurnal variations and levels of radon decay products have shown, that the quantification of the influence of the natural ventilation is indeed possible and gives reliable results. In fact, natural ventilation reduces the radon progeny concentration indoors. However, short ventilation periods as applied here are not a sufficient mean to reduce the indoor concentration of radon decay products to an acceptable level in areas with high radon emanation into buildings.

Further experiments involving a representative sample of buildings and varying ventilation periods are required in order to generalize our findings.

Acknowledgement

This work was partially supported by the Bundesamt für Energiewirtschaft grant No. 0.805.391.02/6 and by the Bundesamt für Gesundheitswesen grant No. 453.38

6. REFERENCES

1. Committee on the Biological Effects of Ionizing Radiation, Health risks of radon and other internally deposited alpha emitters: BEIR IV. Washington DC, National Academy Press, 1988
2. KUNZ, E., SEVEC, J. and PLACEK, V.
"Lung cancer mortality in uranium miners"
Health Phys. 35, 1978, pp579-580
3. JACOBI, W. and PARETZKE, H. G.
"Risk assessment for indoor exposure to radon daughters"
Sci. Tot. Environ. 45, 1985, pp551-562
4. BURKART, W.
"Assessment of the lung cancer risk from radiation exposures due to airtightening of dwellings for energy conservation"
Live Sciences 124, 1987, pp139-145
5. NERO, A. V. and NAZAROFF, W. W.
"Characterising the source of radon indoors"
Radiat. Prot. Dosim. 7, 1984, pp23-39
6. CRAMERI, R., FURRER, D. AND BURKART, W.
"Some building characteristics affecting the indoor radon level of dwellings in the Swiss alpine areas"
CIB Conference, Stockholm, September 5-8, 1988
7. DOWNARD, T. R., GEIGER, E. L. and MILLARD, J. B.

- "Field evaluation of Eberline's radon daughter working level monitor"
In: Indoor Air, Vol. 2, B. Berglund, T. Lindvall and J. Sundell, eds. Lieber Tryck AB, Stockholm, 1984.
8. SCARTEZZINI, J. L., ROULET, C. A. and JOLLIET, O.
"Continuous air renewal measurements in different inhabited buildings"
6th AIC Conference, September 16-19, Netherlands 1985.
9. HANS, J. M. and LYON, R. J.
"Seasonal variations of radon and radon decay products concentrations in single family homes"
U. S. Environmental Protection Agency 520/1-86-0154, Las Vegas, Nevada, 1986.

EFFECTIVE VENTILATION

9th AIVC Conference, Gent, Belgium
12-15 September, 1988

Poster 15

IEA ANNEX XIV: ENERGY AND CONDENSATION.

ERIK SENAVER

Katholieke Universiteit Leuven
Faculteit der Toegepaste Wetenschappen
Laboratorium Bouwfysica
Kasteel van Arenberg
3030 Heverlee
BELGIUM

This paper reviews research activities undertaken in the framework of IEA Annex XIV, "Energy and Condensation". It outlines the objectives and working scheme. The importance of ventilation as an influencing factor and a remedial measure is investigated.

0. Introduction

The central theme of the IEA workshop, held in Leuven in September 1985, was the problem of condensation. During the workshop, it was proposed that an international programme of research should be set up to study the relation between condensation and energy saving, and to develop curative and preventive measures to combat the problem of moisture.

The research programme was formally initiated at a meeting in Utrecht in April 1987, the participating countries being Belgium, Italy, The Netherlands, Germany and Great Britain. Belgium was to act as international coordinator.

1. Brief outline of IEA ANNEX XIV

Following structure is defined to organize the work to be done (fig.1):

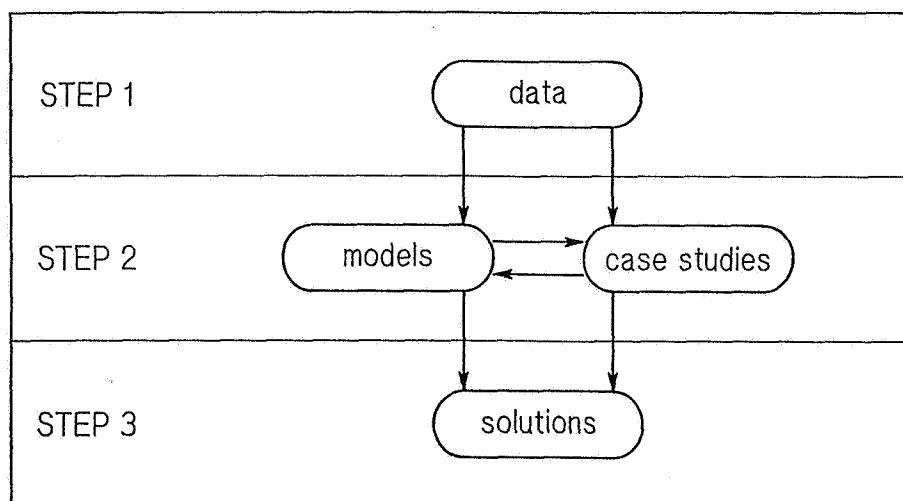


fig.1: structure of IEA ANNEX XIV

STEP 1: The collection of data, mostly concerning (critical) mould growth conditions and hygro-thermal material properties

STEP 2: Models are (further) developed in order to describe heat, moisture and air transport in buildings (interroom transfer), in rooms, on surfaces and to a lesser extent in the building construction, as far as they deal with the problem of surface condensation.

The case studies, one pro country, serve as points of reference for the models. They consist of a detailed study of the indoor climate (temperature, humidity, air movement) in one or more problem dwellings. Curative measures would also have to be evaluated.

STEP 3: Formulation of economically acceptable measures. Such measures should be either curative or preventive.

Each participant should do a case study and be involved in step 3, solutions. So, models may be verified and solutions may be found, adapted to the construction methods and the meteorological conditions in the different countries.

The development of calculation models is optional. The same applies to the collection and deduction of data on the properties of building materials and mould growth.

The success of the annex does not depend on calculation models. Nevertheless, these models are of great importance in achieving the objectives.

In figure 2 the time schedule, based upon research steps as previously mentioned is shown.

The bars indicate the international meetings. Light-grey tint corresponds with preparation period or period of extension of the research step.

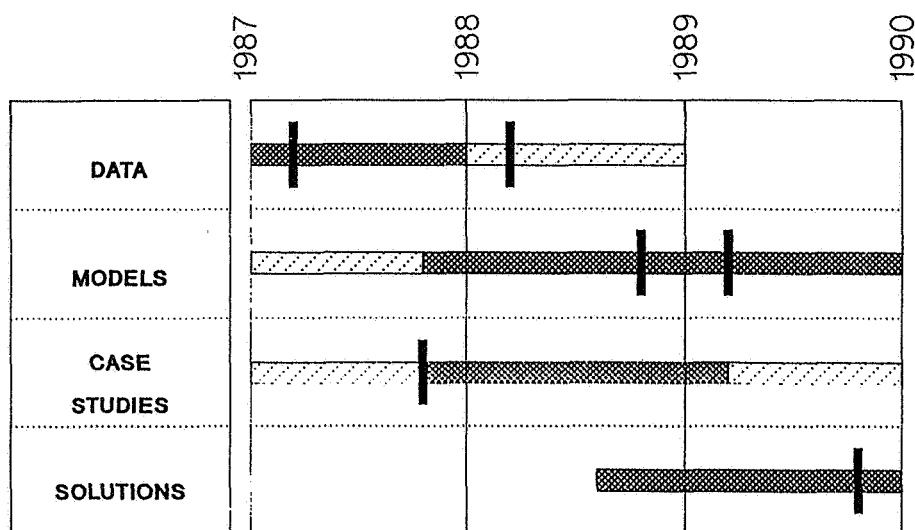


fig.2: research steps IEA ANNEX XIV

Each participant will be responsible for a part of the final report. The research steps are for this purpose divided into a number of subjects, more or less independent of each other. Figure 3 illustrates the allocation of subjects.

STEPS		NL	FRG	GB	I	B
DATA	MATERIAL PROPERTIES	▨	▨	▨	▨	■
	MOULD	▨	▨	■	▨	▨
MODELS	THERMAL MODELS	▨	▨	▨	■	▨
	HYGROSCOPIC MODELS	▨	▨	▨	▨	■
	COMBINED MODELS	■	▨	▨	▨	▨
	BOUNDARY CONDITIONS	▨	■	▨	▨	▨
CASE STUDIES	CASE STUDIES	■				
SOLUTIONS	FINAL TECHNICAL REPORT	▨	▨	▨	▨	■
	PRACTICAL CONCLUSIONST	■				

fig.3: allocation of subjects

Each participant presents an independent report on the case study being undertaken in his own country.

The final, technical report, to be made by the operating agent, will be translated in the various languages, drawing practical conclusions, appropriate to the building practice in his country. It should be emphasized that figure 3 does not illustrate the research activities of the country in question. The aim is to allow participants to gain experience in as wide a field as possible.

2. What about "ventilation and condensation"?

Surface condensation occurs as soon as the dewpoint of the air is above the surface temperature.

The dewpoint of the air is HIGHER, and consequently the risk of surface condensation rises if...

factor

-
1. The moisture content of the external air is higher: marine climate
 2. The moisture production inside is higher: more intense

- occupation, specific moisture sources (laundry drying, many plants, moist walls due to rising damp...)
3. The dwelling is less ventilated: airtight dwellings, bad ventilation habits or possibilities...
 4. The volume of the dwelling is limited
 5. There are less condensing surfaces! (e.g. simple glazing)
-

The surface temperature is LOWER, and consequently the risk of surface condensation HIGHER if...

factor

6. The inside temperature is lower: not or almost not heated rooms
 7. The outside temperature is lower: cold weather
 8. The wall is badly insulated
 9. The room has many cold walls (limited radiative heat exchange) and/or there is not much air movement (limited convective heat exchange), e.g. behind wardrobes
 10. There is important thermal bridging
-

It is clear that all these factors are influenced either by the occupants, the dwelling or the outside climate.

Figure 4 gives a review of all the factors according to this division.

Remarks: 1. In non steady state conditions also the thermal capacity of the wall plays an important role.
2. When we are speaking about mould growth, also the nature of the finishing material must be taken into account.

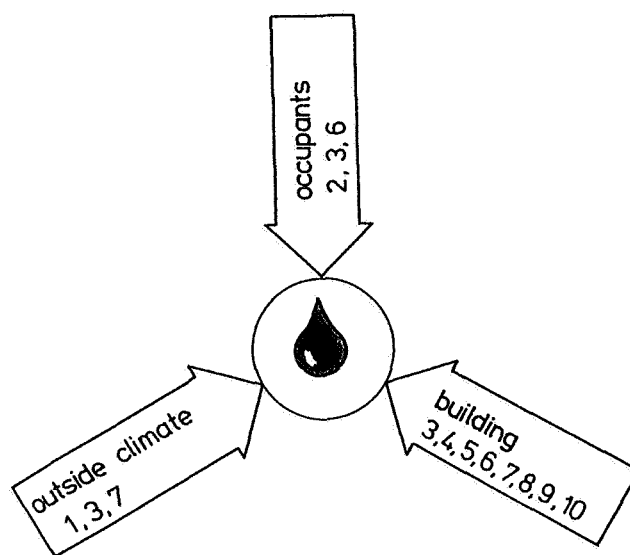


Fig.4: influencing factors

As we see in figure 4, ventilation interferes on many levels with surface condensation:

- through the occupants: ventilation habits: how much and how long which windows and which doors are opened, or in other words: how efficient do people ventilate
- through the building:
 - . implantation (terrain characteristics)
 - . efficient ventilation: position of (openable) windows and air ducts
 - . mechanical ventilation
 - . natural ventilation possibilities
 - . interroom air (and humidity) transfer
- through the outside climate: temperature/wind speed

Therefore ventilation is an important tool in combating surface condensation; but it is not the only one. Figure 5 overviews the possible remedial measures.

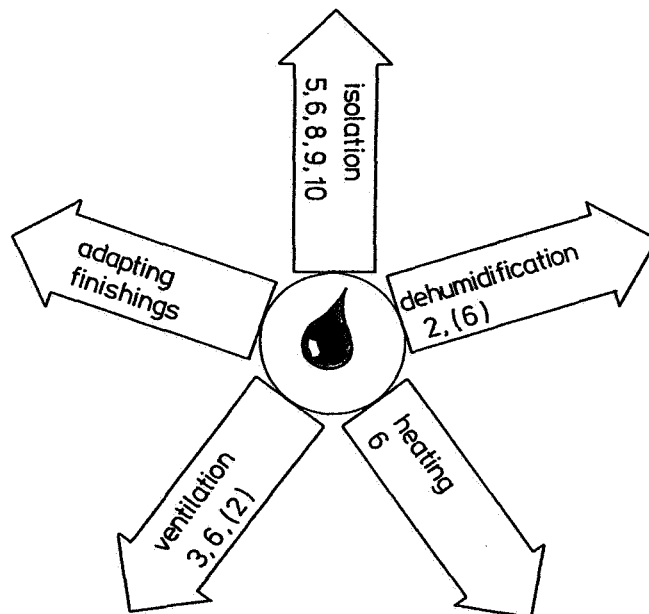


fig.5: remedial measures

The solution in a specific case will mostly be a combination of these measures.

In case of ventilation for example the dewpoint drops when ventilation is increased. However, if heating or the insulation of the dwelling is not enhanced, the inside temperature will lower and the risk of condensation may remain.

It is the aim of the Annex to develop models as well as simple guidelines to find combinations of these factors that cure or prevent moisture problems in the economically most acceptable way.

EFFECTIVE VENTILATION

9th AIVC Conference, Gent, Belgium
12-15 September, 1988

Poster 16

**EXAMINATIONS ABOUT THE AIR HUMIDITY IN LIVED DWELLINGS
DEPENDING ON DIFFERENT AIR VENTILATION SYSTEMS
USING A NEW CHARACTERISTIC VALUE**

SCHMICKLER, FRANZ - PETER

**EBM - Energieberatung Münster Ingenieurgesellschaft mbH
R.T.Hahues - B.Telohe
Weseler Str. 593; Postfach 2560
4400 Münster
West - Germany**

1. SUMMARY

This work deals with problems of the air humidity in inhabited dwellings. A new approach is presented here which renders the definite diagnosis of humidity problems possible.

The room air humidity from two buildings with different air ventilation systems with eight dwellings each is examined. The efficiency of the different ventilation systems is presented applying the new value, the so called "standardized room air humidity".

The results can be summarized as follows:

1.) The mechanical permanently balanced ventilation has essential advantages over the natural exhaust air ventilation in buildings.

2.) Dwellings with permanently balanced ventilation show distinct advantages concerning air humidity. The values of absolute air humidity are lower in these dwellings than in dwellings with natural exhaust air.

3.) By applying the "standardized room air humidity" the problem of humidity can be shown quantitatively. It could be proved that the standardized value expresses the real situation.

4.) In dwellings with permanently balanced ventilation there is no danger of humidity problems. The average natural exhaust air in dwellings reaches dangerous limits, some of them exceed the limit considerably.

5.) A definite correlation between outdoor temperature and the standardized room air humidity has been proved.

2. INTRODUCTION

Humidity problems have more often occurred during the last years. Mostly mould grove is the consequence, which does not only look dirty but also smells foul. In most of the cases mould grove and its spurs cause diseases such as of allergies. Apart from the inhabitants, who are worried about hygienie and their health, the building sponsors and architects are more and more interested in avoiding humidity damages. Mould grove reduces the quality of living. The causes for humidity damages are numeroes and influence themselves contrarily. Often the reason cannot be fully confirmed. Therefore many cases have to be settled in court.

In the past few years this topic has often been dis-

cussed in the media. The reasons are: Allergies are frequent, houses become tighter and tighter and the awareness for environmental problems is increasing.

3. INTRODUCTORY REMARKS ABOUT INDOOR AIR HUMIDITY

First it has to be mentioned that humidity damages being caused by long-lasting condensation processes on surfaces are described in this report. Apart from condensation there are many damages caused by leaks. In most of the cases these can be repaired easily. The condensation humidity causes damages which are long lasting and which can hardly be repaired.

First it will be shown which factors influence the condensation on the wall surface. One has to differentiate between structural statics and constructive influential factors and the user behaviour.

In Germany the building cover has to be build in accordance with many rules. For example, DIN 4108 /1/ prescribes the insulation of a building. By this it is made sure that the inner wall surface temperature does not lead to condensation under normal circumstances. However this is actually much more difficult because there are heat bridges, constructive errors and other characteristics of the respective building. Critical surface temperatures are seldom found on the plane wall, but mostly in corners (geometrically caused higher k-value) and on window surfaces (higher k-value as compared with a plane wall).

The user also exerts a certain influence on the humidity condensation. The daily life in a dwelling causes a lot of humidity: Washing, cooking, cleaning, man himself, animals and plants are humidity producers. In a dwelling humidity would increase continually if natural ventilation did not diminish it. A much smaller amount is absorbed in the upper wall surface.

In the past dwellings have often been so untight that natural ventilation carried away all humidity. The exchange of the old untight windows for new energy saving ones with double sealing makes these dwellings absolutely airtight. A sufficient ventilation of these dwellings is only possible by opening the windows. This way of ventilation, however, is "uncontrolled" and wastes energy.

Thus it is reasonable to install ventilation systems in modern buildings. These systems guarantee "controlled" exhaust and supply of air. Furthermore it is possible to regenerate the high energy of the exhaust air and to add it to the fresh air again.

4. THE RESEARCH PROJECT

The results presented here were gained during a research project /4/, in which dwellings with different ventilation systems were compared. All dwellings had the same groundfloor plan and were inhabited except for one research dwelling. The research dwelling was not inhabited and served as reference.

Some dwellings are ventilated and exhausted mechanically, some are ventilated conventionally. Figure 1 shows the groundfloor plan of each dwelling.

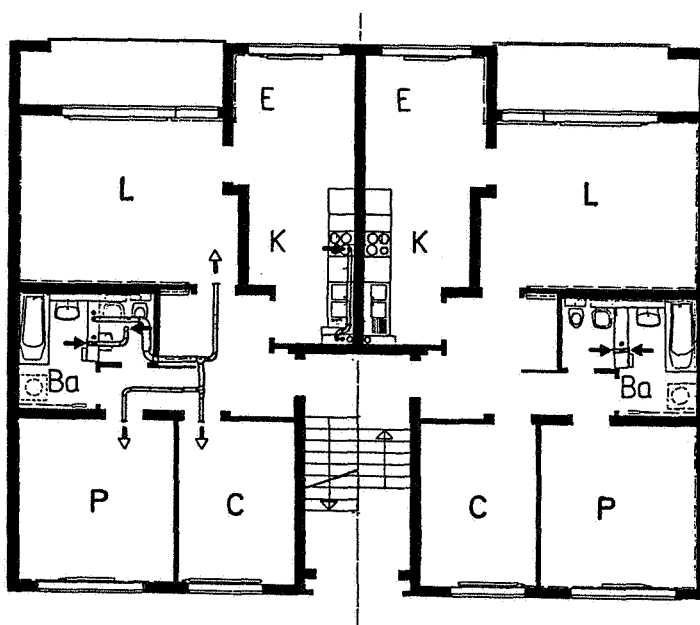


Fig. 1: Groundfloor plan. On the left hand: mechanical ventilation system. On the right hand: balanced ventilation

In Germany rule DIN 18017 /2/ requires that inner rooms without windows have to be ventilated. In rented flats mostly a simple shaft ventilation is installed, the so-called "Kölner Lüftung" /2/. Some of the dwellings of the research project are equipped with this system (here called conventional or natural ventilation).

The other dwellings have a mechanical system of ventilation. The air is exhausted in the inner rooms, toilet, bathroom and kitchen, there humidity and smell are very prominent. The fresh air is warmed up and led to the livingroom, children's room and bedroom. The hall serves as the zone of overflowing.

Fresh and exhausted air are led separately. The central unit is equipped with a recuperative heat exchanger where the energy of the exhaust air warms up the fresh air. Both streams of air are not mixed. The fresh air is entirely outdoor air. This system can be made more efficient by using an heat pump, but this will not be discussed here.

Temperature and air humidity are continually measured and registrated in all rooms, in the exhaust and fresh air as well as in weather station outside the building. Based on the number of dwellings, one can say that the statements made are realistic.

5. THE STANDARDIZED ROOM AIR HUMIDITY - A NEW VALUE

The measured results of these dwellings at first did not allow definite statements. Therefore the author introduced a new value - the so-called standardized room air humidity. The until today mainly used value - the relative air humidity - only describes the air condition based on a certain temperature at a certain place. The relative air humidity is a generally used value, but it cannot be applied when comparing different flats.

The absolute air humidity directly shows the amount of humidity in a room, but it does not include the dew-point. The standardized air humidity X avoids these disadvantages and makes it possible to show the influence of outdoor humidity.

The value is defined as follwos:

$$X = \frac{x_i - x_a}{x_{sio} - x_a}$$

x_i absolute indoor air humidity

x_a absolute outdoor air humidity

x_{sio} absolute saturation of dew humidity on an inner surface

6. RESULTS OF THE STUDY

With the help of the presented definition the standar-dized room air humidity can be calculated, if the unfavourable wall surface is known. For the following examinations the window surface was chosen for calculating the dewpoint humidity because the k-value of the windows have a lower value as the walls of the research building. The results are gained for each dwelling and

presented in the following graphs as day mean values. Two different forms of presentation are chosen. The first form shows the results chronologically during the year. In a second form the values are presented according to the outdoor temperature.

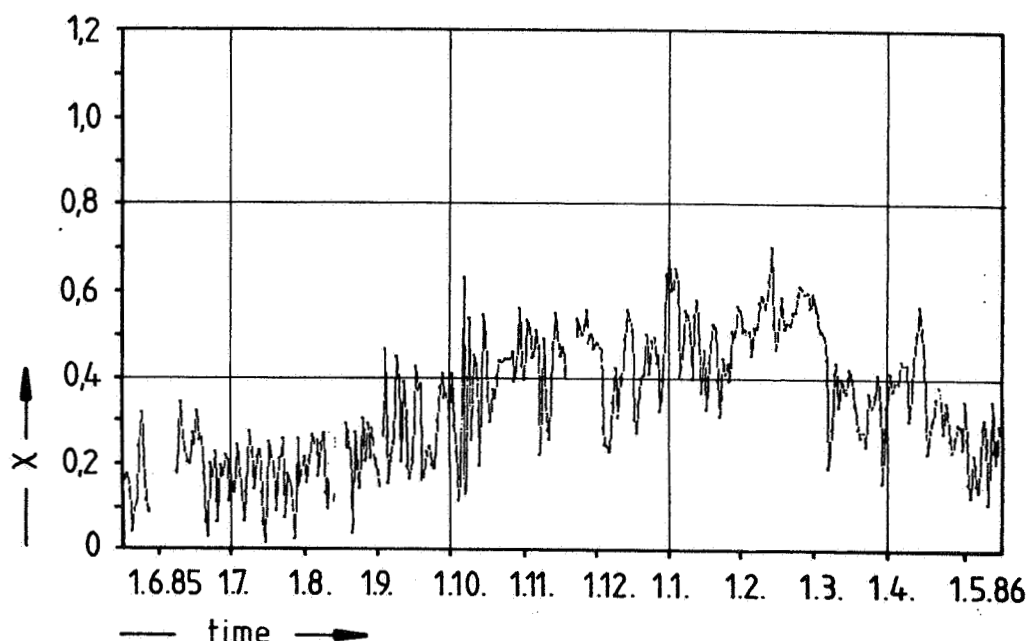


Fig. 2: The standardized air humidity during the year

Figure 2 shows the typical course of the standardized air humidity of an inhabited dwelling with mechanical ventilation during the year. By this figure the possible values of the standardized air humidity are shown. X-values between 0.5 and 0.8 suggest normal use of the flat. X-values higher than 1 imply that the dew-point on this surface is exceeded. Values lower than 0.5 indicate that humidity is hardly produced, or, that efficient ventilation has exhausted the produced humidity.

Figure 3 presents the comparison of the different dwellings and ventilation systems. The values are plotted over the outdoor temperature. The results can be marked by straight lines being highly accurate (see /3/).

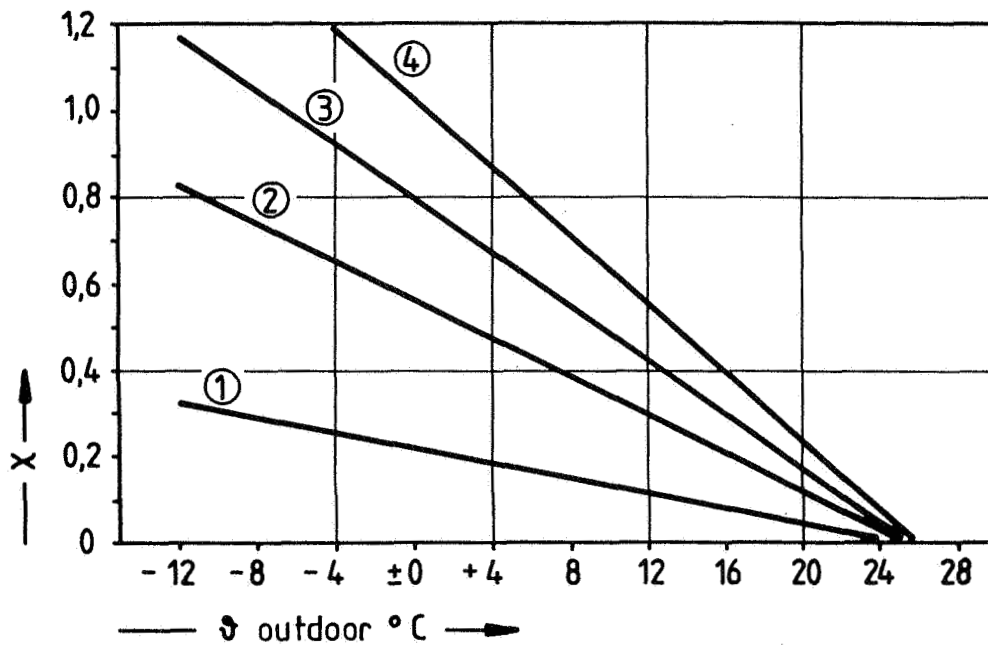


Fig. 3: The standardized room air humidity depending on the outdoor temperature with different ventilation systems (Presentation by equalized straight lines)

- 1 uninhabited research dwelling
- 2 mean value of 6 mechanically ventilated dwellings
- 3 mean value of 8 naturally ventilated dwellings
- 4 maximum value of a naturally ventilated dwellings

7. CONCLUSIONS

The following statements can be deduced from figure 3:

- 1.) In all graphs (including the ones not given here) a linear relationship between the standardized air humidity X and the outdoor temperature can be detected.
- 2.) There is no tendency to greater humidity problems during the transitional period. This would become obvious by bending the straight lines at outdoor temperatures of 4 to 12 °C.
- 3.) The source of all straight lines, i.e. the value $X = 0$ and thus $x_i = x_a$, lies at $t = 25$ °C. This effect is independent from different ventilation systems and an indication for window ventilation in summertime. My own observations during high outdoor temperatures confirm

this theory. The opening of windows increases the air change ratio considerably, by this inner and outdoor air humidity are balanced immediately.

4.) The maximum values of the standardized air humidity are reached during low outdoor temperatures. Primarily they depend on the different ventilation systems, than on the behaviour of the user. In dwellings with mechanical ventilation systems there are no humidity problems to be expected. In all natural ventilated dwellings, however, critical values are reached during lower temperatures. A few dwellings have X-values over 1 which means that humidity problems are to be expected. When visiting these dwellings, humidity damages have been found.

8. LITERATUR

- /1/ DIN 4108 (1981): Wärmeschutz im Hochbau
(Teil 1 - 4)
- /2/ DIN 18017: Lüftung von Bädern und Spülaborten ohne Außenfenster, Blatt 1 - 4
- /3/ Schmickler, F.-P.: Untersuchungen über die Luftfeuchte von Wohnungen in Abhängigkeit von unterschiedlichen Lüftungssystemen unter Verwendung einer neuen Kennzahl, Dissertation Universität Dortmund, 1987
- /4/ Trümper, H.; Hain K.; Schmickler, F.-P.; et.al.: Verschiedene Forschungsberichte, Demonstrationsvorhaben Duisburg, BMFT Bonn (Hrsg.)

EFFECTIVE VENTILATION

9th AIVC Conference, Gent, Belgium
12-15 September, 1988

Poster 17

FIELD EXPERIENCES OF AIRBORNE MOISTURE TRANSFER IN RESIDENTIAL
BUILDINGS

J. OLDENGARM

TNO Institute of Applied Physics
(Technisch Physische Dienst TNO-TH)
P.O. Box 155
2600 AD Delft
The Netherlands

SYNOPSIS

This paper deals with field experience of airborne moisture transfer problems in houses. Two types of phenomena are discussed in more detail: the infiltration of moist air from crawl spaces and the propagation of moist air produced in kitchens. A modified depressurisation test is described to determine the air tightness of ground floors. A case study is briefly discussed where different remedial measures have been tested to evaluate the moisture removal effectiveness in kitchens. A multi-channel dewpoint measurement system has been used to determine the ventilation efficiency experimentally.

1. INTRODUCTION

During the last few years we experienced a growing interest for moisture problems in houses. In many cases we were involved in investigations requested by building owners. The surveys we carried out were very practical and were directed to the determination of the cause of the problems and the solution for remedial actions.

The most common type of moisture problem is mould growth on wall surfaces and furniture, caused by surface condensation. Although the mechanism of surface condensation is fairly well understood, it is not easy to establish adequate proposals for cost-effective remedial actions. Surface condensation and the associated mould growth can be generated by a complex interaction of different factors, such as:

- low thermal quality of the building envelope (e.g. thermal bridges);
- insufficient ventilation;
- excessive moisture sources.

In addition to these the behaviour of the occupants may play a crucial role.

In a number of field surveys we were able to study the moisture balance in houses in more detail. In some cases the special interest was directed to airborne moisture transfer. Two distinct moisture sources are of particular importance when considering airborne moisture transfer:

- infiltration of moist air from spaces under suspended floors (in many countries denoted as crawl spaces) to living areas;
- moist air originating from water vapour producing activities in kitchens.

In this paper we will present some field experience related to these two items.

2. MULTI-CHANNEL DEWPOINT MEASUREMENT SYSTEM

The multi-channel dewpoint measurement system proved to be a very

powerful instrument to study airborne moisture transfer. The principle of the system is outlined in figure 1. The system has been developed at our institute and it has been used in several case studies.

An important feature of the dewpoint measurement system is its ability to detect accurately small differences of vapour concentration between two locations. Because a single sensor is used for all measuring locations, an accuracy of 0.05 g/kg is achieved when measuring the instantaneous difference in vapour concentrations at different points. In general vapour concentration gradients in a single room are very small and can be detected only by a system as described above.

3. AIRBORNE MOISTURE TRANSFER FROM CRAWL SPACES

Crawl spaces below the ground floor are very common in the Netherlands. In a large part of the country it is also common to find the ground water level only a few centimeters below the crawl space bottom surface and in some regions an open water surface is present during a large period of the year. Hence, it is not surprising to find high humidity levels in crawl spaces. A relative humidity of $RH = 95\%$ is quite normal. Figure 2 shows the dynamic behaviour of the vapour concentration in crawl spaces as calculated by a computer model. It demonstrates that particularly in the winter period the excess vapour concentration will be high. It is believed that many mould problems in Dutch houses are related to moisture transport from crawl spaces. Field studies have shown that infiltration of moist air through air leakages in the ground floor construction is the most important mechanism. A simple calculation here might demonstrate the potential risks. During the winter period the excess water vapour concentration in crawl spaces can exceed 5 g/m^3 (with respect to outdoor air). Due to the stack effect the crawl space has always an overpressure with respect to the living space. For a typical overpressure of 3 Pa and a relatively small air leakage area of $5 \times 5 \text{ cm}^2$ the airborne moisture contribution to living area will be about 2.5 kg moisture per 24 hours. From field experiences we know, however, that air leakages in ground floors very often are larger than the 25 cm^2 used in the example.

3.1 Air tightness of ground floor constructions

In the past little attention was paid to the air tightness of ground floors. In the near future new building regulations will be established, in which requirements will be stated for a certain level of air tightness of ground floor constructions. Hence, test methods will be needed to determine the level of air tightness. Conventional pressurisation techniques are not applicable for ground floors.

Therefore, we developed a modified depressurisation test that is enable to measure the air tightness of ground floors. The principle of this test method is outlined in figure 3. The method

is based on the measurement of the increasing vapour concentration due to the infiltration of moist air through the ground floor during depressurisation.

4. MOISTURE IN KITCHENS

The household activities in the kitchen lead to the most important moisture source in houses. Due to cooking and dish washing an amount of 1 to 4 kg moisture per day can be produced. In properly ventilated kitchens, which are separated from the rest of the house, no problems will occur. However, in practical situations kitchen moisture can easily move to other rooms. This is in particular true in cases where the kitchen is in open connection to other zones.

4.1 A case study

We studied airborne moisture in a case study requested by a building owner. The measurements were made in an occupied house from a stock of 150 single family terraced houses. A high percentage of these houses suffered from mould problems. From an introductory survey it was concluded that ineffective moisture removal from the kitchen was a major point. The kitchen in these houses is in open connection with the living room. An exhaust opening connected to a mechanical ventilation system was present as outlined in figure 4.

A test house was selected in which several remedial measures were tested. With respect to airborne moisture problems the following experiments were accomplished (see figure 5):

1. Replacement of the flueless gas-fired DHW-supply (Domestic Hot Water) by a closed system.
2. Installation of a fume hood exhaust connected to the mechanical ventilation system.
3. Installation of a vapour shield to reduce the moisture transfer from the kitchen.
4. Improvement of the ventilation balance and the fresh air supply.

4.2 Moisture removal effectiveness

During these tests the moisture removal effectiveness was evaluated using the dewpoint measurement system described before. A commonly used figure of merit is the coefficient for the ventilation efficiency. In the case of moisture control the following definition could be used:

$$E = \frac{C_x - C_e}{C_i - C_e}$$

where:

E = the moisture removal effectiveness;

C_x = the water vapour concentration measured at the ventilation exhaust;

C_e = the water vapour concentration measured outdoor;

C_i = the water vapour concentration measured indoor at a relevant location.

For the case of a complete mixing of the moisture source with indoor air the effectiveness will be $E = 1$ (because $C_x = C_i$). In unfavourable conditions the coefficient may take value lower than $E = 1$. This occurs for example if "short circuiting" occurs between the fresh air supply and the exhaust opening (which will result in $C_x < C_i$). For situations where source ventilation is applied (e.g. using a fume hood exhaust) the value for E should be larger than 1 (the goal should be $C_x \gg C_i$).

The definition for the ventilation efficiency as introduced before proved not to be very practical for our purpose. Variations in the outdoor humidity and moisture storage effects have a strong influence when determining the ratio E on the basis of vapour concentration measurements.

For our purpose we found that the effectiveness of moisture removal can be better evaluated by a figure of merit expressed by the following formula:

$$E = \frac{C_x - C_{ia}}{C_i - C_{ia}}$$

where C_{ia} is long term average (a 24 hour period is recommended) of the indoor vapour concentration. From a view point of moisture control this proved to be a useful figure of merit for the effectiveness of moisture removal.

4.3 Results and conclusions

To illustrate the moisture behaviour in the test house two 24-hour records of vapour concentration measurements shown in figure 6. These records show that vapour concentration gradients exist only during and after moisture producing activities. A surprising conclusion is that during nighttime an almost perfect equilibrium seems to be settled: all locations show exactly the same vapour concentration. Other conclusions from this case study associated with airborne moisture transfer problems were:

- Flueless gas heaters give rise to an important contribution to the moisture load (1 to 2 kg moisture per day).
- A ventilation scheme that uses a single exhaust opening is not very effective with respect to moisture removal in kitchens. Measurements have shown that complete mixing occurs and as a result of this humid air is propagated to other zones in the house.

- The installation of a vapour shield has very little impact on the moisture removal effectiveness. The effect is noticeable during moisture production peaks but the overall result is not significant with respect to the reduction of condensation risks.
- As expected the installation of a fume hood improves the moisture removal effectiveness, but not at a quite satisfactory level. Only 20% of the moisture produced in the kitchen is removed by source ventilation. Inadequate behaviour of the occupants with respect to the use of the fume hood and the opening of windows was found to be an important reason.
- By routine the occupants opened a window in the kitchen area during the household activities. In contrast to the anticipation of the occupants the effect on moisture removal appeared to be negative. Suggestions to open a window at the opposite façade resulted in air draught complaints.

DISCUSSION AND CONCLUSIONS

The paper discusses two types of airborne moisture transfer problems:

1. Infiltration of moist air from crawl space,
2. Moisture propagation from kitchens to other zones.

The crawl space problem can be solved by creating a sufficient air tight ground floor construction. Test methods are needed to evaluate the air tightness of ground floors. A feasible technique is described in this paper.

Moisture control in kitchens seems to be more difficult to handle, in particular when kitchens are in open connection with other zones. In new built houses balanced ventilation might be a satisfactory solution. In existing houses the moisture removal effectiveness from kitchens will highly rely on the use of the ventilation provisions by the occupants.

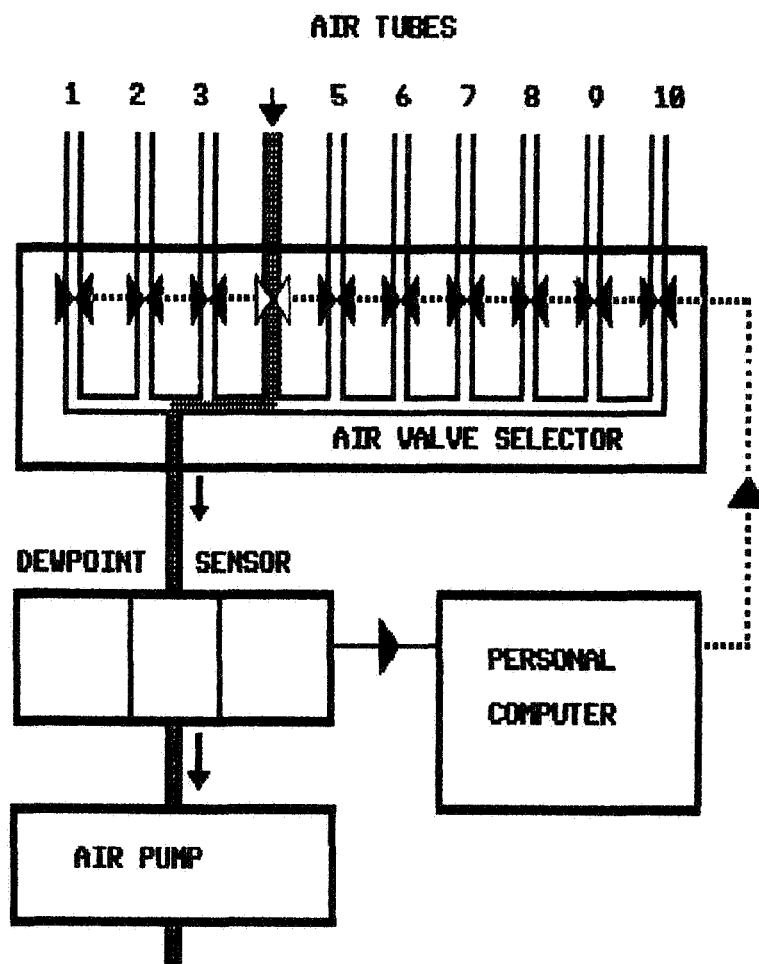


Figure 1: The multi-channel dew point measurement system.

This system is used in field studies on airborne moisture transfer for the monitoring of indoor and outdoor air humidities. The operating principle is based on the measurement of the dew point temperature in air samples extracted through small air tubes from different locations in the house. The air valves in the selector box are controlled by a computer programme. The measuring locations are scanned within a few minutes, depending on the length of the air tubes. The computer also computes the water vapour concentration from the dew point temperature data (equivalent denotations are "air humidity by mass [g/kg]" or "air humidity" by volume [g/m³]).

AIR HUMIDITY
[g/m³]

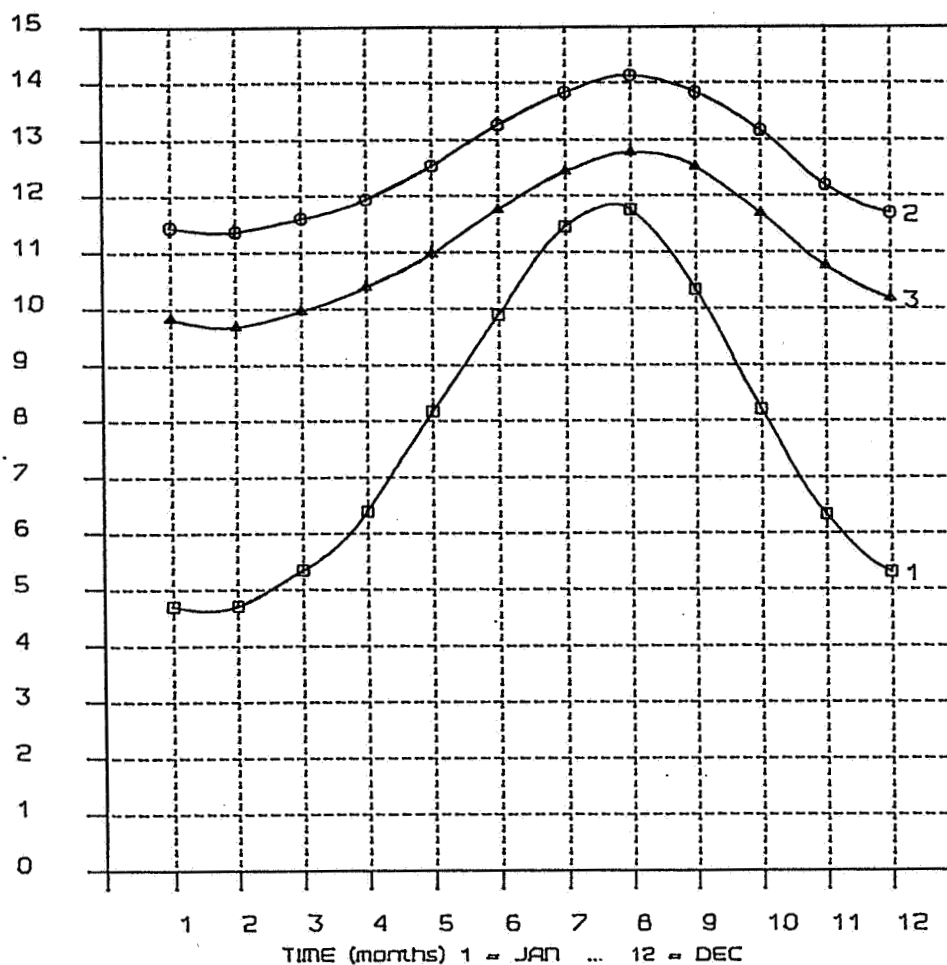


Figure 2: Water vapour concentration in crawl spaces.

- 1: Outdoor air.
- 2: Air humidity in a crawl space without any insulation in the ground floor.
- 3: Air humidity in a crawl space where the ground floor is provided with a 5 cm insulation layer.

The curves are computed by TH3DR, a dynamic thermal model based on combination of heat and moisture balances.

$$\text{AIR LEAKAGE RATIO : } \frac{Q_k}{Q_t} = \frac{\Delta C_i}{C_k - C_e}$$

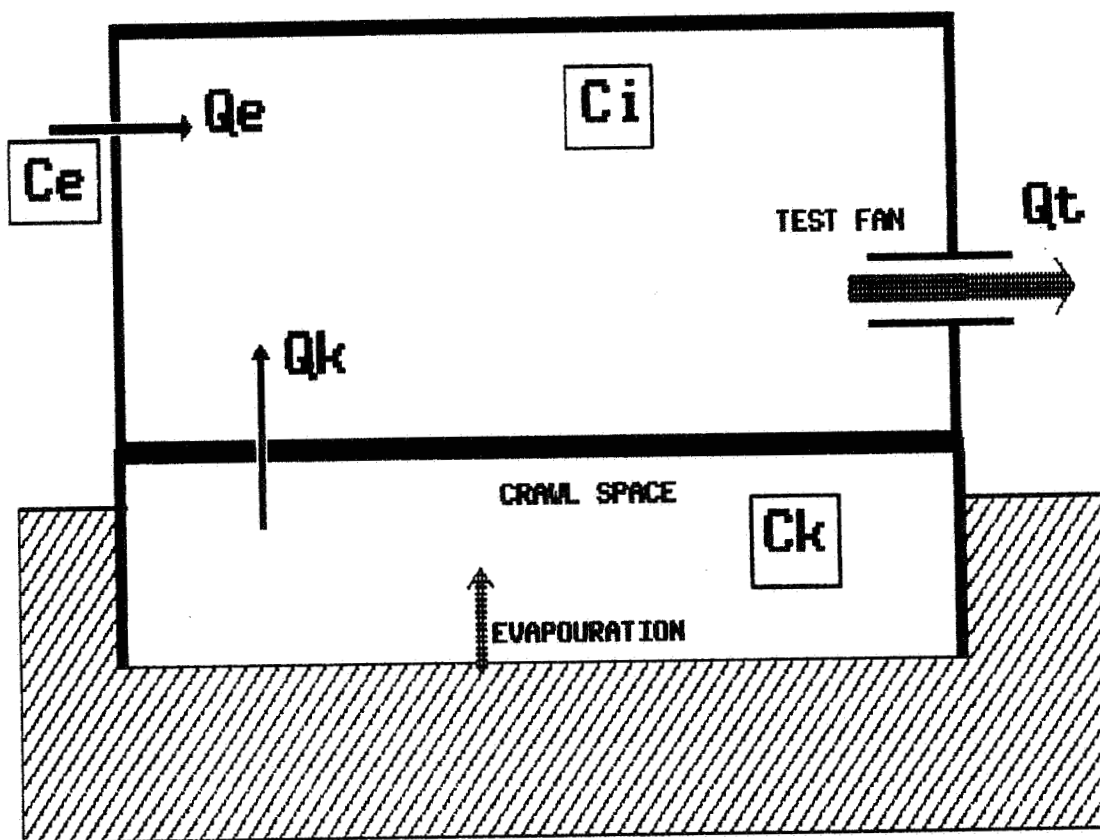


Figure 3: Air tightness of ground floors.

Depressurisation method to test the air tightness of ground floors above humid crawl spaces. In addition to the conventional "blower door test" the dew point system from figure 1 is employed to detect the infiltration of moist air. The air leakage ratio is determined from vapour concentration measurements as shown above.

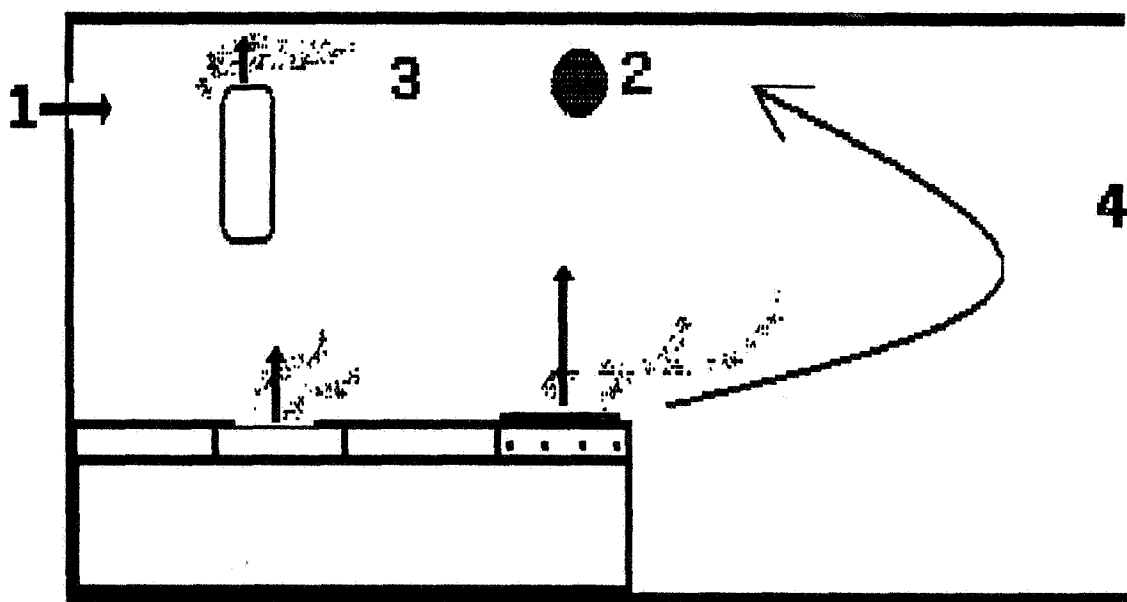


Figure 4: Airborne moisture transfer in kitchens.

View of the kitchen zone in the test house. The locations for the vapour concentration measurements are shown:

- 1: Outdoor air (C_e).
- 2: Ventilation exhaust (C_x).
- 3: Kitchen area.
- 4: Living room zone at 6 m distance from location 1 (C_i).

Humidity measurement data from these locations have been used to evaluate the moisture removal effectiveness E .

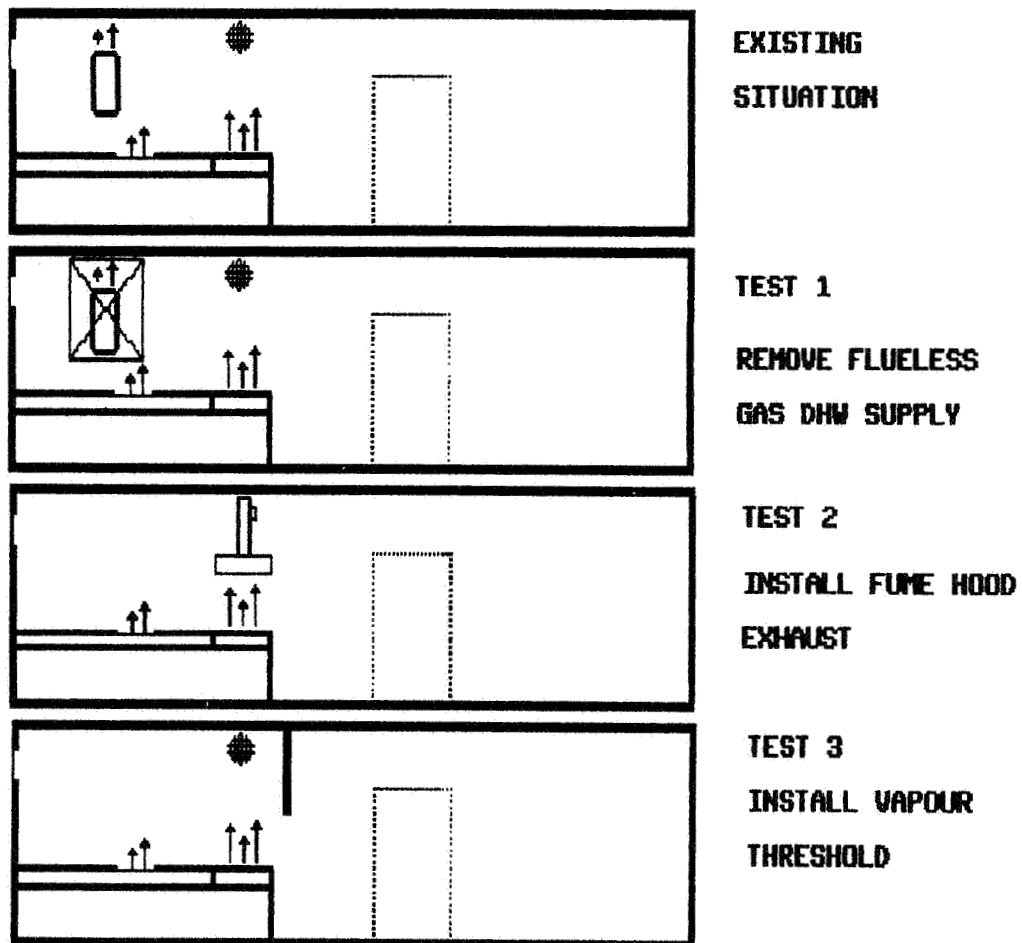


Figure 5: Remedial actions.

Schematic view of the remedial actions to improve the moisture removal effectiveness.

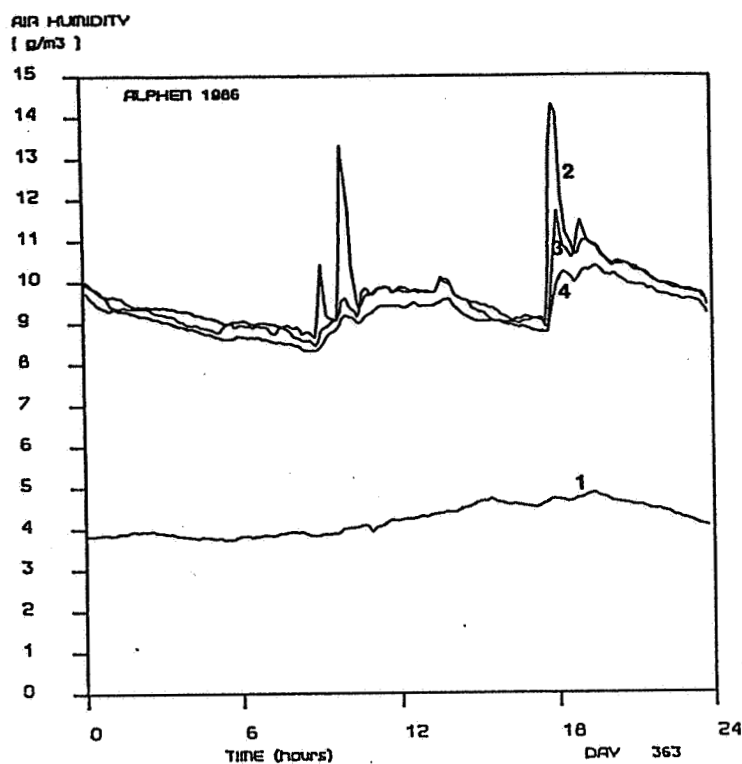
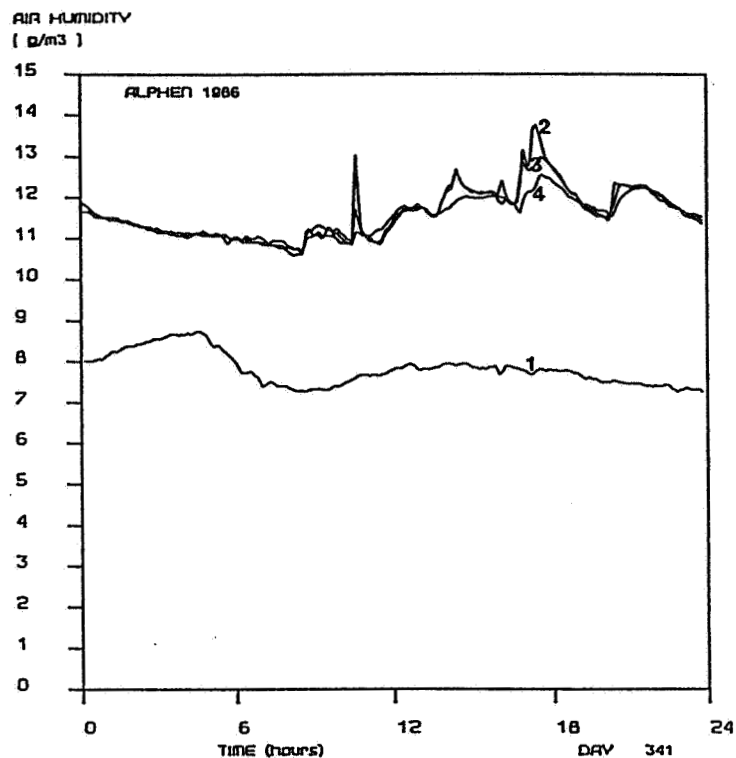


Figure 6: Airborne moisture propagation from kitchens.

Recorded vapour concentrations in the test house for two cases:
a. Reference situation (above), b. Fume hood installed (below).

- 1: Outdoor air.
- 2: Ventilation exhaust opening.
- 3: Kitchen zone.
- 4: Living room at 6 m distance from location 1.

EFFECTIVE VENTILATION

9th AIVC Conference, Gent, Belgium
12-15 September, 1988

Poster 18

VENTILATION HABITS IN RESIDENTIAL BUILDINGS

HANS ERHORN

Fraunhofer-Institut für Bauphysik
(Bereich Wärme/Klima)
(Dir.: Prof. Dr.-Ing. habil. K.A. Gertis)
P.O.B. 80 04 69
D-7000 Stuttgart 80 (W. Germany)

0. SYNOPSIS

Experimental investigations concerning energy savings achieved in buildings with passive solar components (e.g. large south-front windows, sunspaces or Trombe walls) have already been effected under test conditions. Since, however, the influence of occupants' behaviour on energy consumption was generally found to be a very strong one, the main purpose of the present project was to analyze inhabitants' acceptance and use of various components like shading devices, movable heat insulation, manual ventilation, room temperatures, and heating systems. The study is based on extensive measurements performed on 25 occupied single-family houses in Germany. Results concerning the influence of occupants' behaviour will be given.

1. OBJECTIVES

There are still many possibilities to cut down on energy consumption, both in modernizing old buildings and in constructing new ones. In the long run, the heating energy demand for dwellings in the Fed. Rep. of Germany could be reduced to less than a third of today's consumption by consequently applying all of the advanced building concepts and technologies presently available which to date have only been applied with hesitation. It was for these reasons that the German Federal Ministry for Research and Technology decided to give an actual demonstration of the practical implementation by funding the present pilot project.

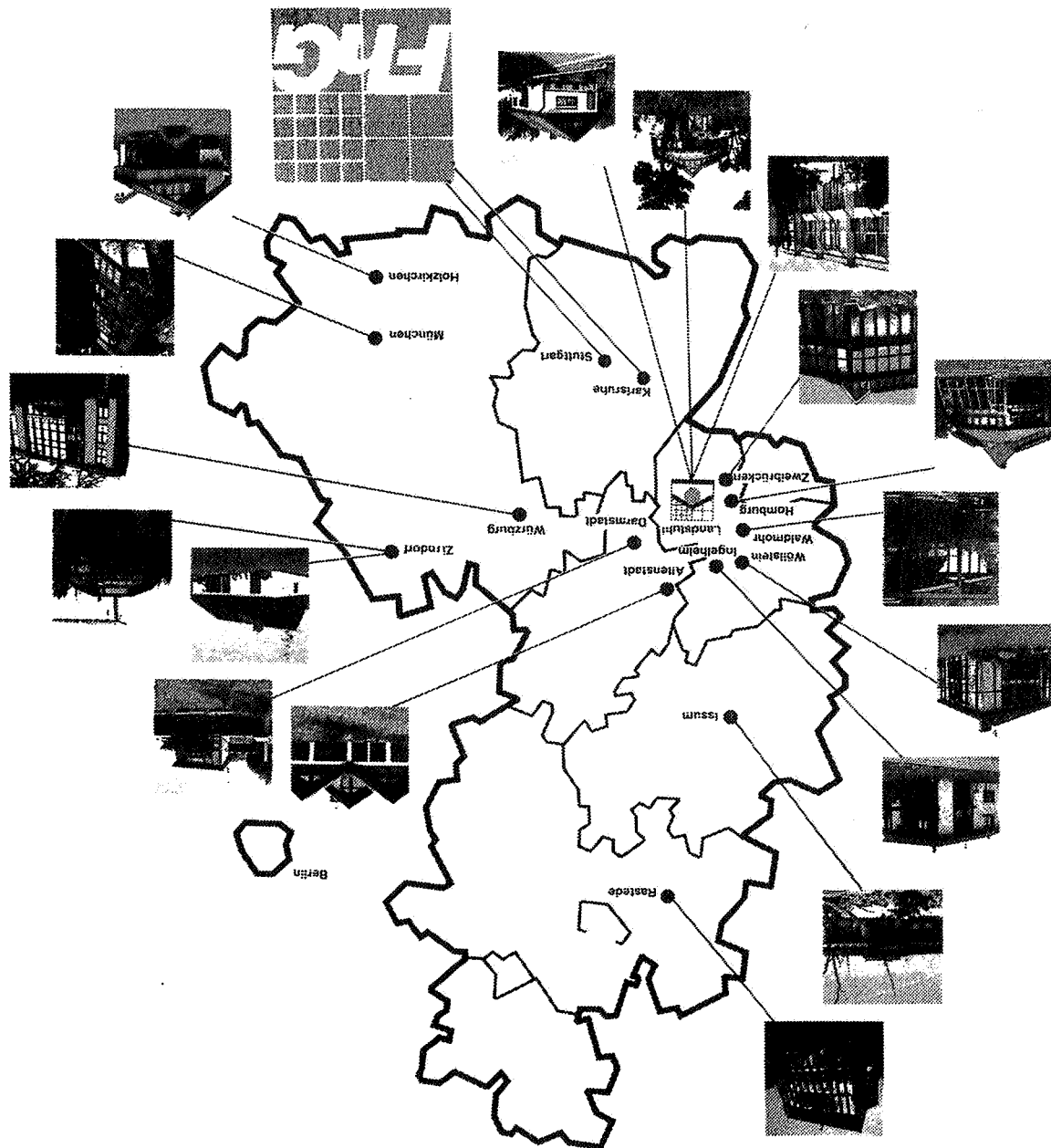
The demonstration project is aimed at:

- implementing promising solutions for single-family dwellings with low heating energy demand
- proving functionality, efficiency and economical feasibility of the new technologies and building concepts
- pointing out inherent technical problems and contributing to their elimination.

2. SCOPE OF THE PROJECT

In Fig. 1 views and locations of the buildings included in the study are given. At Landstuhl, eight buildings with the same floor plan (namely, that of House no. 8) were measured. In all of the 25 buildings various concepts of low-energy construction methods were realized. Most of the buildings have an excellent thermal insulation.

Fig. 1 Views and locations of the buildings included in the study (numbers are related to project participants)



All houses were occupied and provided with a sophisticated measuring equipment. Figure 2 gives a survey of all the values that were continuously recorded for each house. There were also discontinuous tracer gas measurements.

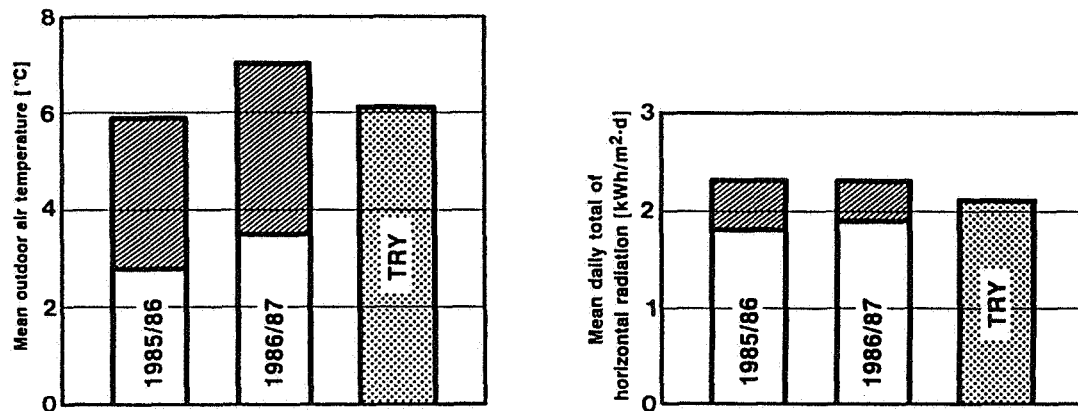


Fig. 2 Measured mean outdoor temperatures and daily totals of global solar radiation during 1985/86 and 1986/87 heating seasons as compared to Test Reference Year (TRY) values for average German climate conditions. The shaded area indicates the range of variation between the building sites.

3. METEOROLOGICAL BOUNDARY CONDITIONS

As the buildings under survey are located in different places all over West Germany, a detailed analysis of climate parameters had to be conducted in order to include also climate-induced effects in the final comparison. Figure 3 presents the mean values of outdoor temperatures and the daily totals of horizontal global solar radiation recorded during the 1985/86 and 1986/87 heating cycles. The shaded area indicates the range of variations between the locations. For comparison, long-term TRY mean values for average German climate conditions are given.

- During both heating cycles, average temperatures fell below Test Reference Year values. The first heating period was the colder one. The differences stated between the locations are significant.
- The mean variation in global solar radiation is low for different locations. On average, it was found not to vary from TRY values.

Measured values

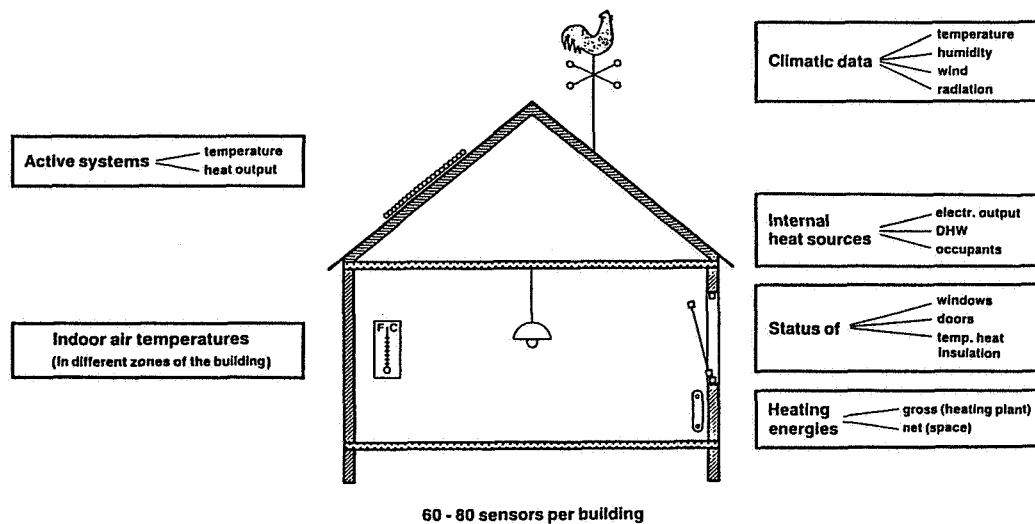


Fig. 3 Instrumentation of the 25 buildings under survey.

4. RESULTS OF THE MEASUREMENT AND INVESTIGATION PROGRAMME

4.1 Investigations concerning occupant behaviour

Among the 25 buildings under survey, 11 buildings were equipped with conventional hot water heating systems (radiators, floor heating) and 14 with warm air heating systems. All of the air heating systems were operated with a partial supply of fresh air; the respective supply rates were at variance. In the following, user-related criteria will be examined separately for the buildings with hot water heating and for those with air heating systems.

4.2 Indoor air temperatures

During the entire monitoring period, all indoor air temperatures were recorded hourly. In Fig. 4 the measured indoor air temperatures are contrasted with the corresponding outdoor air temperatures. The measured values are indicated in the hatched areas. It becomes evident that indoor air temperatures decrease with decreasing outdoor air temperatures. Obviously, there is a tendency for the occupants to accept lower indoor air temperatures more

readily when outside temperatures are low, too, which seems to be a deviation from user patterns during interseasonal heating periods. This tendency proved to be independent of the selected type of heating system. The fluctuation of indoor air temperatures is about the same for all heating systems under study which allows the conclusion that the type of heating system has no part in the user's selection of temperature. User-specified variations in indoor air temperatures are ranging between 4 and 5 K.

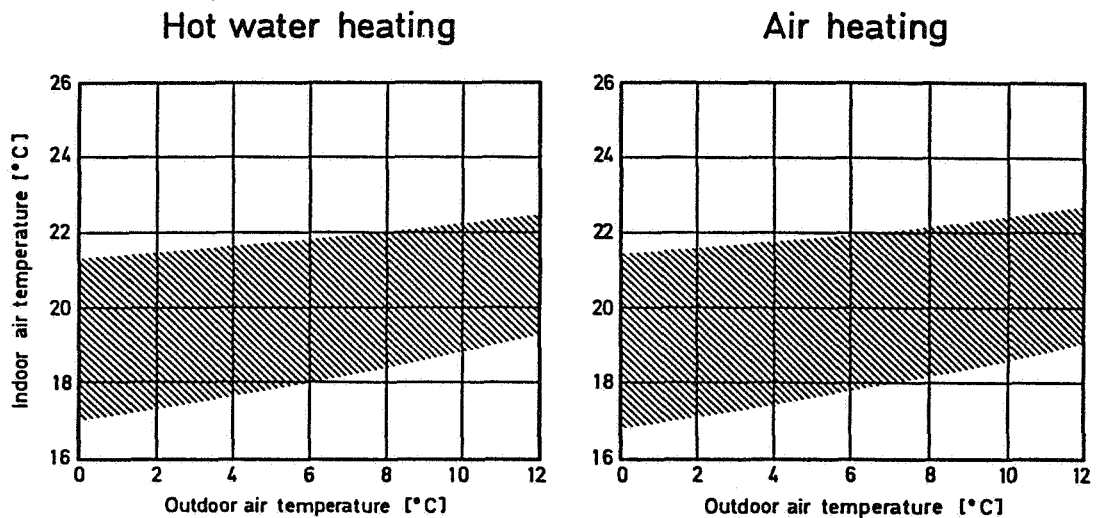


Fig. 4 Measured indoor air temperatures versus outdoor air temperatures for the surveyed buildings with hot water and air heating systems. The range of measured values is hatched.

4.3 Inhabitants' behaviour with regard to opening windows

User patterns that bear relevance to a building's energy performance may not only be described by recording indoor air temperatures but also by examining the occupants' habits and preferences with regard to ventilation. In residential buildings, the occupants' ventilation strategies are characterized by the duration of leaving windows open. In Fig. 5 the measured duration of window ventilation versus outdoor air temperatures is given separately for the buildings with hot water heating and for those with air heating systems. Obviously, the windows were opened significantly less frequently in low outdoor air temperatures than in milder outside air temperatures. While the windows were opened on average for only 2 minutes per hour in low outdoor air temperatures, they were kept open for about 10 minutes on average per hour in milder weather.

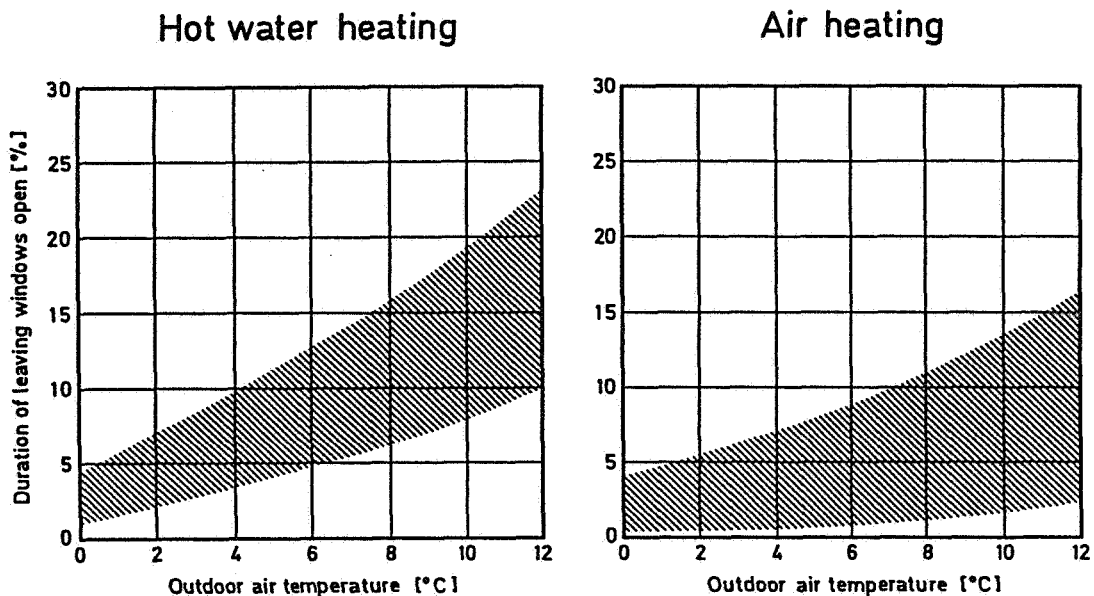


Fig. 5 Measured duration of window ventilation versus outdoor air temperatures for the surveyed buildings with hot water and air heating systems. The range of measured values is hatched.

Considering the duration of window ventilation, pronounced variations are to be observed which are associated with different types of heating systems. In the buildings equipped with hot water heating systems, windows were on average kept open longer than in air-heated buildings, particularly in mild weather. Actually, this tendency was to be expected, since all of the air heating systems were operated with a partial fresh-air supply, i.e. the required air change was already provided via the heating system.

In air-heated dwellings, too, there is a tendency to be observed towards opening windows when outdoor temperatures are rising which may be attributed to psychological rather than physical reasons. In future, this finding which has already been established in [1] for multi-family housing must not be disregarded when planning buildings and installations. As a general rule, windows in residential buildings should be openable and have defined degrees of airtightness when closed. When calculating rates of efficiency and potentials for saving energy by using mechanical ventilation systems in the housing sector, the user-specified "basal air change" resulting from opening windows should always be borne in mind.

When comparing these user habits to those already stated in [1] for multi-family dwellings, occupants of multi-family dwellings are found to open their windows more frequently than occupants of single-family houses (see Fig. 6). This is probably not so much a matter of distinct ventilation strategies characteristic of multi-storey buildings but rather due to the varied number and size of windows depending on the type of construction. This is

why a direct comparison of results is not possible.

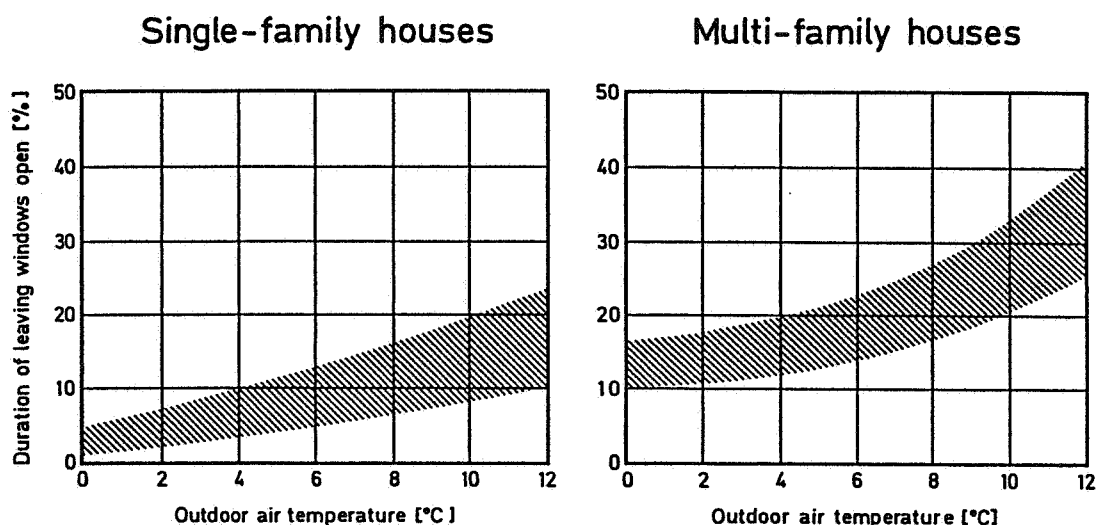


Fig. 6 Measured duration of window ventilation versus outdoor air temperatures for single-family and multi-family buildings acc. to [1], without mechanical ventilation. The range of measured values is hatched.

5. CONCLUSIONS

The study on the energetic performance of occupied single-family houses included monitoring of occupants' behaviour. It was found that there is no significant distinction between buildings with different heating and ventilating systems as regards temperatures. In all of the buildings under survey indoor air temperatures were found to decrease with decreasing outdoor temperatures.

As for ventilation patterns, a direct correlation between the respective type of heating and ventilating system was confirmed. In buildings with air heating systems (all of which were operated with varied portions of fresh air) windows were opened for a significantly shorter period than in buildings with hot water heating and in those without mechanical ventilation. Though, in buildings equipped with mechanical ventilation windows were never found to be absolutely locked. The present findings suggest that a minimum air change via window ventilation is a basic need irrespective of the actual indoor air quality in residential buildings. In future planning, this fact will have to be duly considered.

6. REFERENCES

- [1] Erhorn, H.: Influence of the meteorological conditions on the inhabitants' behaviour in dwellings with mechanical ventilation. Proc. 7th AIC Conference, pp. 11.1-11.15, Stratford upon Avon (1986).

EFFECTIVE VENTILATION

9th AIVC Conference, Gent, Belgium
12-15 September, 1988

Poster 19

FLOW CONDITIONS IN A MECHANICALLY VENTILATED ROOM WITH
A CONVECTIVE HEAT SOURCE

PER HEISELBERG, PETER V. NIELSEN

University of Aalborg,
Sohngårdsholmsvej 57, DK-9000 Aalborg, Denmark

SYNOPSIS

The ventilation of a test room ($L \times W \times H = 5.4 \times 3.6 \times 2.4$ m) with a wall mounted heat source is investigated for two different air terminal devices.

The properties of each air terminal device are described by measuring the velocity decay of the primary wall jet below the ceiling.

The velocity distribution in the plume above the heat source has been measured at different heat loads as a function of the distance to the wall and the distance to the heat source.

The measurements have led to an estimate of the maximum velocity in the plume and of the volume flow rate as a function of the heat load and the distance to the heat source.

In order to find the influence of the convective heat source on the flow conditions in the room, the velocity distribution in the occupied zone and the normalized concentration distribution along a vertical line through the middle of the room has been determined as a function of the specific flow rate and the heat load.

The convective heat source is found to have significant influence on the flow conditions in the room. This paper shows lower velocities in the occupied zone and a more uniform concentration distribution in the room.

1. INTRODUCTION

In many buildings mechanical ventilation is combined with convective heating and/or cooling. The purpose of the ventilation system is therefore only to supply the building with fresh air (outdoor air).

When designing the system, it is normally assumed that the room temperature is constant, that the convective source does not affect the flow conditions in the room and that the air supply is isothermal.

This paper deals with the flow conditions in a mechanically ventilated room with a convective heat source. The mean room temperature is kept constant in the experiments with ventilation and thermal load and at the same level as in the experiments without ventilation. The heat loss by ventilation is therefore always zero and not dependent on volumetric flow rate and heat load.

The paper is a continuation of the isothermal measurements given earlier by Høiselberg and Nielsen¹.

The room is placed in a laboratory hall and has the dimensions $L \times W \times H = 5.4 \times 3.6 \times 2.4$ m. Experiments are made with two different supply openings and both of them are placed close to the ceiling at one of the end walls. Two return openings are located at the other end wall 0.7 m above the floor. The heater is placed at the same wall as the supply openings with the top 0.7 m above the floor. The situation is illustrated in figure 1.

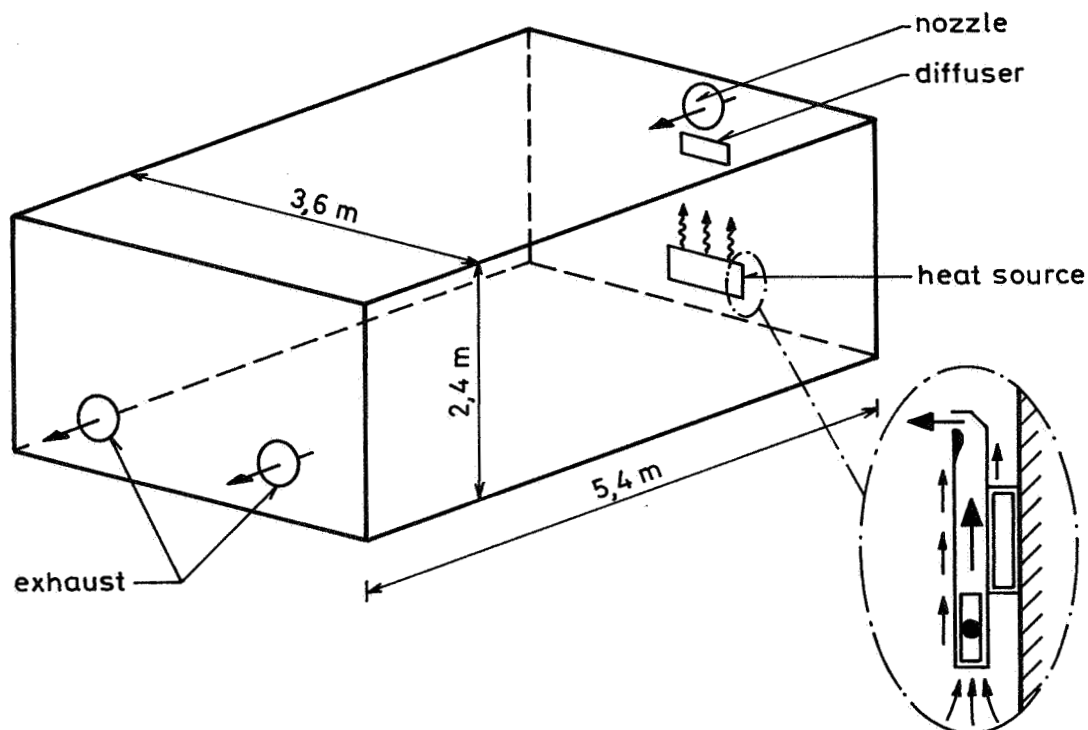


Figure 1. Location of supply-, return openings and convective heat source in the test room.

The two different supply openings are a nozzle (A) with a diameter of 132 mm and a diffuser PVD-10 (D) from STIFAB.

The convective heat source is an electrically heated radiator consisting of a heating element with fins built into a metal cabinet as shown in figure 1.

The heater is mounted on the wall. The main flow goes through the heater and leaves it horizontally from the front.

2. VELOCITY MEASUREMENTS

The velocity decay of the primary jet is measured for both air terminal devices. The result gives a good description of the properties of the air terminal devices and makes it possible to determine the maximum permissible supply velocities and volumetric flow rates based on the throw of the jets.

The velocity distribution in the middle of the hot plume is measured to find the maximum velocity and volume flow as a function of the power supplied and the distance to the heat source.

The maximum velocity of the recirculating flow is measured as a function of the volumetric flow rate and the power supply to the heat source. Applying these results and the comfort requirements by Fanger and Christensen² to the air velocity in the occupied zone, it is possible to find the maximum supply velocity or volumetric flow rate based on comfort requirements.

2.1 Wall jet conditions

For a three-dimensional wall jet the expression for the maximum velocity of the primary jet as a function of the distance to the supply opening is given by

$$\frac{V_x}{V_0} = K_a \frac{\sqrt{a_0}}{x+x_0} \quad (1)$$

The K_a -value, the effective supply area, a_0 , and the distance to virtual origin, x_0 , are found for both air terminal devices (A) and (D). The result is shown in figure 2.

AIR TERMINAL DEVICE	DISTANCE TO CEILING (m)	K_a	a_0 (10^{-3} m^2)	x_0 (m)
A	0.067	9.5	14.0	0.55
D	0.300	1.9	7.3	0.14

Figure 2. K_a -value, effective supply area, a_0 , and distance to virtual origin, x_0 , are given for both air terminal devices.

Figure 2 shows that the K_a -values differ with the factor 5. As expected, the nozzle has the highest value and the diffuser the lowest. The K_a -value for diffuser D is a typical value for a commercial diffuser design.

2.2 Air exchange at constant throw

The maximum permissible supply velocity V_o is found for each air terminal device for a throw which is equal to the room length, L , and the corresponding terminal velocity equal to 0.25 m/s. The result is shown in figure 3 together with the air supply flow rate and the specific flow rate.

The specific flow rate is defined as

$$n = \frac{q_o}{LWH} \quad (h^{-1}) \quad (2)$$

where q_o is the air supply flow rate.

AIR TERMINAL DEVICE	V_o m/s	q_o m ³ /h	n h ⁻¹
A	1.3	67	1.4
D	8.1	213	4.6

Figure 3. Maximum permissible supply velocity, air supply flow rate and specific flow rate for each air terminal device for a throw which is equal to the room length.

Figure 3 shows a significant difference between the maximum permissible volumetric flow rates for the two air terminal devices.

2.3 Convective flow above the heat source

The air velocities in the convective plume above the heat source are measured as functions of the distance from the top of the source, the distance to the wall and of the power supplied. Four distances from the heat source have been measured, namely 0.11 m, 0.70 m, 1.28 m and 1.55 m, and the power supplied to the source was 256 W/m, 513 W/m, 769 W/m and 1026 W/m, respectively.

In figure 4 the velocities are shown as functions of the distance to the wall for 4 distances from the top of the heat source and a power supply of 256 W/m.

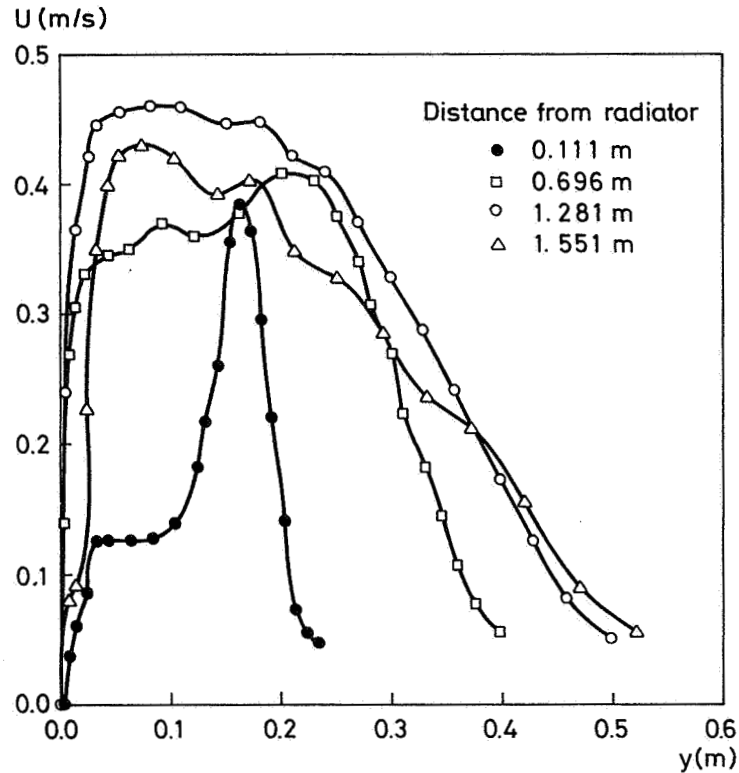


Figure 4. Air velocities in the convective plume above the heat source as functions of the distance to the wall. The measurements have been made at 4 distances from the top of the source and at a power supply of 256 W/m.

Near the heat source the velocities are low close to the wall and high over a small range about 0.15 m from the wall. This is due to the design and the mounting of the heater. The heater is placed 0.05 m from the wall and the main plume leaves the heat source horizontally at the front. Bouyance changes the flow to a vertical plume and the plume turns into a wall plume at some distance from the heat source.

The relation between the maximum velocity in the convective plume, the distance from the top of the heater and the heat load may be expressed by

$$U_{\max} = 0.085 Q_C^{0.3} y^{0.06} \text{ (m/s)} \quad (3)$$

where

Q_C is the convective heat load per length (W/m)

y is the distance from the top of the heater (m)

The volume flow in the convective plume can be calculated from the measured velocity distribution in the plume by integrating from the wall to δ , the distance where the velocity is zero. The volume flow is calculated as:

$$q_y = \ell \int_0^{\delta} U dx \quad (m^3/s) \quad (4)$$

where

q_y is the volume flow in the convective plume

ℓ is the length of the heater

δ is the width of the plume

U is the measured velocity

The volume flow in the plume depends on heat load and distance from the heater

$$q_y = 0.016 Q_C^{2/5} y^{1/2} \ell \quad (m^3/s) \quad (5)$$

The supply openings are located 1.5 m above the heater and at this height the volume flow varies between 0.14 m³/s and 0.24 m³/s corresponding to a specific flow rate of 11 - 19 h⁻¹. This volume flow is very large compared to the volume flow of fresh air (1 - 5 h⁻¹).

2.4 Room air velocities

The air velocities in the occupied zone are measured at 5 different specific flow rates and at 5 different heat loads for both air terminal devices. In figure 5 the velocity 0.1 m above the floor is shown for the nozzle (A) under isothermal conditions and with a heat load of 800 W.

The result of the velocity measurements in the occupied zone contains several characteristics.

At isothermal conditions and at specific flow rates exceeding 2 - 3 h⁻¹ there is a linear correlation between air velocity and specific flow rate. This means that the flow has a fully developed turbulent level in the room and that the normalized values are independent of the velocity, see Nielsen³.

The same correlation does not appear with heat load in the room. The velocities are considerably lower with heat

load in the room than under isothermal conditions. The supply air is mixed with air from the hot plume above the heat source. Totally this gives a plume or jet which is warmer than the room air. Due to bouyancy the velocity in the downward flow at the opposite wall will decrease more rapidly than under isothermal conditions giving lower velocities in the occupied zone.

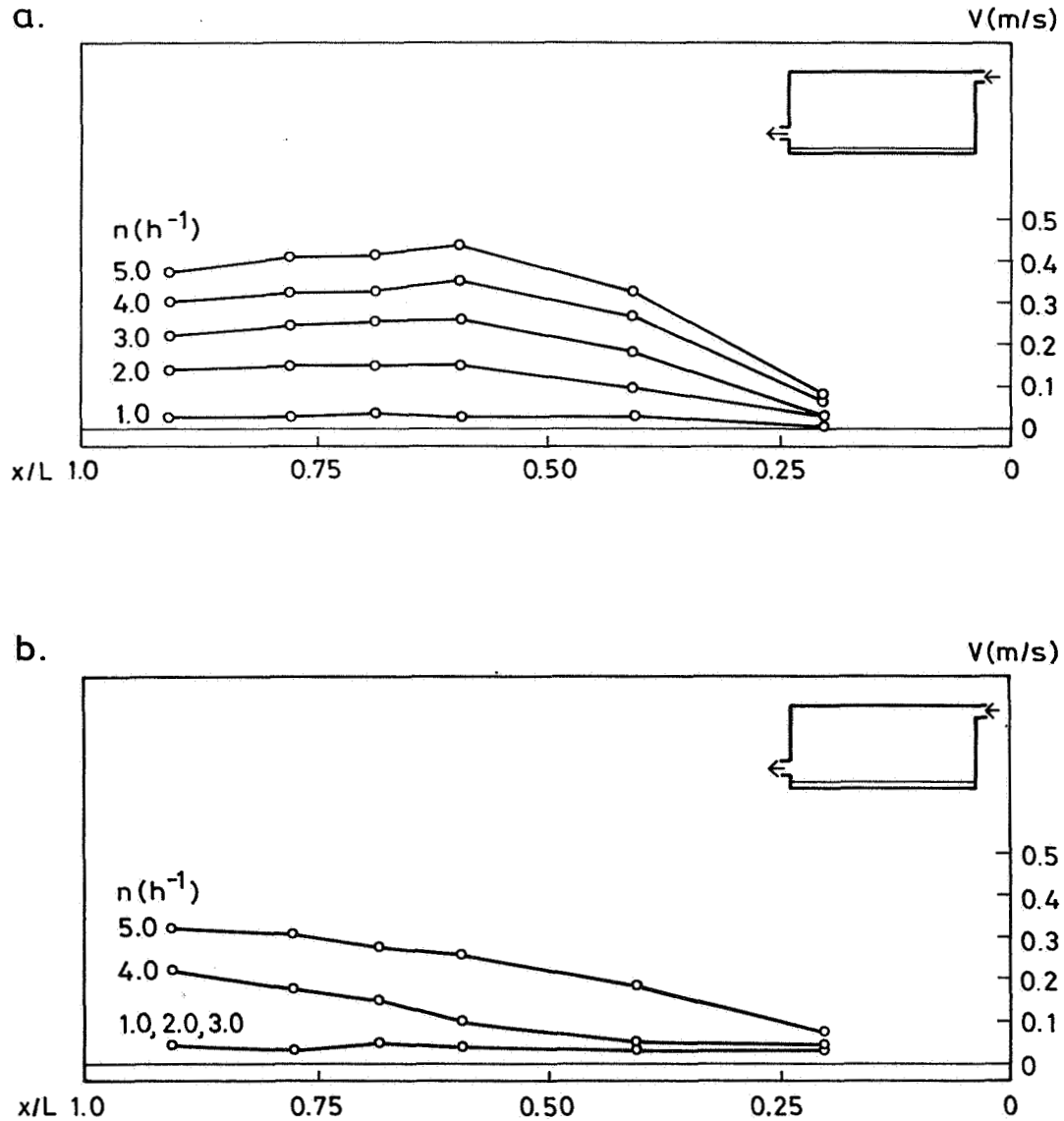


Figure 5. Air velocities in the occupied zone at 5 different specific flow rates for the nozzle (A) measured 0.1 m above the floor under: a) isothermal conditions, and b) with a heat load of 800 W in the room.

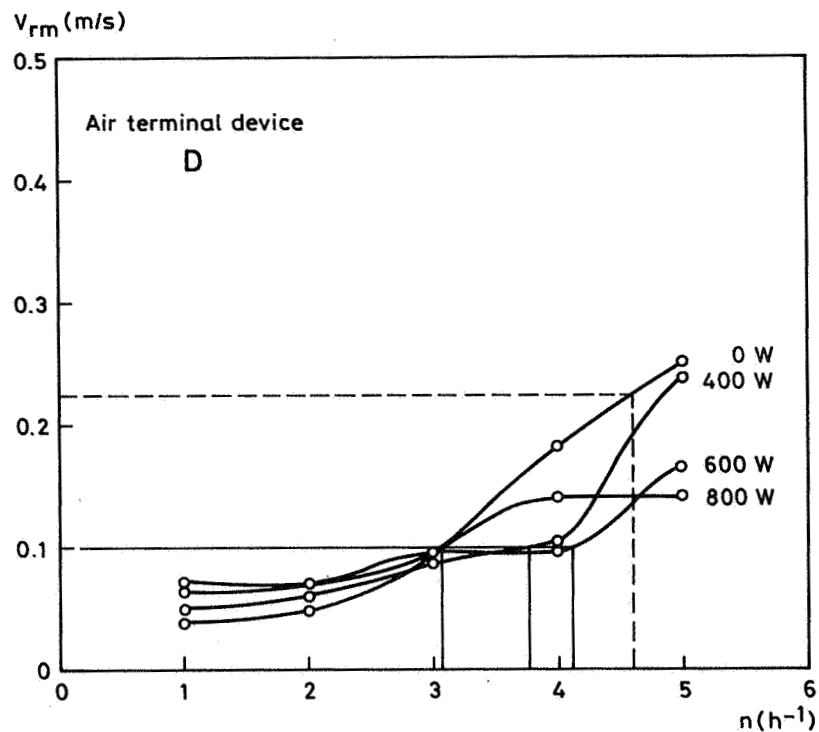
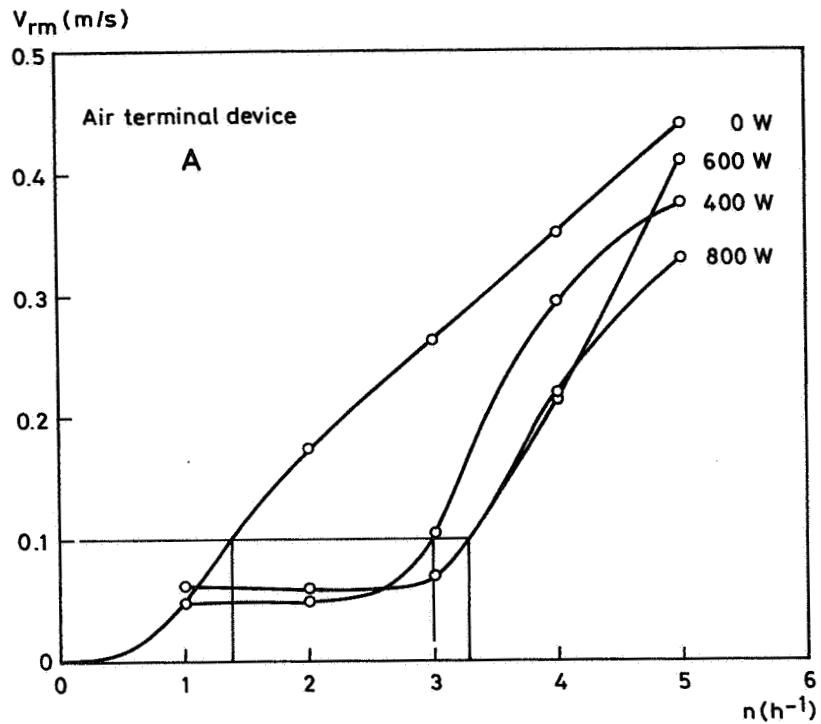


Figure 6. The maximum air velocity in the occupied zone as a function of the specific flow rate and the heat load for air terminal devices (A) and (D).

The maximum air velocity in the occupied zone cannot be completely determined from the measurements. However, it is estimated from the measured velocities at 18 points that the correct value is not considerably higher than the measured value. Therefore, in the following the maximum air velocity in the occupied zone is assumed to be equal to the maximum measured air velocity.

In figure 6 the maximum measured air velocity is shown as a function of the specific flow rate and the heat load for both air terminal devices.

As expected figure 6 shows that the maximum velocity in the occupied zone is much higher for ventilation with the nozzle than for ventilation with the diffuser at the same specific flow rate. This means that the diffuser (D) allows the highest specific flow rate in the room at the same velocity level in the occupied zone.

Figure 6 also shows, especially for the nozzle (A), that the maximum velocity in the occupied zone is much lower with heat load in the room than under isothermal conditions. The difference in velocity decreases at increasing specific flow rate and decreasing heat load.

2.5 Comfort demands

Determination of the comfort limit for air velocity in the occupied zone in a room depends on the acceptable level of discomfort. In an ordinary office a dissatisfaction rate of 10% is acceptable. According to Fanger and Christensen² the comfort limit for air velocity should in this case be $V_{rm} = 0.1$ m/s. This value is adequate within the normal temperature range in ventilated work rooms.

The maximum specific flow rate can be found from the comfort limit and figure 6. The results are shown for both air terminal devices in figure 7.

AIR TERMINAL DEVICE	ISOTH. COND.		THERM. COND.	
	$n(h^{-1})$	$q_o(m^3/h)$	$n(h^{-1})$	$q_o(m^3/h)$
A	1.4	66	3.0-3.3	140-154
D	3.1	145	3.1-4.1	145-191

Figure 7. Maximum specific flow rate and air supply flow rate for air terminal devices (A) and (D) for $V_{rm} = 0.1$ m/s.

The result from figure 3 is included in figure 6 together with the comfort requirements. Apparently a design with a throw equal to the room length functions satisfactorily for the nozzle under isothermal conditions. It is further shown that the non-isothermal conditions (at the given location of heat source and supply temperature equal to return temperature) allows a specific flow rate from the nozzle (A) which is high compared to the value found for the throw equal to room length.

Diffuser D and a throw equal to the room length gives a maximum air velocity of 0.23 m/s in the occupied zone. This corresponds to a dissatisfaction rate of 40% which is clearly unacceptable. The reason for the failure of the simple design method may be that the wall jet from the diffuser spreads quickly and occupies a large area of the room which increases the velocity level in the return flow.

The need for fresh air in the room depends on its use. If the room is used as a conference room with space enough for 6 - 8 persons, the necessary specific flow rate of fresh air to the room will be either 5.4 h^{-1} or 3.7 h^{-1} dependent on whether or not smoking is allowed⁴. It will not be possible to supply the room with fresh air through the nozzle in this case, if the comfort demands are to be fulfilled.

3. CONCENTRATION MEASUREMENTS

The concentration measurements were performed to determine the distribution of contamination in the room under different circumstances. The measurements are performed under stationary contaminant, air and temperature distribution conditions. The measuring points are evenly distributed along a vertical line through the middle of the room. The tracer gas is supplied through a point source (diameter 30 mm) placed 1.1 m above the floor in the middle of the room. For both air terminal devices the room has been ventilated with specific flow rates of 1 h^{-1} , 2 h^{-1} and 3 h^{-1} , respectively. The heat load has been varied between 0 W, 400 W and 800 W, respectively.

3.1 Normalized concentration distribution

The concentration measurements are normalized in relation to the concentration m_R in the return opening. A concentration of m/m_R of e.g. 2.0 will indicate that the local concentration is twice as high as the concentration in the return opening

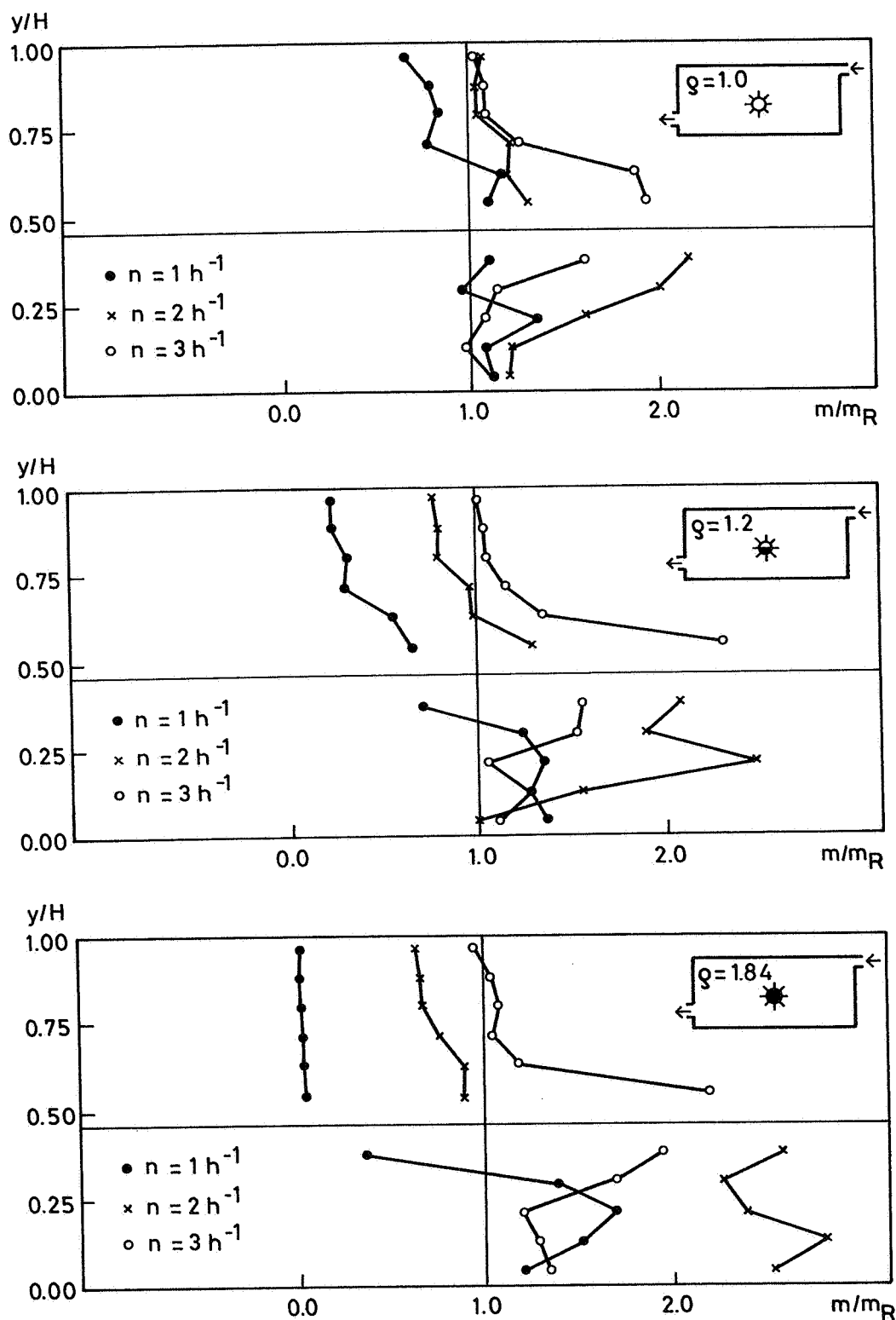


Figure 8. Normalized concentration distribution along a vertical line through the middle of the room for air terminal device (D) under isothermal conditions. Specific flow rates of 1 h^{-1} , 2 h^{-1} and 3 h^{-1} and a tracer gas densities of 1.0 kg/m^3 , 1.2 kg/m^3 and 1.84 kg/m^3 .

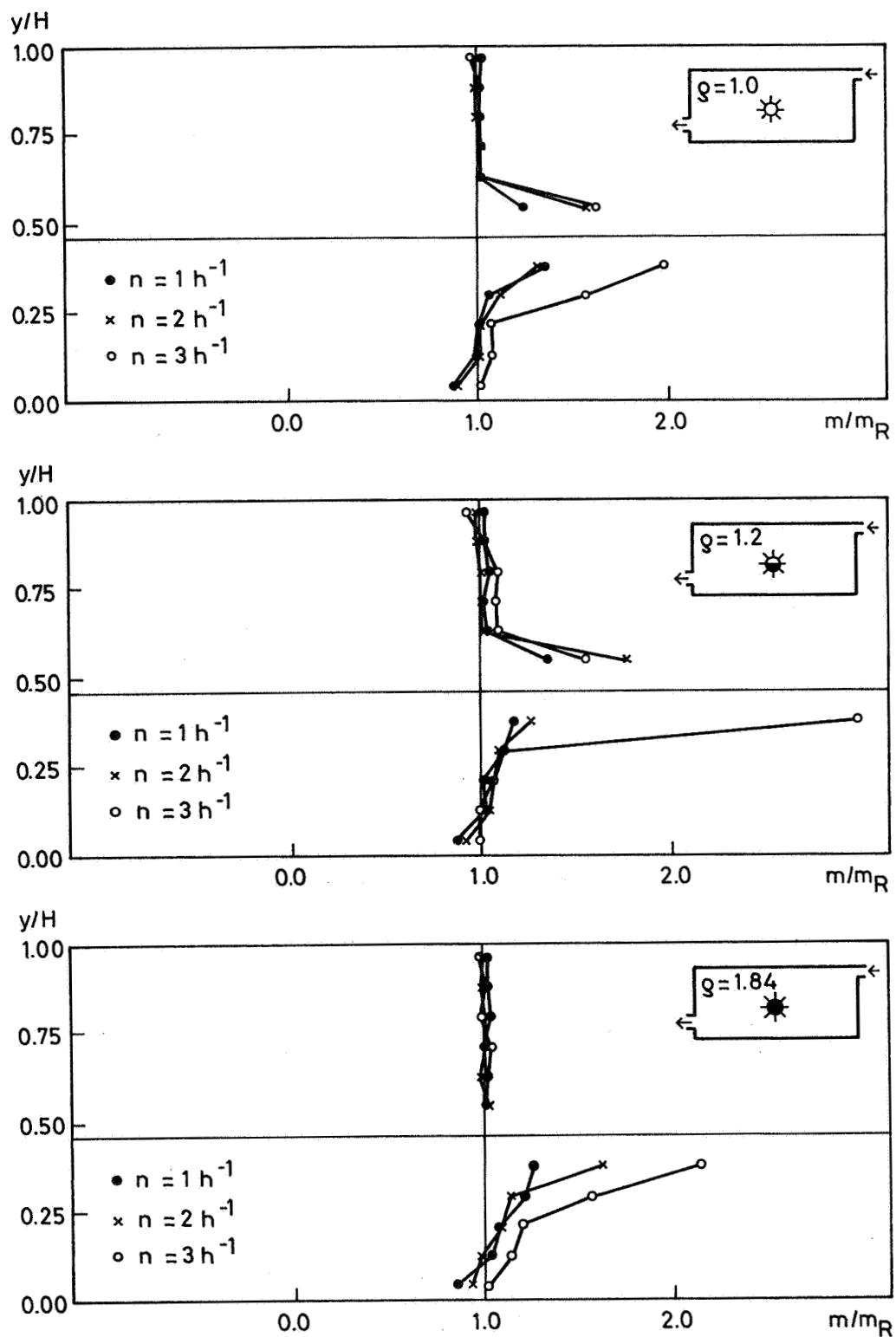


Figure 9. Normalized concentration distribution along a vertical line through the middle of the room for air terminal device (D). Heat load equal to 800 W. Specific flow rates of 1 h^{-1} , 2 h^{-1} and 3 h^{-1} and a tracer gas densities of 1.0 kg/m^3 , 1.2 kg/m^3 and 1.84 kg/m^3 .

The result in figure 8 shows a concentration distribution in the wall jet created by entrainment of the contaminated room air into the primary air. The concentration is highest around and directly below the source. The source is placed in an area of the occupied zone where the air velocity is very low, and the tracer gas will reach a high concentration level before it is entrained and discharged with the other air in the room. Measurements by Oppl⁵ show a similar effect when the source is placed in an area with a low velocity.

With increasing specific flow rate it is seen that the contaminant distribution m/m_R is approximating the distribution under high turbulent flow conditions in the room. It is characteristic of this distribution that it is independent of the specific flow rate, see Nielsen⁶. It is seen that the tracer gas density affects the distribution. Above the source level the highest concentrations were measured by using tracer gas of low density, and the lowest concentrations were measured by using tracer gas of high density. The reverse condition applies below source level. However, the influence decreases at increasing specific flow rate.

The result in figure 9 shows a concentration distribution which is rather independent of specific flow rate and tracer gas density. As under isothermal conditions the concentration is highest around and just below the source. In the rest of the room the concentration level is the same as in the return opening. The distribution may be explained by the large amount of air which is circulated by the convective heat source, and it may also be explained by a slightly increased velocity around the source which is measured in the case of heat load in the room.

4. CONCLUSION

The design of air terminal devices in ventilated rooms with a throw equal to the room length does not always ensure thermal comfort. The air velocity in the occupied zone does not only depend on the proportions of the supply opening but also on the flow conditions in the room.

A convection heat source in the room gives rise to a large internal volume flow in the room and this means an equally distributed concentration m/m_R in the room independent of the specific flow rate.

5. REFERENCES

1. HEISELBERG, P. and NIELSEN, P.V.,
"The contaminant distribution in a ventilated room
with different air terminal devices",
Room Vent 87, Stockholm, June 1987.
2. FANGER, P.O. and CHRISTENSEN, N.K.,
"Perception of draught in ventilated spaces",
Ergonomics, 1986, vol. 29, No. 2, 215-235.
3. NIELSEN, P.V.,
"Flow in air conditioned rooms",
(English translation of Ph.D.-thesis from the tech-
nical University of Denmark, 1974) Danfoss A/S, 1976.
4. "Code of Practice for Ventilation Installation",
Danish standard, DS 447, Dec. 1981.
5. OPPL, L.,
"Luftströmung in gelüfteten Räumen",
Öl- und Gasfeuerung, Nr. 9, 1969.
6. NIELSEN, P.V.,
"Contaminant distribution in industrial areas with
forced ventilation and two-dimensional flow",
IIR-Joint Meeting, Commission E1, Essen, Sept. 1981.

EFFECTIVE VENTILATION

9th AIVC Conference, Gent, Belgium
12-15 September, 1988

Poster 20

VENTILATION AND INDOOR AIR QUALITY IN A MODERN
OFFICE BUILDING

R.A. GROT, A. PERSILY* AND A.T. HODGSON, J.M. DAISEY°

*Centre for Building Technology
National Institute of Standards and Technology
Gaithersburg, MD 20899
U.S.A.

°Indoor Environment Program
Lawrence Berkeley Laboratory
Berkeley, CA 94720
U.S.A.

Introduction

The National Institute of Standards and Technology (formerly the National Bureau of Standards) has through an interagency agreement with the Public Building Service of the General Services Administration performed an evaluation of the thermal and environmental performance of a new Federal office building in Portland OR. The building was constructed during the 1986 and 1987 and occupancy began in August of 1987.

This evaluation is part of a research effort by the Center for Building Technology of NIST to develop methods for evaluating advanced technology buildings. The procedure used for this evaluation was to install in the new office building a diagnostic center capable of monitoring important environmental parameters of the building. The measurements made consisted of 1.) air infiltration and ventilation rates, building envelope tightness, interzone air movement, detection of envelope thermal deficiencies, envelope thermal resistance and the levels of indoor contaminants. The indoor contaminants measured include carbon dioxide, carbon monoxide, respirable particulates in the 0.3 to 10 micron range, formaldehyde, radon and volatile organic compounds which could be emitted either by the new building materials and furnishings or the activities of the building occupants. Much of the measurements were made in real time. There are over 100 monitoring points in the building installed both in the interior space of the building, the building HVAC systems and the underground parking garage.

Description of the Building

The new Federal office building is a seven-story office building with a one-story basement and a two and one-half story underground garage (see figures 1 to 7). Attached to the building are a dining room and kitchen (figures 3 and 4). The penthouse of the building houses a mechanical equipment room which serves the first through seventh floors. There are three main HVAC systems which serve respectively the east, center and west cores of the building. These three systems have a total capacity of approximately 140 m³/s (about 3 air changes per hour). Each HVAC system has one return fan, two cold supply fans and a hot supply fan. These three HVAC systems are variable-air-volume systems (VAV). On the B1 level (occupied basement level-figure 5) there are four air handling systems which serve various sections of the basement. The B1 level also contains the loading dock. Above and to the north of the loading dock is an air handler system for the dining room. In the underground garages there are four exhaust fans which are activated when the carbon monoxide levels in the garage reach 50 ppm. The occupied area of the building is approximately 46,000 m² and has a volume of 180,000 m³. The garage is connected to the occupied space by several stair and elevator shafts. The general interior plan of the building (figures 6,7) is that of an open architecture which each occupant having a space enclosed by 5 ft. partitions. On most floors there are enclosed offices for supervisors and enclosed conference rooms that do not have separate air handling systems. The second floor of the building contains a computer facility.

Description of Measurement Methods

A diagnostic center was installed in the building during the later stages of construction. A schematic of this diagnostic center is shown in figure 8. The instrumentation [1] of the diagnostic center was designed to measure automatically the air infiltration and ventilation rates of various parts of the building, internal temperatures and humidity, exterior temperature, wind speed and direction, the indoor and outdoor levels of carbon dioxide and carbon monoxide and the indoor levels of respirable particles in six size ranges (0.3-0.5, 0.5-0.7, 0.7-1.0, 1-5, 5-10 and >10 microns). Figure 9 shows a view of the instrumentation systems installed in the diagnostic center. In addition check measurements were made of the concentrations of formaldehyde, radon and volatile organic compounds.

The air exchange rate measurements were made using the tracer gas decay technique with an automated measuring system. This system has been used previously to provide continuous measurements of building air exchange rates in office buildings [2]. For these measurements the system injects sulfur hexafluoride (SF_6) into the building supply fans every two or three hours, allows the tracer gas to mix, and then monitors the decay in tracer concentration at several locations within the building. The tracer gas decay procedure is based on the sample on the assumption that the tracer gas is well-mixed with the interior air, and sampling of the SF_6 concentration at several locations enables the verification of this assumption. The rate of decay of the tracer gas concentration provides an estimate of the whole building air exchange rate under the conditions that exist during the measurement. This estimate includes both air exchange due to the internal intake of outside air through the air handlers and uncontrolled, unintentional air exchange through leaks in the building envelope.

The automated system is controlled by a microcomputer that controls the tracer gas injection and air sampling, records the SF_6 concentrations, and monitors and records the outdoor weather, indoor temperatures and fan operation. Two such systems were employed in the new office buildings enabling sampling of tracer concentrations at twenty locations. These systems operate unattended for long periods of time (approximately one month).

The sampling locations in the building were placed both in the interior space and in the air handling systems. In general each air handling system had three air sampling locations: one down-stream of the intake fans, one up-stream of the intake fan and one in the return fan. These sampling points were connected directly to the diagnostic center through 5/8 inch OD nylon or polyethylene tubing. Each air handling system had two injection points for injecting tracer gas (one up-stream and one down-stream of the supply air fans). These points were collected to injection manifolds with 1/8 inch nylon tubing. On each floor there were between 8 to 12 interior space sampling location at a height of approximately 5 ft. above the floor (figures 10,11). In addition there were sampling points in the exhaust stream of each air handling system. Typical locations of these sampling points can be seen in figures 4 - 6. These floor sampling locations were collected to floor panel boxes by either nylon or polyethylene 5/8 inch tubing for runs under the raise floor or 5/8 copper tubing (a fire requirement) for runs through the ceiling return air plenum. Each floor panel had six 5/8 inch polyethylene tubes which ran to the diagnostic center on the B1 level. These six tubes were patched to the desired floor sample locations. This permitted easy changing of sampling locations and also through the use of tees

and jumpers the creation of a large variety of average sampling strategies. (One particularly useful strategy was to tee together one central location from each floor to obtain a average interior space concentration.) Similar sampling locations were installed on each level of the underground garages. In addition sampling location were placed in the exhaust air of the garage's four exhaust fans. Sampling points were also installed at two locations outdoors on the roof and at two locations outdoors at street level.

The levels of pollutants were measured using a variety of techniques. Carbon monoxide (CO) and carbon dioxide (CO₂) were measured with an automated system employing infrared absorption analyzers for determining concentrations and a microcomputer to switch among the sampling locations and to record data. This system automatically monitored the CO and CO₂ concentrations at ten locations in the building, each location being monitored once every ten minutes. Particle concentrations were monitored with a light-scattering particle counter that determines particle concentrations in six different size ranges (0.3-0.5, 0.5-0.7, 0.7-1.0, 1-5, 5-10 and >10 microns). Cumulative particle counts were recorded on a disk by a microcomputer based data acquisition system. Formaldehyde concentrations were measured with a passive monitor based on absorption onto a sodium-bisulfite treated filter and analysis by the chromotropic acid colorimetric method. These passive samplers yield average formaldehyde concentrations for periods from 5 to 7 days. Radon concentrations were measured with charcoal canisters for periods of about 3 days, and a working level monitor was used to obtain hourly measurements of radon progeny levels.

Volatile organic compounds were measured using active sampling on Tenax and/or charcoal with analysis by a gs/Ms. Air samples were collected on multisorbent samplers containing three sorbent materials in series: Tenax-TA, Ambersorb XE-340, and activated carbon. Samples were analyzed using a thermal desorption and sample concentrating device (Model 810, Envirochem, Inc.) a capillary gas chromatograph (Model 5790A, Hewlett-Packard, Inc.) equipped with an on-column cryogenic focusing device, and a mass-selective detector (Model 5970B, Hewlett-Packard, Inc.). Following thermal desorption, a portion of the sample was split off to a flame-ionization detector for a measurement of total organic carbon. The mass-selective detector was operated in scan mode for qualitative analyses and in selected ion mode for quantitative analyses.

Results of the First Year Evaluation

The building ventilation and air infiltration rates are shown in figure 12 as a function of inside-outside temperature difference. Building ventilation rates (open diamonds) are between 0.4 to 2.2 air changes per hour during periods when the building is occupied with the most typical values being about 1.0 to 1.2 air changes per hour. The extreme of 0.4 occurs during extremely hot summer conditions or extremely cold (for Portland, OR) winter conditions. For comparison, the new ASHRAE ventilation standard requires 20 cfm per person for office buildings. This is equivalent to 0.8 to 0.9 air changes per hour if the building is occupied at a density of one person per 135 ft.².

The building air leakage (uncontrolled air exchange when the HVAC fans are off during unoccupied hours - solid squares) is between 0.2 and 0.4 air changes per hour. This is a building designed to be energy efficient and these values indicate that the exterior walls of the building are not tight by what we would consider typical of US office buildings. (Note: The surface to volume ratio of an office building is about 1/6 th that of a home. Therefore the walls of this building are equivalent to the walls of a house with an air leakage of about 1.2 to 2.4 air changes per hour - very loose).

The maximum daily carbon dioxide levels for the months of January through April are shown in figure 14. Figure 15 shown the maximum daily CO₂ level as a function of air exchange rate. Carbon dioxide levels are seldom over 600 ppm on a building average and only a couple of times ever over 1000 ppm at any location in the building. (The new ASHRAE standard proposes a maximum level of 1000 ppm, complaints from building occupants begin to occur when levels excess 600 ppm). A closer examination of the hourly CO₂ levels in the building shows that the obtain levels are never at steady state and usually have two daily peaks - one around 11 am and the other around 3 pm. It is also shown by the values of the constants of the fitted curve in figure 15. The value of 100 is approximately 1/3 the expected equilibrium value based on the occupancy of the building.

A detailed examination of the SF₆ and CO₂ data shows that the air handling system can easily control the amount of air required for the building. The outside air is well distributed and there is little or no evidence of short circuiting of the outside supply air or poor mixing due to the operation of the variable volume air handling system. In the summer and warmer periods of the fall and spring the typical operational mode of this air handling system runs the system at 100 percent outside from early morning to a point in the day when the outside temperature researches about 26 degrees C at which point the point the system is run at between 10 to 20 percent outside air. In the winter a economizer mode of operation was used last winter in which the amount of outside air was determined by the cooling requirements of the building.

The levels of carbon monoxide in various parts of the building are shown in figures 15 through 20. Figure 15 gives the daily maximum carbon monoxide levels in the interior space for the months of February through May. Figure 16 shows the high levels of CO occurring in the elevator level of the sixth floor. Figure 17 shows the daily peaks of CO on the B2 garage level. Figure 18 gives the peak reading in CO for the elevator lobby on the B1 level. Figure 19 shows similar maxima for the B1 level loading dock. An examination of the data in these figures and the more detailed hourly data shows that during the fall and early winter months, there were occasional incidents of excessive carbon monoxide levels (greater than 10 ppm) in the upper building (figure 16) due to the flow of air from the under ground parking garage toward the elevator shafts and stairwells. (Note the ASHRAE required level is 10 ppm, complaints begin to occur at 5 ppm.) It seems that the automated sensors in the garage, though functioning as designed (to activate the garage's exhaust fans when the level in the garage exceeds 50 ppm (see figure 17)), will not prevent the transport of CO up the elevator shafts (figure 16) and stairwells in extreme weather conditions when the stack effort is strongest. Once the garage exhaust fans (at least two of the four) were operated continuously during occupied hours, the CO level in the office space never exceeded 5 ppm.

Figures 21 and 22 shows the results of the radon testing in the building. The measured radon levels in the building are below 0.007 working levels (the ASHRAE level is 0.01 working levels, the EPA action level is 0.02 working levels) as measured in terms of the equivalent radiation impact of the radon daughters and less than 1.2 pCi/l (the ASHRAE recommended level is 2 pCi/l, the EPA action level is 4 pCi/l) in terms of the amount of radon gas. The radon levels in the low garage levels are higher than those of the upper floors. It is interesting to note that the upper floors of the occupied space are consistently higher in radon level than the lower above ground levels. This can be attributed to the fact the air flows into the elevator shafts and stairwells on the lower levels and out of these shafts on the upper levels.

Figure 23 shows the maximum daily concentrations of respirable particles in the six size ranges of 0.3-0.5, 0.5-0.7, 0.7-1.0, 1-5, 5-10 and greater than 10 microns. The levels of the fine particles in the 0.3 to 0.5 remain fairly constant and show little hourly or daily variation. The three size range of 0.5-0.7, 0.7-1.0 and 1.0 -5.0 have much more pronounced variations. The two size range greater than 5 microns are not considered respirable. The high levels of particles in the ranges 0.7-1.0 and 1.0-5.0 micron for the period around October 15 were caused by the sweeping of the parking garage with street-type sweeping machines. The building maintenance staff reported that all filters in the air handlers had to be replaced after the sweeping of the garages. In general the levels of respirable particle levels in the building (particles of a size less than 3 microns) are in the 10 to 15 million particles per cubic meter range, typical for office buildings without smoking which we have measured (data from a limited number of buildings). It is difficult to compare the measured particle levels with established standards since the standards are given in micrograms per cubic meter and there is great uncertainty in converting from particle counts per cubic meter to micrograms per cubic meter without more detailed analysis of the composition of the particles present in the building.

The level of formaldehyde in the building was measured in August 1986 during the period when the new furniture was being installed and the occupants were moving into the building. The carpeting (a removable type of carpet squares with a pressure sensitive adhesive) was installed during the months of April through July in most parts of the building. The results of these measurements are shown in figure 24. The measured formaldehyde levels are less than 0.056 ppm (the ASHRAE level is 0.1 ppm, complaints begin at 0.06 ppm, outside levels are typically 0.04 ppm). There is little or no outgassing of formaldehyde from the building's furnishing and carpets.

The last class of pollutants measured was the volatile organics. The results are given in Table 1. The measurements were made on three different occasions: August 4, 1987 when the occupants were moving into the building, October 14, 1987 and January 13, 1988. On each of these dates the building was being operated with three distinct air exchange rates (0.5, 1.36 and 0.24 changes per hour) due to the prevailing exterior weather conditions. Figure 25 shows the effect of building ventilation rate on the total VOC concentration. The curve in figure 25 represents the predicted level in the building using the source strengths in table 1. The source strength of total VOC is remarkably constant over the five month period between the first and last measurements. We have measured and identified 37 volatile organic compounds in the interior building space. There are 5 oxygenated compounds, 6 halogenated compounds, 16 alkanes, 6 cycloalkanes and alkenes, and 5 aromatic hydrocarbons. All are at levels less than 1/1000 th of the OSHA standard environmental levels of industrial work spaces. (Note: The

ASHRAE standard recommends that for indoor air quality the level be not more than 1/10 of OSHA SEL's.) The largest amount of the mass of the VOC's is concentrated in the alkane class (C_{10} to C_{12} branched decanes and undecanes). These are not particularly irritating compounds and there are no OSHA recommended levels for these substances. However very limited studies done in Denmark by Dr. Molhave [3] indicated that many complaints will occur when the total levels of VOC's exceeds 5 mg/m^3 and it has been recommended by researchers [4] at EPA Research Triangle Park that a prudent target level for total VOC's be 1 mg/m^3 . All three measurements sets that were made in the building were greater than 1 mg/m^3 and the building exceeded 5 mg/m^3 when the ventilation rate was below 0.5 air changes per hour. The sources of these compounds have not yet been identified; however we have tested the major building components and furnishings for outgassing and these are not the sources. We suspect that they are activity related and we are making an effort at identifying these activities. Though operating the ventilation system always at 100 percent outside air would keep the levels near the target of 1 mg/m^3 , identification and limitation of the sources is a better strategy.

Summary

The new office building studied is being investigated in order to establish a long-term record of a modern office building's thermal and environmental performance and to document what parameters in the design, construction and operation of a new office building will effect this performance. Other than initial problems associated with "debugging" the HVAC system and controls, the building has adequate ventilation under most operating conditions. The envelope of the building is not tight for a new office building and infiltration is a significant source of building air exchange. The levels of CO_2 , HCHO, radon and respirable particles are well within the established guidelines. An area of concern is the airflow from the garage into the occupied space. This airflow can cause high levels of CO in the vicinity of elevator shafts and stairwells on the upper levels and near the loading dock. The garage exhaust fans are adequate to reverse this flow, but in the automatic mode they currently do not operate for a sufficient amount of time to do so. A change in their controls, or an attempt to isolate the vertical shafts (stairs and elevators) from the garage, would alleviate these problems. There is no evidence of any significant outgassing of pollutants from the building's materials and furnishings. There is however a total of at least 37 volatile organic compounds in the building air which seem to be related to the activities occurring in the building. The levels of all these compounds are of at least two orders of magnitude below established limits (1/10th of the TLV's). However the vast amount of VOC's found in the building are compounds for which no extensive amount of research has been done to establish irritant levels and therefore these compounds could be a source of complaints from the building's occupants at low ventilation rates.

Acknowledgments

The authors wish to acknowledge the support of the US General Services Administration in conducting this research. Also without the efforts of Douglas Pruitt, Sandra Krause and Samuel Silberstein of NIST and Richard Syldowski of LBL in installing the miles of tubing, wiring and measuring equipment, this project would not have been possible. The assistance of

W. Stuart Dols of NIST in processing and analyzing the tracer gas and CO₂ data must also be acknowledged. Finally the cooperation of the GSA region 9 field staff and the Bonneville Power Administration (BPA) building facility staff was indispensable.

References

- [1] Persily, A., "Specifications for Thermal and Environmental Evaluation of Advanced-Technology Office Buildings, NBSIR 86-3462, NBS, 1986
- [2] Grot, R.A. and A. Persily "Measured Air Infiltration and Ventilation in Eight Federal Office Buildings", in Measured Air Leakage of Buildings, ASTM, STP 904, H.R. Treschel and P.L. Lagus, editors
- [3] Molhave, L., "Volatile Organic Compounds as Indoor Air Pollutants" in Indoor Air and Human Health, P. Gammage and S. Kaze editors, Lewis Publications, 1984
- [4] Tucker, G., "Factors Influencing Indoor Air Pollutants Originating from Surface Materials" in preprints of conference "Heathy Buildings 88", Swedish Council for Building Research, Stockholm, Sweden, 1988.



Figure 1. Exterior View of the New Federal Office Building

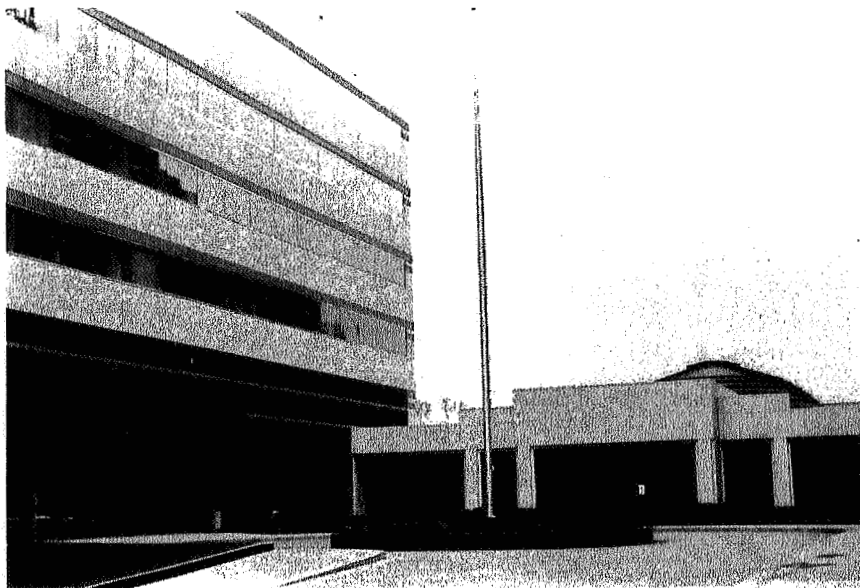


Figure 2. Front Entrance of Building

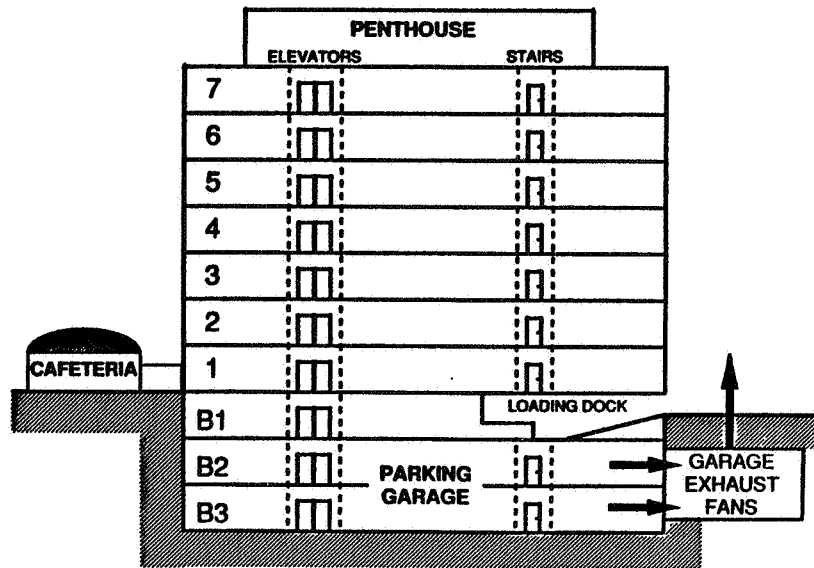


Figure 3. Schematic of the New Federal Office Building

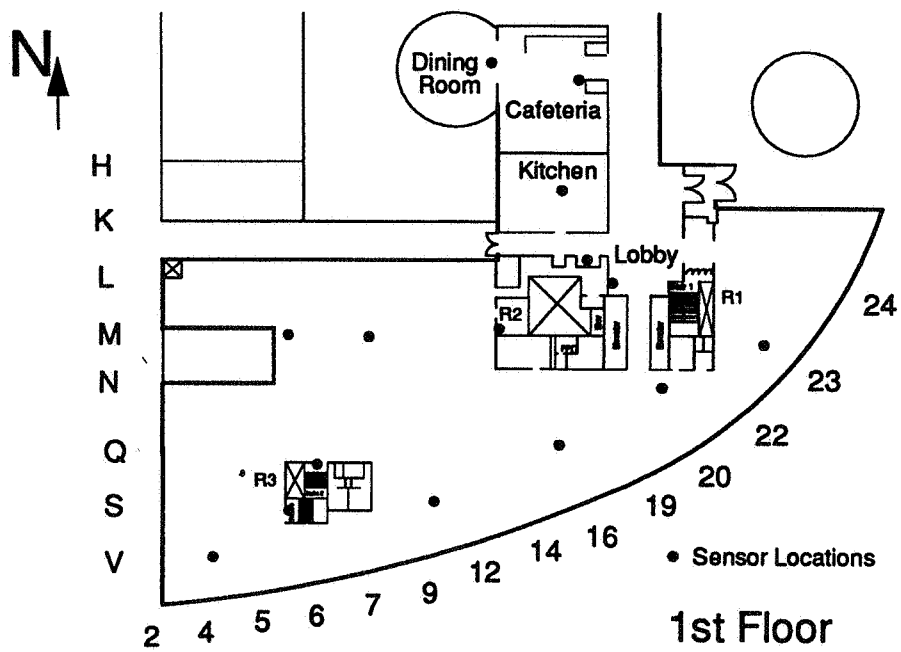


Figure 4. Schematic of First Floor

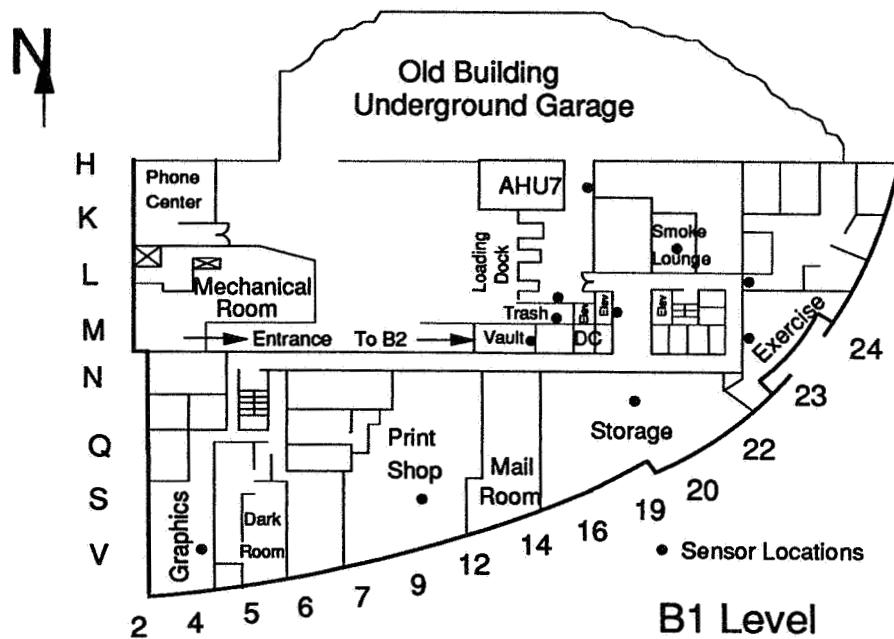


Figure 5. Schematic of B1 Level

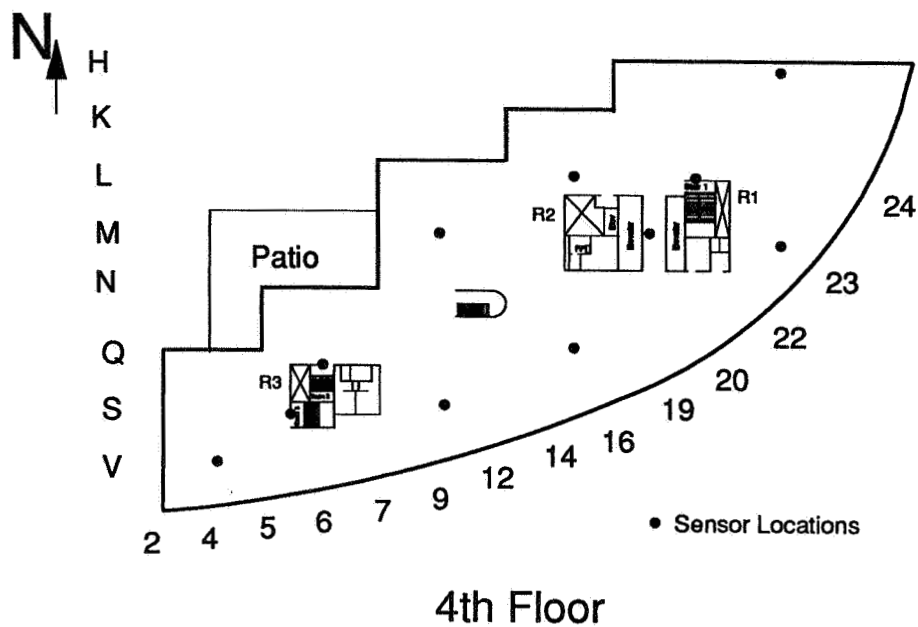


Figure 6. Schematic of Fourth Floor



Figure 7. View of Building Interior

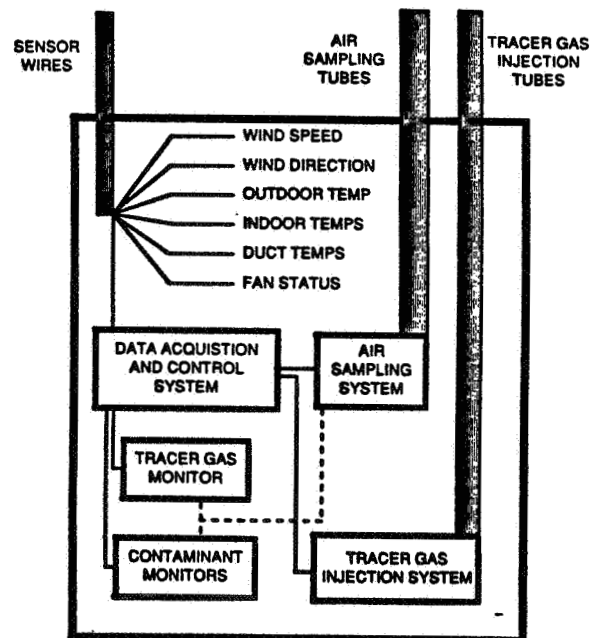


Figure 8. Schematic of Diagnostc Center



Figure 9. View of Diagnostic Center

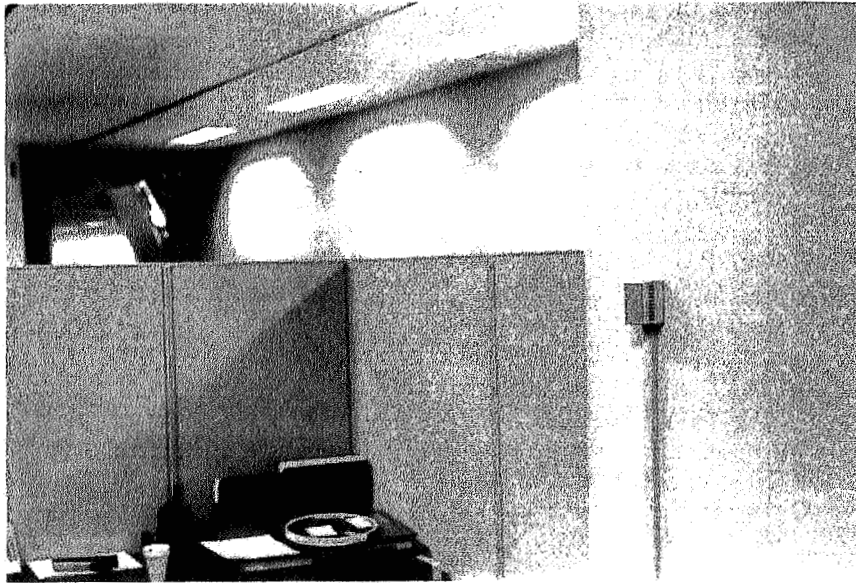


Figure 10. Space Air Sampling Location

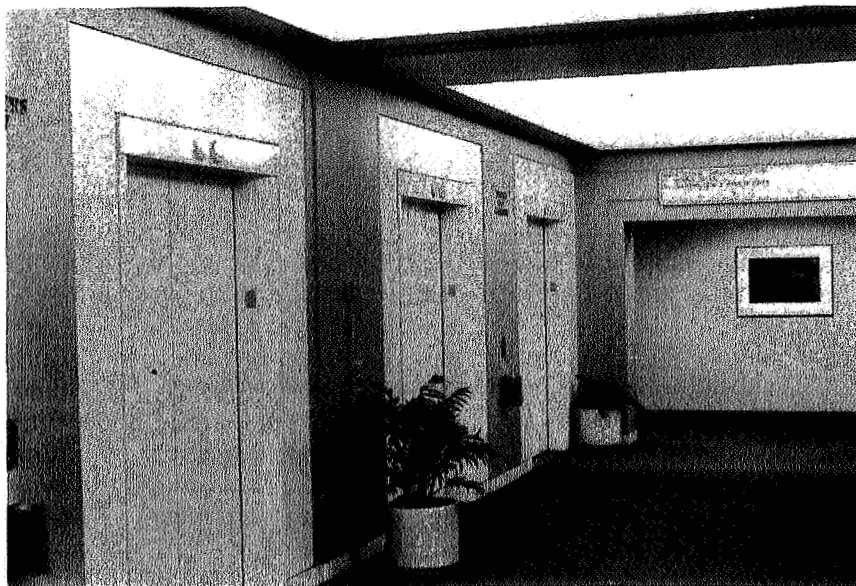


Figure 11. Elevator Lobby Air Sampling Location

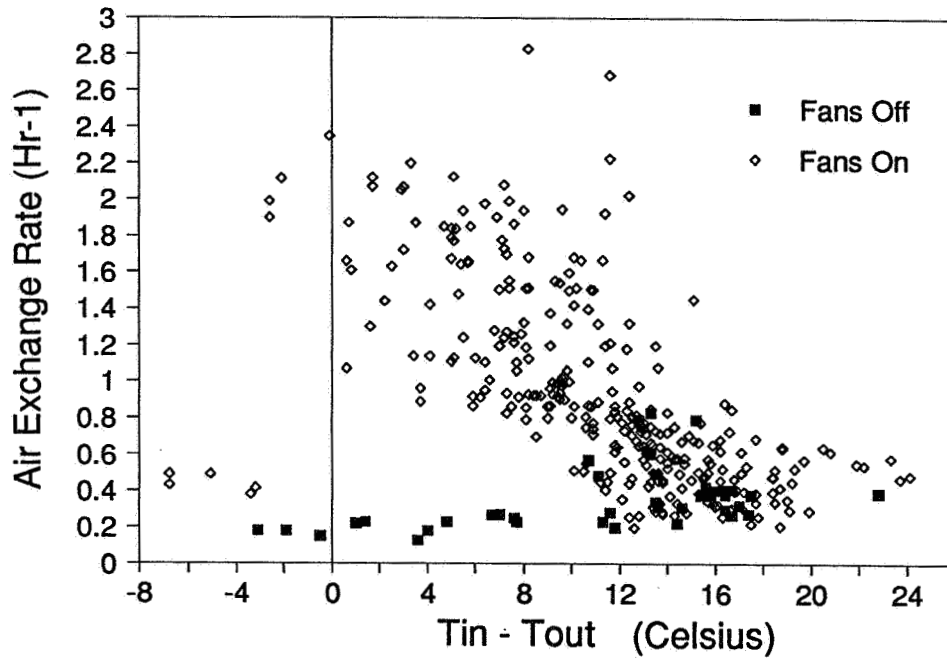


Figure 12. Air Exchange Rate versus Inside-Outside Temperature Difference

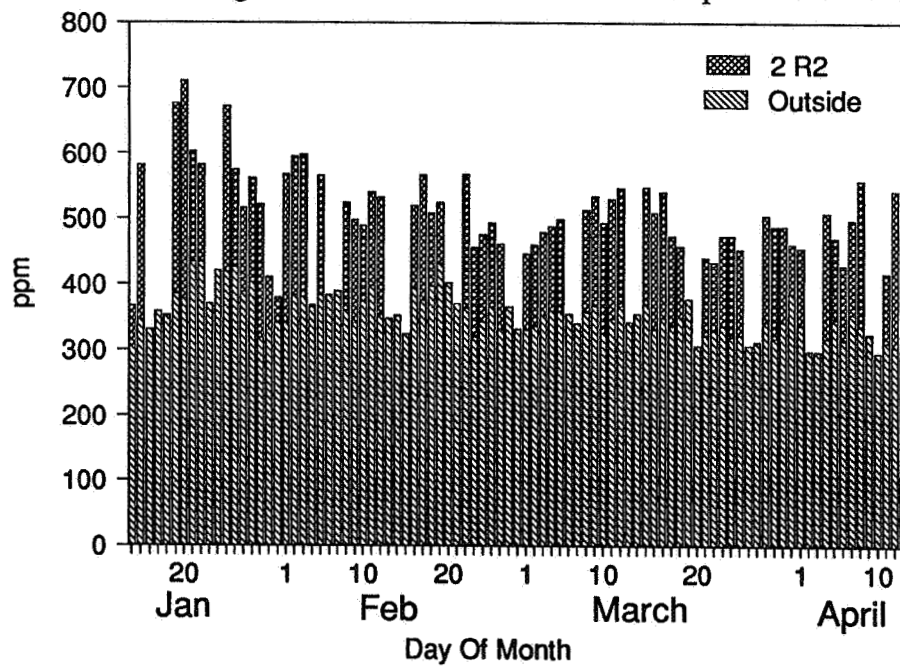


Figure 13. Daily Maximum Carbon Dioxide Levels for Months of January through April 1988

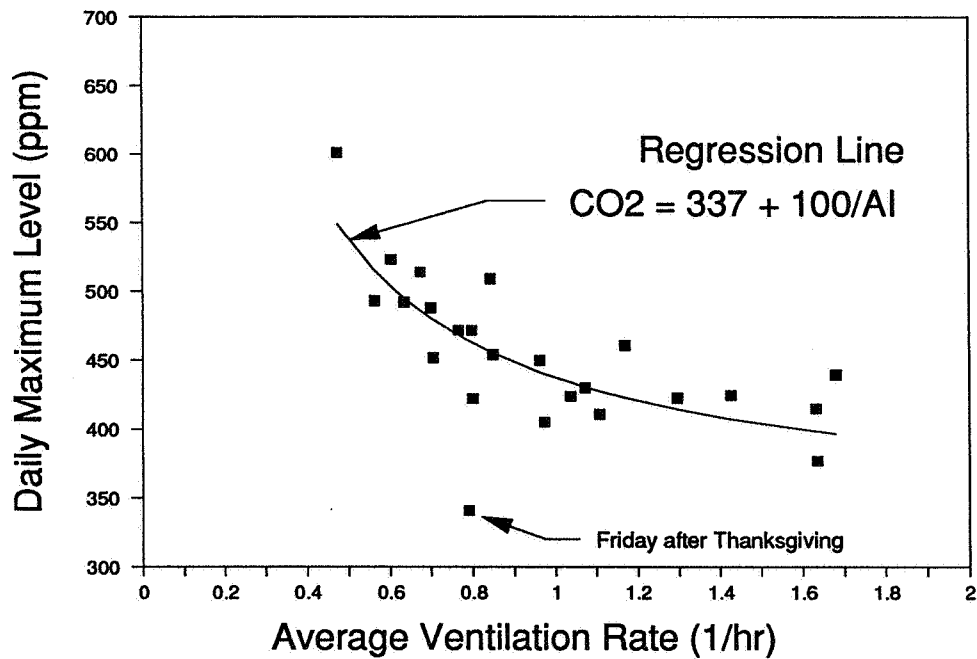


Figure 14. Carbon Dioxide Level versus Ventilation

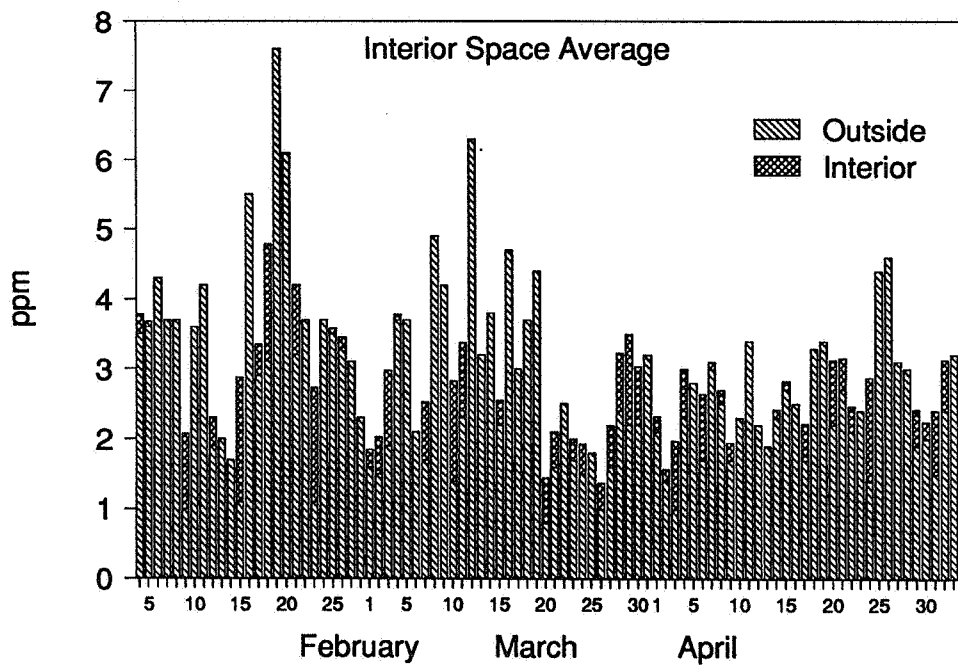


Figure 15. Daily Maximum Carbon Monoxide Level in Interior Office Space for Months of February to May

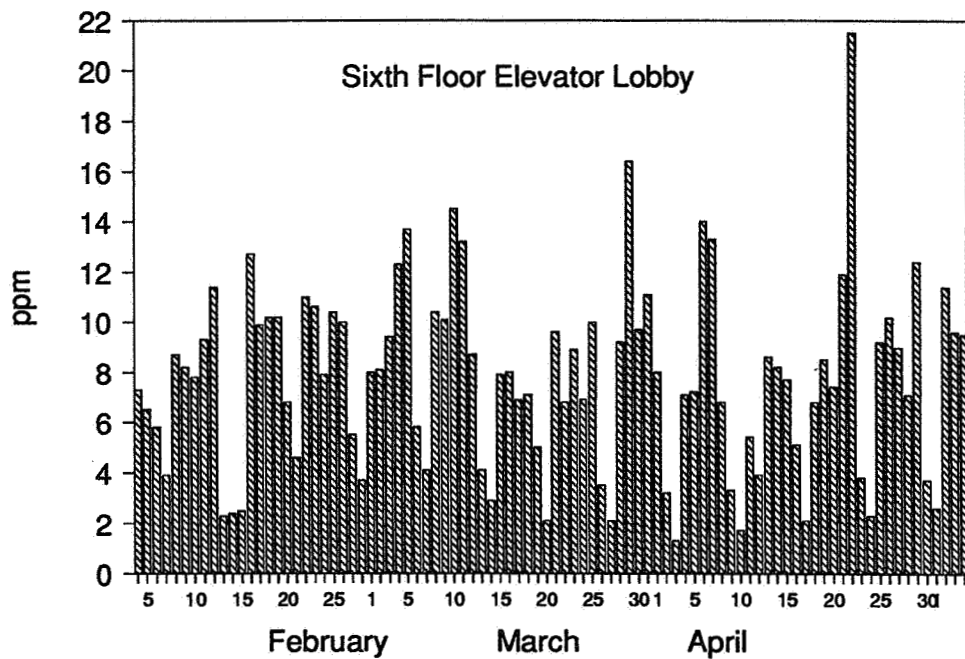


Figure 16. Daily Maximum Carbon Monoxide Level in Sixth Floor Lobby for Months of February to May

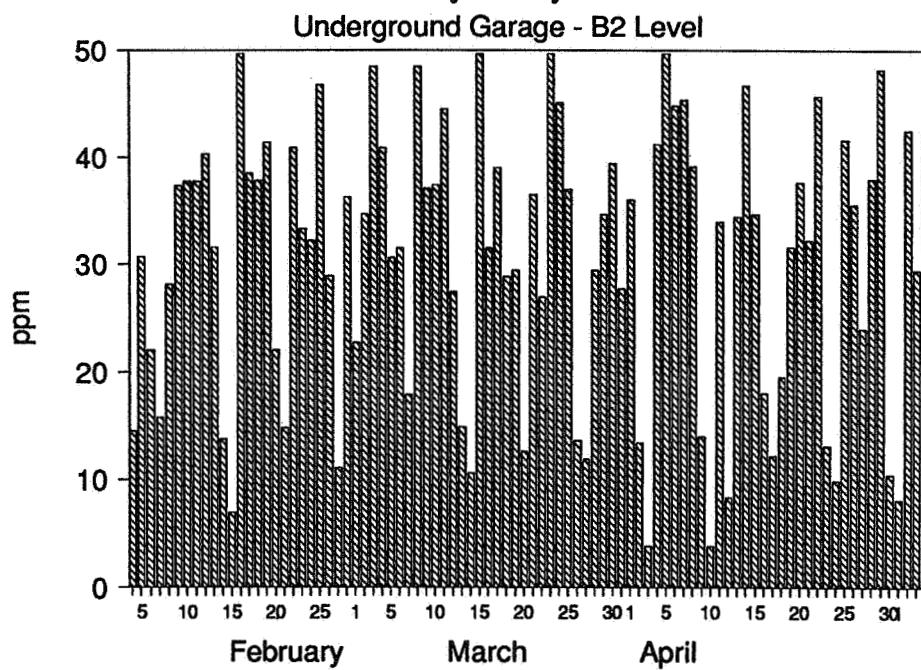


Figure 17. Daily Maximum Carbon Monoxide on B2 Level for Months of February to May

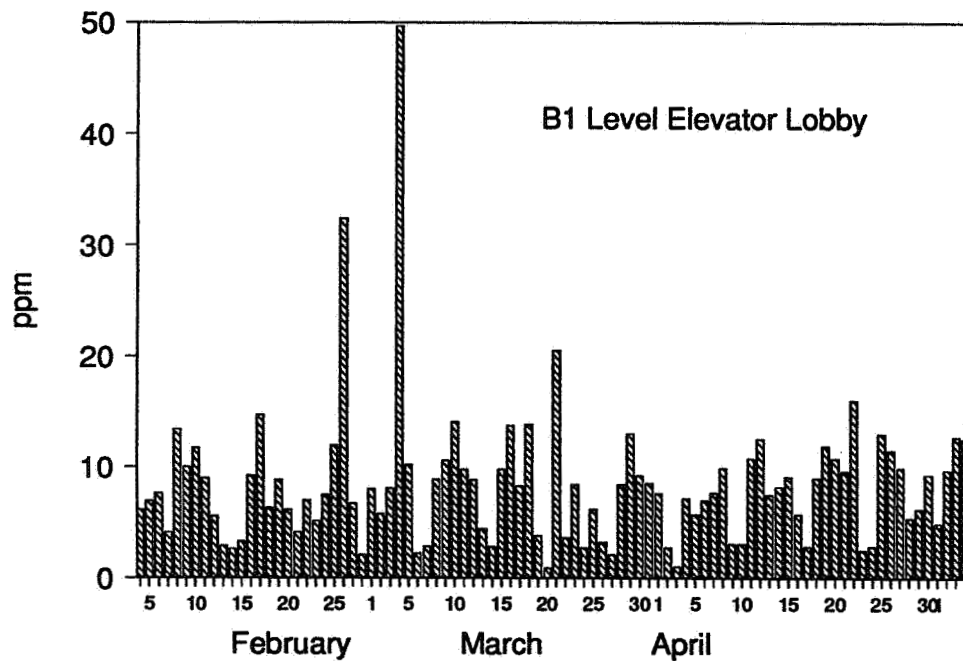


Figure 18. Daily Maximum Carbon Monoxide Level on B1 Level for Months of February to May

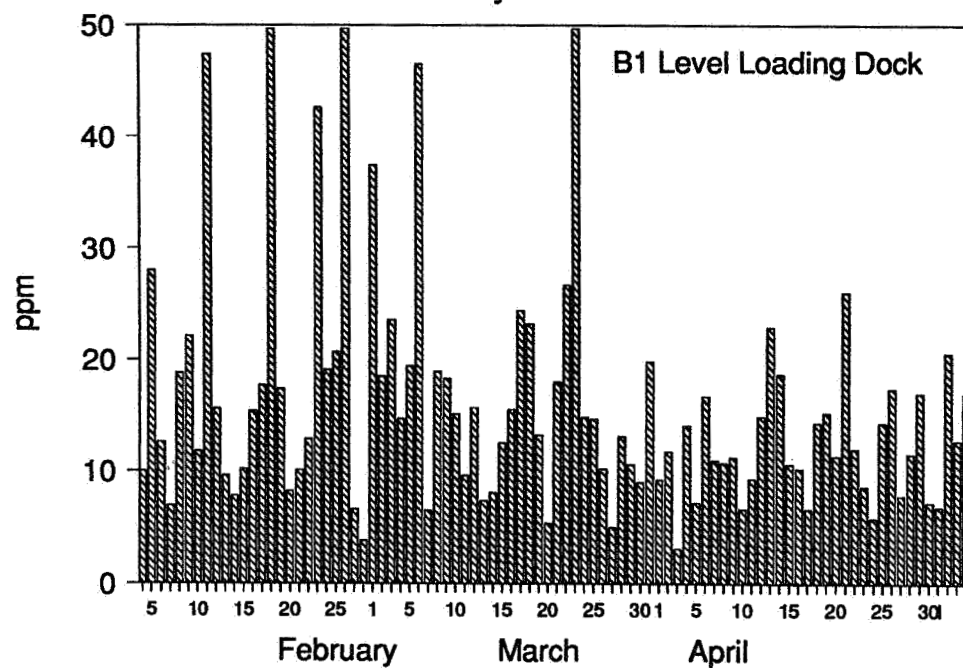


Figure 19. Daily Maximum Carbon Monoxide Level on Loading Dock for Months of February to May

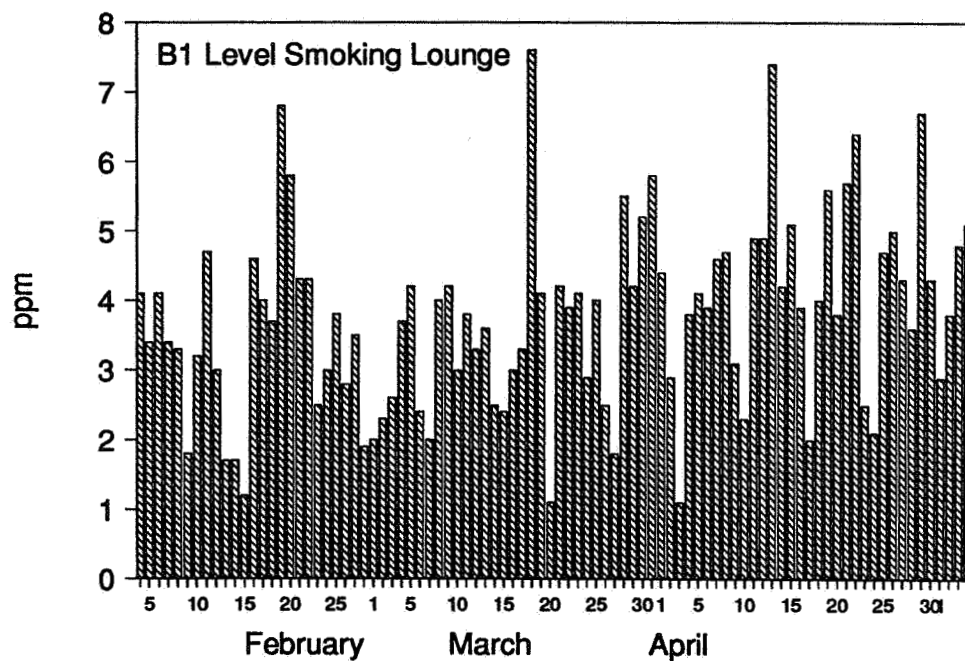


Figure 20. Daily Maximum Carbon Monoxide Level in Smoking Lounge B1 Level for Months of February to May

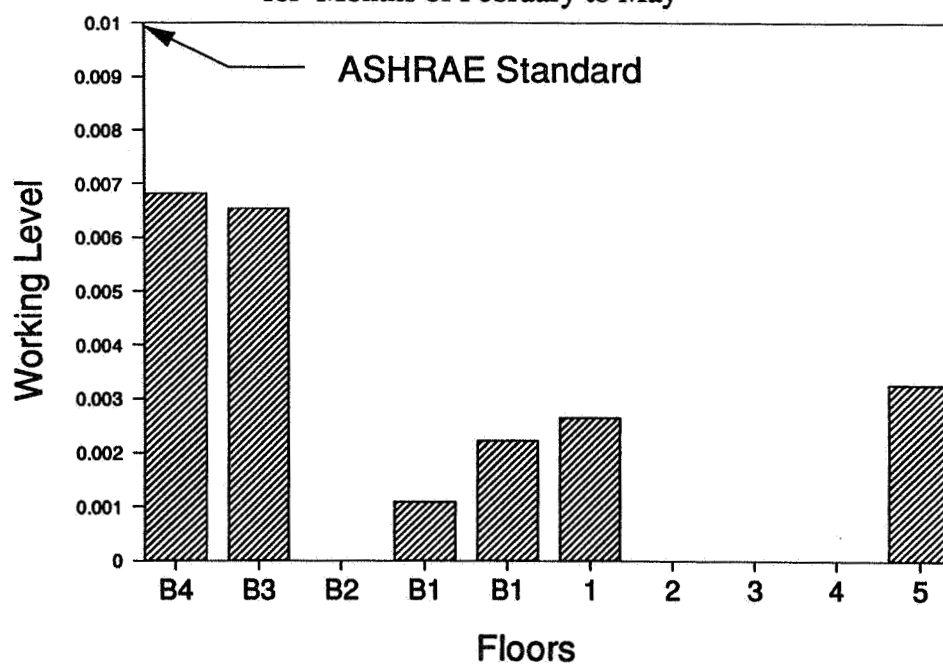


Figure 21. Working Levels of Radon Daughters

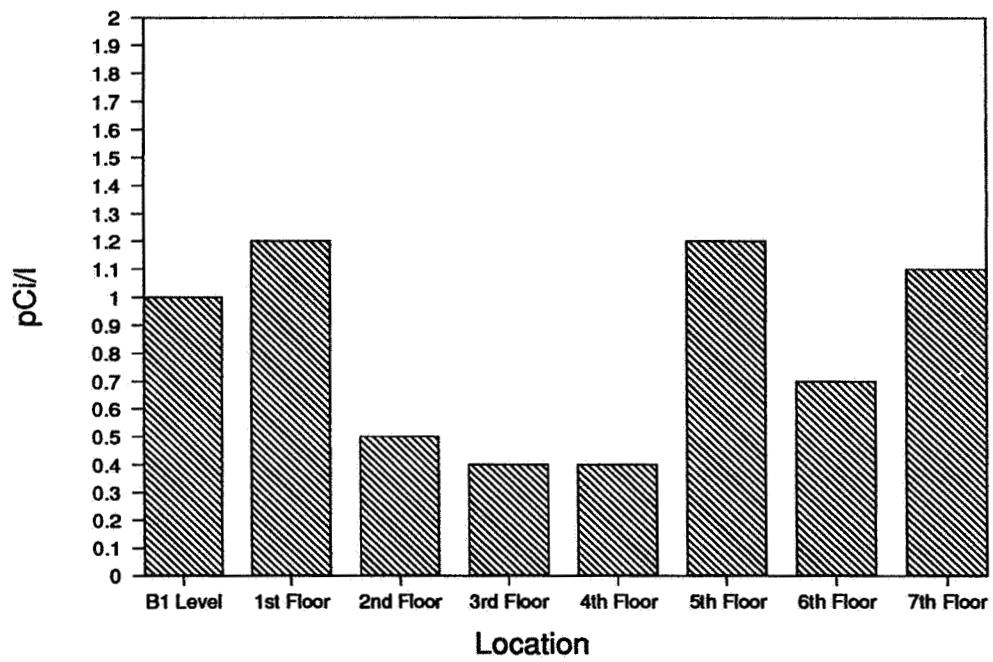


Figure 22. Radon Levels as Measured with Charcoal Canisters

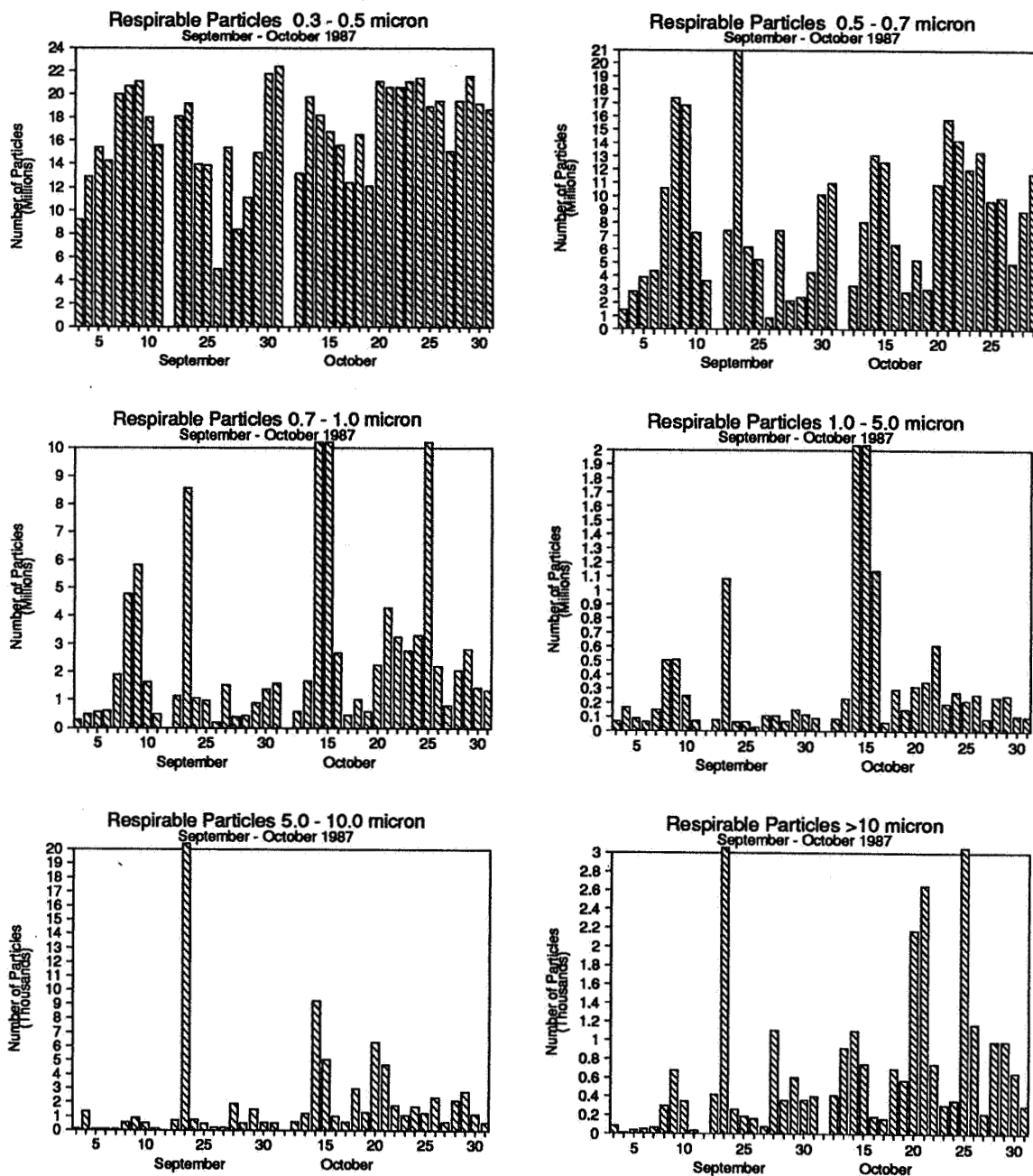


Figure 23. Respirable Particles in Various Size Ranges for Months of September and October 1987

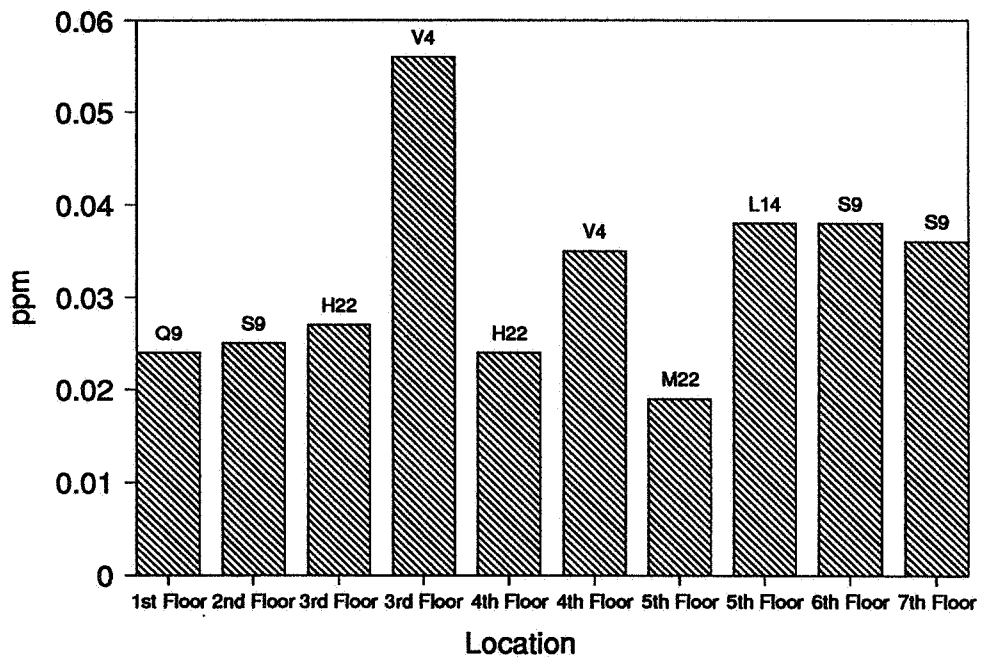


Figure 24. Formaldehyde Levels in Building

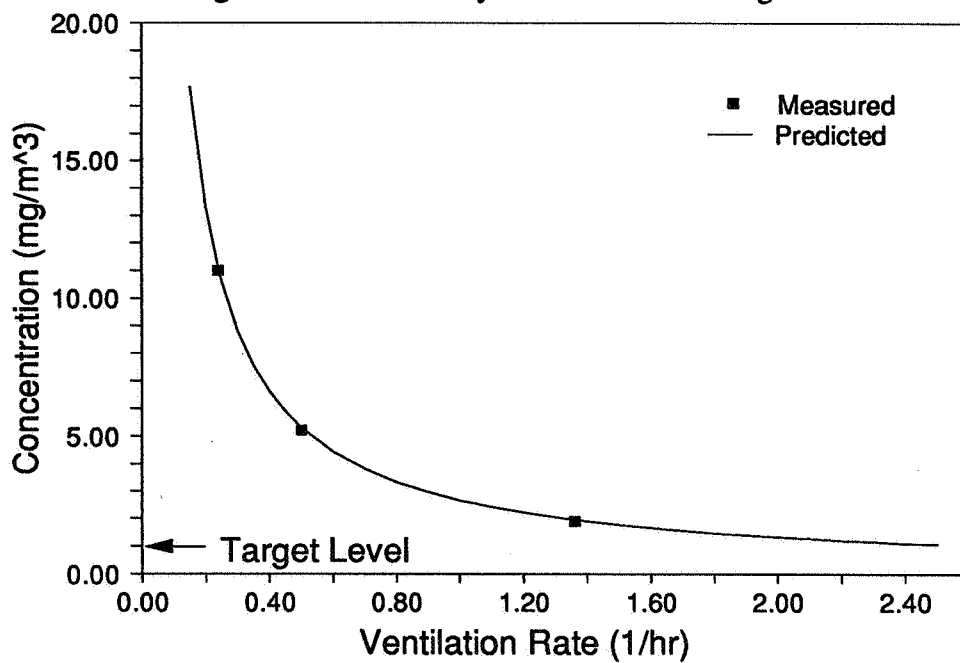


Figure 25. Total Volatile Organics versus Ventilation Rate

Table 1. Total Volatile Organics							
	Date	Concentration ($\mu\text{g}/\text{m}^3$)			Source Strength ($\mu\text{g}/\text{m}^3\text{-h}$)		
		8/4/87	10/14/87	1/13/88	8/4/87	10/14/87	1/13/88
Air Exchange Rate		0.5	1.36	0.24	0.5	1.36	0.24
Oxygenated							
2-Propanol		14.8	20.2	137.2	5.8	21.9	31.6
2-Propanone		50.1	28.8	66.6	22.1	26.0	14.9
2-Butanone		40.9	5.2	15.3	19.0	2.5	2.0
Halogenated							
Trichlorofluoromethane			48.0	26.6		62.3	5.6
Dichloromethane		32.4	2.6	13.4	15.9	1.3	2.7
1,1,1-Trichloroethane		13.5	13.8	119.7	5.4	13.6	27.5
Trichloroethane		16.4	7.2	58.2	8.2	9.7	11.0
Alkane + Cycloakane							
2-Methylbutane		31.9	53.8	81.6	13.1	31.7	16.1
n-Hexane		11.3	10.0	24.0	5.7	6.7	3.7
Cyclohexane		5.7			2.4		
n-Heptane		4.8	3.1	12.6	2.0	2.7	0.2
3-Methylhexane		6.0	4.0	14.7	2.4	3.1	0.0
Methylcyclohexane		5.1			2.4		
2,2,4-Trimethylpentane		2.4	1.8	8.0	1.0	1.3	0.7
1,4-Dimethylcyclohexane		3.1			1.6		
n-Nonane		39.6	10.6	149.1	19.7	11.4	11.7
2,2,5-Trimethylhexane		2.4			1.2		
n-Decane		147.0	82.5	638.7	72.8	104.2	151.7
n-Undecane		115.6	57.3	831.3	55.2	71.3	196.8
n-Dodecane		49.1	10.6	280.8	21.8	5.9	67.0
n-Tridecane			6.0	111.9		5.8	526.2
n-Tetradecane			36.1	245.3		43.0	57.9
Aromatic							
Toluene		60.4	81.3	91.0	22.7	80.9	13.7
Ethylbenzene		11.8	7.0	18.7	5.3	4.9	2.3
1,2-Dimethylbenzene		17.2	8.7	25.8	7.6	5.8	4.1
1,3-,1,4-Dimethylbenzene			18.1	54.5		11.7	8.8
1,3,5-Trimethylbenzene		4.1			1.6		
Totals							
Sum of individual compounds		685.5	517.7	3025.1	314.8	528.7	679.6
Total volatile carbon		5200.0	1900.0	11000.0	2500.0	2400.0	2500.0

EFFECTIVE VENTILATION

9th AIVC Conference, Gent, Belgium
12-15 September, 1988

Poster 21

APPLICATION OF MATHEMATICAL MODELING TO THE
EVALUATION OF BUILDING VENTILATION SYSTEMS

J.B. FANG, R.A. GROT*AND T. KURABUCHI^o

*Centre for Building Technology
National Institute of Standards and Technology
Gaithersburg, MD 20899
U.S.A.

^oDepartment of Architecture
University of Tokyo
Tokyo
Japan

ABSTRACT

Numerical modeling is performed for three-dimensional turbulent buoyant flows emerging from an air diffuser in an air-conditioned, ventilated room. The velocity and temperature distributions of air in the room are calculated, and the calculated results are found to be in reasonable agreement with published experimental observations. Calculations of Air Diffusion Performance Index (ADPI) for a sidewall grille are carried out for different flow rates of air supply. The predicted ADPI values are found generally to be consistent with the corresponding experimental values. It is reasonable to apply the numerical modeling technique for practical use in the prediction of various air-conditioned room environments and the design of building ventilation systems.

Keywords: air diffusion performance, K-E turbulence models, mathematical modeling, numerical simulation, room air movement, ventilation systems.

1 Introduction

The velocity and temperature characteristics of air within the occupied zones of a building are important factors in determining the comfort level and indoor air quality experienced by the spaces's occupants. Most heating, ventilation and air-conditioning systems can provide a certain level of air motion and maintain the desired average of temperature and humidity in conditioned spaces. However, there can be areas of excessive air drafts and excessive room air temperature variation, which can be discomforting for the building occupants. Similarly, parts of the space which experience low air flows may have locally high pollutant levels and low ventilation effectiveness. For the design and selection of suitable and effective building ventilation systems, information on the distributions of air flow velocities and temperatures as well as the heating and cooling loads for a given room geometry is needed.

Due to increasing computing speed and decreasing costs with rapid progress in computer technology, numerical simulations of physical systems are potentially a valuable tool for solving fluid flow and heat transfer problems. It can be noted that various experimental techniques such as field tests for measuring local air velocities and temperatures are expensive and time consuming. Mathematical modeling can provide a relatively cheap and rapid means for evaluating the performance of the building ventilation systems and assessing the effects of various system variables such as air supply rate and temperature, and the sizes and locations of air diffusers. In addition to these, numerical modeling can provide the bases for prediction of thermal comfort and air contaminant dispersion.

The performance of air ventilation systems is dependent on the type of air diffuser used as an air inlet, the space heating or cooling load, and the flow rate of air supply to the conditioned spaces. A properly designed, wall or ceiling mounted air diffuser system can not only meet the required heating and cooling loads but also provide comfort thermal conditions and satisfactory air movement environments in the occupied zones.

A comprehensive study of room air distribution performance was conducted by Miller and Nevins [1-4]. They performed extensive laboratory testing of various types of air distributing devices such as sidewall grilles and ceiling diffusers, and evaluated their performances based on the measured air velocities and temperatures in the occupied zone of the test room. Hart and Int-Hout [5] carried out a series of laboratory tests to determine the performance of continuous linear air diffusers in the perimeter zones of both open and closed office configurations. The results of their tests suggest that ceiling mounted linear diffusers can give acceptable thermal environments for a variety of heat loads without the use of convective heaters. Recently, Yamazaki, et al. [6] applied numerical modeling technique to simulate the air-heating environments for both a console type of air heater installed in a residential room and an air diffuser installed on the ceiling, and compared the predicted results with some experimental data.

In this paper, an attempt is made to estimate the air-conditioned environments using mathematical modeling technique for a sidewall grille mounted on a wall and directly above the return air outlet in a room of an office building. The predicted results on the air distribution performance of this air diffuser are compared with the published test results [1-5].

2 Calculation Procedure

A finite difference computer program called EXACT3 [7], which stands for EXPLICIT AlGORITHM for 3-dimensional Continuous Turbulent fluid flow, was modified with addition of a source term to the energy equation and used for predicting indoor air distribution. This computer code was

used for numerical simulation of indoor air movement and local air contaminant dispersion processes under conditions of with and without use of a mechanical ventilation device in a chemical laboratory for isothermal flow situation [8].

The basic equations describing the indoor air flows include the continuity, Navier-Stokes, and energy equations for a turbulent, incompressible fluid, along with two additional transport equations for the turbulence kinetic energy and its dissipation rate, and are expressed by:

$$\frac{\partial U_j}{\partial x_j} = 0 \quad (1)$$

$$\frac{\partial U_i}{\partial t} + \frac{\partial U_i U_j}{\partial x_j} = -\frac{1}{\rho} \frac{\partial P}{\partial x_i} + \frac{\partial}{\partial x_j} \left\{ \nu_{eff} \left(\frac{\partial U_i}{\partial x_j} + \frac{\partial U_j}{\partial x_i} \right) \right\} - \beta g_i \theta \quad (2)$$

$$\frac{\partial \theta}{\partial t} + \frac{\partial \theta U_j}{\partial x_j} = \frac{\partial}{\partial x_j} \left(\alpha_{eff} \frac{\partial \theta}{\partial x_j} \right) + S_\theta \quad (3)$$

$$\frac{\partial \kappa}{\partial t} + \frac{\partial \kappa U_j}{\partial x_j} = \frac{\partial}{\partial x_j} \left(\Gamma_\kappa \frac{\partial \kappa}{\partial x_j} \right) + \nu_t S + G - \epsilon \quad (4)$$

$$\frac{\partial \epsilon}{\partial t} + \frac{\partial \epsilon U_j}{\partial x_j} = \frac{\partial}{\partial x_j} \left(\Gamma_\epsilon \frac{\partial \epsilon}{\partial x_j} \right) + \frac{\epsilon}{\kappa} (c_1 \epsilon \nu_t S - c_2 \epsilon + c_3 G) \quad (5)$$

where

$$\nu_t = C_D \frac{\kappa^2}{\epsilon} \quad \text{eddy viscosity}$$

$$\nu_{eff} = \frac{1}{Re} + \nu_t \quad \text{effective eddy viscosity}$$

$$\alpha_{eff} = \frac{1}{RePr} + \frac{\nu_t}{\sigma_\theta} \quad \text{effective thermal diffusivity}$$

$$S = \left(\frac{\partial U_i}{\partial x_j} + \frac{\partial U_j}{\partial x_i} \right) \frac{\partial U_i}{\partial x_j}$$

$$G = \beta g_j \frac{\nu_t}{\sigma_\theta} \frac{\partial \theta}{\partial x_j}$$

$$\Gamma_\kappa = \frac{1}{Re} + \frac{\nu_t}{\sigma_\kappa}$$

$$\Gamma_\epsilon = \frac{1}{Re} + \frac{\nu_t}{\sigma_\epsilon}$$

U_i are mean velocity components in x_i direction, respectively, x_i are Cartesian coordinates, t is time, ρ is the fluid density, p is the pressure, β is the volumetric coefficient of expansion of the fluid, g_i is gravitational acceleration in x_i direction, θ is the temperature difference between the average indoor temperature and local temperature, S_θ is the volumetric rate of heat generation, κ is turbulence kinetic energy, ϵ is the dissipation rate of turbulence kinetic energy, $Re = L_0 U_0 / \nu$, Reynolds number, in which L_0 is the inlet width of air diffuser and U_0 is the inlet air velocity; $Pr = \nu / \alpha$, in which ν is the kinematic viscosity and α is the thermal diffusivity of the fluid, and $c_1, c_2, c_3, \sigma_\theta, \sigma_\kappa$ and σ_ϵ are empirical constants in κ - ϵ turbulence model.

These equations are converted into a series of finite difference equations and solved simultaneously by using the MAC method [9]. A staggered grid system is used where the velocity components are defined at the center of grid surface and scalar quantities such as pressure and turbulence kinetic energy are defined at the center of grid volume. The computer code uses a hybrid scheme, which utilizes either centered differencing or upwind differencing scheme depending on the local value of cell Peclet number, for the partial derivatives in space, and an explicit scheme for the partial derivative with respect to time. It also uses the pressure relaxation technique to correct the pressure and velocity components simultaneously in order to obtain solutions which satisfy the continuity equation. Using the following values for empirical constants appearing in Equations 1 to 5:

$$c_D = 0.09, \quad c_1 = 1.44, \quad c_2 = 1.92, \quad c_3 = 1.0$$

$$\sigma_\kappa = 1.0, \quad \sigma_\epsilon = 1.3, \quad \sigma_\theta = 0.9$$

and following the MAC method, iterative solving and numerical time integration of these equations were made to obtain the converged solution.

The test room modeled numerically had overall dimensions of 6.10 m wide x 3.66 m long x 2.74 m high simulating an interior room of a multi-story office building [1-4]. The energy input to the room consisted of uniform heating loads from finstrip heaters located around the center of the room floor and having a total heat output of 22.07 W/m² over a 3.66 x 1.52 m floor area, and a concentrated load composed of a 0.97 x 0.91 x 0.31 m angle iron framework installed 0.20 m from the south wall, and having a heat output rate of 40.98 W/m² of floor area. A sidewall grille measuring 0.61 m wide by 0.15 m high was located in the center of the 3.66 m long north wall, with its horizontal center line 0.15 m below the ceiling. A 0.76 m x 0.42 m high return air grille was situated directly beneath the supply air grille, 0.71 m above the floor. Local air temperatures and velocities within the occupied zone of the test room were measured at 216 locations using anemometers and thermocouples. The air supply grilles had two rows of 19 mm wide adjustable vanes and both sets of vanes were straight for all tests performed. For all tests, the test room was maintained at an average temperature of 23.33 ± 0.39 °C during the course of the test. Under a total heating load of 63.05 W/m² of floor area, the flow rates of air supply to the room varied from 10.97 to 91.44 m³/h - m² of floor area.

Mathematical modeling was performed to simulate six air distribution tests on the sidewall grille installed in a ventilated room. A numerical grid with the room being subdivided non-uniformly into 29 x 27 x 20 rectangular parallelepiped cells was used with six different air flow rates including 10.97, 18.29, 36.58, 54.86, 73.15 and 91.44 m³/h-m² of floor area. In order to deal with boundary conditions, one or two dummy cells with the same cell intervals as that of the terminal real cell were added to outside of the boundary. The temperature difference between the supply air and the room air for each flow rate was calculated based on an overall energy balance around the whole room. The calculated values of temperature difference between the supply air and the

room air, θ_o , for different rates of air inflow are tabulated in Table 1 along with the Reynolds number and the Archimedes number, which determines the effect of buoyancy on the flow field and is defined as $Ar = \beta g L_o \theta_o / V_o^2$.

The incoming air was colder than the bulk air in the room to compensate for the input of the room heating load, simulating a ventilation situation in summer. Numerical modeling corresponding to the test conditions was made with a nonuniform mesh layout for a symmetric half portion of the flow domain including the concentrated and uniform heating loads, and an inlet and an outlet opening. Fine grid spacing was used in the vicinity of the walls, the heating loads, and the inlet and outlet openings.

The sidewall grille used for air distribution was assumed to be a 50% free area air diffuser. The boundary conditions for the velocity and turbulence properties included zero gradients in the exit plane and logarithmic wall functions to describe the near-wall or solid surface regions. All surfaces were assumed to be adiabatic except a portion of floor around the room center and the top face of the concentrated load, where constant heat input rates were prescribed. Heat was supplied at a rate of 88.3 W/m² from uniform load at the center of room floor, and at 3279 W/m² from the concentrated load in the vicinity of wall opposite to the inlet. As illustrated in Table 1, the inlet temperatures for six air inflow rates varying from 10.97 to 91.44 m³/h-m² were respectively 17.3, 10.4, 5.2, 3.5, 2.6 and 2.1 °C lower than the average temperature of the room of 23.3 °C. The calculations of air velocity and temperature distributions for three-dimensional turbulent buoyant flows in a ventilated room were performed using the Cyber 205 supercomputer at the National Institute of Standards and Technology

3 Calculated Results

Figures 1 to 6 show the calculated velocity distribution in the vertical center plane of the test room for different air inflow rates. As shown in Figure 1, the cold air coming from the inlet travelled down towards the floor due to the downward directed buoyancy force. A portion of flows circulated around the lower left corner of the room and exited through the return air grille. The remaining portions of flows proceeded along the floor surface, turned upward after impinging onto the concentrated load and being accelerated by merging with the hot gas stream rising from the concentrated load, spread radially along the ceiling and entrained into the main flows from the inlet. One small recirculating zone was observed in the top right corner of the room. The air distribution patterns on the vertical center plane of the room obtained with smoke filaments for different flow rates [3,4] are given in Figure 7 for comparison with the predictions. As shown in Figures 1 and 7.a, the predicted general flow structure agrees quite well with the corresponding experimental observations. In Figure 2, the inflows following the ceiling spread radially toward the floor and the wall opposite to the entrance because of increased inlet velocity and decreased downward directed buoyancy effects. The flows are then curved along the wall and floor, and entrained into the jet stream or depart from the test room. It can be seen that a secondary recirculation is created in the vicinity of the floor and the concentrated heat source. There are some discrepancies between prediction and experimental observations on flow patterns by comparison of Figures 2 and 7.b. This may be due to relatively low value for Archimedes number used in the calculations causing the temperature difference between the room air and the supply air to be underestimated compared to actual value of the test.

Figures 3 through 6 show that a turbulent buoyant wall jet issuing from the inlet grille, spreading along the ceiling and turning downward and horizontally toward the outlet after impinging onto the opposite wall. A recirculating flow structure appeared in the whole flow domain with its center located near the concentrated load. The predicted flow patterns shown in Figures 3 to 6 are generally consistent with the corresponding experimental observations illustrated in Figure 7.

The Air Diffusion Performance Index (ADPI) is commonly used to specify the performance of an air diffuser system, and defined as the percentage of the locations in the occupied zone, which meet acceptable limits of effective draft temperatures between - 1.7 °C and +1.1 °C, and local air velocity of less than 0.35 m/s [10]. The effective draft temperature, ϕ , can be calculated from the equation below:

$$\phi = (T_x - T_c) - 8.0(v_x - 0.15) \quad (6)$$

where T_x is the local air temperature, in °C, T_c is the room average temperature, in °C and v_x is the local air velocity, in m/s.

The air diffusion performance indexes for the sidewall grille are calculated for different flow rates of supply air and listed in Table 2 along with the corresponding experimentally determined values. The ADPI calculations were based on predicted air temperatures and velocities at 96 locations, which were uniformly distributed throughout the occupied space in the one-half portion of the flow domain. The occupied zone was situated at 0.28 m from the wall of the inlet, 0.31 m from side walls, 0.79 m from the wall opposite to the inlet, and 0.17 m from the floor extending up to 1.87 m above the floor.

With the exception of the two highest air inflow rates, the predicted ADPI and drafty percentage values are generally in good agreement with the experimental ADPI and drafty percentage values. It can be noted that the experimental values were derived based on 216 measurement locations distributed evenly in a room space situated 0.92 m from the wall opposite to the inlet, 0.31 m from side walls and the wall of air inlet, 0.10 m from the floor, and 0.81 m from the ceiling or 1.93 m above the floor. At the highest two air inflow rates, there are noticeable discrepancies between the predicted and experimental ADPI results. This may be attributed to over-predicting the spread of the air wall jet after impinging onto the opposite wall and deflecting and reversing direction of flows as local air velocities decreased so rapidly as shown in Figures 5 and 6. There are significant inconsistencies between the predicted and experimental results on the percentages of stagnant cold and stagnant hot locations in the occupied zone. The use of lower values for temperature differential between the room air and the inlet air in calculations, for instance, 17.2 °C versus 19.4 °C [1], which was actually used to make up the 63.05 W/m² heating load for the test with a flow rate of 10.97 m³/h-m², undoubtedly contribute to a part of this discrepancy. It was also noted that at higher flow rates, the results of the simulation were greatly influenced by the assumed inlet flow velocity even through the volumetric flow remained constant (that is, by increasing or decreasing the assumed effective area of the grille).

As illustrated in Table 2, the predicted ADPI values have a maximum at air inflow rate of 36.58 m³/h-m². At low rates of air injection, the jet of cool air fell downward due to strong buoyancy effect and did not fill the room. Under these conditions, there were thus numerous locations within the room at which the local temperatures were far below and above the control temperature causing the effective draft temperature to be outside the comfort limits and therefore leading to low ADPI values. With an increase in the supply of air, the ADPI values were

increased to reach a maximum because of better mixing occurring within the room. However, a further increase in the volume of air supply resulted in decrease in ADPI value since the number of locations with local air velocities greater than the 0.35 m/s limit was increased.

4 Conclusions

Prediction of buoyancy-affected air flows emerging from an air diffuser in a ventilated room has been demonstrated in a wide range of air inflow rates with constant heating loads using the numerical technique presented in this paper. The three-dimensional distributions of air velocity and temperature in an air conditioned room are calculated, and the calculated velocity distributions are generally in reasonably good agreement with experimental observations obtained with smoke filaments.

The Air Diffusion Performance Indexes (ADPI) for a sidewall grille are calculated for six air flow rates and the calculated results are compared with the corresponding published experimental values. A good agreement is obtained for flow rates ranging between 10.97 and 54.86 m³/h-m² of floor area, and a fair agreement is found for flow rates greater than 73.15 m³/h-m² which is probably due to use of smaller values for the heating loads and temperature differential between the room air and the inlet air in numerical simulations compared to experimental values. The ADPI value is found to be a function of air inflow rate and room heating load as would be expected. The procedure for calculating three velocity components and temperature in a ventilated room involves the solution of three-dimensional transient equations for conservation of mass, momentum, energy, and turbulence kinetic energy and its dissipation rate. The calculation procedure is practically useful in the design of building ventilation systems and prediction of various air-conditioned room environments.

5 References

1. Miller, P. L. and R. G. Nevins, 'An Analysis of the Performance of Room Air Distribution Systems; ASHRAE Transactions, 78, Part I, 191-198, (1972).
2. Miller, P. L., 'Room Air Distribution Performance of Four Selected Outlets', ASHRAE Transactions, 77, Part II, 194-204, (1971).
3. Miller, P. L. and R. T. Nash, 'A Further Analysis of Room Air Distribution Performance; ASHRAE Transactions, 77, Part II, 205-212, (1971).
4. Nevins, R. G., 'Air Diffusion Dynamics--Theory, Design and Application', Business News Publishing Co., Birmingham, Michigan, 1976.
5. Hart, G. H. and D. Int-Hout, 'Thermal Performance of a Continuous Linear Air Diffuser in the Perimeter Zone of an Office Environment', ASHRAE Transactions, 86, Part 2, 107-124, (1980).
6. Yamazaki, K., M. Komatsu and M. Otsubo, 'Application of Numerical Simulation for Residential Room Air Conditioning', ASHRAE Transactions, 93, Part 1, 210-225, (1987).
7. Kurabuchi, T., 'Numerical Calculation Method of Indoor Air Flow by Means of k-E Turbulence Model, NBSIR Report (In Process).
8. Kurabuchi, T. and T. Kusuda, 'Numerical Prediction for Indoor Air Movement', ASHRAE Journal, December 1987, pp 26-30.

9. Harlow, F. H. and J. E. Welch, 'Numerical Calculation of Time Dependent Viscous Incompressible Flow of Fluid with Free Surface', *Physics of Fluids*, 8, 2182-2189 (1965).
10. American Society of Heating, Refrigerating and Air-Conditioning Engineers, 'ASHRAE Handbook - 1985 Fundamentals', Atlanta, GA, 1985.

Table 1. The Calculated Values of Temperature Difference between the Supply Air and the Room

Parameters Used in Numerical Simulations				
Inlet Flow Rate (m ³ /h-m ²)	Velocity (m/s)	Temperature Difference (θ°C)	Reynolds Number	Archimedes Number
10.97	1.463	17.20	57990	0.162630
18.29	2.438	10.36	96640	0.035125
36.58	4.877	5.180	193290	0.004391
54.86	7.315	3.452	289930	0.001301
73.15	9.754	2.589	386580	.000549
91.44	2.19	2.071	483220	0.00028

Table 2. Calculated ADPI Values for Different Flow Rates of Air Supply and the Corresponding Experimentally Determined Values

Inflow (m ³ /h-m ²)	ADPI (%)	V > 0.35 m/s Drafty (%)	T > -2.8 °C ϕ < -1.7 °C Stagnant Cold (%)	T < 2.8 °C ϕ > 1.1 °C Stagnant Hot (%)
10.97	64	7.3	36.5	0.0
	(68)	(2.3)	(4.2)	(23.6)
18.29	80	4.2	16.7	3.1
	(79)	(3.7)	(6.9)	(10.2)
36.58	81	11.5	13.5	5.2
	(82)	(5.1)	(0.5)	(12.0)
54.86	73	20.8	21.9	5.2
	(74)	(25.9)	(0.5)	(0.0)
73.15	62	28.1	28.1	4.2)
	(31)	(68.1)	(0.9)	(0.0)
91.44	54	40.6	33.3	3.1
	(20)	(79.2)	(0.5)	(0.0)

Note: The values in parentheses are the experimentally determined values.

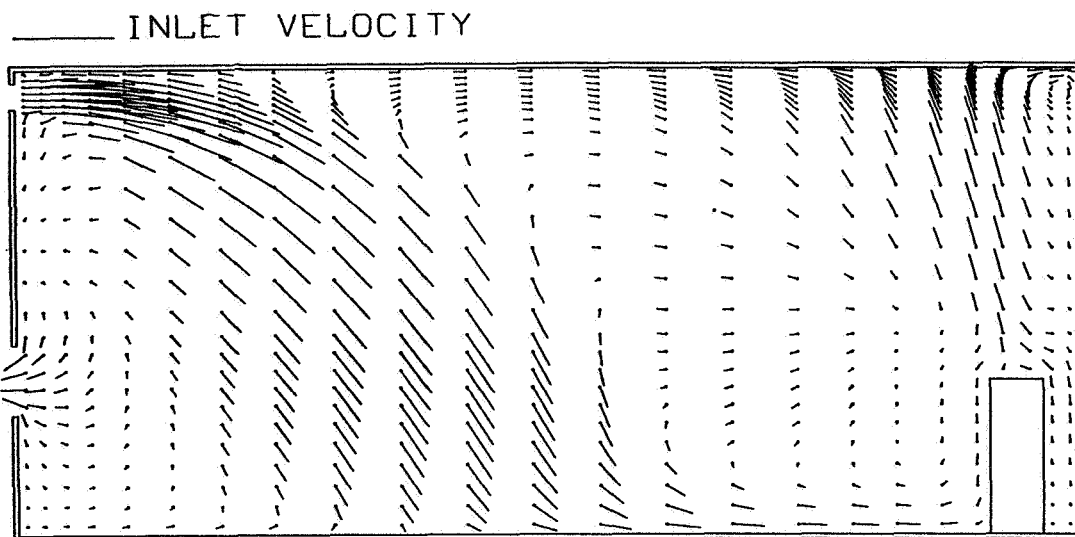


Figure 1. Distribution of Calculated Velocity Vectors in the Center Plane for Inflow Rate of $10.97 \text{ m}^3/\text{h-m}^2$

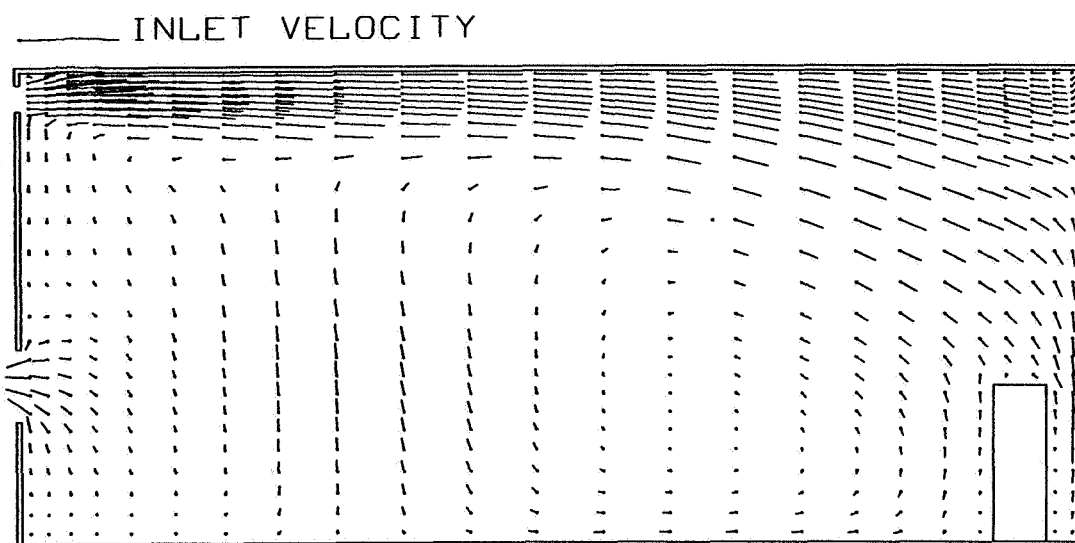


Figure 2. Distribution of Calculated Velocity Vectors in the Center Plane for Inflow Rate of $18.29 \text{ m}^3/\text{h-m}^2$

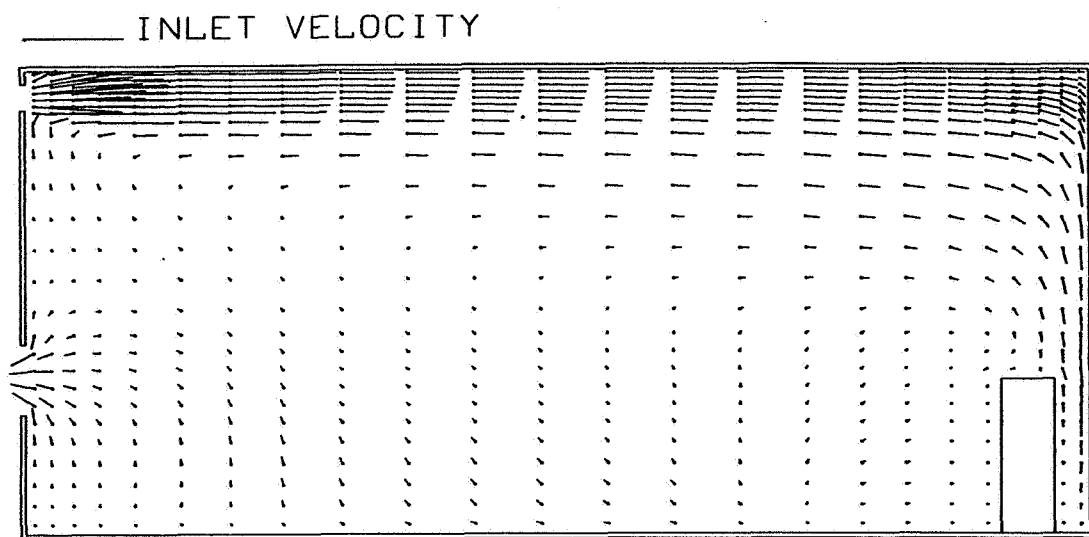


Figure 3. Distribution of Calculated Velocity Vectors in the Center Plane for Inflow Rate of $36.58 \text{ m}^3/\text{h-m}^2$

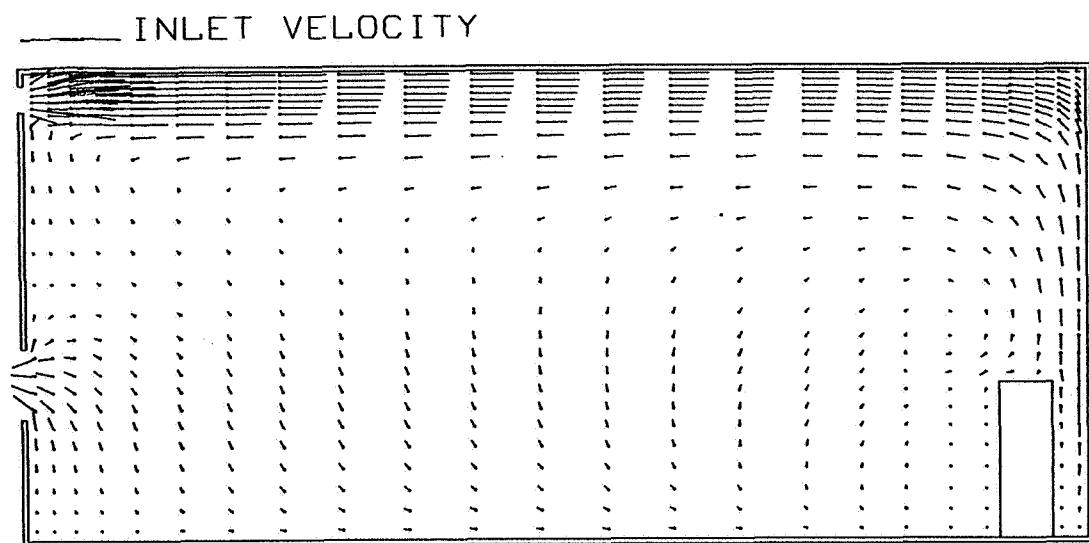


Figure 4. Distribution of Calculated Velocity Vectors in the Center Plane for Inflow Rate of $54.86 \text{ m}^3/\text{h-m}^2$

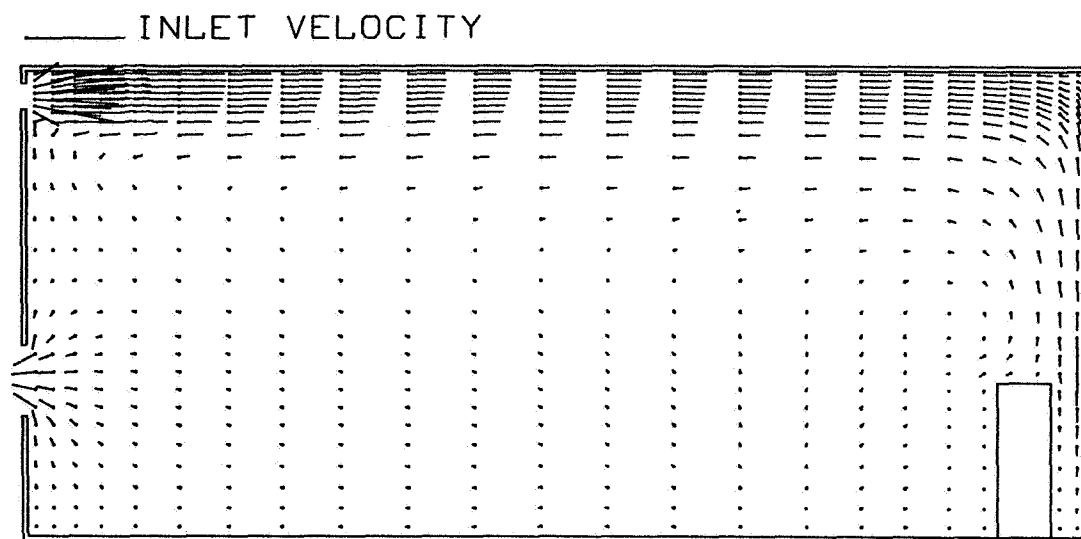


Figure 5. Distribution of Calculated Velocity Vectors in the Center Plane for Inflow Rate of $73.15 \text{ m}^3/\text{h-m}^2$

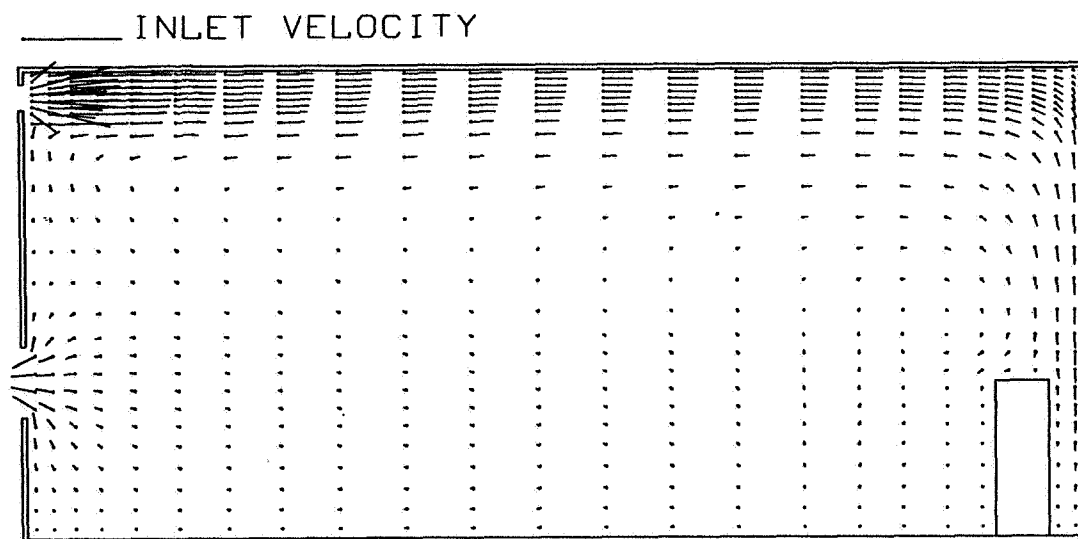
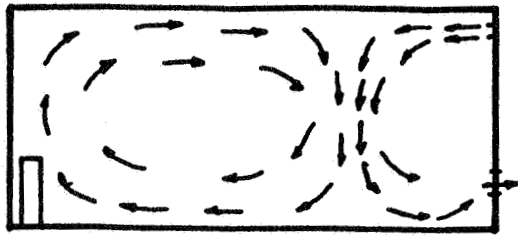
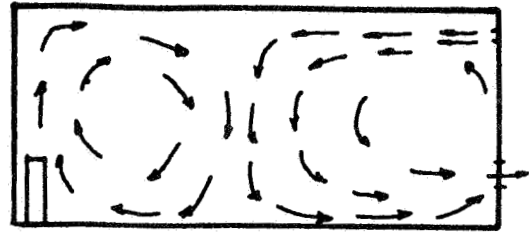


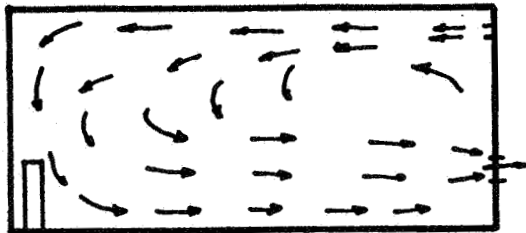
Figure 6. Distribution of Calculated Velocity Vectors in the Center Plane for Inflow Rate of $91.44 \text{ m}^3/\text{h-m}^2$



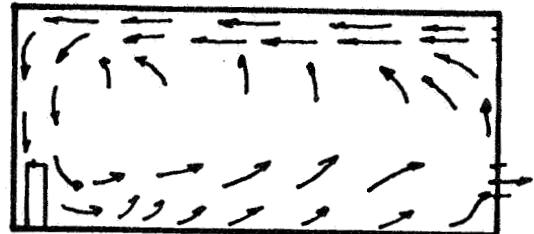
a. Inflow rate = $10.97 \text{ m}^3/\text{h-m}^2$



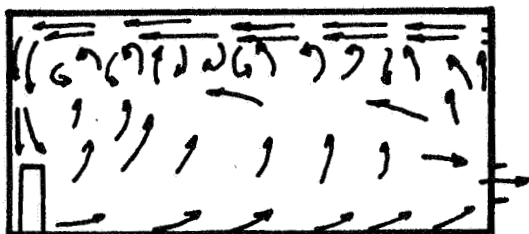
b. Inflow rate = $18.29 \text{ m}^3/\text{h-m}^2$



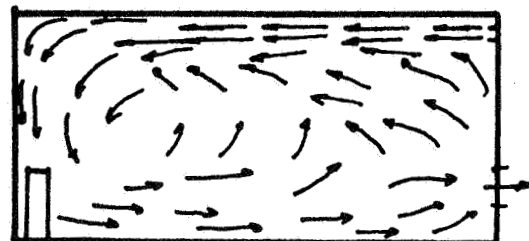
c. Inflow rate = $36.58 \text{ m}^3/\text{h-m}^2$



d. Inflow rate = $54.86 \text{ m}^3/\text{h-m}^2$



e. Inflow rate = $73.15 \text{ m}^3/\text{h-m}^2$



f. Inflow rate = $91.44 \text{ m}^3/\text{h-m}^2$

Figure 7. Measured Air Flow Patterns for Different Air Flow Rates

